University of Groningen

Dissecting diversity

Jacobs, Sabrina

IMPORTANT NOTE: You are advised to consult the publisher's version (publisher's PDF) if you wish to cite from it. Please check the document version below.

Document Version
Publisher's PDF, also known as Version of record

Publication date:
2021

[Link to publication in University of Groningen/UMCG research database](#)

Dissecting diversity

Clonal analysis of normal and malignant hematopoiesis using cellular barcodes

Sabrina Jacobs

rijksuniversiteit
groningen

Dissecting diversity

Clonal analysis of normal and malignant hematopoiesis using
cellular barcodes

Proefschrift

ter verkrijging van de graad van doctor aan de
Rijksuniversiteit Groningen
op gezag van de
rector magnificus prof. dr. C. Wijmenga
en volgens besluit van het College voor Promoties.

De openbare verdediging zal plaatsvinden op

maandag 27 september 2021 om 12:45 uur

door

Sabrina Jacobs

geboren op 11 november 1990
te Zeist

Promotor
Prof. dr. G. de Haan

Copromotores
Dr. L. Bystrykh
Dr. M.E. Belderbos

Beoordelingscommissie
Prof. dr. F. Foijer
Prof. dr. B. Fehse
Prof. dr. H. Vormoor

TABLE OF CONTENTS

Chapter 1

Introduction and thesis outline

INTRODUCTION

Concepts of clonal heterogeneity

The term *clone* was first described in agriculture and botany. In 1903 H.J. Webber wrote that "clons" are "groups of plants that are propagated by the use of any form of vegetative parts such as bulbs, tubers, grafts, etc., and are simply parts of the same individual"[1]. Since this initial description, the study of clones has received increasing attention in various fields of research, in particular stem cell biology and cancer.

Tissue-specific stem cells are a rare population of undifferentiated cells that are characterized by their capacity to self-renew, thereby maintaining a population of undifferentiated stem cells, and to give rise to a larger, multi-lineage progeny of differentiated cells[2]. In recent decades, advances in flow cytometry, genomics and bio-informatics have greatly increased our understanding of stem cells. In particular, the possibility to trace individual stem cells and their clonal progeny, *lineage tracing*, has allowed quantification of the number of stem that contribute to tissue formation and into the clonal dynamics of tissue (re-)generation. Previously, it was thought that hematopoietic stem cells (HSCs) were identical and contributed equally to hematopoiesis. However, lineage tracing of individual stem cells shows that the hematopoietic system can be repopulated by only a few HSCs *in vivo* and that they differ in their lineage output[3,4]. While some HSCs can generate a multi-lineage output, others are restricted to either the lymphoid or myeloid lineage. Moreover, the study of monozygotic twins, which are in essence clones as both embryos are derived from a single fertilized ovum, shed light on the development of pediatric leukemia[5]. For example, this study shows a common clonal origin and additional genomic aberrations are required to develop leukemia.

According to the theory of Webber, all descendants that are derived from the same parental stem cell are considered to be part of a clone, and thus to share certain features. However, contrary to Webbers proposal, it is becoming increasingly clear that these descendants are not completely identical. Throughout life, cells in all tissues (e.g. blood[6], colon[7,8], esophagus[9], skin[10]) accumulate (epi-)genetic alterations. These alterations cause descendants from the same ancestor to diversify, so called *clonal heterogeneity*. Furthermore, these genomic alterations may change essential cell functions. Upon exposure to the relevant selective pressures, clones with an evolutionary advantage will expand at the cost of other clones, resulting in *clonal selection*. This dynamic process of clonal (epi-)genetic diversification, selection, expansion and further (epi-)genetic diversification is known as *clonal evolution* (figure 1). This process of clonal evolution results in a continuously changing heterogeneous population of cells in many living tissues, as well as in cancer[11–16].
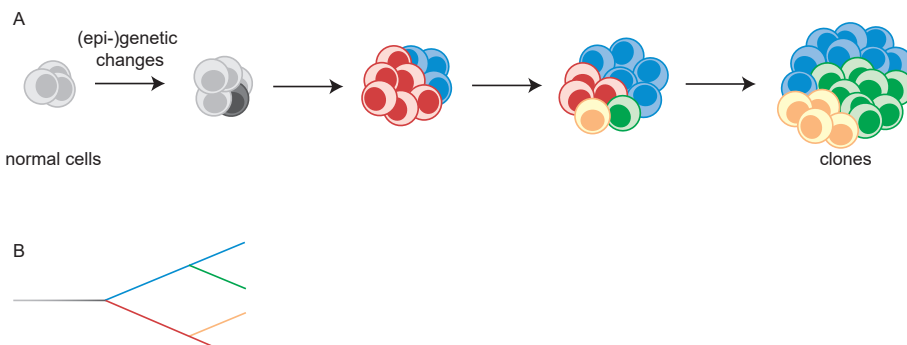
Figure 1. Clonal evolution. A. Stepwise accumulation of (epi-)genetic alterations in normal tissue, which could potentially result in a malignant transformation. Colored populations are clones carrying the same (epi-)genetic alterations. The presence of multiple clones with distinct combinations of genetic mutations provides clonal diversity, upon which selection may act followed by clonal expansion. B. Clonal evolution is thought to follow a complex branching pattern that results in a continuously changing heterogeneous population of cells.

Although the biological definition of a clone may seem rather straightforward, its experimental measurement is rather complex and not straightforward. One source of complexity results from the definition of a clone relative to the clone-marking event (figure 2)[2]. Experimental studies commonly rely on artificially introduced markers (e.g. DNA barcodes and fluorescent tags) to trace the clonal offspring of a single cell. In these experiments, the introduction of such markers is the clone-defining event, which is thus a single moment in time (figure 2A-C). In contrast, many cancer studies use combinations of naturally occurring mutations as clonal markers (figure 2D). As the accumulation of mutations is a dynamic process, the degree of clonal complexity depends on the time cancer cell populations are assessed. As an extreme example, a cancer cell population will be defined as monoclonal when the initial molecular event that contributed to a malignant transformation is chosen as the clone-defining event. However, when mutations that arise at later stages during cancer development are chosen as clone-defining events, this same population of cells can be defined as oligo- or polyclonal. Note that, due to clonal evolution and the chosen clone-defining event, (1) a single clone could consist of multiple subclones and (2) a single cell could belong to multiple clones[2]. Moreover, (3) as the various clone-tracing methods differ in their clone-defining event, a population of cells might be defined as monoclonal by one method whereas it might be oligo- or polyclonal by another method[2]. Therefore, conclusions regarding clonal composition of a given tissue or population of cells need to be interpreted in the context of the employed clonal marker. With respect to DNA barcoding, the applied method throughout this thesis, the term *clone* refers to all cells that share the same barcode sequence and are therefore derived from the same ancestor. Due to ongoing clonal evolution, cells constituting a

barcode clone might be genetically different and therefore a barcode clone might consist of multiple subclones.
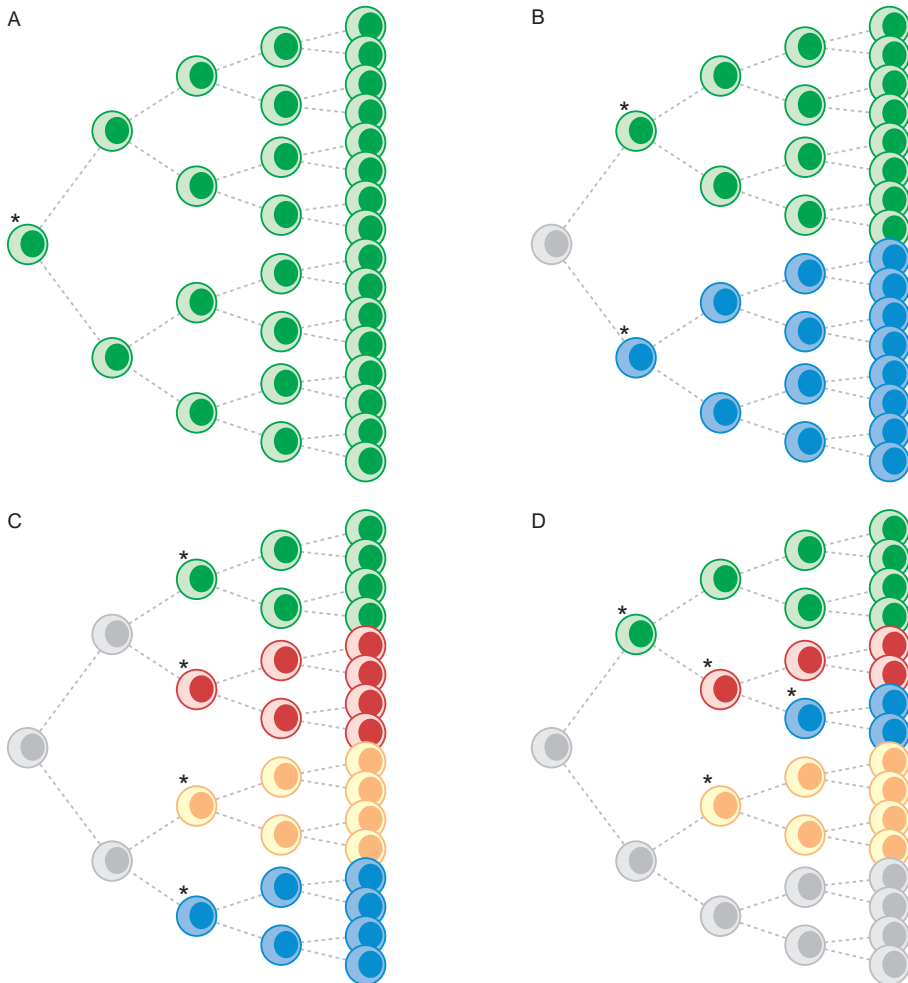
Figure 2. Schematic representation of clonal diversity relative to the clone-defining event. A-D. As clone-tracing methods vary in their clone-defining event, the degree of clonal complexity of a population of cells can differ between these clone-tracing methods. When the clone-defining event is a single moment in time and occurs in the cell of origin, the resulting population will be mono-clonal (A). If the event that defines a clone occurs after one and two cell divisions, the resulting population of cells will consist of respectively two (B) or four clones (C). In case the chosen clonal marker is acquired across multiple time points, such as the accumulation of mutations, the clonal diversity depends on the time cell populations are assessed (D). Asterisk refers to clone-defining event. Figure adapted from Glauche, I. *et al*.

Clone-tracing methods

There are a wide variety of clone-tracing methods to track individual cells and their (clonal) progeny. These methods range from naturally occurring (e.g. somatic mutations and antigen-receptor gene rearrangements) to experimentally introduced (e.g. vector integration sites and barcoding) clonal markers, which have been extensively reviewed in the past[17–19]. The degree of accuracy to detect and quantify clones differs between these approaches. Where some methods mark the actual progeny that arises from a single ancestor, other methods aim clonal quantification by retrospective reconstruction of evolutionary trajectories from ancestor to progeny. Therefore, the chosen method should be carefully selected based on the experimental question that needs to be addressed[2,20]. As these methods differ in their definition, identification and approach to trace clones, we will briefly discuss the most common applied methods below (table 1).

Stem cell assays

For the murine hematopoietic system there are a range of *in vitro* and *in vivo* stem cell assays, which aim to detect and quantify the number of stem or progenitor cells[21,22]. For example, in the presence of reliable phenotypic markers, flow cytometry is the fastest approach to detect and quantify stem cells. However, flow cytometry is not a functional assay and does not inform on the repopulation potential and lineage output. Another example is the limiting dilution assay, which relies on the *in vitro* culture or *in vivo* (serial) transplantation of a range of cell dilutions. The frequency and repopulation potential of tissue-specific stem cells or cancer stem cells are estimated by Poisson statistics[22–24]. The limiting dilution approach is a useful method when unique, phenotypic markers to identify stem cells are lacking. However, this approach is time-consuming and expensive, especially when conducted *in vivo*. Moreover, it shows the potential of an individual stem cell, but it does not take into account the genetic diversity of individual stem cells, nor the potential competitive or cooperative behavior of multiple stem cells and their progeny.

Naturally occurring somatic mutations

Naturally occurring somatic mutations are unique cell-intrinsic inheritable markers, which include microsatellites (i.e. small simple repeat regions), single-nucleotide variants and copy number alterations. Sequencing these somatic mutations has been instrumental in our understanding on clonal evolution in healthy tissues[6–10] and cancer[25–28]. An important advantage of this method is that it does not rely on artificial markers. Accordingly, it can be performed on human tissues, even retrospectively. Sequencing of naturally occurring mutations has initially been performed in bulk population of cells, which is an affordable method that allows accurate detection of high-frequency mutations[29]. Moreover, it does not require *in vitro* cell culture and manipulation to experimentally

Table 1. Overview of the advantages and disadvantages of the various clone-tracing methods.

	Flow cytometry	Limiting dilution assay	Naturally occurring somatic mutations		Antigen-receptor gene rearrangements	Integration site analysis	Multicolor barcoding		DNA barcoding	
			Bulk	Single cell			Viral transduction	Endogenous	Viral transduction	Endogenous
Affordability	++	+	-	--	-	+	++	++	+	+
Applicability in human patients	Yes	NA	Yes	Yes	Yes	Yes*	No	No	No	No
Clonal complexity	Low	NA	High	High	Low	High	Low	Low	High	Moderate
Live clone-tracing	No	No	No	No	No	No	Yes	Yes	No	No
Reproducibility	Yes	Yes	No	No	No	No	Yes	No	Yes**	No
Clone identification	Prospective	Prospective	Retrospective	Retrospective	Retrospective	Prospective	Prospective	Prospective	Prospective	Prospective
Stability	Debatable	NA	No	No	Debatable	Yes	Yes	Yes	Yes	Yes
Quantitative	Good***	Estimate	Low	Moderate	Low	Moderate	Moderate	Low	Good****	Moderate

* Patients undergoing gene-therapy treatment.

** Depends on library production.

*** In the presence of reliable phenotypic stem cell markers.

**** Accuracy depends on barcode structure, amplification by universal set of primers and upfront knowledge of library size.

introduce a clonal marker. Bulk sequencing of naturally occurring mutations is used to reconstruct evolutionary trajectories[14,16,29]. However, the identification of low-frequency mutations is inaccurate and as a consequence, some clones may remain undetected[29]. Although it allows quantification of relative clone sizes, it does not allow absolute quantification of the number of clone-forming stem cells. With the introduction of single-cell sequencing techniques, the detection of rare mutations in individual cells improved and as a result the degree of clonal heterogeneity increased[29,30]. One challenge, however, is the discrimination of 'true' mutations from sequencing noise[31]. To obtain sufficient amounts of DNA, single-cell sequencing requires pre-amplification through single-cell *in vitro* expansion or DNA amplification by PCR, which introduces noise[29]. In addition, the detection of minor subclonal populations remains challenging. As more cells need to be sequenced to obtain sufficient and reliable data to reconstruct an evolutionary trajectory, single-cell sequencing is also more expensive compared to bulk sequencing[29]. Finally, reconstruction of the evolutionary trajectory and quantification of cell fractions harboring specific mutations require complex mathematical modelling which relies on a number of assumptions[29]. Although the use of naturally occurring somatic mutations as clonal marker faces some challenges, it's a valuable method especially in human patients where the use of experimentally introduced clonal markers is generally not an option.

Antigen-receptor gene rearrangements

Antigen-receptor genes provide an alternative method to trace clonal expansions of lymphocytes. In fact, immunoglobulin gene and T-cell receptor gene rearrangements are the most widely applied clinical method to assess minimal residual disease in lymphoid malignancies. During early B- and T-cell development, the germline variable, diverse and joining fragments of the antigen-receptor genes are rearranged. This results in the generation of unique immunoglobulin and T-cell receptor genes within each lymphocyte[32,33]. Because of the wide range of possible rearrangements, the estimated diversity of immunoglobulin molecules is in the order of 10^{12}. Each rearrangement is independent and unique, with negligible probability that two unrelated cells share the same sequence. Therefore, when two cells have the same antigen-receptor gene rearrangement, they are likely derived from the same ancestor. Moreover, as antigen-receptor rearrangement is a relatively early event in lymphocyte development, lymphocytic neoplasms are characterized by a single, unique antigen-receptor rearrangement. Detection of rearranged antigen-receptor genes by Southern blotting, polymerase chain reaction, Sanger sequencing and more recently by next generation sequencing, have been used to study clonal heterogeneity in hematological malignancies[33]. However, antigen-receptor-gene rearrangements face limitations related to low complexity and instability. A recent publication by Li *et al.* showed, using RNA sequencing, that the majority of B-cell acute lymphoblastic leukemia patients harbor a maximum of two IGH rearranged clones[34] Al-

though other, more sensitive methods to identify antigen-receptor gene rearrangements may be capable of detecting somewhat more clones, the number of antigen-receptor-rearranged clones within a lymphocytic neoplasm seems to be low[34–36]. Moreover, ongoing rearrangements have been shown to occur during the development of hematological malignancies, arguing that antigen-receptor rearrangements are instable at least in a part of the patients[36]. Although these rearrangements have proven to be a powerful method to identify minimal residual disease, they are of limited use in the identification and tracking of subclones[33].

Integration site analysis

Using viral transduction, vectors are randomly integrated into the genome of the target cells[20]. Integration sites are then identified and quantified through DNA fragmentation, PCR amplification and next-generation sequencing. As these integration sites are unique and random, they allow tracking of an unlimited number of clones. Viral integration site analysis was one of the first techniques to experimentally introduce clonal markers. However, the quantification of clone numbers and sizes remains inaccurate[37,38]. First, the required use of restriction enzymes results in only the detection of integration sites in genomic regions that consist of restriction sites. Second, the variable lengths of the DNA fragments and their structural differences result in amplification bias. Although quantification of clone numbers and sizes remains challenging, it is an extraordinary useful clone tracing method. Currently it is the only experimentally introduced clonal marker that can be applied in human patients, specifically those that are undergoing gene therapy[39,40].

Multicolor barcoding

As cells can be labelled with fluorescent proteins, imaging-based clone tracing could be an alternative to genome-based clone-tracing methods. Imaging-based clone-tracing relies on combinations of multiple fluorescent proteins as a clonal marker[41–45]. These fluorescent proteins can be introduced by red-green-blue viral transduction. Alternatively, the Cre-LoxP switching color cassettes can be used. Upon Cre-induction, the LoxP sites are randomly recombined and the targeted cells express different fluorescent proteins. Multicolor lineage tracing has the advantage that individual clones can be sorted and live-traced in living animals. Moreover, the use of Cre-LoxP switching color cassettes allows direct application in transgenic models and circumvents *in vitro* manipulation. However, due to the limited number of distinguishable color combinations and recombination bias when using the Cre-LoxP-based system[46], accurate quantitative analysis in highly polyclonal samples remains difficult.

Endogenous DNA barcoding

Two well-known methods that allow for *in vivo* DNA barcoding are based on the Cre-LoxP and CRISPR-Cas9 system. The Cre-LoxP DNA barcoding system is similar to multicolor lineage tracing and uses DNA sequences instead of color cassettes to mark individual cells and their progeny[47,48]. The DNA sequences are identified through DNA isolation, PCR amplification and next-generation sequencing of the barcoded locus. The use of DNA sequences increases the number of traceable clones, but individual clones can no longer be sorted by flow cytometry. Moreover, quantification of the clone numbers and sizes remains inaccurate. The composition of the library is unknown and as a consequence, it is difficult to discriminate between noise and actual DNA barcode sequences. Moreover, Cre-LoxP faces the problem of recombination bias, which makes it possible for two clones to be marked with the same DNA sequence[46]. The CRISPR-Cas9-based system relies on the introduction of insertions or deletions (i.e. 'scars') in targeted genomic or synthetic DNA sequences (e.g. GFP-repeats) by the Cas9 and guide RNA complex[49,50]. The 'scarring' of the genome occurs in the time window that the Cas9 enzyme is active and is commonly used to reconstruct developmental lineage trees of tissues and organs. Developmental studies in zebrafish showed that thousands of scars can be generated, with only a few clusters of 'scars' contributing to the development of specific organs[49,50]. The number of traceable clones can be increased with the use of homing guide RNAs, where the homing guide RNA repeatedly targets its own locus[51]. However, bias in the introduction of specific 'scars' and reconstruction of the clonal signature faces, similar to the Cre-LoxP system, problems of low complexity and redundancy of scars. Although CRISPR-Cas9 requires further optimization, it has emerged as a promising new method which can be combined with single-cell transcriptomics[52–54].

DNA barcoding by viral transduction

DNA barcoding relies on the viral integration of (semi-)random, unique DNA sequences of a predetermined length (i.e. "barcode") in the genome of target cells. DNA barcoding marks all target cells at the same time and is therefore independent of (epi-)genetic makeup. For detection barcode sequences are first amplified by PCR using unique sets of primers and subsequently identified by multiplexed next-generation sequencing (figure 3)[55–59]. In contrast to some of the above-mentioned techniques, DNA barcoding is subjected to several selective bottlenecks (e.g. *in vitro* cell culture and *in vivo* transplantation) and cannot be applied to human patients. Moreover, clonal dynamics are retrospectively assessed and individual clones cannot be sorted. However, DNA barcoding also does not face the many challenges of the above-mentioned methods. It is a relatively simple method that does not require complex mathematical modelling. In general, data analysis includes several pre-filtering steps (i.e. quality control, de-multiplexing and barcode retrieval) and removal of sequencing noise and multiple barcode integrations into a single

cell. In our studies we used a semi-random barcode sequence, which is characterized by alternating fixed nucleotides (i.e. backbone) and variable nucleotides. The presence of the backbone has the advantage that barcode sequences can be easily retrieved from the sequencing data. DNA barcoding is an affordable method, as multiple heterogeneous population of cells can be combined into a single sequencing run due to the use of unique sets of primers. Moreover, in our studies we used a barcode library of known size (i.e. complexity), which facilitates signal-to-noise discrimination and allows for more accurate, quantitative clonal analysis. This quantitative analysis is further facilitated by the structural similarities and predetermined length of the barcode sequences, which reduces amplification bias. Moreover, the detection of barcode sequences is independent of the integration site and does not rely on the use of restriction enzymes. Finally, minor barcode fractions can be detected as well. These advantages make barcoding a relevant and useful method for quantitative, high-throughput clone tracing, especially for highly polyclonal samples.
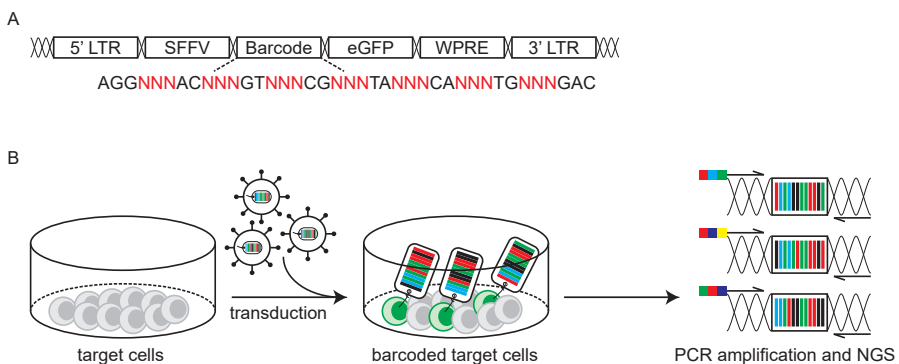
Figure 3. Cellular barcoding. A. The barcode sequence consists of fixed nucleotides (black) to enhance barcode retrieval from sequencing data and random nucleotides (red) to generate a diversity of barcodes. The barcode sequence is ligated in a vector together with an enhanced Green Fluorescent Protein (eGFP) to identify barcoded cells. The expression of the barcode and eGFP is regulated by the spleen focus forming virus (SFFV) promoter. B. Barcode sequences are integrated into the genome of the target cells via lentiviral transduction. Barcode sequences are retrieved by isolation of genomic DNA followed by polymerase chain reaction (PCR) amplification using uniquely indexed forward primers and a universal reverse primer. Next, polyclonal barcoded cell populations are subjected to multiplex next-generation sequencing (NGS).

Clonal heterogeneity in acute lymphoblastic leukemia

Cancer results from a reiterative process of genetic diversification, clonal expansion, and clonal selection. Accordingly, clone-tracing methods provide a unique strategy to gain insight into the occurrence and evolution of malignancy. In children, B- progenitor cell acute lymphoblastic leukemia (B-ALL) is the most common malignancy[60,61]. Due to improved treatment protocols and supportive care, the 5-year event free survival is now

approaching 90%[62,63]. However, approximately 10% of these children suffer from relapse and especially this group of patients have a poor prognosis[64–66]. Multiple studies have shown that B-ALL is characterized by a heterogeneous population of cells, consisting of multiple clones with distinct genomic aberrations[15,67–70]. Moreover, it has been shown the majority of the relapses is caused by a minor clone that was already present at diagnosis, which often acquired additional (therapy-induced) genomic aberrations, indicative of ongoing clonal evolution[14,16,71]. This clonal heterogeneity is thought to be a key contributor in the initiation, progression and relapse of B-ALL, and perhaps of cancer in general. Using cellular barcoding we could potentially address some key questions on clonal heterogeneity in B-ALL, including the number of leukemia-propagating cells, the distribution of clones across different anatomical locations and the clonal dynamics in response to selective bottlenecks, such as chemotherapy. In conclusion, clone-tracing methods could further improve our understanding of clonal heterogeneity in B-ALL and cancer in general.

OUTLINE OF THESIS

The aim of this thesis is to provide insights into the applicability and relevance of cellular barcodes to study the clonal dynamics of individual cells in a heterogeneous population of cells. Therefore, we applied cellular barcoding to normal, non-malignant hematopoietic stem cells and B-ALL cells and studied their behavior in murine xenografts.

In **chapter 2**, we emphasize on the influence of different data analysis methods to study the frequency and clonal dynamics through cellular barcoding and xenotransplantation of hematopoietic stem cells (HSCs) derived from human umbilical cord blood. Different barcode data analysis methods might directly affect the experimental results and as a consequence the biological interpretation. The importance of the different parameters in barcode library design, barcode library validation, experimental design, the identification and quantification of barcodes and reporting on them, have been extensively reviewed by us in the past[58]. Here, we applied different data analysis methods to the same dataset. We demonstrate that conclusions on the number of HSCs in the same sample can vary by several orders of magnitude, depending on the applied methods for data filtering and definitions of clonal diversity. Moreover, using the Shannon-diversity index, which we identified as the most robust method of clone-quantification, we demonstrate marked heterogeneity in the frequency of HSCs and their lineage output between different umbilical cord blood donors.

In **chapter 3**, we demonstrate that applying cellular barcodes to murine xenograft models is a reliable method to study the clonal dynamics of pediatric B-ALL. The identification and tracking of individual leukemia clones using cellular barcoding was first

validated in the SupB15 cell line *in vitro* and *in vivo*. We subsequently applied this to patient-derived B-ALL cells and show that murine xenografts harbor tens to hundreds of leukemia clones which undergo clonal selection and evolution. As we only analyzed a fraction of the total number of leukemia cells in the donating patient, the real number of clones is likely much higher. Moreover, we demonstrate that barcoded B-ALL clones are asymmetrically distributed in xenografts (i.e. spatial heterogeneity), implying that single site sampling does not fully capture the clonal heterogeneity.

In **chapter 4**, we use cellular barcoding to study the anatomic distribution of human leukemia clones in murine xenografts in more detail and assess the quantitative distribution of leukemia clones at different stages of leukemia development. We show that, at end stage disease, murine xenografts harbor millions of leukemia cells, of which the majority localize in the spine and the spleen. The leukemia cell content in skeletal sites is proportional to, and limited by, the size of the location. In line with chapter 3, leukemia clones are asymmetrically distributed across the murine body. Using quantitative barcode tracing, we calculate the probability for a given clone to escape detection when only a single anatomic site is assessed.

In **chapter 5**, we demonstrate that cellular barcoding of patient-derived leukemia cells in murine xenografts is an effective model to assess the impact of single chemotherapeutic agents on clonal dynamics and heterogeneity. We observed that individual leukemia clones differ in their response to chemotherapy. By applying differential gene expression analysis to our barcode DNA sequencing data of mice transplanted with SupB15 cell line and patient-derived leukemia cells we could discriminate between clonal patterns developed through clonal drift or selection. We show that this model enables identification of chemotherapy-resistant clones and allows assessment of the effect of chemotherapeutic agents on spatial heterogeneity.

In **chapter 6** we summarize the results described in this thesis, discuss the relevance of cellular barcodes to study the clonal behavior of individual cells in a heterogeneous population of cells and suggest future perspectives.

REFERENCES

1. Webber HJ. NEW HORTICULTURAL AND AGRICULTURAL TERMS. *Science (80-)*. 1903;18(459):501-503. doi:10.1126/science.18.459.501-b

2. Glauche I, Bystrykh L, Eaves C, Roeder I. Stem cell clonality — Theoretical concepts, experimental techniques, and clinical challenges. *Blood Cells, Mol Dis*. 2013;50(4):232-240. doi:10.1016/j.bcmd.2013.01.007

3. Lemischka IR, Raulet DH, Mulligan RC. Developmental potential and dynamic behavior of hematopoietic stem cells. *Cell*. 1986;45(6):917-927. doi:10.1016/0092-8674(86)90566-0

4. Jordan CT, Lemischka IR. Clonal and systemic analysis of long-term hematopoiesis in the mouse. *Genes Dev*. 1990;4(2):220-232. doi:10.1101/gad.4.2.220

5. Greaves MF, Maia AT, Wiemels JL, Ford AM. Leukemia in twins: lessons in natural history. *Blood*. 2003;102(7):2321-2333. doi:10.1182/blood-2002-12-3817

6. Watson CJ, Papula AL, Poon GYP, et al. The evolutionary dynamics and fitness landscape of clonal hematopoiesis. *Science (80-)*. 2020;367(6485):1449-1454. doi:10.1126/science.aay9333

7. Blokzijl F, de Ligt J, Jager M, et al. Tissue-specific mutation accumulation in human adult stem cells during life. *Nature*. 2016;538(7624):260-264. doi:10.1038/nature19768

8. Lee-Six H, Olafsson S, Ellis P, et al. The landscape of somatic mutation in normal colorectal epithelial cells. *Nature*. 2019;574(7779):532-537. doi:10.1038/s41586-019-1672-7

9. Yokoyama A, Kakiuchi N, Yoshizato T, et al. Age-related remodelling of oesophageal epithelia by mutated cancer drivers. *Nature*. 2019;565(7739):312-317. doi:10.1038/s41586-018-0811-x

10. Martincorena I, Roshan A, Gerstung M, et al. High burden and pervasive positive selection of somatic mutations in normal human skin. *Science (80-)*. 2015;348(6237):880-886. doi:10.1126/science.aaa6806

11. Nowell P. The clonal evolution of tumor cell populations. *Science (80-)*. 1976;194(4260):23-28. doi:10.1126/science.959840

12. Greaves M, Maley CC. Clonal evolution in cancer. *Nature*. 2012;481(7381):306-313. doi:10.1038/nature10762

13. Ferrando AA, López-Otín C. Clonal evolution in leukemia. *Nat Med*. 2017;23(10):1135-1145. doi:10.1038/nm.4410

14. Mullighan CG, Phillips LA, Su X, et al. Genomic Analysis of the Clonal Origins of Relapsed Acute Lymphoblastic Leukemia. *Science (80-)*. 2008;322(5906):1377-1380. doi:10.1126/science.1164266

15. Anderson K, Lutz C, van Delft FW, et al. Genetic variegation of clonal architecture and propagating cells in leukaemia. *Nature*. 2011;469(7330):356-361. doi:10.1038/nature09650

16. Ma X, Edmonson M, Yergeau D, et al. Rise and fall of subclones from diagnosis to relapse in pediatric B-acute lymphoblastic leukaemia. *Nat Commun*. 2015;6(1):6604. doi:10.1038/ncomms7604

17. Woodworth MB, Girskis KM, Walsh CA. Building a lineage from single cells: genetic techniques for cell lineage tracking. *Nat Rev Genet*. 2017;18(4):230-244. doi:10.1038/nrg.2016.159

18. Baron CS, van Oudenaarden A. Unravelling cellular relationships during development and regeneration using genetic lineage tracing. *Nat Rev Mol Cell Biol*. 2019;20(12):753-765. doi:10.1038/s41580-019-0186-3

19. Wu S-H (Sam), Lee J-H, Koo B-K. Lineage Tracing: Computational Reconstruction Goes Beyond the Limit of Imaging. *Mol Cells*. 2019;42(2):104-112. doi:10.14348/molcells.2019.0006

20. Bystrykh L V, Verovskaya E, Zwart E, Broekhuis M, de Haan G. Counting stem cells: method-ological constraints. *Nat Methods*. 2012;9(6):567-574. doi:10.1038/nmeth.2043

21. van Os R, Kamminga LM, de Haan G. Stem Cell Assays: Something Old, Something New, Something Borrowed. *Stem Cells*. 2004;22(7):1181-1190. doi:10.1634/stemcells.2004-0095

22. Purton LE, Scadden DT. Limiting Factors in Murine Hematopoietic Stem Cell Assays. *Cell Stem Cell*. 2007;1(3):263-270. doi:10.1016/j.stem.2007.08.016

23. Roeder I, Horn K, Sieburg H-B, Cho R, Muller-Sieburg C, Loeffler M. Characterization and quantification of clonal heterogeneity among hematopoietic stem cells: a model-based ap-proach. *Blood*. 2008;112(13):4874-4883. doi:10.1182/blood-2008-05-155374

24. Hu Y, Smyth GK. ELDA: Extreme limiting dilution analysis for comparing depleted and enriched populations in stem cell and other assays. *J Immunol Methods*. 2009;347(1-2):70-78. doi:10.1016/j.jim.2009.06.008

25. Navin N, Kendall J, Troge J, et al. Tumour evolution inferred by single-cell sequencing. *Nature*. 2011;472(7341):90-94. doi:10.1038/nature09807

26. Baca SC, Prandi D, Lawrence MS, et al. Punctuated Evolution of Prostate Cancer Genomes. *Cell*. 2013;153(3):666-677. doi:10.1016/j.cell.2013.03.021

27. Zhang J, Fujimoto J, Zhang J, et al. Intratumor heterogeneity in localized lung adenocar-cinomas delineated by multiregion sequencing. *Science (80-)*. 2014;346(6206):256-259. doi:10.1126/science.1256930

28. Gao R, Davis A, McDonald TO, et al. Punctuated copy number evolution and clonal stasis in triple-negative breast cancer. *Nat Genet*. 2016;48(10):1119-1130. doi:10.1038/ng.3641

29. Kuipers J, Jahn K, Beerenwinkel N. Advances in understanding tumour evolution through single-cell sequencing. *Biochim Biophys Acta - Rev Cancer*. 2017;1867(2):127-138. doi:10.1016/j.bbcan.2017.02.001

30. Gawad C, Koh W, Quake SR. Dissecting the clonal origins of childhood acute lymphoblastic leukemia by single-cell genomics. *Proc Natl Acad Sci*. 2014;111(50):17947-17952. doi:10.1073/pnas.1420822111

31. Malikic S, Jahn K, Kuipers J, Sahinalp SC, Beerenwinkel N. Integrative inference of subclonal tumour evolution from single-cell and bulk sequencing data. *Nat Commun*. 2019;10(1):2750. doi:10.1038/s41467-019-10737-5

32. Meffre E, Casellas R, Nussenzweig MC. Antibody regulation of B cell development. *Nat Im-munol*. 2000;1(5):379-385. doi:10.1038/80816

33. Gazzola A, Mannu C, Rossi M, et al. The evolution of clonality testing in the diagnosis and monitoring of hematological malignancies. *Ther Adv Hematol*. 2014;5(2):35-47. doi:10.1177/2040620713519729

34. Li Z, Jiang N, Lim EH, et al. Identifying IGH disease clones for MRD monitoring in child-hood B-cell acute lymphoblastic leukemia using RNA-Seq. *Leukemia*. 2020;34(9):2418-2429. doi:10.1038/s41375-020-0774-4

35. Beishuizen A, Hählen K, Hagemeijer A, et al. Multiple rearranged immunoglobulin genes in childhood acute lymphoblastic leukemia of precursor B-cell origin. *Leukemia*. 1991;5(8):657-667.

36. Gawad C, Pepin F, Carlton VEH, et al. Massive evolution of the immunoglobulin heavy chain locus in children with B precursor acute lymphoblastic leukemia. *Blood*. 2012;120(22):4407-4417. doi:10.1182/blood-2012-05-429811

37. Gabriel R, Eckenberg R, Paruzynski A, et al. Comprehensive genomic access to vector inte-gration in clinical gene therapy. *Nat Med*. 2009;15(12):1431-1436. doi:10.1038/nm.2057

38. Harkey MA, Kaul R, Jacobs MA, et al. Multiarm High-Throughput Integration Site Detection: Limitations of LAM-PCR Technology and Optimization for Clonal Analysis. *Stem Cells Dev*. 2007;16(3):381-392. doi:10.1089/scd.2007.0015

39. Biasco L, Pellin D, Scala S, et al. In Vivo Tracking of Human Hematopoiesis Reveals Patterns of Clonal Dynamics during Early and Steady-State Reconstitution Phases. *Cell Stem Cell*. 2016;19(1):107-119. doi:10.1016/j.stem.2016.04.016

40. Six E, Guilloux A, Denis A, et al. Clonal tracking in gene therapy patients reveals a diversity of human hematopoietic differentiation programs. *Blood*. 2020;135(15):1219-1231. doi:10.1182/blood.2019002350

41. Livet J, Weissman TA, Kang H, et al. Transgenic strategies for combinatorial expression of fluorescent proteins in the nervous system. *Nature*. 2007;450(7166):56-62. doi:10.1038/nature06293

42. Weber K, Thomaschewski M, Warlich M, et al. RGB marking facilitates multicolor clonal cell tracking. *Nat Med*. 2011;17(4):504-509. doi:10.1038/nm.2338

43. Weber K, Thomaschewski M, Benten D, Fehse B. RGB marking with lentiviral vectors for multicolor clonal cell tracking. *Nat Protoc*. 2012;7(5):839-849. doi:10.1038/nprot.2012.026

44. Weissman TA, Pan YA. Brainbow: New Resources and Emerging Biological Applications for Multicolor Genetic Labeling and Analysis. *Genetics*. 2015;199(2):293-306. doi:10.1534/genetics.114.172510

45. Thomaschewski M, Riecken K, Unrau L, et al. Multi-color RGB marking enables clonality assessment of liver tumors in a murine xenograft model. *Oncotarget*. 2017;8(70):115582-115595. doi:10.18632/oncotarget.23312

46. Weber TS, Dukes M, Miles DC, Glaser SP, Naik SH, Duffy KR. Site-specific recombinatorics: in situ cellular barcoding with the Cre Lox system. *BMC Syst Biol*. 2016;10(1):43. doi:10.1186/s12918-016-0290-3

47. Pei W, Feyerabend TB, Rössler J, et al. Polylox barcoding reveals haematopoietic stem cell fates realized in vivo. *Nature*. 2017;548(7668):456-460. doi:10.1038/nature23653

48. Pei W, Wang X, Rössler J, Feyerabend TB, Höfer T, Rodewald H-R. Using Cre-recombinase-driven Polylox barcoding for in vivo fate mapping in mice. *Nat Protoc*. 2019;14(6):1820-1840. doi:10.1038/s41596-019-0163-5

49. McKenna A, Findlay GM, Gagnon JA, Horwitz MS, Schier AF, Shendure J. Whole-organism lineage tracing by combinatorial and cumulative genome editing. *Science (80-)*. 2016;353(6298):aaf7907. doi:10.1126/science.aaf7907

50. Junker JP, Spanjaard B, Peterson-Maduro J, et al. Massively parallel whole-organism lineage tracing using CRISPR/Cas9 induced genetic scars. *bioRxiv*. January 2016:56499. doi:10.1101/056499

51. Kalhor R, Kalhor K, Mejia L, et al. Developmental barcoding of whole mouse via homing CRISPR. *Science (80-)*. 2018;361(6405):eaat9804. doi:10.1126/science.aat9804

52. Spanjaard B, Hu B, Mitic N, et al. Simultaneous lineage tracing and cell-type identification using CRISPR–Cas9-induced genetic scars. *Nat Biotechnol*. 2018;36(5):469-473. doi:10.1038/nbt.4124

53. Raj B, Gagnon JA, Schier AF. Large-scale reconstruction of cell lineages using single-cell readout of transcriptomes and CRISPR–Cas9 barcodes by scGESTALT. *Nat Protoc*. 2018;13(11):2685-2713. doi:10.1038/s41596-018-0058-x

54. Raj B, Wagner DE, McKenna A, et al. Simultaneous single-cell profiling of lineages and cell types in the vertebrate brain. *Nat Biotechnol*. 2018;36(5):442-450. doi:10.1038/nbt.4103

55. Gerrits A, Dykstra B, Kalmykowa OJ, et al. Cellular barcoding tool for clonal analysis in the hematopoietic system. *Blood*. 2010;115(13):2610-2618. doi:10.1182/blood-2009-06-229757

56. Bystrykh L V. Generalized DNA Barcode Design Based on Hamming Codes. Stanton J-AL, ed. *PLoS One*. 2012;7(5):e36852. doi:10.1371/journal.pone.0036852

57. Bystrykh L V, de Haan G, Verovskaya E. Barcoded Vector Libraries and Retroviral or Lentiviral Barcoding of Hematopoietic Stem Cells. In: Bunting KD, Qu C-K, eds. New York, NY: Springer New York; 2014:345-360. doi:10.1007/978-1-4939-1133-2_23

58. Bystrykh L V, Belderbos ME. Clonal Analysis of Cells with Cellular Barcoding: When Numbers and Sizes Matter. In: Turksen K, ed. *Stem Cell Heterogeneity: Methods and Protocols*. New York, NY: Springer New York; 2016:57-89. doi:10.1007/7651_2016_343

59. Thielecke L, Aranyossy T, Dahl A, et al. Limitations and challenges of genetic barcode quantification. *Sci Rep*. 2017;7(1):43249. doi:10.1038/srep43249

60. Pui C-H, Robison LL, Look AT. Acute lymphoblastic leukaemia. *Lancet*. 2008;371(9617):1030-1043. doi:10.1016/S0140-6736(08)60457-2

61. Bhojwani D, Yang JJ, Pui C-H. Biology of Childhood Acute Lymphoblastic Leukemia. *Pediatr Clin North Am*. 2015;62(1):47-60. doi:10.1016/j.pcl.2014.09.004

62. Hunger SP, Lu X, Devidas M, et al. Improved Survival for Children and Adolescents With Acute Lymphoblastic Leukemia Between 1990 and 2005: A Report From the Children's Oncology Group. *J Clin Oncol*. 2012;30(14):1663-1669. doi:10.1200/JCO.2011.37.8018

63. Pieters R, de Groot-Kruseman H, Van der Velden V, et al. Successful Therapy Reduction and Intensification for Childhood Acute Lymphoblastic Leukemia Based on Minimal Residual Disease Monitoring: Study ALL10 From the Dutch Childhood Oncology Group. *J Clin Oncol*. 2016;34(22):2591-2601. doi:10.1200/JCO.2015.64.6364

64. Ko RH, Ji L, Barnette P, et al. Outcome of Patients Treated for Relapsed or Refractory Acute Lymphoblastic Leukemia: A Therapeutic Advances in Childhood Leukemia Consortium Study. *J Clin Oncol*. 2010;28(4):648-654. doi:10.1200/JCO.2009.22.2950

65. van den Berg H, de Groot-Kruseman HA, Damen-Korbijn CM, de Bont ESJ., Schouten-van Meeteren AYN, Hoogerbrugge PM. Outcome after first relapse in children with acute lymphoblastic leukemia: A report based on the Dutch Childhood Oncology Group (DCOG) relapse all 98 protocol. *Pediatr Blood Cancer*. 2011;57(2):210-216. doi:10.1002/pbc.22946

66. Bhojwani D, Pui C-H. Relapsed childhood acute lymphoblastic leukaemia. *Lancet Oncol*. 2013;14(6):e205-e217. doi:10.1016/S1470-2045(12)70580-6

67. Mullighan CG, Goorha S, Radtke I, et al. Genome-wide analysis of genetic alterations in acute lymphoblastic leukaemia. *Nature*. 2007;446(7137):758-764. doi:10.1038/nature05690

68. Mullighan CG, Miller CB, Radtke I, et al. BCR–ABL1 lymphoblastic leukaemia is characterized by the deletion of Ikaros. *Nature*. 2008;453(7191):110-114. doi:10.1038/nature06866

69. Yang JJ, Bhojwani D, Yang W, et al. Genome-wide copy number profiling reveals molecular evolution from diagnosis to relapse in childhood acute lymphoblastic leukemia. *Blood*. 2008;112(10):4178-4183. doi:10.1182/blood-2008-06-165027

70. Bardini M, Woll PS, Corral L, et al. Clonal variegation and dynamic competition of leukemia-initiating cells in infant acute lymphoblastic leukemia with MLL rearrangement. *Leukemia*. 2015;29(1):38-50. doi:10.1038/leu.2014.154

71. Li B, Brady SW, Ma X, et al. Therapy-induced mutations drive the genomic landscape of relapsed acute lymphoblastic leukemia. *Blood*. 2020;135(1):41-55. doi:10.1182/blood.2019002220

Chapter 2

Donor-to-donor heterogeneity in
the clonal dynamics of transplanted
human cord blood stem cells in murine
xenografts

Mirjam E. Belderbos, Sabrina Jacobs, Taco K. Koster, Albertina Ausema,
Ellen Weersing, Erik Zwart, Gerald de Haan and Leonid V. Bystrykh

ABSTRACT

Umbilical cord blood (UCB) provides an alternative source of hematopoietic stem cells (HSCs) for allogeneic transplantation. Administration of sufficient donor HSCs is critical to restore recipient hematopoiesis and to maintain long-term polyclonal blood formation. However, due to lack of unique markers, the frequency of HSCs among UCB CD34$^+$ cells is subject of ongoing debate, urging for reproducible strategies for their counting.

Here, we employed cellular barcoding to determine the frequency and clonal dynamics of human UCB HSCs, and to determine how data analysis methods impact on these parameters. We transplanted lentivirally barcoded CD34$^+$ cells from 20 UCB donors into Nod/Scid/IL2Ry-/- (NSG) mice (n=30). Twelve recipients (of 8 UCB donors) engrafted with >1% GFP$^+$ cells, allowing for clonal analysis by multiplexed barcode deep sequencing.

Using multiple definitions of clonal diversity and strategies for data filtering, we demonstrate that differences in data analysis can change clonal counts by several orders of magnitude, and propose methods to improve their consistency. Using these methods, we show that the frequency of NSG-repopulating cells was low (median ~1 HSC/10^4 CD34$^+$ UCB cells) and could vary up to 10-fold between donors. Clonal patterns in blood became increasingly consistent over time, likely reflecting initial output of transient progenitors, followed by long-term HSCs with stable hierarchies. The majority of long-term clones displayed multilineage output, yet clones with lymphoid- or myeloid-biased output were also observed.

Altogether, this study uncovers substantial inter-donor and analysis-induced variability in the frequency of UCB CD34$^+$ clones that contribute to post-transplant hematopoiesis. As clone tracing is increasingly relevant, we urge for universal and transparent methods to count HSC clones, during normal aging and upon transplantation.

INTRODUCTION

Human umbilical cord blood (UCB) is an established source of hematopoietic stem cells (HSC) for allogeneic transplantation of patients with a variety of diseases[1]. Compared to other stem cell sources, UCB has the advantages of being readily available and permitting a higher degree of donor-recipient mismatch[1]. However, its main disadvantage is the limited number of cells that can be obtained from a single UCB unit, which may contribute to an increased risk of non-engraftment, delayed hematopoietic recovery and immune reconstitution[2–5]. Accordingly, HSC content, currently measured as CD34+ cells/kg recipient, is a major criterion used to select the optimal UCB unit for transplantation. However, the CD34+ population is highly heterogeneous, with few cells fulfilling the (functional) definition of a "true" HSC[6–8]. Accordingly, the frequency of HSCs among the CD34+ cell population may vary between different UCB donors, thereby potentially explaining the occurrence of graft failure in patients transplanted with seemingly adequate CD34+ HSC doses. Finally, as (age-related) reduction in the number of HSC clones is associated with various adverse health effects, administration of sufficient HSCs may be favorable on the long-term as well[9–11]. Altogether, to improve the use of UCB in experimental and clinical transplants, insight into the frequency of HSCs among UCB CD34+ cells, their clonal contribution to post-transplant hematopoiesis and the potential variability in these parameters between individual UCB donors is urgently needed.

Due to lack of unambiguous phenotypic markers, stringent definition of an HSC relies on its capacity to self-renew and to produce robust multi-lineage progeny. Various experimental methods have been employed, using limiting-dilution transplantation[12], viral integration sites[13,14], genetic barcodes[15,16], fluorescent markers[17–19], CRISPR-Cas9 genome editing[20], or Cre-*loxP* recombination[21], to trace the clonal outgrowth of HSCs in unperturbed hematopoiesis, or in autologous, syngeneic, or xenogeneic recipients. Using cellular barcodes to count and trace murine LSK48-150+ hematopoietic stem- and progenitor cells (HSPCs) in murine recipients, we previously demonstrated that only a minor fraction of this highly purified population produces clonal offspring, and that their quantitative output and lineage commitment are stable over time[15,22]. Similar results have been obtained by other groups, using transplantation of barcoded murine HSPCs in syngeneic recipients[23,24], autologous transplantation of genome-edited HSPCs in nonhuman primates[25,26], or fluorescent markers to trace native hematopoiesis in zebrafish[17]. Regardless of the exact species or experimental model, these studies unequivocally demonstrate that long-term hematopoiesis is maintained by a rare population of cells, with stable multi-lineage reconstitution over time.

In marked contrast, data on the frequency and lineage commitment of transplanted human HSCs remains scarce and controversial. On the one hand, gene therapy studies estimate that 1 in 10^5-10^6 gene-corrected CD34+ HSPC has the potential to engraft long-term,

and that their lineage commitment is stable for several years after transplantation[14,27]. On the other hand, *in vivo* lineage tracing studies suggest a considerable higher HSC frequency, indicating that 0.2% of barcoded human CD34^{+} UCB cells produce multi-lineage progeny upon xenotransplantation in mice, with variable lineage commitment and with the majority of clones only present at a single time point[16]. In addition to obvious differences in the nature of the recipient (human vs murine) and in the employed method to identify and trace HSC clones, this discrepancy could also be due to differences in analytical methods to assess HSC frequency. Besides, as these studies used autologous transplantation[13,14,28] or pooled CD34^{+} cells from >100 donors[16], the inter-donor heterogeneity in HSC frequency and lineage commitment remain unknown, yet highly relevant for optimization of HSC transplantation (HSCT) and donor selection protocols.

Here, we have exploited quantitative, high-throughput barcoding technology to characterize the frequency and lineage commitment of CD34^{+} cells from 8 individual human UCB donors, and to quantify the potential impact of inter-donor and analytical variability on these parameters. We show that the frequency of Nod-SCID-IL2Ry^{-/-} (NSG)-repopulating cells and their lineage contributions differ substantially between human UCB donors, stressing the importance of accurate quantification of graft HSC content. Moreover, we demonstrate that estimates of HSC clone numbers in the same sample can vary several orders of magnitude, depending on the used method of analysis, and we provide guidelines to select the optimal analytical method. Altogether, our findings partially explain some of the discrepancies in HSC frequency in previous studies, and urge for uniform and transparent data analysis methods to count HSC clones during normal ageing and upon transplantation.

METHODS

Data sharing statement

We adhere to the recent consensus of the StemCellMathLab for utility and reproducibility of clonal tracking studies[29]. Accordingly, data tables containing all raw barcode data included in this study are publicly available through the online repository (Table S1).

Barcode library

The barcode library used for the current studies was described in detail previously[30,31]. Briefly, we cloned synthetic random barcode sequences with two similar backbones AG-GNNNACNNNGTNNNCGNNNTANNNCANNNTGNNNGAC or GAANNNACNNNGTNNNC-GNNNTANNNCANNNTAAGGACG in the modified pGIPZ lentiviral vector, and collected over 800 individual DNA-preps and *E. coli* stocks[30,31]. These preps were then pooled at equimolar concentrations to generate the 800-barcode libraries used to transduce target

cells, with conventional lentiviral transduction protocols with p8.91 CMV and VSV-G viral plasmids[32].

Cord blood CD34$^+$ cell isolation, transduction and xenotransplantation

UCB was collected from 20 individual donors, directly after uncomplicated vaginal delivery, using citrate phosphate dextrose-containing collection bags (MacoPharma, Utrecht, NL), according to procedures approved by the Medical Ethical Committee of the University of Groningen. CD34$^+$ HSPC were isolated within 24 hours after birth by Ficoll gradient centrifugation (Sigma Aldrich, Zwijndrecht, NL), and subsequent positive selection using CD34-magnetic beads (Miltenyi, Leiden, NL). Two types of culture medium were used to maintain UCB-derived CD34$^+$ HSPC throughout the transduction procedure: StemSpan supplemented with recombinant human thrombopoietin (rhTPO, 100 ng/mL, Preprotech, London, United Kingdom), stem cell factor (100 ng/mL, R&D systems, Minneapolis, MN) and FLT3-ligand (100 ng/mL, R&D Systems, UCB donor 1-3); or StemSpan supplemented with rhSCF (10 ng/mL), rhTPO (20 ng/mL), mIGF-2 (20 ng/mL, R&D systems) and rhFGF (10 ng/mL, Preprotech, UCB donor 4-20). The type of medium did not impact significantly on the kinetics of engraftment or on the number of HSC clones (data not shown). UCB CD34$^+$ HSPC were transduced with the lentiviral barcode library for 24h *in vitro*, after which the cells were washed and cultured for another 24h. After a total duration of 48h, cells were counted using trypan blue, and transduction efficiency was assessed by flow cytometry for GFP. Cells were subsequently transplanted in bulk in sublethally irradiated NSG mice (n=30, 1-2 Gy) with a minimum dose of 1.0×10^5 CD34$^+$GFP$^+$ cells/recipient.

Detection of human blood cells in murine xenografts

Human chimerism and lineage differentiation were monitored in mouse blood at selected time points after transplantation, and in bone marrow and spleen at sacrifice. Single-cell suspensions were prepared as described previously[15,30]. Differential blood counts were performed on a Medonic CA620 Hematology Analyzer (Boule Medical AB, Spanga, Sweden). Flow cytometry was used to identify human B-cells (hCD45$^+$hCD19$^+$), T-cells (hCD45$^+$hCD3$^+$) and granulocytes (FSC/SSC high, hCD45$^+$hCD16$^+$) and presence of the barcode vector (GFP$^+$). Engraftment for each lineage was defined as ≥1% fluorophore-positive cells among total live PMBC[32]. Lineage-sorted cell fractions were obtained using a MoFlo flow cytometer (Beckman Coulter, Woerden, Netherlands), employing the same markers as for flow cytometry.

DNA isolation and barcode sequencing

Genomic DNA was isolated from unsorted cells and sorted cell populations (table S1) using the DNeasy Blood&Tissue Kit (Qiagen, Venlo, The Netherlands), according to the

manufacturer's instructions. For samples with low cell numbers (blood), the DNA micro kit was used (Qiagen). Barcode sequences were amplified in a 35-cycle PCR reaction using primers for the flanking EGFP (forward) and WPRE (reverse) sites, and sequenced in multiplex format on an Illumina HiSEQ 2500 Platform (BaseClear, Leiden, Netherlands), as described previously[30,31].

Data analysis

Barcode sequence extraction, noise filtering and data processing were performed as previously described[30,31]. Briefly, all unique sequences were first collapsed with the script provided on Github (https://github.com/erikzwart/collapse-multiplex-barcodes). Subsequently, unique sequences were demultiplexed by primer tag and split among experiments. Barcode sequences were extracted using custom scripts searching for the barcode backbone motif. Highly similar barcodes were merged using a Hamming distance threshold of ≥1. The resulting list of barcode reads per sample was grouped in tables per experiment. All these tables are available in the supplementary files. Consistency in barcode patterns was expressed as Spearman correlation. Differences between groups were calculated using the Mann-Whitney U-test for non-normally distributed variables (e.g. consistency in barcode patterns over time), or the Student's T-test for normally distributed variables. Paired measurements (e.g. the number of barcodes in blood versus bone marrow) were compared using the Wilcoxon signed rank test.

Definitions and calculation of barcode diversity

We used and compared different parameters to assess the diversity of the retrieved barcodes. The first and most simple is *nominal count*, being the number of different barcodes in a given sample.

Second, the *Shannon count* (Sh count) is derived from population dynamics, and takes into account both the number of barcodes as well as their relative abundance. The Shannon count for a given sample is determined by first calculating the *Shannon index* (H):

$$H = - \sum_{j=i}^{s} p_i \ln(p_i)$$

Where s is the total number of observed barcodes in a given sample, and p is the proportion of reads belonging to the ith barcode in the sample. The Shannon index is subsequently converted to the Shannon count:

$Sh_{count} = e^{H}$

When all barcodes in a sample are equally distributed, the nominal count and Shannon count are equal, whereas skewed barcode distributions will result in a lower Shannon count (also minimizing its sensitivity to PCR noise)[31].

Third, we calculated several commonly used predictors of population diversity: the Abundance-based Coverage Estimate (ACE), the Chao2 estimator and the Goods completeness coefficient[33,34]. These parameters generally predict total population diversity based on the number of distinct measurements in a given sample, correcting for a certain degree of unseen diversity. For example, the *Chao estimators* are commonly used in ecology and sporadically in gene therapy studies, when it is assumed that only a fraction of the total body "true" clonal diversity is captured in a (blood/bone marrow) sample[34–36]. Chao1 is calculated as:

$$S_1 = S_{obs} + \frac{F_1^2}{2F_2}$$

Where S_{obs} is the number of species/barcodes, F_1 is the number of singletons and F_2 is the number of doubletons. Because read frequencies cannot be interpreted in terms of single- or double detection of species, we used the Chao2 index, which is conceptually similar to Chao1, but defines single- and doubletons as species/barcodes present only in one or two samples. All other predictors were defined and calculated using the python scikit-diversity-alpha package (http://scikit-bio.org/docs/0.5.1/generated/skbio.diversity.alpha.html).

RESULTS

Barcoded human cord blood CD34+ cells produce multi-lineage progeny in murine xenografts

We set out to quantify the frequency of HSC and their lineage contribution among different UCB donors. CD34+ cells from 20 individual UCB donors were subjected to lentiviral barcoding and transplanted into a total of 30 NSG mice, at a minimum dose of 1.0×10^5 CD34+GFP+ cells/recipient (figure 1A, table 1). In total, 29 recipients engrafted, defined as ≥1% human CD45+ cells in peripheral blood, at a median interval of 6 weeks (range 4-36) after transplant (Figure 1B-C, table 1). Of these, 12 recipients (of 8 UCB donors) had sufficient GFP+ cells for barcode analysis (table 1). The kinetics of engraftment varied between leukocyte subtypes: B-cells were the most abundant and first to appear at a median time of 10 weeks after transplant (range 4-36), followed by T-cells (10 weeks, range 8-42) and myeloid cells (10 weeks, range 9-42, figure 1D). Ten (34%) mice did not have any human T-cell engraftment and 13 (45%) did not have granulocyte engraftment. The interval until human cell engraftment tended to shorten with increasing CD34+ cell dose, yet this was not significant (Spearman ρ=-0.25, p=0.20, figure 1E).
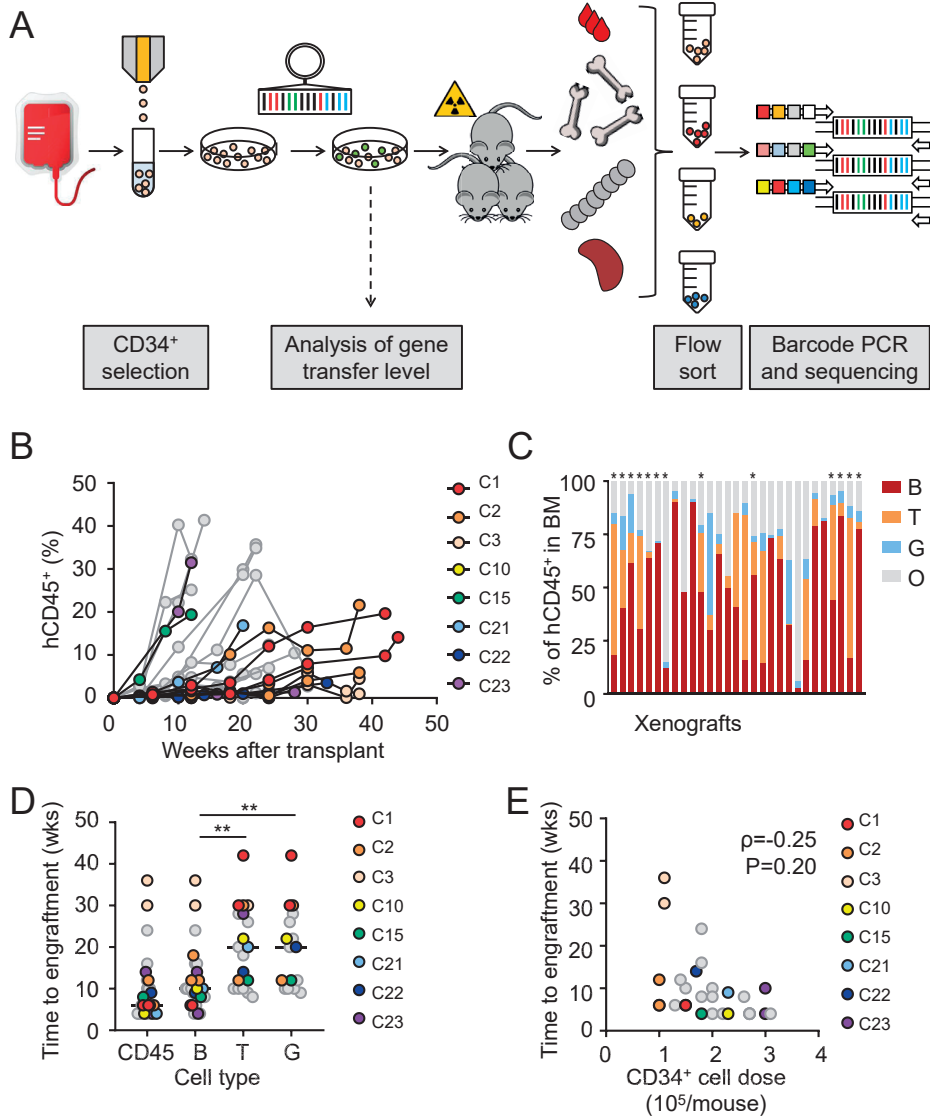
Figure 1. Engraftment and multilineage differentiation of human UCB CD34⁺ cells in murine xenografts

(A) Experimental design. Human cord blood CD34⁺ cells from 20 individual donors were isolated by positive selection using CD34 magnetic beads, followed by lentiviral cellular barcode transduction as previously described[30]. Transduction efficiency was determined by flow cytometry, after which cells were transplanted into sublethally irradiated NSG mice (n=30) at a minimum dose of 1×10^5 GFP⁺ cells per recipient. Human chimerism and lineage differentiation were monitored by flow cytometry in blood throughout the experiment, and in blood, bone marrow and spleen at termination. Unsorted samples and lineage-sorted cell populations were subjected to barcode polymerase chain reaction (PCR), deep sequencing and data processing as described previously[30,31]. (B) Frequency of human CD45⁺ cells (of total live PBMC) in the peripheral blood of mice over time. Connected

dots represent one xenograft. Colors are used to depict mice engrafted with sufficient GFP$^+$-cells for clone tracking using barcode analysis, as described in figures 2-4. (C) Lineage commitment of human HSCs in bone marrow of murine xenografts. Each bar represents one mouse. Asterisks depict mice with sufficient GFP$^+$ cells for barcode analysis. (D) Time to engraftment of human CD45$^+$ cells, human B-cells (CD45$^+$/CD19$^+$), human T-cells (CD45$^+$/CD3$^+$) and human granulocytes (CD45$^+$CD16$^+$). Engraftment was defined as levels above 1% of live PBMC, which is the threshold for detection by flow cytometry. Each dot represents one xenograft. Colored dots represent xenografts with GFP$^+$ engraftment, and correspond to the data in panel 1C. (E) Time to human CD45$^+$ cell engraftment as a function of transplanted CD34$^+$ cell dose. Abbreviations: B; B-cells; T; T-cells; G; granulocytes; O; other, defined as CD45$^+$CD19$^-$CD3$^-$CD16$^-$.

Table 1. Overview of cord blood samples.

| Donor	Barcoding efficiency (%)	Total cell dose/ mouse (10^6)	GFP$^+$ cell dose/ mouse (10^6)	No. of mice transplanted	No. of mice engrafted (≥1% hCD45)	No. of mice with GFP$^+$ engraftment (≥1% GFP$^+$)	Lineage engraftment (≥1% of hCD45$^+$)
1	40	0.38	0.15	2	2	2	B, T, G
2	18	.50	0.10	3	3	3	B, T, G
3	30	.37	0.11	2	2	2	B, G
6	10	1.4	0.13	1	1	0	B
8	14	1.00	0.14	1	1	1*	B, G
9	11	1.36	0.15	1	1	0	B, T, G
10	7	2.89	0.23	1	1	1	B, T, G
11	8	2.86	0.22	1	1	1*	B, T, G
12	18	1.00	0.18	2	2	1*	B, T, G
13	21	0.86	0.18	1	1	0	B
14	12	2.07	0.26	1	1	0	B, T, G
15	18	1.00	0.18	1	1	1	B, G
16	13	.210	0.27	2	2	0	B, T, G
17	21	.95	0.20	2	1	0	B, T, G
18	16	1.70	0.27	2	2	0	B, T, G
19	53	0.59	0.31	1	1	0	B, T, G
20	25	0.80	0.20	2	2	0	B, G
21	65	0.35	0.23	1	1	1	B, T, G
22	81	0.21	0.17	1	1	1	B, G
23	29	1.05	0.30	2	2	1	B, T, G

Overall, 12 mice (from 8 different donors) provided enough material for reliable barcode deep sequencing. These mice are depicted in bold and were used for the rest of the story. * ≥1% GFP positive cells in bone marrow, but insufficient barcode retrieval by deep sequencing.

Definitions of clonal diversity impact several orders of magnitude on the number of retrieved clones

Previous studies aimed at counting HSC clones used different definitions of clonal diversity, barcode libraries of varying (known/unknown) sizes, and various analytical methods for data filtering and barcode retrieval[16,17,27,29,36]. To reliably quantify the number of clones in our data, we first assessed the impact of these analytical differences on the number of retrieved HSPC.

We observed that the log2-transformed barcode distributions in the barcode library (figure 2A) and in UCB CD34^{+} cells prior to transplantation (figure 2B) were close to normal, reflecting the presence of multiple clones without clonal selection. In contrast, barcode distributions in samples from UCB xenografts showed skewed/bimodal barcode distribution, with a few high-frequency barcodes and many low-frequency reads (representative example in figure 2C). The first category, high frequency barcodes, likely contains true clones that survived evolutionary selection, whereas the low-frequency reads will reflect small clones as well as sequencing artefacts. To assess the impact of this distribution on clonal counts, we calculated the number of barcodes in each xenograft, using different definitions of clonal diversity and different thresholds for data filtering. Using nominal counts and unfiltered sequencing results, we found a median of 235 barcodes per xenograft, which were reduced several-fold when data were filtered using increasingly stringent criteria (figure 2D). In marked contrast, the Shannon count, which incorporates both the number of unique barcodes and their relative abundance, provided a ten-fold lower barcode number, which remained stable across data filtering steps (figure 2E). To reconcile this apparent paradox, we calculated the clonal diversity in all experiments using different filtering thresholds and estimates of clonal diversity, and compared the results with the size of the 800-barcode library (supplementary figure S6 and figure 2F). Theoretically, the cumulative number of barcodes in any experiment should rise asymptotically with repetitive sampling, and cannot exceed the size of the library. As expected, the nominal barcode count was always equal to the (arbitrarily defined) filtering threshold (i.e. when the top 200 barcodes are filtered, the nominal barcode count is 200). Remarkably, the ACE and Chao2 estimators, which predict clonal diversity based on the observed number of barcodes and a certain degree of unseen diversity, reported clonal diversities that were several-fold higher, grew steadily (instead of asymptotically) upon repetitive sampling, and exceeded the size of the library several-fold, likely reflecting their sensitivity to noise. In contrast, the Shannon count reported barcode frequencies that were several-fold lower, remained below the library-threshold and remained stable throughout data-filtering steps, reflecting its ability to reliably detect major barcode clones. Altogether, this shows that definitions of clonal diversity and thresholds for data filtering can affect clone counts by several-folds magnitude, with the Shannon count being the most consistent, least sensitive to sequencing noise and thus

the preferred method. Overall, these findings demonstrate that detailed description of the used data filtering protocols and methods for clone counting is crucial to assess and compare clonal counts within and across studies.
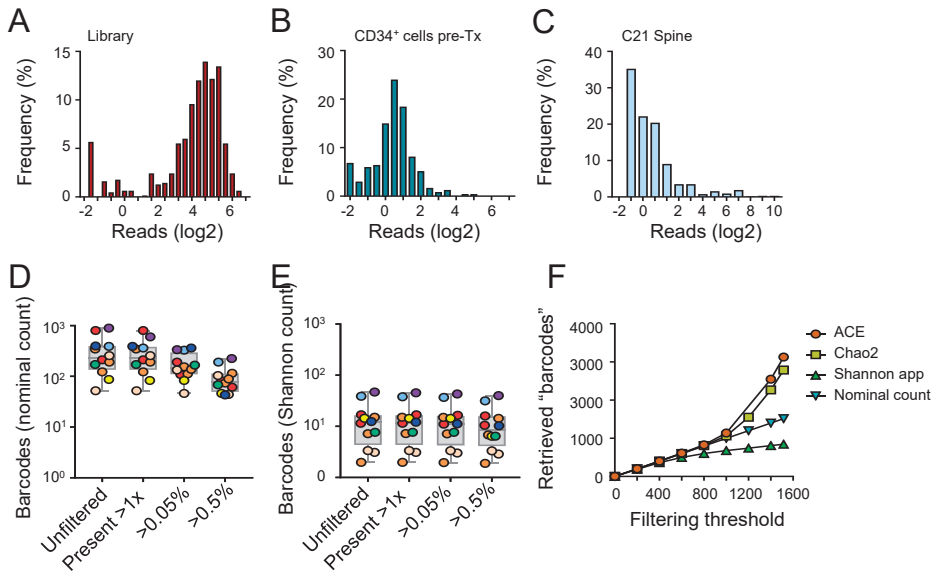

Figure 2. Impact of data analysis methods on quantification of HSPC clone numbers
(A-C) Histograms depicting barcode distribution in: (A) the barcode library prior to target cell transduction; (B) transduced CD34$^+$ cells prior to transplantation; (C); a representative example of an *in vivo* sample from a barcoded CD34$^+$ UCB xenograft. (D) Impact of data filtering on the number of retrieved HSPC clones, assessed by nominal counts. Each dot represents bone marrow of an individual UCB xenograft, colors correspond to colors in figure 1. (E) HSPC clone numbers in the same dataset as panel D, but now using the Shannon count to quantify clonal diversity. (F) Estimated barcode frequencies, using different data filtering thresholds and estimators of diversity (for more detailed information, see figure S1).

Inter-donor variability in HSPC frequency among cord blood CD34$^+$ cells

We subsequently used the preferred barcode method to determine the frequency of HSPCs among UCB CD34$^+$ cells. Hereto, we longitudinally traced the barcode patterns in blood and bone marrow of GFP$^+$ engrafted mice (n=12 recipients of 8 donors) for up to 10 months after transplantation (table 1). GFP-levels in bone marrow varied between recipients, and were unrelated to administered cell dose or to pre-transplant transduction efficiency (figure S2). Analysis of barcode patterns in longitudinally obtained blood samples identified tens to hundreds of barcodes at each individual time point (figure 3A-B). Early after transplantation clone numbers were more variable, and generally stabilized within 16-20 weeks after transplantation (figure 3B). At sacrifice, we observed a median of 12.7 (range 4 to 167, Shannon count) clones in blood, and 15.0 (range 2 to 43) in bone marrow.
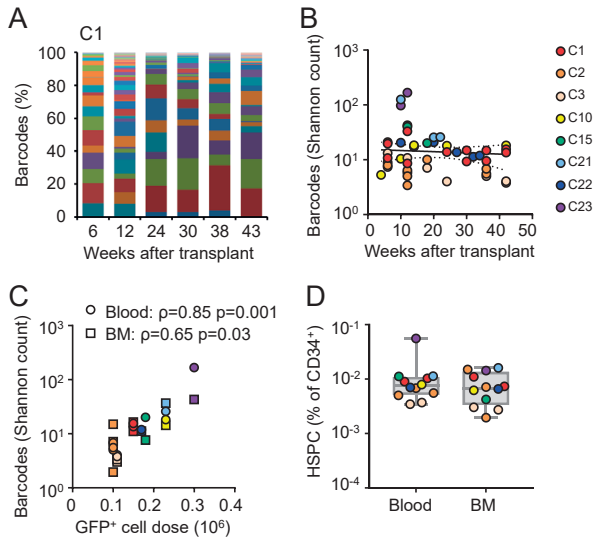
Figure 3. Frequency and inter-donor variability of HSPC among UCB CD34$^+$ cells revealed by cellular barcodes

Barcode composition in longitudinally obtained blood samples of a representative mouse. Each color represents an individual barcode. (B) Summary of clonal diversity in blood of twelve xenografts transplanted with eight individual UCB donors. Xenografts transplanted from the same donor are indicated with similar colors. (C) Correlation between GFP$^+$ CD34$^+$ cell dose and the number of barcodes in blood (circles) and bone marrow (squares) of murine xenografts. (D) Summary of HSPC frequency, calculated by dividing the number of clones in blood or BM (Shannon count), by the transplanted GFP$^+$ cell dose.

The numbers of clones in blood and bone marrow of individual recipient were highly similar, and correlated with barcoded CD34$^+$ cell dose (figure 3C). Relating the number of retrieved barcodes to the administered GFP$^+$CD34$^+$ cell dose, we found that a median of 0.007% (range 0.002-0.056) of CD34$^+$ cells produced long-term clonal progeny in our model, and that clonogenic-cell frequency could vary up to 10-fold between UCB donors (figure 3D). Notably, a higher number of clones was not significantly associated with faster donor engraftment, but did correlate with increased levels of human GFP$^+$CD45$^+$ cells in bone marrow at sacrifice (ρ=0.68, p=0.02, figure S3). These data indicate that the NSG-repopulating cell frequency in an enriched population of CD34$^+$ UCB cells is very low and can vary up several-fold between donors. Moreover, they suggest that early donor engraftment and long-term hematopoiesis may be mediated by distinct HSPC clones.

Initial engraftment is supported by transient clones and followed by long-term HSPC with stable clonal output

To further characterize the engraftment dynamics of individual HSPC clones, we compared clonal patterns at multiple time intervals (figure 4). Early after transplantation,
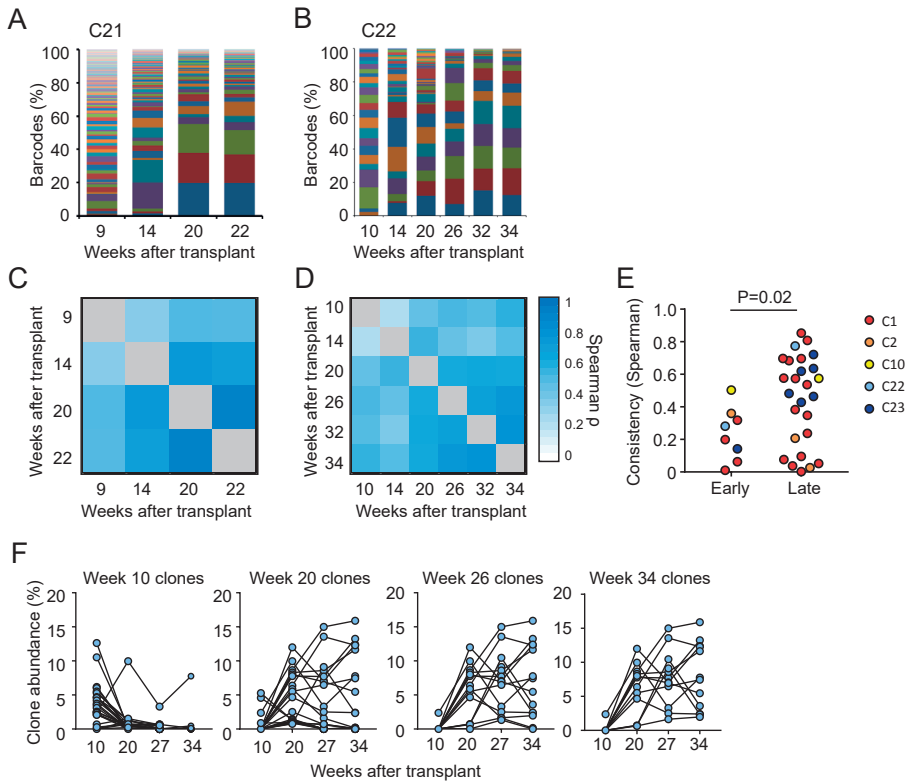
Figure 4. Blood cells are produced by transient clones early after transplantation, followed by hematopoiesis by long-term clones with stable output.
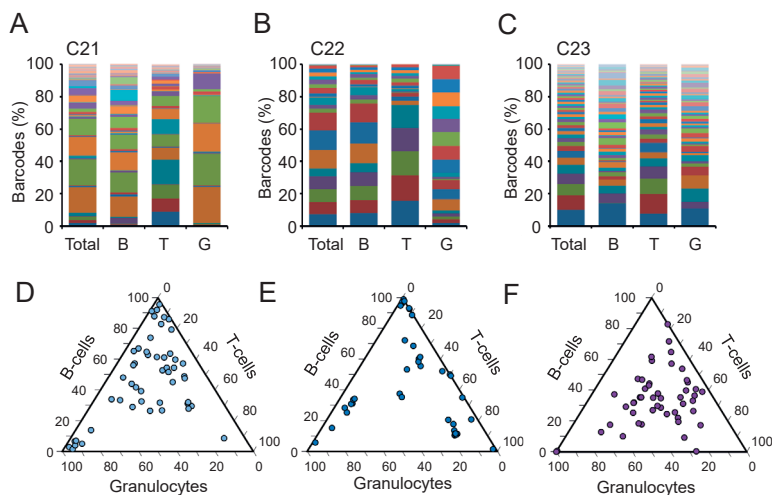(A) and (B): Representative examples of barcode distribution in peripheral blood of individual cord blood CD34+ xenografts. Each bar represents one time point, colors are used to depict different barcodes. (C) and (D); Correlation matrix depicting Spearman correlation between barcode composition (top 100 most abundant clones) in blood drawn at different time points after transplantation. (E) Spearman correlations between blood samples drawn early after transplantation (first half of mouse life) vs those drawn at later time points (second half of mouse life). (F) Longitudinal patterns of clone sizes over time of individual barcode clones in a representative xenografts (C22). For each time point, the most abundant clones (Shannon approximation) are shown.

we found a relatively high number of HSPC clones in blood, many of which were small in size and transient (representative patterns in figure 4A-B, quantification in figure S4). The short-term presence of these early clones was reflected by a relatively low Spearman correlation between barcode patterns in sequentially obtained blood samples at early time points (figure 4C-D). In contrast, at later time points, the number of contributing HSPC clones became smaller and their contribution more consistent, reflected by higher Spearman correlations between barcode patterns at sequential time points (figure 4C-E). Interestingly, the majority of HSPC clones contributing to long-term blood formation were already present (usually as a minor clone) at the earliest time point, yet gradually

grew to become dominant over time (figures 4F and S4B). Altogether, these data demonstrate that hematopoiesis is supported by a relatively high number of transient clones early after transplant, followed by long-term hematopoiesis by a limited number of HSPCs with stable clonal output.

The majority of long-term HSPC clones have multilineage potential

To assess the lineage contribution of these long-term HSPC clones, we compared barcode patterns between sorted human cell populations from bone marrow of xenografts with robust polyclonal multi-lineage engraftment (C21, C22, C23, figure 1c). Although B-cells were the most abundant human cell type in the majority of xenografts, which is a known feature of the NSG-model[16], we were able to isolate sufficient numbers of granulocytes and T-cells for barcode analysis. The majority of HSPC clones had multilineage potential: Of the top 50 most abundant barcodes in each recipient, a median of 72% (range 32-100%) were found in all lineages, with varying abundance (figure 5). Multipotent barcode clones were generally larger than lineage-restricted clones (figure S5), which may reflect a biological feature of multipotent clones, and/or a detection-issue for minor barcodes in smaller samples. Altogether, these data demonstrate that the majority of major long-term NSG-repopulating UCB CD34$^+$ cells have multilineage potential, yet clones with uni- or bilineage potential were also present.

Figure 5. Multilineage engraftment of human HSPCs in murine xenografts.
(A-C): Representative examples of barcode distribution in total bone marrow and in sorted B-cells (CD45$^+$CD19$^+$), T-cells (CD45$^+$CD3$^+$) and granulocytes (CD45$^+$CD16$^+$) of individual cord blood CD34$^+$ xenografts. Each panel represents one mouse, colors are used to depict different barcodes. (D-F) Ternary (triangle) plots of the clonal contribution of individual HSPCs to T-cells, B-cells and granulocytes in bone marrow at termination of the experiments. Each dot within the triangle represents on individual barcode (clone).

DISCUSSION

HSCT is the only routinely used stem cell therapy in humans, which is used in over 30.000 patients annually[37]. Its success relies critically on administration of sufficient numbers of HSCs, which may be a limiting factor, especially when UCB donors are used. Very little is known about the frequency of functional long-term repopulating HSCs in UCB, and how these clones behave over time. Here, we used cellular barcodes to quantitatively trace the clonal behavior of CD34+ HSPC from individual UCB donors upon transplantation in murine xenografts. We demonstrate that only ~0.007% of CD34+ cells enriched from UCB establishes long-term progeny in murine xenografts, and that this frequency can vary several-fold between different donors. Moreover, we found that quantification of clone frequencies is largely dependent on the used definitions of clonal diversity and on the analytical methods for their quantification. Altogether, our findings suggest that functional analyses and/or additional HSC markers are needed to optimize UCB donor donor selection protocols. In addition, as clone-tracing studies are increasingly used to understand age-related clonal hematopoiesis and the evolution of malignancy and relapse, it is of crucial importance to develop transparent and uniform methods for HSC counting to reconcile their results.

Assessment of HSC frequency in human cell populations

In contrast to mice, in which phenotypic markers allow for the isolation and enumeration of HSCs to near-purity[6], evidence regarding the phenotype and frequency of human HSCs remains controversial. Using a functional definition of HSCs and an unbiased, quantitative lineage-tracing method, we demonstrate that 0.007% of UCB CD34+ produces multilineage progeny in NSG mice. Our estimates are consistent with human gene therapy studies, which demonstrate that 0.001-0.01% of gene-corrected CD34+ cells has the potential to engraft long-term[14,28,38]. In marked contrast, a previous barcoding study, which used pooled UCB CD34+ cells from >100 donors, report HSC frequencies several fold higher[16]. This discrepancy may be due to the *in vitro* methods for lentiviral transduction, the use of single versus multiple donors, and/or to differences in the transplantation procedure[39]. In particular, in contrast to this previous study[39], we did not add any CD34- competitor cells to our transplants. Although this has the advantage of preventing experimental variation due to differences in donor immunity between UCB units, the lack of donor T-cells may have compromised the ability of the donor HSCs to engraft the recipient's marrow. In future, co-transplantation experiments, in which barcoded HSCs are administered together with purified CD34-negative cell populations, will be of interest to elucidate the impact of each of these populations on HSC engraftment. Moreover, in addition to these experimental differences, the analytical methods for barcode

retrieval and clone counting differ markedly between these studies, and have significant impact on estimates on clonal diversity, as elaborated below.

Short-term progenitors are followed by long-term multilineage HSCs

Our data are in line with previous clonal tracking studies, identifying two phases of post-transplant hematopoietic reconstitution[14,15,24,25,40]. The first phase is characterized by clonal instability/succession, and likely reflects the output of committed progenitor cells which may be more abundant and proliferative, yet lack the capacity to long-term self-renew. Over time, these clones are replaced by long-term multipotent HSCs, which produce stable clonal offspring for several months after transplantation. Retrospectively, we were able to detect many of these long-term clones at minor frequencies at early time points, confirming their relative quiescence compared to short-lived progenitors. The majority of long-term clones produced all blood lineages, yet clones with uni- or bi-lineage contribution were also found. Accordingly, the absence of granulocyte- or T-cell engraftment in some recipients may be due to lack of true multi-lineage HSCs in the graft, which may be at limiting dilution. Insight into the fundamental properties of each of these progenitor cell populations is of great interest, biologically as well as for therapeutic purposes. Can we identify phenotypic or functional markers that discriminate long-term HSCs from transient progenitors? What are the mechanisms that guide HSC self-renewal and differentiation? How does transplantation impact on HSC mutagenesis, clonal fitness and age-related clonal hematopoiesis? In future, integrated approaches, combining genetic lineage tracing with single-cell transcriptomics[41], will provide detailed characterization of the developmental and functional properties of single human HSCs. This will contribute to better understanding of human HSC biology, and may identify novel targets for increasing the number of HSCs and/or to improve their long-term contribution to hematopoiesis.

Impact of data analysis methods on the number of retrieved clones

The large variation in reported HSPC frequencies in our study and in other clonal tracing studies in mice and men[6,8,14–16], triggered us to investigate the impact of data analysis on the number of retrieved clones. Using multiple parameters of clonal diversity on the same (filtered and unfiltered) datasets, we demonstrate that methodological differences can cause several-fold difference in the number of reported clones. Of all used parameters for clonal diversity, the Shannon count was most reproducible and least sensitive to (arbitrary) data filtering decisions. However, most current studies, both in mice and humans, report nominal counts, either/not with correction for unseen diversity[14,16,35,36,42]. Depending on the robustness of the barcode signal and methods of data filtering, these studies may dramatically overestimate true clonal diversity. Accordingly, detailed information on sample preparation and data processing (e.g. transplantation parameters,

barcode calling, thresholds for noise filtering, estimators for clonal diversity) is essential for independent data interpretation, yet this is often difficult to find. To enhance reproducibility and cross-study comparisons, guidelines for uniform and transparent reporting of data-analysis decisions have recently been published[29].

To search the unknown: The impact of library size

One factor that can greatly facilitate the reliability barcode retrieval and noise filtering, is to use a library of known complexity. Using our 800-barcode library of known content, we were able to assess commonly used strategies for data filtering and to validate the reliability of the retrieved barcodes. Importantly, we demonstrated that any overestimation of the library size greatly increases the number of false-positive barcode calls, with diversity estimates sometimes exceeding the size of the library by several-fold. Knowledge of the size of the library can thus improve data filtering significantly. However, especially for larger libraries, quantifying its exact size is not trivial, as this often relies on sequencing of (part of) the library, which is subject to the same technical artefacts as described above. Here, we provide an alternative, more error-proof method of library size prediction. Using the cumulative number of unique barcodes in sequentially added samples, we observed an asymptotic increase in overall barcode diversity, which ultimately approached the size of the library. Therefore, multiple samples and/or repeated sequencing of the same samples may allow for more accurate estimation of the library size and improved data filtering methods.

This study provides the first quantitative assessment of inter-donor variation in clonogenic cell frequencies among CD34^{+} cells from different UCB donors. Our findings may (in part) explain the occurrence of non-engraftment in HSCT recipients transplanted with adequate CD34^{+} cell doses. Notably, as we only assessed a limited number of donors, true inter-donor variability in UCB HSC frequency, and its consequences for clinical/experimental transplants, may be even larger, However, we realize that the lentiviral transduction and xenograft model may significantly impact on our assessments on HSC frequency and function. In the future, innovative methods that allow for the tracing of unmanipulated HSCs in human recipients[43–45] will be needed to validate our findings. Ultimately, these studies will provide unprecedented insights into the clonal behavior of single human HSCs, which may allow for novel strategies to optimize their use in clinical HSCT and gene therapy protocols.

ACKNOWLEDGMENTS

expert assistance in cell sorting; H. Schepers for assistance in the barcode transduction procedure, and R. van Os for valuable discussions.

AUTHORSHIP AND CONFLICT-OF-INTEREST STATEMENTS

FINANCIAL DISCLOSURE STATEMENT

REFERENCES

1. Ballen KK, Gluckman E, Broxmeyer HE. Umbilical cord blood transplantation: the first 25 years and beyond. *Blood*. 2013;122(4):491–498.

2. Wagner JE, Barker JN, DeFor TE, et al. Transplantation of unrelated donor umbilical cord blood in 102 patients with malignant and nonmalignant diseases: influence of CD34 cell dose and HLA disparity on treatment-related mortality and survival. *Blood*. 2002;100(5):1611–1618.

3. Barker JN, Davies SM, DeFor T, et al. Survival after transplantation of unrelated donor umbilical cord blood is comparable to that of human leukocyte antigen-matched unrelated donor bone marrow: Results of a matched-pair analysis. *Blood*. 2001;97(10):2957–2961.

4. Laughlin MJ, Eapen M, Rubinstein P, et al. Outcomes after Transplantation of Cord Blood or Bone Marrow from Unrelated Donors in Adults with Leukemia. *N. Engl. J. Med.* 2004;35122:.

5. Eapen M, Rocha V, Sanz G, et al. Effect of graft source on unrelated donor haemopoietic stem-cell transplantation in adults with acute leukaemia: a retrospective analysis. *Lancet Oncol.* 2010;11(7):653–660.

6. Notta F, Doulatov S, Laurenti E, et al. Isolation of single human hematopoietic stem cells capable of long-term multilineage engraftment. *Science*. 2011;333(6039):218–221.

7. Majeti R, Park CY, Weissman IL. Identification of a hierarchy of multipotent hematopoietic progenitors in human cord blood. *Cell Stem Cell*. 2007;1(6):635–45.

8. Park CY, Majeti R, Weissman IL. In vivo evaluation of human hematopoiesis through xeno-transplantation of purified hematopoietic stem cells from umbilical cord blood. *Nat. Protoc.* 2008;3(12):1932–1940.

9. Steensma DP, Bejar R, Jaiswal S, et al. Clonal hematopoiesis of indeterminate potential and its distinction from myelodysplastic syndromes. *Blood*. 2015;126(1):9–16.

10. Jaiswal S, Natarajan P, Silver AJ, et al. Clonal Hematopoiesis and Risk of Atherosclerotic Cardiovascular Disease. *N. Engl. J. Med.* 2017;377(2):111–121.

11. Jaiswal S, Fontanillas P, Flannick J, et al. Age-Related Clonal Hematopoiesis Associated with Adverse Outcomes. *N. Engl. J. Med.* 2014;371(26):2488–2498.

12. Sieburg HB, Cho RH, Dykstra B, et al. The hematopoietic stem compartment consists of a limited number of discrete stem cell subsets. *Blood*. 2006;107(6):2311–2316.

13. Boztug K, Schmidt M, Schwarzer A, et al. Stem-Cell Gene Therapy for the Wiskott–Aldrich Syndrome. *N. Engl. J. Med.* 2010;363(20):1918–1927.

14. Biasco L, Pellin D, Scala S, et al. In Vivo Tracking of Human Hematopoiesis Reveals Patterns of Clonal Dynamics during Early and Steady-State Reconstitution Phases. *Cell Stem Cell*. 2016;19(1):107–119.

15. Gerrits A, Dykstra B, Kalmykowa OJ, et al. Cellular barcoding tool for clonal analysis in the hematopoietic system. *Blood*. 2010;115(13):2610–2618.

16. Cheung AMS, Nguyen L V, Carles A, et al. Analysis of the clonal growth and differentiation dynamics of primitive barcoded human cord blood cells in NSG mice. *Blood*. 2013;122(18):3129–37.

17. Henninger J, Santoso B, Hans S, et al. Clonal fate mapping quantifies the number of haematopoietic stem cells that arise during development. *Nat. Cell Biol.* 2017;19(1):17–27.

18. Yu VWC, Yusuf RZ, Oki T, et al. Epigenetic Memory Underlies Cell-Autonomous Heterogeneous Behavior of Hematopoietic Stem Cells. *Cell*. 2016;167(5):1310–1322.e17.

19. Sykes SM, Scadden DT. Modeling Human Hematopoietic Stem Cell Biology in the Mouse. *Semin. Hematol.* 2013;50(2):92–100.

20. McKenna A, Findlay GM, Gagnon JA, et al. Whole-organism lineage tracing by combinatorial and cumulative genome editing. *Science (80-.)*. 2016;353(6298):aaf7907.

21. Pei W, Feyerabend TB, Rössler J, et al. Polylox barcoding reveals haematopoietic stem cell fates realized in vivo. *Nature*. 2017;548(7668):456–460.

22. Verovskaya E, Broekhuis MJC, Zwart E, et al. Heterogeneity of young and aged murine hematopoietic stem cells revealed by quantitative clonal analysis using cellular barcoding. *Blood*. 2013;122(4):523–32.

23. Lu R, Neff NF, Quake SR, Weissman IL. Tracking single hematopoietic stem cells in vivo using high-throughput sequencing in conjunction with viral genetic barcoding. *Nat. Biotechnol.* 2011;29(10):928–33.

24. Naik SH, Perié L, Swart E, et al. Diverse and heritable lineage imprinting of early haematopoietic progenitors. *Nature*. 2013;496(7444):229–232.

25. Wu C, Espinoza DA, Koelle SJ, et al. Geographic Clonal Tracking in Macaques Provides Insights into HSPC Migration and Differentiation. *J. Exp. Med.* 2017;215(1):217–232.

26. Wu C, Li B, Lu R, et al. Clonal tracking of rhesus macaque hematopoiesis highlights a distinct lineage origin for natural killer cells. *Cell Stem Cell*. 2014;14(4):486–99.

27. Aiuti A, Biasco L, Scaramuzza S, et al. Lentiviral Hematopoietic Stem Cell Gene Therapy in Patients with Wiskott-Aldrich Syndrome. *Science*. 2013;

28. Aiuti A, Slavin S, Aker M, et al. Correction of ADA-SCID by stem cell gene therapy combined with nonmyeloablative conditioning. *Science*. 2002;296(5577):2410–2413.

29. Lyne A-M, Kent DG, Laurenti E, et al. A track of the clones: new developments in cellular barcoding. *Exp. Hematol.* 2018;68:15–20.

30. Belderbos ME, Koster T, Ausema B, et al. Clonal selection and asymmetric distribution of human leukemia in murine xenografts revealed by cellular barcoding. *Blood*. 2017;129(24):3210–3220.

31. Bystrykh L V, Belderbos ME. Clonal Analysis of Cells with Cellular Barcoding: When Numbers and Sizes Matter. *Methods Mol. Biol.* 2016;

32. Radtke S, Adair JE, Giese MA, et al. A distinct hematopoietic stem cell population for rapid multilineage engraftment in nonhuman primates. *Sci. Transl. Med.* 2017;9(414):eaan1145.

33. Chao A, Colwell RK, Lin C-W, Gotelli NJ. Sufficient sampling for asymptotic minimum species richness estimators. *Ecology*. 2009;90(4):1125–33.

34. Chao A, Bunge J. Estimating the number of species in a stochastic abundance model. *Biometrics*. 2002;58(3):531–9.

35. De Ravin SS, Wu X, Moir S, et al. Lentiviral hematopoietic stem cell gene therapy for X-linked severe combined immunodeficiency. *Sci. Transl. Med.* 2016;8(335):335ra57.

36. Cooper AR, Lill GR, Shaw K, et al. Cytoreductive conditioning intensity predicts clonal diversity in ADA-SCID retroviral gene therapy patients. *Blood*. 2017;129(19):2624–2635.

37. Li HW, Sykes M. Emerging concepts in haematopoietic cell transplantation. *Nat. Rev. Immunol.* 2012;12(6):403–16.

38. Boitano AE, Wang J, Romeo R, et al. Aryl Hydrocarbon Receptor Antagonists Promote the Expansion of Human Hematopoietic Stem Cells. *Science (80-.)*. 2010;329(5997):1345–1348.

39. Nguyen L V., Pellacani D, Lefort S, et al. Barcoding reveals complex clonal dynamics of de novo transformed human mammary cells. *Nature*. 2015;

40. Dykstra B, Olthof S, Schreuder J, Ritsema M, de Haan G. Clonal analysis reveals multiple functional defects of aged murine hematopoietic stem cells. *J. Exp. Med.* 2011;208(13):2691–2703.

41. Kester L, Van Oudenaarden A. Cell Stem Cell Review Single-Cell Transcriptomics Meets Lineage Tracing. *Stem Cell*. 2018;23:166–179.

42. Ott MG, Schmidt M, Schwarzwaelder K, et al. Correction of X-linked chronic granulomatous disease by gene therapy, augmented by insertional activation of MDS1-EVI1, PRDM16 or SETBP1. *Nat. Med.* 2006;12(4):401–409.

43. Alemany A, Florescu M, Baron CS, Peterson-Maduro J, van Oudenaarden A. Whole-organism clone tracing using single-cell sequencing. *Nature*. 2018;556(7699):108–112.

44. Osorio FG, Rosendahl Huber A, Oka R, et al. Somatic Mutations Reveal Lineage Relationships and Age-Related Mutagenesis in Human Hematopoiesis. *Cell Rep.* 2018;25(9):2308–2316.e4.

45. Behjati S, Huch M, van Boxtel R, et al. Genome sequencing of normal cells reveals developmental lineages and mutational processes. *Nature*. 2014;513(7518):422–5.

SUPPLEMENTARY INFORMATION
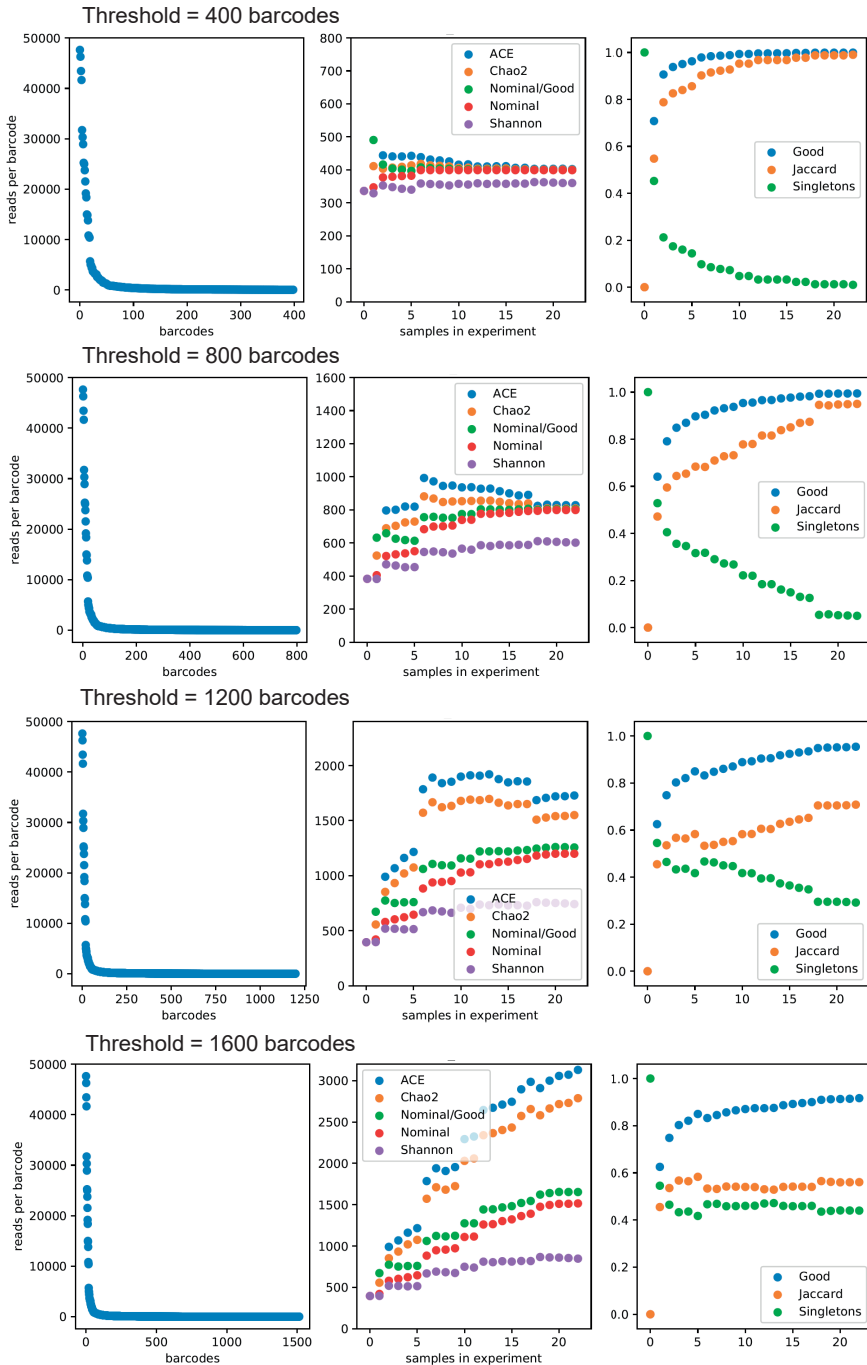
← **Figure S1. Impact of clone definitions and filtering threshold on the number of retrieved barcodes.** Data from recipient C21, using different thresholds for data filtering (top to bottom). Left panels: Cumulative barcodes in the experiment, ranked based on their overall abundance. Middle panels: estimates on clonal diversity, using multiple-samples and different parameters of diversity. Up until a threshold of 800 (the actual library size), estimates on clonal diversity are quite similar. In contrast, increasing the threshold above library size results in large discrepancy in clone counts, likely reflecting false-barcode calls based on sequencing noise.
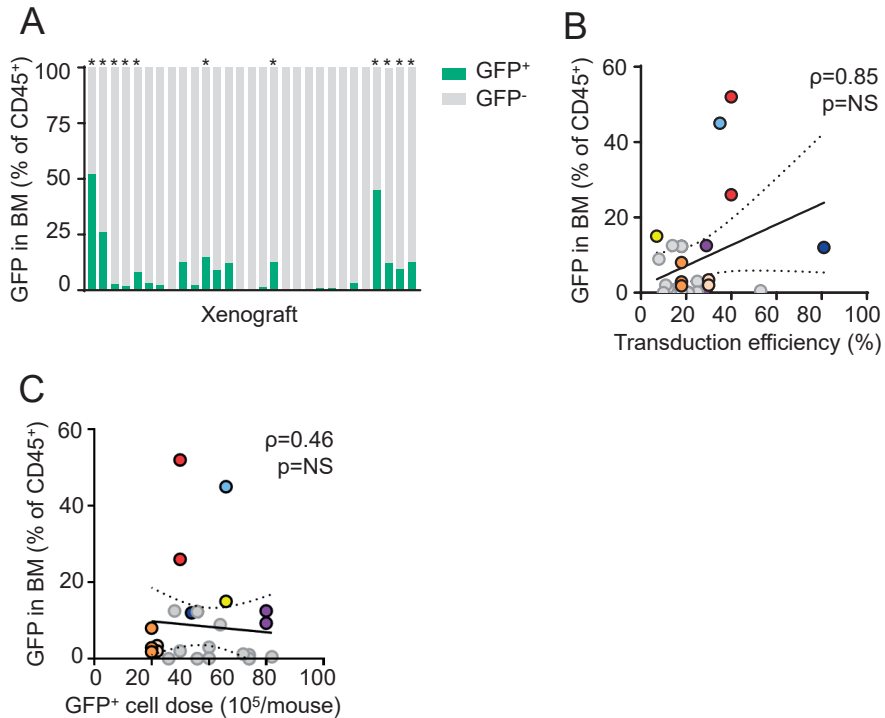
Figure S2. Human GFP⁺ cell engraftment in murine xenografts. (A) GFP⁺ cell engraftment in bone marrow of murine xenografts at sacrifice. Each bar represents one mouse. Asterisks depict mice with sufficient material for barcode analysis. (B) Lack of correlation between GFP⁺ cell percentage in bone marrow and pre-transplant transduction efficiency. (C) Lack of correlation between GFP⁺ cell percentage in bone marrow and tranplanted GFP⁺ cell dose.
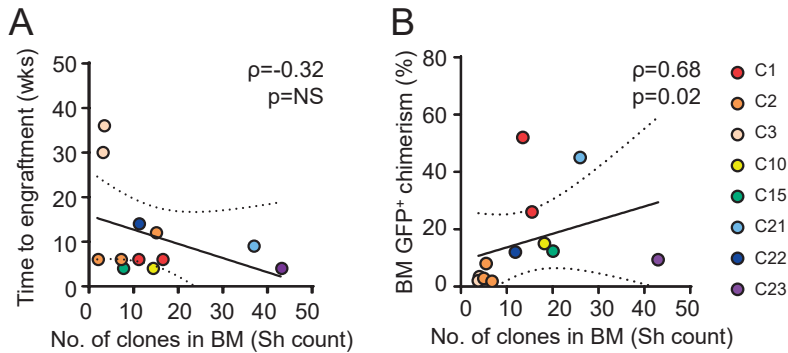
Figure S3. Correlation between the number of HSC clones and engraftment kinetics. (A) Lack of correlation between the number of HSC clones in bone marrow at sacrifice and the time to engraftment (defined as ≥1% hCD45^{+} cells). Each dot represents one mouse. Colors are used to depict individual UCB donors and correspond to the colors used in figure 1. Lines depict regression line +/- 95%CI. (B) Correlation between the number of HSC clones and GFP[+] human chimerism in bone marrow at sacrifice.
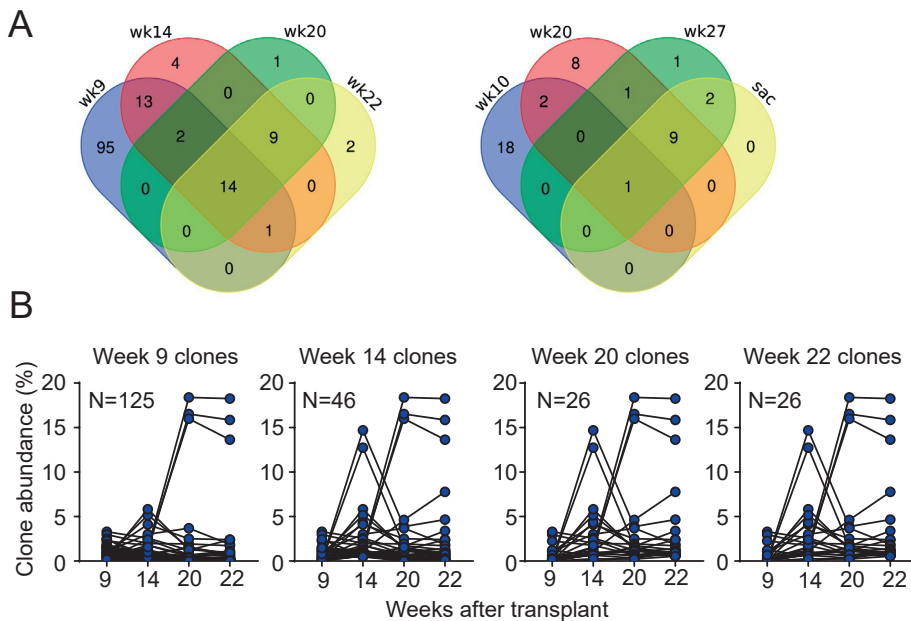
Figure S4. Blood cells are produced by transient clones early after transplantation, followed by hematopoiesis by long-term clones with stable output (continued)

(A) Venn diagram displaying presence of barcode clones in blood at several time points after transplantation. For each time point, clones were sorted in based on their relative abundance, and only the most abundant clones (based on Shannon approximation) were used for analysis. Depicted are representative examples of two individual recipients (C21). (B) Longitudinal patterns of clone sizes over time of individual barcode clones in xenografts of C1. For each time point, the most abundant clones (Shannon approximation) are shown.
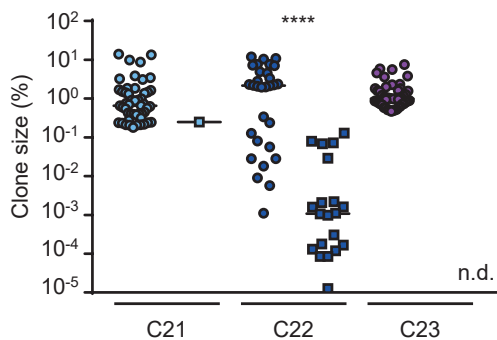
Figure S5. Clones with multilineage contribution are larger than clones with restricted lineage potential. Depicted are the top 50 most abundant clones in each xenograft. Clone size was defined as the number of barcode reads assigned to a certain clone, divided by the total number of barcode reads in the sample. Each dot represents a single barcode clone. In C23, all top 50 clones had multilineage output, preventing comparisons of clone sizes. ****; $p<0.0001$ (Mann-Whitney U).

Chapter 3

Clonal selection and asymmetric distribution of human leukemia in murine xenografts revealed by cellular barcoding

Mirjam E. Belderbos, Taco Koster, Bertien Ausema, Sabrina Jacobs, Sharlaine Sowdagar, Erik Zwart, Eveline de Bont, Gerald de Haan and Leonid V. Bystrykh

ABSTRACT

Genetic and phenotypic heterogeneity of human leukemia is thought to drive leukemia progression through a Darwinian process of selection and evolution of increasingly malignant clones. However, the lack of markers to uniquely identify individual leukemia clones precludes high resolution tracing of their clonal dynamics.

Here, we employ cellular barcoding to analyze the clonal behavior of patient-derived leukemia-propagating cells (LPCs) in murine xenografts. Using a leukemic cell line and diagnostic bone marrow cells from six patients with B-progenitor cell acute lympho-blastic leukemia (B-ALL), we demonstrate that patient-derived xenografts were highly polyclonal, consisting of tens to hundreds of LPC clones. The number of clones was stable within xenografts but strongly reduced upon serial transplantation. In contrast to primary recipients, in which clonal composition was highly diverse, clonal composition in serial xenografts was highly similar between recipients of the same donor and reflected donor clonality, supporting a deterministic, clone-size based model for clonal selection. Quantitative analysis of clonal abundance in several anatomic sites identified two types of anatomic asymmetry. First, clones were asymmetrically distributed between different bones. Second, clonal composition in the skeleton significantly differed from extramedullary sites, showing similar numbers but different clone sizes.

Altogether, this study shows that cellular barcoding and xenotransplantation provides a useful model to study the behavior of patient-derived LPC clones, which provides insights relevant for experimental studies on cancer stem cells and for clinical protocols for the diagnosis and treatment of leukemia.

INTRODUCTION

Leukemia is thought to arise through a Darwinian type of clonal evolution, in which acquisition of genetic mutations drives the selection and progression of pre-leukemic clones towards overt leukemia[1–5]. Acquisition of mutations has long been considered a sequential, linear process[6]. However, with the progress of sequencing technology and collection of massive amounts of data, a more complex picture of cancer clonal composition has emerged[71,8]. Insight into clonal heterogeneity of leukemia and its evolution is of utmost importance, as it may fuel emergence of novel, clinically relevant biological features, such as more aggressive growth or drug resistance[9]. However, especially in acute lymphoblastic leukemia, many aspects of clonal evolution are subject to ongoing debate. For instance, the existence of leukemia stem cells (LSCs), their frequency within the total leukemic population and the dynamics of their clonal offspring remain unknown[10,11].

A crucial aspect of studying clonal evolution of leukemia is how to define, identify, and trace individual LSC clones. Currently, identification and enumeration of LSC is hampered by the lack of phenotypic markers that unambiguously discriminate LSC from the bulk leukemic cell population[10,12,13]. Therefore, LSC are commonly defined by their capacity to clonally expand and propagate the disease in immune deficient xenografts. Although the term *clone* is commonly used, its definition is instrumental for the interpretation of clonal tracking studies. Conceptually, a clone represents a group of cells that descends from a common ancestor and therefore share certain heritable and unique genetic features. Experimentally, clones are identified by detecting those features (markers). Clonal markers can be cell-intrinsic (e.g. genetic mutations, immunoglobulin heavy chain rearrangements), induced by cell manipulation (e.g. vector integration, barcodes) or by the experimental design (e.g. limiting dilution or single cell sorting strategies), and should be defined based on the particular experimental question[14,15]. In the present study, we use cellular barcodes to mark and trace patient-derived leukemia cells. We use the term "clone" to refer to a group of cells that carry the same barcode, and therefore derive from the same ancestor, which we call the "leukemia-propagating cell" (LPC).

Previous studies investigating clonal evolution of leukemia have relied on (deep) sequencing of somatic mutations, either in bulk cell populations[4,16] or in single leukemia cells[17]. These studies have been instrumental to demonstrate the existence of clonal heterogeneity[4,10], to identify certain driver mutations[18] and to reconstruct leukemia clonal architecture[4,8]. However, these studies generally provide "snap shots" of mutational landscapes at certain time points (e.g. diagnosis and relapse), and complex mathematical models are employed to reconstruct clonal ancestry[19,20]. Therefore, to validate current views on the clonal pathogenesis of leukemia, there is need for complimentary strategies to ultimately derive a quantitative description of individual leukemia clones and the competitive behavior of their clonal offspring.

Lineage tracking using cellular barcodes provides such a strategy, allowing for simple, high-resolution tracking of individual clones over time[21–23]. Cellular barcoding relies on the viral integration of random DNA sequences of fixed length ("barcodes") into the genome of target cells[22,24,25]. After transplantation of barcoded cells, their offspring can be traced by quantifying the barcode abundance using deep sequencing[25]. So far, few studies have used cellular barcodes to study the clonal dynamics of human leukemia, and they differ in their conclusions. *In vitro*, culture of barcoded patient-derived leukemia cells on human mesenchymal stromal cells resulted in polyclonal cultures which retained their clonal complexity for 4-6 weeks[26]. In addition, barcoding of a KCL-22 chronic leukemia cell line allowed for the detection of small therapy-resistant subclones which would have gone undetected with standard next generation sequencing strategies[27]. In contrast, *in vivo,* leukemia induced by artificial oncogenic overexpression rapidly evolved towards mono- or oligoclonality[28,29]. It is unclear to what extent the murine environment contributes to these differences[30] and whether these models reflect the competitive biological behavior of patient-derived leukemia clones.

In this study, we applied cellular barcoding and xenotransplantation to comprehensively characterize the dynamics of LPC clones derived from pediatric patients with B-progenitor cell acute lymphoblastic leukemia (B-ALL). We identified hundreds of LPC that steadily contributed to the leukemic population in murine xenografts. Many clones were asymmetrically distributed, preferentially localized in either bone marrow or extramedullary sites. Overall, our results demonstrate that cellular barcoding is a reliable method to count and trace patient-derived LPC clones, which can be used to obtain important insights on leukemia clonal evolution.

METHODS

Cells

The pediatric BCR-ABL[+] SupB15 cell line was maintained in DMEM supplemented with 10% fetal calf serum (FCS, Stemcell Technologies, Grenoble, France), 1% penicillin and streptomycin (Gibco, ThermoScientific, Waltham, MA, USA). Cryopreserved diagnostic bone marrow cells from pediatric patients with B-cell acute lymphoblastic leukemia (B-ALL) had been collected as part of routine diagnostics for suspected leukemia. Residual mononuclear cells left after clinical testing were cryopreserved for research purposes (Department of Pediatric Hematology/Oncology, University Medical Center Groningen). Written informed consent was provided by all patients and/or their caregivers. All procedures were approved by the Medical Ethical Committee of the University Medical Center Groningen.

Mice

Immune deficient Nod/SCID/IL2Rγ$^{-/-}$ mice were bred and housed at the Central Animal Facility of the Groningen University. All animal experiments were approved by the Groningen University Animal Care Committee and by the Dutch National Central Animal Experiments Committee.

Barcoded vector library

A barcode library was prepared as previously described, with the modification that each barcoded vector in the current library was isolated and stored separately as DNA prep and E.coli stock[25,31]. For details on barcode library production, see supplementary file S1.

Barcode library validation

The SupB15 pediatric B-ALL cell line was transduced with a lentiviral barcoded pEGZ2 vector library containing ~800 barcodes. 48 hours after the initial transduction, cells were sorted based on GFP-expression ($43x10^6$ cells, 13% GFP$^+$), expanded *in vitro* to $18x10^6$ cells and then transplanted into sublethally irradiated NSG mice ($2.5x10^6$ cells/ mouse; n=5) or split into five parallel cultures (10^6 cells/parallel culture). *In vitro* cultures were maintained for 20 weeks. Twice weekly, $1x10^6$cells of each passage were seeded into the next well (supplementary file S2). Remaining cells were stored as pellets at -20°C for barcode analysis.

Cellular barcoding of patient-derived leukemia cells

Diagnostic B-ALL cells were thawed rapidly. From each patient sample, part of the cells was transplanted directly into immune deficient NSG mice, and part was used for lentiviral barcoding. The direct transplant served as a control to assess loss of engraftment potential during the barcoding procedure and to allow for a potential second barcoding attempt upon sacrifice (figure 2a; supplementary file S3-S4). Cells for barcoding were resuspended into Stem Span medium (Stemcell Technologies, Grenoble, France) containing 10% FCS, recombinant human (rh)IL7 (10 ng/mL, Peprotech, London, United Kingdom), TPO (100 ng/mL, Preprotech), FLT3-L (20 ng/mL, R&D Systems, Minneapolis, MN, USA) and rhSCF (50 ng/mL, R&D Systems, Oxon, UK). 12h after thawing, polybrene was added (2 µg/mL) and cells were transduced in 2 rounds of 12 hours with a lentiviral barcoded pEGZ2 vector library containing ~800 barcodes (ALL-58) or ~500 barcodes (ALL-70). Two days after the initial transduction, GFP$^+$ cells were sorted using a MoFlo flow cytometer (Beckman Coulter, Woerden, Netherlands) and transplanted.

Xenotransplantation of barcoded leukemia cells

Barcoded leukemia cells were transplanted into sublethally irradiated (1-2 Gy) NSG mice by intravenous injection into the retro-orbital plexus (ALL-58, primary transplant) or tail

vein (all other transplants, supplementary file S3-S4). Patient sample ALL-58 required *in vivo* expansion to allow successful barcoding. Bone marrow from two xenografts of unbarcoded leukemia cells was barcoded and transplanted in two separate experiments. Transduction efficiencies were 0.4% (ALL-58.1) and 2.5% (ALL-58.2), resulting in cell doses of 35000 (ALL-58.1) and 400000 (ALL-58.2) per mouse. Patient sample ALL-70 was barcoded successfully immediately upon thawing at a transduction efficiency of 1% and transplanted at 14000 cells/mouse (2 mice) or 140000 cells/mouse (2 mice).

Leukemia development

Leukemia development was monitored based on clinical symptoms and monthly blood analysis. Differential blood counts were performed on a Medonic CA620 Hematology Analyzer (Boule Medical AB, Spanga, Sweden). Leukemic and GFP chimerism were analyzed by flow cytometry[31,32] (supplementary file S5-6). When mice developed symptomatic leukemia, they were sacrificed by cervical dislocation under isoflurane anesthesia and blood, bones, spleen and liver were collected. Bones were isolated according to anatomic location: (1) sternum; (2) spine; (3) left femur and tibia (left hind); and (4) right femur and tibia (right hind). Single cell suspensions were prepared by crushing in lysis solution (NH_4Cl) and/or filtering through a 100 M-filter, as previously described[29,32]. Cells were analyzed by flow cytometry (figure 3b and supplementary file S5) and stored in pellets of $1-5 \times 10^6$ for barcode analysis.

Barcode library production, deep sequencing, barcode data processing and analysis and clonal analysis of non-leukemic hematopoiesis

For methods used for barcode library production, deep sequencing, barcode analysis, the random sampling model, estimation of stochasticity and determinism, clonal analysis of non-leukemic hematopoiesis and general statistical analysis, see supplementary files S1 and S7.

RESULTS

Construction and validation of the barcode library

To allow for robust and reproducible clonal labeling, we generated ~800 individual barcode preps which were pooled into libraries of varying complexity (figure 1a and 1b). Individual preparation of barcodes is useful, since it allows for construction of libraries of known, equimolar barcode content and complexity. In addition, each barcode can be regenerated endlessly from *E. coli* stock, thus enhancing reproducibility of the library and of experimental data[22]. Sequencing analysis of a 500-barcode library confirmed that most barcodes were evenly distributed across the library and present with frequencies

of 0.1-0.2% (figure 1c). To further validate our library and methods for barcode analysis, we mixed individual barcode DNA samples at equimolar ratios into libraries of different sizes and sequenced each mixture in duplicate. We found a nearly perfect 1:1 correlation between the number of barcodes put in each sample and the number of barcodes retrieved from deep sequencing results (Spearman r=1.00, p<0.001; figure 1d).
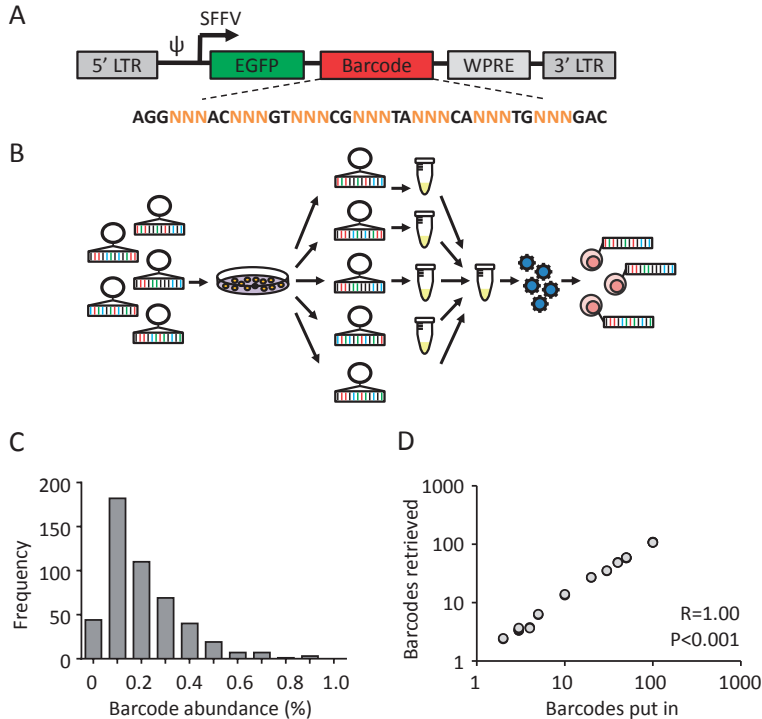
Figure 1. Construction and validation of an equimolar barcode library.
(A) Structure of the barcode linker. The linker contains a variable sequence part which consists of triplets of random (N) nucleotides which generate barcode diversity, flanked by fixed nucleotides which facilitate barcode retrieval in deep sequencing results. (B) Schematic representation of barcode library production and barcoding protocol. (C) Frequency distribution of barcodes in a 500-barcode library, determined by PCR and deep sequencing. (D) Correlation between the number of barcodes in samples submitted for sequencing, and the number of barcodes retrieved in deep sequencing results.

Validation of the barcoding method for highly polyclonal samples

We subsequently aimed to validate our methods for clone identification and tracking. Hereto, we characterized the clonal behavior of a barcoded pediatric leukemia cell line (SupB15) in vitro and in vivo. We presumed that all cells from a cell line are equal, resulting in the highest possible barcode complexity, which would put the maximum challenge on our methods for clone retrieval and data analysis.
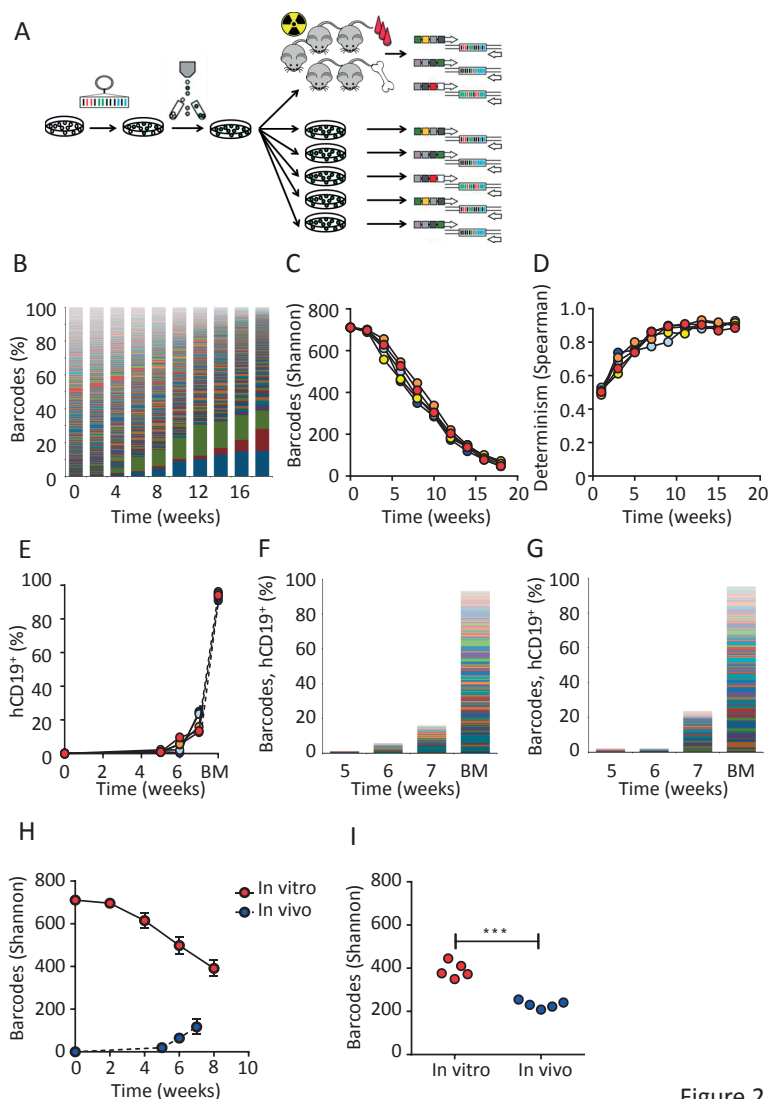
Figure 2. Validation of the barcoding method *in vitro* and *in vivo*.
(A) Experimental design. (B) Barcode composition in one representative cell culture. Each color represents one barcode. (C) Quantification of barcode complexity *in vitro*. (D) Determinism in *in vitro* barcode composition over time, calculated as Spearman rank coefficient between sequential passages of the same parallel culture. (E) *In vivo* human chimerism in xenografts of barcoded SupB15 leukemia cells, measured by flow cytometry for human CD19+ cells. One mouse did not engraft. (F-G) Barcode composition in blood at 5, 6, 7 weeks after transplant and bone marrow (BM) of SupB15 xenografts. Each color represents one barcode, the height of the bars corresponds to the level of human chimerism. Depicted are two representative xenografts. (H) Comparison of barcodes in murine blood and in the *in vitro* culture over time. (I) Comparison of barcode clones in bone marrow at the time of sacrifice with *in vitro* clonality at the corresponding time points.

In vitro, we initiated five parallel cultures of 10^6 barcoded SupB15 cells each (details in methods, growth curve in file S2). Barcode analysis revealed high clonal complexity in the first passages (711 barcodes at week 0, 696 at week 2), closely approaching the size of the used library (figure 2b-c). Afterwards, complexity slowly declined, yet remained polyclonal (figure 2b-c).

To validate our methods in vivo, we transplanted $2,5x10^6$ cells/mouse of the same barcoded cell line into sublethally irradiated NSG mice (n=5). All xenografts developed a polyclonal leukemia, consisting of 7-71 clones in blood (figure 2f-h) and 208-255 clones in bone marrow (figure 2i). Notably, the number of clones retrieved from blood gradually increased over time. This may be due to presence of clones with more dormant behavior, which only reach the threshold for detection at later time points. In addition, the number of clones in bone marrow was markedly higher than in blood.

Comparison of *in vivo* and *in vitro* clonal complexity at corresponding time points demonstrated lower frequencies of LPC clones *in vivo*, both in blood (figure 2h) and in bone marrow (average 390 clones *in vitro* vs 231 clones *in vivo*; p<0.0001, figure 2i). To calculate the survival rate of the transplanted cells needed to achieve such a reduction in clone frequency, we used an *in silico* simulation script (file S7). We found that a survival rate of 1:3000 resembled our observations closely, resulting in approximately 200 surviving clones.

Altogether, these findings validate the usefulness of cellular barcoding for detection and high-resolution tracking of individual leukemia clones *in vitro* and *in vivo*.

Engraftment of patient-derived leukemia

We subsequently aimed to use cellular barcodes to characterize the behavior of patient-derived leukemia clones. Diagnostic bone marrow cells of six patients with B-ALL were subjected to barcoding and transplanted into immune deficient NSG mice. Two samples engrafted and caused a GFP$^+$ leukemia (figure 3a, table 1, details on experimental procedures in files S2-S3). The remaining four samples did not produce any human chimerism up to 28 weeks after transplantation.

Leukemia development was characterized by high chimerism for human CD19$^+$CD34$^+$ cells in peripheral blood and bone marrow (figure 3b-e), of which the majority was GFP$^+$ (supplementary file S6). In addition, leukemic mice displayed clinical symptoms necessitating sacrifice (figure 3f-h), and significantly enlarged spleen size (0.07 vs 0.54 g, p<0.001, figure 3i-j) with >90% CD19$^+$CD34$^+$ B-cells (not shown). Interestingly, compared to non-engrafting samples, the engrafting samples were obtained from patients with more aggressive types of leukemia (BCR-ABL$^+$ of delIKZF1; table 1) and the dynamics of engraftment differed between these samples. Whereas xenografts of the BCR-ABL$^+$ leukemia (ALL-58) all had >90% leukemic chimerism in peripheral blood within 6 weeks after transplant (figure 2c-d), xenografts of the IKZF1-deleted leukemia (ALL-70) demonstrated
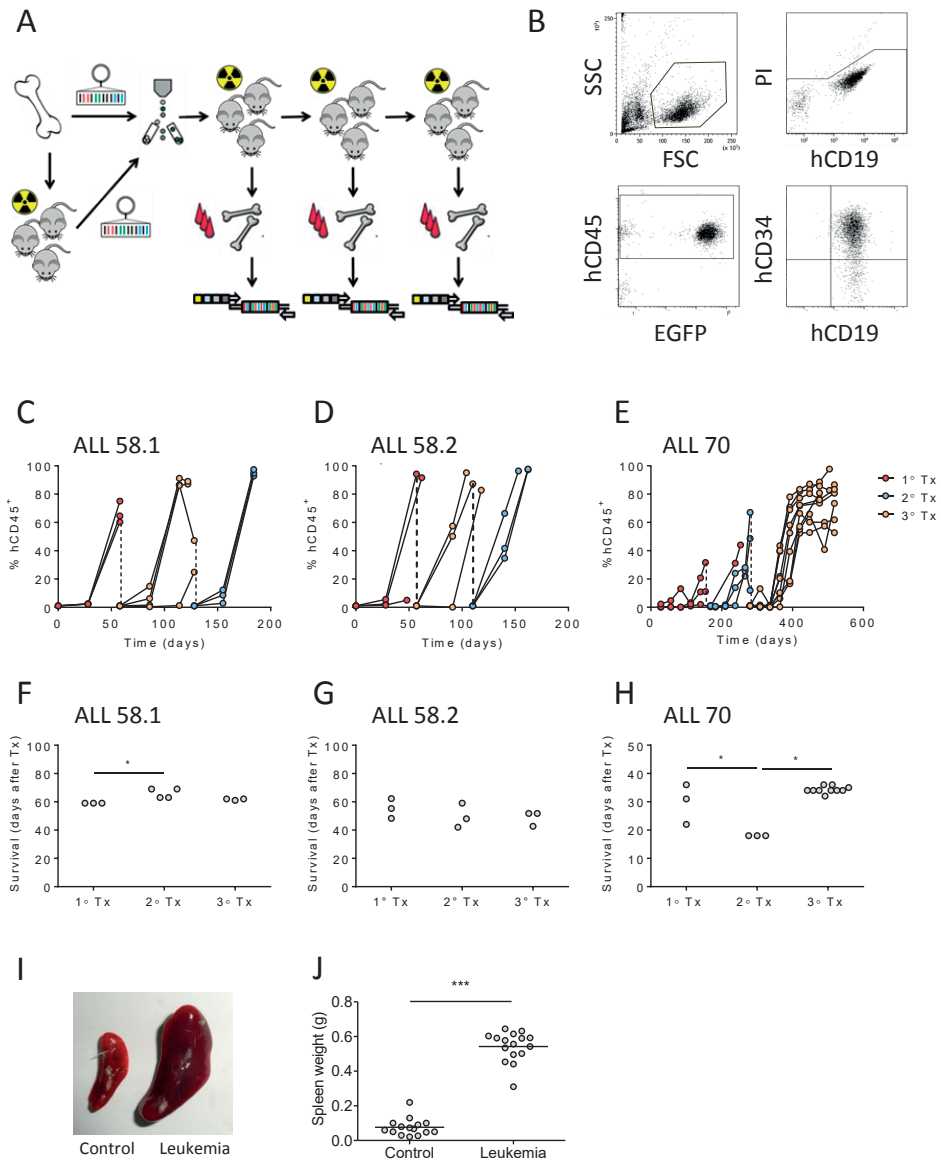
Figure 3. Lentiviral barcoding of primary pediatric leukemia.
(A) Experimental design. (B) Gating strategy for flow cytometric detection of human leukemia cells in mouse blood. (C-E) Percentage of human chimerism (%hCD45$^+$ of live cells) in blood of serial xenografts of patient-derived leukemia. Connected dots represent samples from a single mouse. (F-H) Survival of serial xenografts of patient-derived leukemia. Each dot represents a single mouse. (I-J): Spleen size in control and leukemic mice. Each dot is one mouse. ***; p<0.001.

Table 1. Characteristics of patient samples used for xenotransplantation

Patient sample	Age at diagnosis (yrs)	WBC count (10⁹/L)	Blasts (%)	Karyotype	Cytogenetic aberrations	Outcome	Barcoding	Engraftment
ALL-45	4	7.9	25	46,XX	None	Alive, CR	Yes	No
ALL-58	18	295	79	46,XY	BCR-ABL	Dead	Yes	Yes
ALL-70	6	7.6	45	54,XY,+X,+Y,+8,+9,+14,+18,+21,+21[11]/46,XY[4]	DelKZF1	Dead	Yes	Yes
ALL-78	14	61	90	46,XY,9p-[6]/46,XY,9p+[4]/46,XY[2]	None	Alive, CR	No	Yes
ALL-79	9	25	96	46,XX	None	Alive, CR	No	No
ALL-80	16	3.7	57	64~68,XX,-X,+1,add(1)(p13),-3,-4,+5,+6,add(6)(q13) or del(6)?(q13p23),-7,?add(8)(p11),-13,-15,-16,-17,-19,+?20,-22,+1~7mar[cp8]/46,xx[3]	None	Alive, CR	No	No

slower leukemogenesis and lower levels of blood chimerism at sacrifice, especially in primary xenografts (figure 3e). No engraftment with human T-cells (CD45$^+$CD3$^+$), granulocytes (CD45$^+$CD16$^+$) or mature B-cells (CD45$^+$CD19$^+$CD34$^-$) was observed in any mouse.

Because transduction efficiency of patient samples was rather low, we tested whether the transduction procedure selected for a specific population of more aggressive and/or quiescent clones. We found similar levels of chimerism and rates of survival between recipients of barcoded leukemia cells and non-barcoded cells (supplementary file S8). Analysis of the sorted cells prior to transplantation showed that the patient samples were highly polyclonal, containing 402 (ALL-58.2) and 403 (ALL-70) barcode clones (file S9). This suggests that the barcoded LPC provide a biologically representative sample of the total leukemic population, although some selection may have occurred.

Patient-derived leukemia xenografts are highly polyclonal

Barcode analysis in blood throughout the experiment (figure 4a-c) and bone marrow at sacrifice (figure 4d-f) demonstrated that patient-derived xenografts were highly polyclonal, consisting of tens to hundreds of LPC clones. Within individual xenografts, the numbers and types of clones were stable over time (figure 4a-c), indicating their steady contribution to the leukemic population. Each primary xenograft was repopulated with different types of clones (figure 4a-c). The number of retrieved clones was dependent on the patient sample (figure 4a-f) and on the transplanted cell dose (figure 4h-i). When more cells were transplanted, we retrieved a higher number of barcodes (figure 4h), corresponding to calculated LPC frequencies ranging from 10^{-3} to 10^{-4} (fig.4i). None of the patient-derived leukemia samples proliferated in vitro. The observed patterns of engraftment and clonal dynamics were different from non-leukemic cord blood CD34$^+$ hematopoietic progenitors, which produced slower, multilineage engraftment, with an average of 8 clones (range 3-15) in bone marrow of primary xenografts (file S10). Notably, despite the fact that considerably lower cell doses were used for patient samples than for transplantation of the SupB15 cells (35000 to 400000 cells for patient samples versus 2,5x10^6 cells for the cell line), the number of retrieved clones was significantly higher in patient-derived xenografts compared to cell line xenografts, which may reflect increased capacity of patient-derived clones to survive the xenograft barrier.

Heritability of clonal dominance after serial transplantation

We noticed striking differences in the clonal patterns in primary xenografts transplanted with the same patient sample (figure 4). Theoretically, outgrowth of an LPC clone can be either stochastic (based on chance, thus poorly predictable), or deterministic (reflecting certain clone- of cell-dependent properties that confer a proliferative advantage). To investigate these possibilities, we assessed heritability and predictability of barcode patterns over time *in vitro* and *in vivo* in a serial transplantation model.
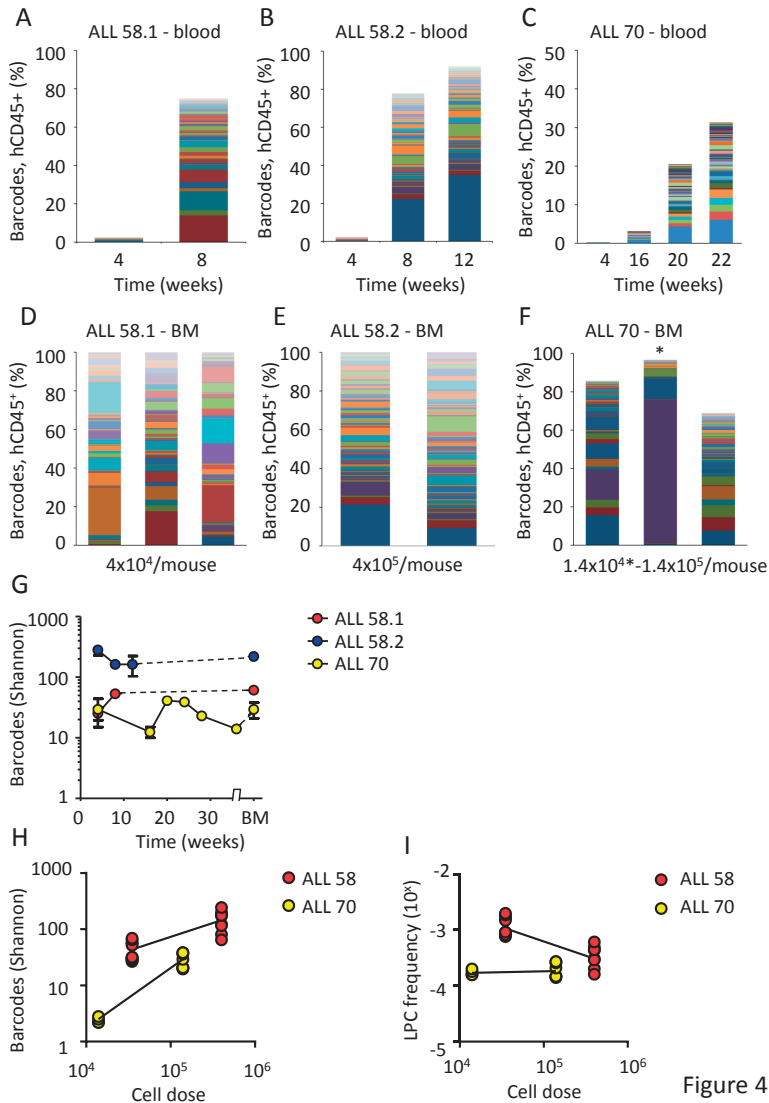
Figure 4. Clonal complexity of patient-derived leukemia subclones

(A-C) Clonal composition in blood of primary xenografts of patient-derived leukemia. Each bar represents one time point, each colored rectangle one barcode. The height of the bars corresponds to the %hCD45+ cells, determined by flow cytometry. (D-F) Clonal composition in bone marrow of primary xenografts at sacrifice. Each bar represents spine bone marrow of one mouse. For ALL-70 (4F), the mouse transplanted with 1.4×10^4 cells is marked with an asterisk. (G) Barcode complexity in blood and bone marrow of primary patient-derived xenografts over time. (H) Plot of retrieved barcode complexity in primary xenografts versus transplanted cell dose. Each dot represents one sample (i.e. one anatomic location). (I) Plot of LPC frequency in primary xenografts versus transplanted cell dose. LPC frequency was calculated by dividing the number of retrieved clones by the administered cell dose.

First, we revisited our *in vitro* cell culture data (figure 2). As expected, in the first passages, clonal selection was largely stochastic, reflected by a low Spearman rank coefficient (figure 2d). In later passages, clonal patterns became increasingly deterministic, meaning that clone order (by size) did not change much.

We subsequently assessed clonal selection patterns of patient-derived leukemia samples in serial transplantation experiments (figure 5, supplementary file S11). We observed
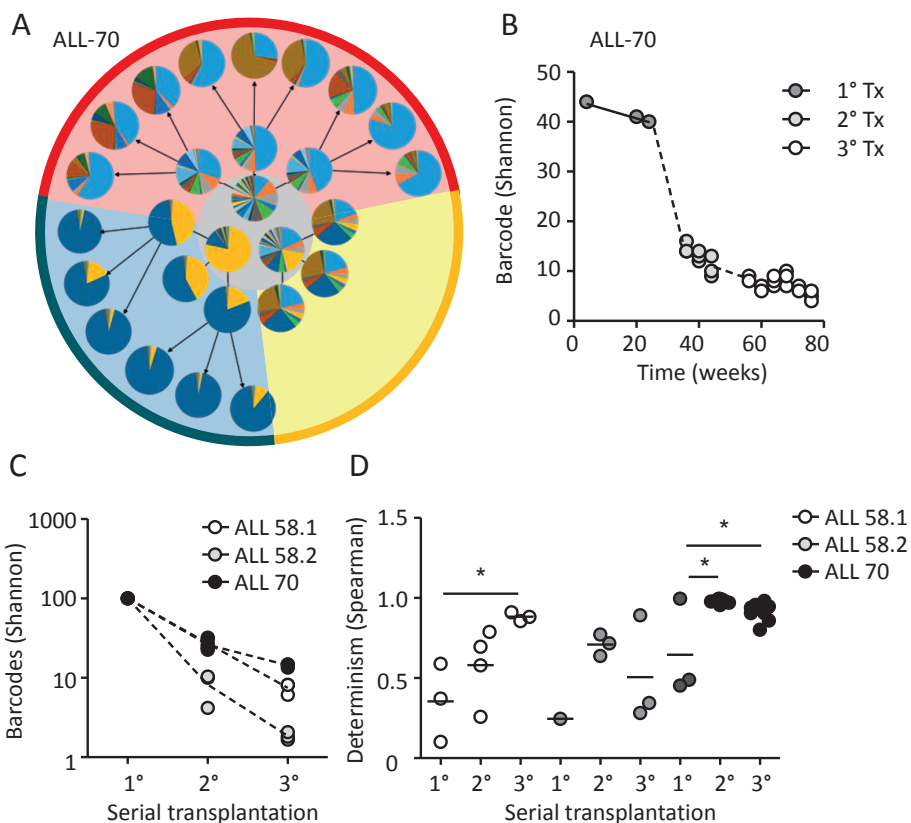
Figure 5. Clonal selection upon serial transplantation
(A) Barcode composition in serial xenografts of donor ALL-70. Each circle represents one mouse. Primary xenografts are depicted in the middle grey circle, arrows connect each donor to its serial recipients. The background colors mark descendants of the same ancestor. (B) Quantification of barcode complexity in blood of serial xenografts of donor ALL-70. Each dot represents one mouse at a certain time point. Dashed lines connect the donor to its serial recipients. (C) Barcode complexity in spine bone marrow of serial recipients. Each dot represents one mouse. Barcode composition of Detailed information on bone marrow composition of all recipients of ALL-58 can be found in file S11. (D) Degree of determinism in barcode composition between recipients of the same donor, expressed by Spearman rank coefficient. For example, for donor ALL-70, we calculated Spearman rank coefficients for barcode composition in spine bone marrow between the three primary recipients (panel a, grey circle); between the secondary recipients and between their tertiary recipients. Only mice receiving the same cell dose (red and yellow area) are plotted.

a strong reduction of clonal complexity in secondary and tertiary recipients compared to their donors (figure 5a-b). With each serial transplantation, 30-90% of clones were lost (figure 5a-c). Using the random sampling simulation model used previously for the cell line (supplementary file S7), we estimated survival rates of 1:20 to 1:100 from primary to secondary xenografts, or from secondary to tertiary xenografts.

In contrast to the primary recipients, which were highly different in their clonal composition (figure 5a, middle circle), we noted that clonal compositions were more similar in secondary and tertiary recipients (figure 5a, outer circles). This was confirmed using unsupervised clustering analysis, in which recipients from the same donor clustered together (supplementary file S12), and by Spearman rank analysis, showing increasing similarity over serial transplantation (figure 5d).
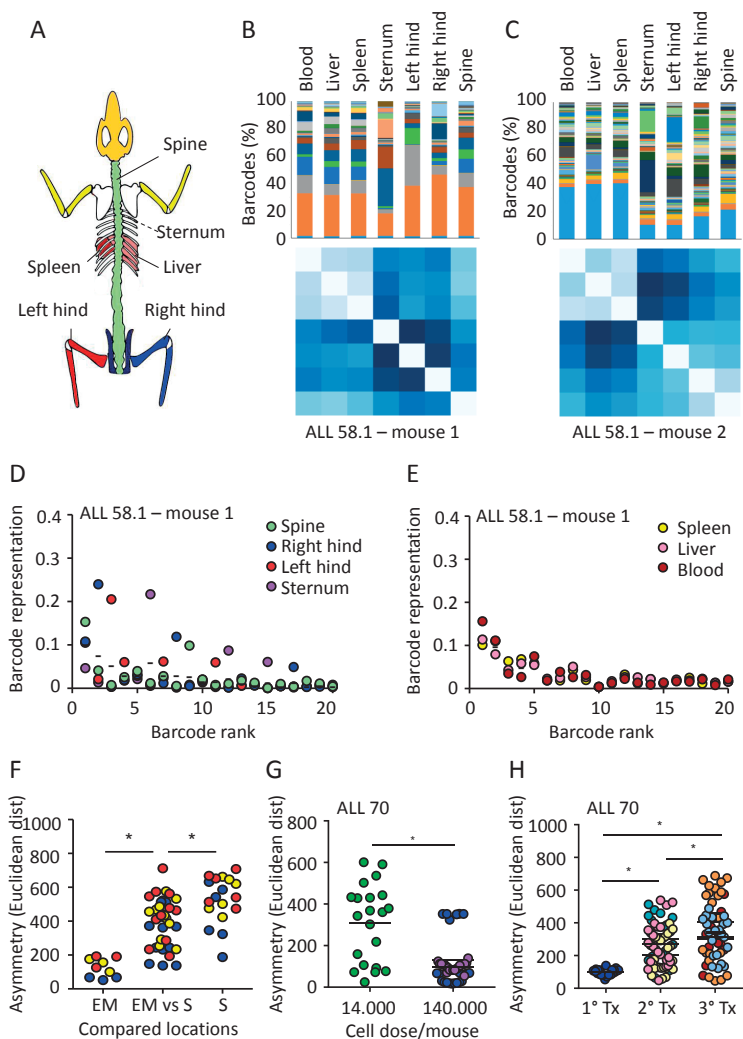
Spatial asymmetry of patient-derived leukemia clones

Despite increasing insight into the importance of the niche microenvironment for leukemia evolution[33–35], the anatomical distribution of individual leukemia clones is unknown[36]. In our study, we compared barcode composition at sacrifice of the mice in four skeletal sites (sternum, left hind leg, right hind leg, spine) and three extramedullary sites (liver, spleen and blood). We identified two types of clonal asymmetry; (1) asymmetry within the skeleton between different bone locations and (2) asymmetry between the skeleton and extramedullary sites (figure 6 and supplementary files S13-S14).

Within the skeleton, we noted that the relative abundance of certain clones differed between bones. For example, in figure 6b (upper panel), the dark grey clone dominated in the left hind leg, but not in any of the other locations. We visualized and quantified this in different ways. First, we compared the variation in clonal abundance per location around their average (overall) abundance (figure 6d-e). We noted that the abundance of some clones was variable, whereas others were symmetrically distributed (figure 6d). Interestingly, extramedullary sites did not show such asymmetry, demonstrated by minimal variation around average (fig 6e). Second, we compared the cumulative variation in clone sizes using Euclidean distances (fig 6b-c, figure 6f-h), which also showed that extramedullary sites are highly similar to each other, whereas bones are more diverse (fig 6f). Of note, the Spearman rank order of clones did not vary much by location (figure S13), indicating that clonal asymmetry is primarily due to variation in clone sizes, rather than their absolute presence/absence.

Notably, when all anatomic locations were cross-compared, we noted a higher degree of asymmetry in xenografts transplanted with a relatively low cell dose (figure 6g). In addition, clonal anatomic asymmetry increased over serial transplantations, with the highest degree of asymmetry observed in the tertiary recipients (figure 6h).

Together, these data demonstrate that LSC are asymmetrically distributed in xenografts, especially in situations or sites where the number of contributing clones is low.

Figure 6. Asymmetric distribution of patient-derived LSC clones in murine xenografts
At sacrifice of the mice, leukemia cells from patient-derived xenografts were isolated from seven anatomic locations, and barcode composition was determined by PCR and deep sequencing. (A) Schematic representation of the skeletal locations that were analyzed. (B-C) Anatomic distribution of barcoded clones in two representative xenografts of ALL-58.1. Top panels: Relative barcode abundance per location. Each color is one barcode clone. Bottom panels: Similarity in clonal distribution, assessed by Euclidean distance (for detailed information on methods, see figure S8). (D-E) Relative clonal abundance per anatomic location. Clones are ranked based on their overall abundance (x-axis). The Y-axis shows the relative abundance of each clone to the total pool in one location. Dots on the same vertical line reflect the size of a particular clone in different anatomic locations. The mean contribution of each clone is shown with a horizontal line. (F-H) Clonal diversity related to anatomical location (F); transplanted cell dose (G) or serial transplantation (H). Depicted are Euclidean distances over all combinations of anatomic locations within individual mice. Different colors are used to depict individual mice.

DISCUSSION

Patient-derived leukemia xenografts are highly polyclonal

Insight into the frequency of LPC and the dynamics of their clonal offspring is important for our understanding of leukemia pathogenesis and progression. Here, we describe the tracking of clonal dynamics of xenografted patient-derived ALL using cellular barcodes. The barcoding model has several advantages over previously used methods of clonal analysis: It is relatively simple, quantitative, and allows for prospective, high-throughput analysis of clonal complexity[20,37]. In addition, it allows to address questions on leukemia clonal evolution which cannot be addressed in patients.

We demonstrate that patient-derived leukemia xenografts are highly polyclonal, consisting of tens to hundreds LPC clones, and provide insights into the mechanisms of their selection. We identify significant skewing in LPC clonal distribution, both within the skeleton and between the skeleton and extramedullary sites. Altogether, these findings are relevant for experimental studies on ALL biology, as well as for clinical protocols for diagnosis and follow-up of patients with leukemia.

Cellular barcoding to characterize clonal evolution of leukemia

In contrast to acute myeloid leukemia, in which a stepwise model of tumor progression is well established[38,39], published studies regarding the cell of origin and its trajectory towards overt leukemia in ALL have been contradictory. Genome-wide analyses of DNA copy number alterations and loss-off-heterozygosity have identified various genetic aberrations associated with ALL progression (e.g. *PAX5, IKZF1, RAG1/2, CREBBP*)[40], which are present in different combinations and frequencies, indicative of the polyclonal nature of the disease. Importantly, in >95% of patients, at least part of the genetic aberrations present at diagnosis are retrieved at relapse, suggestive of a common clonal ancestor[4]. With the advent of modern sequencing technology, more genetic aberrations and an even higher degree of diversity will likely be uncovered. This will increase the challenge of discriminating driver mutations from innocent bystander effects, of identifying mutations causing chemotherapeutic resistance and of reconstructing clonal hierarchies. Our results provide a novel perspective on ALL clonal evolution, which identifies and counts clones based on their proliferative capacity, rather than their mutational load (which may change over time). In future, correlated clonal dynamics, simultaneously assessed by genomic aberrations and by cellular barcodes, may provide a more thorough picture of leukemia clonal dynamics.

Patterns of clonal selection

The observation that leukemia clonal complexity is greatly reduced upon serial transplantation raises the question to which extent functional differences between individual

leukemia clones dictate their survival and/or drive their selection. Here, we provide evidence for both stochastic (random) and deterministic (predictable) patterns of clonal behavior. We show that clonal selection is largely stochastic in initial *in* vitro passages and in primary xenografts, and becomes increasingly deterministic over time. Deterministic behavior has also been shown to apply to other tumor types[41], and is commonly explained by the existence of certain clonal inequalities driving their selection. However, it should be noted that the observed patterns of selection here may also be explained by the very properties of the barcoding method, which marks any cell and counts those that proliferate. Although initial marking will be random, upon proliferation, each clone will be represented by a large number of cells. Accordingly, serial transplantation/passaging will likely result in reproducible clonal hierarchies if the number of passaged cells representing each clone is sufficiently high. In the future, ascertainment of potential functional differences between cancer clones will need to take into account the stochastic patterns intrinsic to these types of experiments.

Asymmetric distribution of patient-derived leukemia clones

The observation that leukemia clones are asymmetrically distributed within the skeleton and between the skeleton and extramedullary sites is in line with earlier observations from our group, demonstrating skewed skeletal localization of murine normal (non-malignant) hematopoietic clones[32]. Based on this, one may speculate that interactions between LPCs and niche cells may define clone homing preferences[32,42–44]. However, our results support an alternative explanation, indicating that stochastic effects play substantial role in clone distribution. Accordingly, it may not be surprising that asymmetry increases when fewer LPCs are present. As an extreme example, a single LPC can only home to and engraft in one site. Nonetheless, it is striking that despite weeks of incubation and massive proliferation, the offspring of certain LPC still fail to mobilize and fully equilibrate over the body. Notably, once they do occupy extramedullary sites, they efficiently and equally distribute over different anatomic locations (resembling our previously reported G-CSF mobilized HSC)[32]. We did not find any evidence for selective clone preference to certain sites, suggesting that clonal distribution is stochastic[42] and that, once engrafted, differences in proliferation and/or mobilization, perhaps dictated by the bone marrow niche, account for the observed asymmetry.

Asymmetry in spatial distribution of leukemia clones has important experimental and translational implications, suggesting that sampling of a single anatomic site may underestimate the clonal repertoire and may miss certain (potentially relevant) clones located elsewhere. Further identification of potential skeletal asymmetry in patients, and of the clone- and/or niche specific differences dictating this asymmetry will be relevant for the diagnosis, treatment and follow-up of leukemia.

In conclusion, this study demonstrates that cellular barcoding and xenotransplantation is a simple and useful strategy to model the clonal evolution of human leukemia cells. In the future, combining cellular barcoding with *in vivo* chemotherapy and/or genomic mutation analysis will provide a powerful tool to study the clonal evolution of chemotherapeutic resistance and to optimize patient treatment.

ACKNOWLEDGMENTS

FINANCIAL DISCLOSURE STATEMENT

CONFLICT OF INTEREST DISCLOSURES

None of the authors has any conflict of interest to declare.

AUTHORSHIP CONTRIBUTIONS

MB, GdH and LB designed the research. MB, TK, SJ, BD-A, SS and LB performed the research. EdB contributed vital reagents and patient samples. MB, EZ and LB analyzed the data. MB, GdH and LB wrote the manuscript.

REFERENCES

1. Anderson K, Lutz C, van Delft FW, et al. Genetic variegation of clonal architecture and propagating cells in leukaemia. *Nature*. 2011;469(7330):356–361.

2. Greaves M, Maley CC. Clonal evolution in cancer. *Nature*. 2012;481(7381):306–13.

3. Ma X, Edmonson M, Yergeau D, et al. Rise and fall of subclones from diagnosis to relapse in pediatric B-acute lymphoblastic leukaemia. *Nat. Commun.* 2015;6:6604.

4. Mullighan CG, Phillips LA, Su X, et al. Genomic analysis of the clonal origins of relapsed acute lymphoblastic leukemia. *Science*. 2008;322(5906):1377–1380.

5. Notta F, Mullighan CG, Wang JC, et al. Evolution of human BCR-ABL1 lymphoblastic leukaemia-initiating cells. *Nature*. 2011;469(7330):362–367.

6. Knudson AG. Mutation and cancer: statistical study of retinoblastoma. *Proc. Natl. Acad. Sci. U. S. A.* 1971;68(4):820–3.

7. Gao R, Davis A, McDonald TO, et al. Punctuated copy number evolution and clonal stasis in triple-negative breast cancer. *Nat. Genet.* 2016;48(10):1119–1130.

8. Mullighan CG. Genomic characterization of childhood acute lymphoblastic leukemia. *Semin. Hematol.* 2013;50(4):314–324.

9. Aparicio S, Caldas C. The implications of clonal genome evolution for cancer medicine. *N. Engl. J. Med.* 2013;368(9):842–51.

10. le Viseur C, Hotfilder M, Bomken S, et al. In childhood acute lymphoblastic leukemia, blasts at different stages of immunophenotypic maturation have stem cell properties. *Cancer Cell*. 2008;14(1):47–58.

11. Bernt KM, Armstrong SA. Leukemia stem cells and human acute lymphoblastic leukemia. *Semin. Hematol.* 2009;46(1):33–38.

12. Castor A, Nilsson L, Astrand-Grundstrom I, et al. Distinct patterns of hematopoietic stem cell involvement in acute lymphoblastic leukemia. *Nat. Med.* 2005;11(6):630–637.

13. Cox C V, Evely RS, Oakhill A, et al. Characterization of acute lymphoblastic leukemia progenitor cells. *Blood*. 2004;104(9):2919–2925.

14. Glauche I, Bystrykh L, Eaves C, Roeder I, participants other. Stem cell clonality -- theoretical concepts, experimental techniques, and clinical challenges. *Blood Cells. Mol. Dis.* 2013;50(4):232–240.

15. Baldow C, Thielecke L, Glauche I. Model Based Analysis of Clonal Developments Allows for Early Detection of Monoclonal Conversion and Leukemia. *PLoS One*. 2016;11(10):e0165129.

16. Clappier E, Gerby B, Sigaux F, et al. Clonal selection in xenografted human T cell acute lymphoblastic leukemia recapitulates gain of malignancy at relapse. *J. Exp. Med.* 2011;208(4):653–61.

17. Gawad C, Koh W, Quake SR. Dissecting the clonal origins of childhood acute lymphoblastic leukemia by single-cell genomics. *Proc. Natl. Acad. Sci. U. S. A.* 2014;111(50):17947–17952.

18. Mullighan CG, Zhang J, Kasper LH, et al. CREBBP mutations in relapsed acute lymphoblastic leukaemia. *Nature*. 2011;471(7337):235–239.

19. El-Kebir M, Oesper L, Acheson-Field H, Raphael BJ. Reconstruction of clonal trees and tumor composition from multi-sample sequencing data. *Bioinformatics*. 2015;31(12):i62-70.

20. Bystrykh L V, Verovskaya E, Zwart E, Broekhuis M, de Haan G. Counting stem cells: methodological constraints. *Nat. Methods*. 2012;9(6):567–574.

21. Blundell JR, Levy SF. Beyond genome sequencing: lineage tracking with barcodes to study the dynamics of evolution, infection, and cancer. *Genomics*. 2014;104(6 Pt A):417–30.

22. Bystrykh L V, Belderbos ME. Clonal Analysis of Cells with Cellular Barcoding: When Numbers and Sizes Matter. *Methods Mol. Biol.* 2016;

23. Cheung AMS, Nguyen L V, Carles A, et al. Analysis of the clonal growth and differentiation dynamics of primitive barcoded human cord blood cells in NSG mice. *Blood*. 2013;122(18):3129–37.

24. Bystrykh L V. Generalized DNA barcode design based on Hamming codes. *PLoS One*. 2012;7(5):e36852.

25. Gerrits A, Dykstra B, Kalmykowa OJ, et al. Cellular barcoding tool for clonal analysis in the hematopoietic system. *Blood*. 2010;115(13):2610–2618.

26. Pal D, Blair HJ, Elder A, et al. Long-term in vitro maintenance of clonal abundance and leukaemia-initiating potential in acute lymphoblastic leukaemia. *Leukemia*. 2016;30(8):1691–700.

27. Bhang HC, Ruddy DA, Krishnamurthy Radhakrishna V, et al. Studying clonal dynamics in response to cancer therapy using high-complexity barcoding. *Nat. Med.* 2015;21(5):440–8.

28. Cornils K, Thielecke L, Hüser S, et al. Multiplexing clonality: combining RGB marking and genetic barcoding. *Nucleic Acids Res.* 2014;42(7):e56.

29. Klauke K, Broekhuis MJ, Weersing E, et al. Tracing dynamics and clonal heterogeneity of cbx7-induced leukemic stem cells by cellular barcoding. *Stem cell reports*. 2015;4(1):74–89.

30. Klco JM, Spencer DH, Miller CA, et al. Functional Heterogeneity of Genetically Defined Subclones in Acute Myeloid Leukemia. *Cancer Cell*. 2014;25(3):379–392.

31. Verovskaya E, Broekhuis MJC, Zwart E, et al. Heterogeneity of young and aged murine hematopoietic stem cells revealed by quantitative clonal analysis using cellular barcoding. *Blood*. 2013;122(4):523–32.

32. Verovskaya E, Broekhuis MJC, Zwart E, et al. Asymmetry in skeletal distribution of mouse hematopoietic stem cell clones and their equilibration by mobilizing cytokines. *J. Exp. Med.* 2014;211(3):487–97.

33. Antonelli A, Noort WA, Jaques J, et al. Establishing human leukemia xenograft mouse models by implanting human bone marrow-like scaffold-based niches. *Blood*. 2016;

34. Zambetti NA, Ping Z, Chen S, et al. Mesenchymal Inflammation Drives Genotoxic Stress in Hematopoietic Stem Cells and Predicts Disease Evolution in Human Pre-leukemia. *Cell Stem Cell*. 2016;19(5):613–627.

35. Schepers K, Campbell TB, Passegué E. Normal and leukemic stem cell niches: insights and therapeutic opportunities. *Cell Stem Cell*. 2015;16(3):254–67.

36. Williams MTS, Yousafzai YM, Elder A, et al. The ability to cross the blood-cerebrospinal fluid barrier is a generic property of acute lymphoblastic leukemia blasts. *Blood*. 2016;127(16):1998–2006.

37. Bystrykh L V, de Haan G, Verovskaya E. Barcoded vector libraries and retroviral or lentiviral barcoding of hematopoietic stem cells. *Methods Mol. Biol.* 2014;1185:345–60.

38. Hotfilder M, Rottgers S, Rosemann A, et al. Immature CD34+CD19- progenitor/stem cells in TEL/AML1-positive acute lymphoblastic leukemia are genetically and functionally normal. *Blood*. 2002;100(2):640–646.

39. Ding L, Ley TJ, Larson DE, et al. Clonal evolution in relapsed acute myeloid leukaemia revealed by whole-genome sequencing. *Nature*. 2012;481(7382):506–510.

40. Inaba H, Greaves M, Mullighan CG. Acute lymphoblastic leukaemia. *Lancet*. 2013;381(9881):1943–1955.

41. Eirew P, Steif A, Khattra J, et al. Dynamics of genomic clones in breast cancer patient xeno-grafts at single-cell resolution. *Nature*. 2014;518(7539):422–426.

42. Hawkins ED, Duarte D, Akinduro O, et al. T-cell acute leukaemia exhibits dynamic interactions with bone marrow microenvironments. *Nature*. 2016;538(7626):518–522.

43. Lo Celso C, Scadden DT. The haematopoietic stem cell niche at a glance. *J. Cell Sci.* 2011;124(21):.

44. van der Velden VHJ, Jacobs DCH, Wijkhuijs AJM, et al. Minimal residual disease levels in bone marrow and peripheral blood are comparable in children with T cell acute lymphoblastic leukemia (ALL), but not in precursor-B-ALL. *Leukemia*. 2002;16(8):1432–6.

SUPPLEMENTARY INFORMATION

Supplementary information of raw sequencing reads is available via the online version of this paper.

File S1: Methods for barcode library production, deep sequencing, barcode data processing and analysis and clonal analysis of non-leukemic hematopoiesis.

Barcode library production

The current library was based on the pGIPZ vector (GE Dharmacon, Lafayette, CO), in which the IRES-puro-miR cloning site was cut with BsrgI-MIuI restriction enzymes and replaced with a short linker carrying *Cla*I, *Bam*HI and *Sma*I restriction sites. The pCMV promoter was further replaced by the pSFFV promotor and the resulting vector was named pEGZ2. Barcodes were cloned via *Bsrg*I-*Bam*HI sites by ligation as previously described>. To allow for assessment of library skewing, we used two different barcode structures; either GAANNNACNNNGTNNNCGNNNTANNNCANNNTAAGGAC or AGGNNNACNNNGTNNNCGNNNTANNNCANNNTGNNNGAC. Competent *E. Coli* were transduced with the resulting barcoded vectors and cultured on LB-Agar plates. After 24h, individual colonies were picked, cultured individually for another 24h in liquid LB medium. Afterwards, plasmid DNA was isolated, checked for barcode presence and stored at -20°C. In addition, each colony was also stored in 50% glycerol at -80°C. Using this protocol, ~800 barcodes were generated and pooled at equimolar ratios to provide libraries for target cell transduction.

Clonal analysis of non-leukemic hematopoiesis

Cord blood was collected directly after uncomplicated vaginal delivery from the umbilical cord and placenta. CD34$^+$ hematopoietic progenitor cells were isolated by Ficoll gradient centrifugation (...) and subsequent positive selection using CD34$^+$ magnetic beads (Miltenyi, Leiden, NL). Cord blood CD34$^+$ hematopoietic progenitor cells from donor 1-3 were barcoded *in vitro* in stem span medium supplemented with recombinant human thrombopoietin (rhTPO, 100 ng/mL), stem cell factor (100 ng/mL) and FLT3 ligand (100 ng/mL). For donors 4-10, we used stem span with rhSCF (10 ng/mL), rhTPO (20 ng/mL), mIGF-2 (20 ng/mL) and rhFGF (10 ng/mL). On day 3 of the barcoding procedure, cells were counted, the % of GFP-positive cells was measured by flow cytometry and cells were transplanted into sublethally irradiated NSG mice. Human chimerism was monitored by flow cytometry for human CD45, CD19, CD3, CD16 and GFP. Barcode analysis was performed by PCR and deep sequencing in blood at several time points during the experiment, and in bone marrow at sacrifice.

Deep sequencing

Genomic DNA was isolated from leukemia cell samples using the REDExtract-N-Amp Tissue PCR kit (Sigma-Aldrich), followed by a clean-up step using the Nucleospin Plasma XS kit (BioKe, Macherey Nagel), according to the manufacturer's instructions. Barcode sequences were amplified in a 35-cycle PCR reaction using uniquely indexed eGFP forward primers and a WPRE reverse primer (5' GGAGAAAATGAAAGCCATACGGGAAGC 3'). Subsequently, samples were combined into pools of 200-400 samples, which were sent for next generation sequencing on an Illumina HiSEQ 2500 Platform (BaseClear, Leiden, The Netherlands).

Barcode data processing and analysis

Data extraction was performed using in-house scripts as previously described >. In short, high-quality reads were extracted and compressed into sets of unique sequences. Sequences were assigned to a sample based on exact matching the primer tag. Barcode sequences were extracted using Motif Occurrence Detection Suite (MOODS). Read frequencies of barcodes pairs varying by a single nucleotide were merged, assuming that these are more likely sequencing errors than truly unique barcodes. Samples from the same experiment were joined into one table. Low frequency barcodes (<0.5% of all reads) or barcodes that were observed <2 times were excluded from the analysis. Samples with <500 reads were excluded from the analysis.

Random sampling model

To validate and quantify our assumptions on clonal survival, we designed an *in silico* model for clonal sampling using a simple python script (figure S7). First, we generated a list of random characters, with defined diversity corresponding to the number of barcodes in the library, and with excessive repetition of certain characters, representing stem cells carrying the same barcode. From this list, we performed random subsampling and tested the resulting list for frequency and relative size of each character (representing barcode frequency and size). Parameters of this model (barcode diversity, hypothetical clone size, subsampling degree) were adjusted to match experimental details.

Estimation of stochasticity and determinism

The Spearman rank index was used to compare samples and to quantify stochasticity and determinism in clonal selection. If the order of barcoded clones in sample B (sorted by size) can be predicted by the order in sample A, this results in a high Spearman index, which indicates a high degree of determinism and low stochasticity. In contrast, a low Spearman rank index (scipy.stats.spearmanr) between two biologically related samples indicates a low degree of determinism and high degree of stochasticity. Euclidean dis-

tance (scipy.spatial.distance.euclidean) was used for the quantification of stochasticity and determinism and distribution while taking into account clone sizes as well.

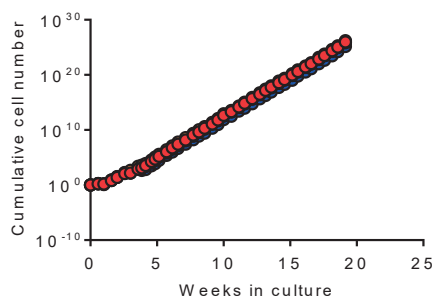### General statistical analysis

Differences of normally distributed variables (survival, spleen size, number of clones in bone marrow) were tested using the Student's T-test (two groups) or by one-way ANOVA with post-hoc Bonferroni correction (multiple groups). The number of barcodes within a sample was expressed as the Shannon diversity index, as previously described[1,3,>].The correlation between barcode library size and the number of barcodes retrieved in deep sequencing results was analyzed by Spearman correlation. Similarity between clonal composition in different samples was analyzed using Euclidean distance. Statistical analyses were performed in GraphPad Prism (La Jolla, CA, USA). Statistical significance was defined as $P<0.05$.

References

1. Gerrits A, Dykstra B, Kalmykowa OJ, et al. Cellular barcoding tool for clonal analysis in the hematopoietic system. *Blood*. 2010;115(13):2610-2618. doi:10.1182/blood-2009-06-229757; 10.1182/blood-2009-06-229757.

2. Verovskaya E, Broekhuis MJC, Zwart E, et al. Heterogeneity of young and aged murine hematopoietic stem cells revealed by quantitative clonal analysis using cellular barcoding. *Blood*. 2013;122(4):523-532. doi:10.1182/blood-2013-01-481135.

3. Bystrykh L V, Belderbos ME. Clonal Analysis of Cells with Cellular Barcoding: When Numbers and Sizes Matter. *Methods Mol Biol*. April 2016. doi:10.1007/7651_2016_343.

4. Bystrykh L V, Verovskaya E, Zwart E, Broekhuis M, de Haan G. Counting stem cells: methodological constraints. *Nat Methods*. 2012;9(6):567-574. doi:10.1038/nmeth.2043; 10.1038/nmeth.2043.

File S2: Growth curve of barcoded SupB15 cells *in vitro*.

Barcoded SupB15 cells were cultured in three parallel cultures for 20 weeks (41 passages). Twice weekly, cells were counted and 1×10^6 cells was used to initiate the next culture. Dots represent the cumulative cell number at each time point. Different colours are used to depict different parallel cultures.

File S3: Experimental details for patient-derived xenografts.

Sample	No. of viable cells (10⁶)			Transduction %	Cell dose/mouse transplanted (10⁶)	No. of mice transplanted	Engraftment	No. of viable cells (10⁶)		Transduction %	Cell dose/mouse transplanted (10⁶)	No. of mice transplanted	Engraftment
		Primary barcoding attempt							Secondary barcoding attempt				
	Frozen in vial	*Thawed (day 0)*	*After barcoding (day 3)*					*Used for barcoding (day 0)*	*After barcoding (day 3)*				
ALL-45	100	75	40	33	25000-2500000	6	No	n/a	n/a	n/a	n/a	n/a	n/a
ALL-58.1	100	80	67	0	2500000	3	Yes	100	23	0.4	35000	3	Yes
ALL-58.2	100	80	67	0	2500000	3	Yes	100	50	2.5	400000	3	Yes
ALL-70	100	100	86	1	14000-140000	4	Yes	n/a	n/a	n/a	n/a	n/a	n/a
ALL-78	67	53	<10	0	2500000	2	Yes	100	<10	0	n/a	n/a	n/a
ALL-79	100	75	<10	0	2500000	2	No	n/a	n/a	n/a	n/a	n/a	n/a
ALL-80*	67	1,0	n/a	0	450000	2	No	n/a	n/a	n/a	n/a	n/a	n/a

* For sample ALL-80, due to a low number of viable cells retrieved upon thawing, no primary barcoding attempt was performed, and all cells were used for xenotransplantation.

n/a: not applicable.

File S4: Experimental design for clonal analysis of patient-derived leukemia (detailed).

Diagnostic bone marrow cells from pediatric patients with acute lymphoblastic leukemia were serially transplanted into immune deficient NSG mice. Each rectangle represents an individual mouse. White rectangles represent mice that were transplanted with un-barcoded leukemia cells; grey rectangles represent mice that did not develop leukemia. Experimental details for each serial transplantation are shown in the table.
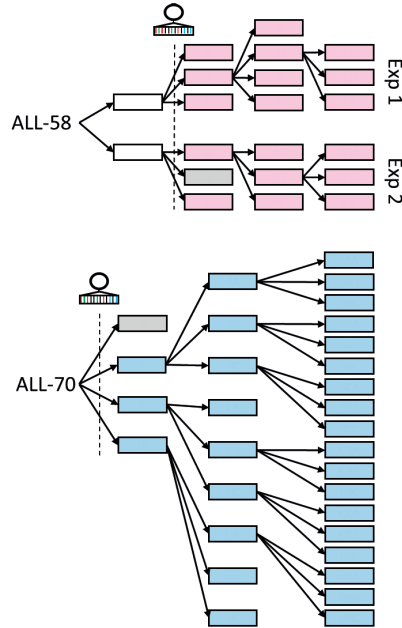

Patient sample	Experiment	Serial Tx	Cell dose /mouse	Mice transplanted (n)	Mice engrafted (n)
ALL-58	1	1	35.000	3	3
ALL-58	1	2	400.000	4	4
ALL-58	1	3	400.000	3	3
ALL-58	2	1	400.000	3	2
ALL-58	2	2	1.200.000	3	3
ALL-58	2	3	1.200.000	3	3
ALL-70	n/a	1	14.000	2	1
ALL-70	n/a	1	140.000	2	2
ALL-70	n/a	2	2.500.000	9	9
ALL-70	n/a	3	2.500.000	15	15

File S5: Flow cytometric detection of human leukemia in mouse blood.

Human leukemia cells in mouse blood and tissues were detected by flow cytometry. Cells were stained using the following antibodies: CD10-BV605 (clone HI10a), CD19-PE (clone HIB19), CD20-BV421 (clone 2H7), CD34-APC (clone 8G12) and CD45 PECy7 (clone HI30). Propidium iodide was used to exclude dead cells. Potential chimerism with human

non-leukemic cells was analyzed using antibodies against CD3-APC (clone UCHT1) and CD16-BV421 (clone 3G8). The anti-CD34 antibody was obtained from EBioscience (San Diego, CA, USA), all others were from Biolegend (San Diego, CA, USA). To validate this approach, primary B-ALL cells were titrated in mouse blood at increasing percentages and subsequently used for flow cytometry. The correlation between spiked B-ALL cells and % of human cells was determined using Spearman correlation.
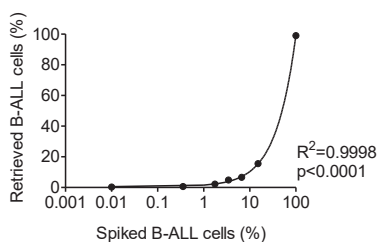
File S6: Dynamics of GFP$^+$ cells within the population of CD45$^+$ cells.

Patient-derived leukemia cells were barcoded, sorted for GFP at a sorting purity of >99% and transplanted into immune deficient NSG mice. Human leukemia cells in mouse blood and tissues were detected by flow cytometry for human CD19, CD45, CD10, CD20 and CD45.

Despite high sorting efficiency, some mice were partially repopulated with GFP$^-$ cells. These may result from promotor silencing and/or from outgrowth of cells which did not integrate the vector (either rare GFP-negative cells which were wrongly sorted, or cells in which GFP was originally expressed from the viral cDNA and which did not integrate into the host cell genome). Note that GFP-expression does not affect barcode analysis, which depends on the presence of the vector in the genomic DNA, rather than its expression.
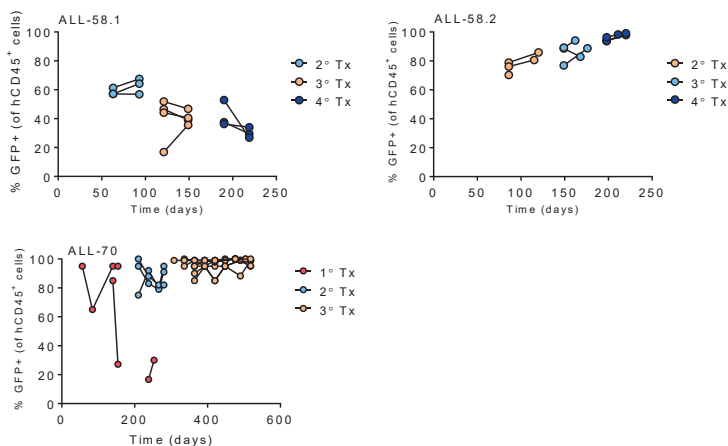
File S7: *In silico* model for clonal sampling.

An *in silico* model for clone sampling was designed using python script, to validate the observed clonal dynamics in our experiments. First, we generated a list of random characters. The diversity of characters corresponds to the number of barcodes in the library/sample, the repetition of each character to the relative size of the barcode within the sample. From this list, we performed random subsampling and tested the resulting list for frequency and size of each number (representing barcode frequency and size). Parameters of this model (barcode diversity, hypothetical clone size, subsampling degree) were compared with and adjusted to match experimental details (see below).
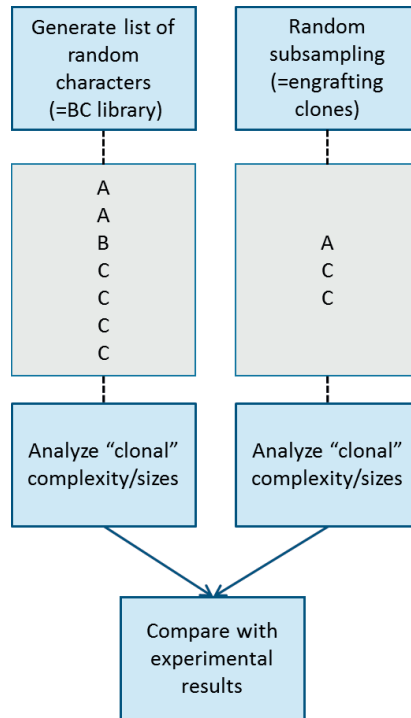
Detailed explanation of model and parameters

SupB15 cell line xenografts

Barcoded SupB15 cells were transplanted into sublethally irradiated NSG mice (2.5×10^6 cells/mouse). Barcode analysis showed a maximum barcode complexity in spine of ~200 barcodes.

Question: What is the fraction of surviving cells (survival rate) explaining such a barcode reduction upon transplantation?

Methods: Random sampling model in python. Parameters:

– Initial barcodes: 800 (=library complexity)
– Initial barcode frequency: ~3000 (=number of cells per barcode)
– Final barcode frequency: 200 (=engrafting clones)

Subsampling rate=Initial barcodes * Initial BC frequency / Fold reduction

Results: A 2-fold reduction results in a final barcode frequency of ~200. Accordingly, the net survival rate upon transplantation was ~1:5000.

Serial transplantation of patient-derived leukemia

Patient-derived leukemia cells were serially transplanted into sublethally irradiated NSG mice. For example, in 58.2, barcode complexity decreased from ~150 in primary recipients to ~10 in secondary and tertiary recipients.

Question: What is the fraction of surviving cells explaining such a barcode reduction upon serial transplantation?

Model parameters:

– Initial barcodes: 100 (=primary recipient)
– Initial barcode frequency: 10
– Final barcode frequency: 10 (=secondary recipient)

Subsampling rate=Initial barcodes * Initial BC frequency / Fold reduction

Results: A 100-fold reduction results in a final barcode frequency of ~8-10. Accordingly, the net survival rate upon transplantation is one in 100.

Of note: The initial barcode frequency, representing the number of LSC carrying the same barcode, is unknown. If we reduced this number to 4 (2 symmetrical LSC cell divisions), the survival rate was one in 20.

File S8: Human chimerism and survival in xenografts of unbarcoded cells and xenografts of barcoded cells.

Depicted are serial xenografts of ALL-58.2. (A) Human chimerism in blood, determined by flow cytometry for human CD45^{+} cells among the total population of PBMC. Connected dots represent individual mice. (B) Survival of serial xenografts of ALL 58.2. Each dot represents one individual mouse.
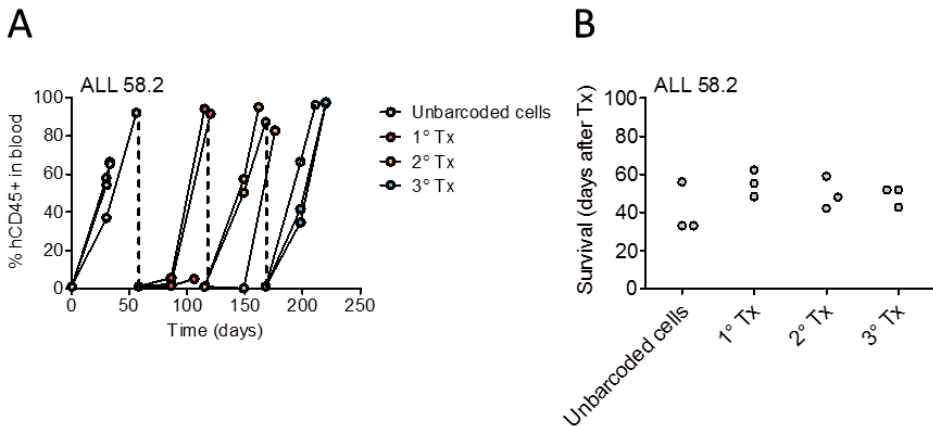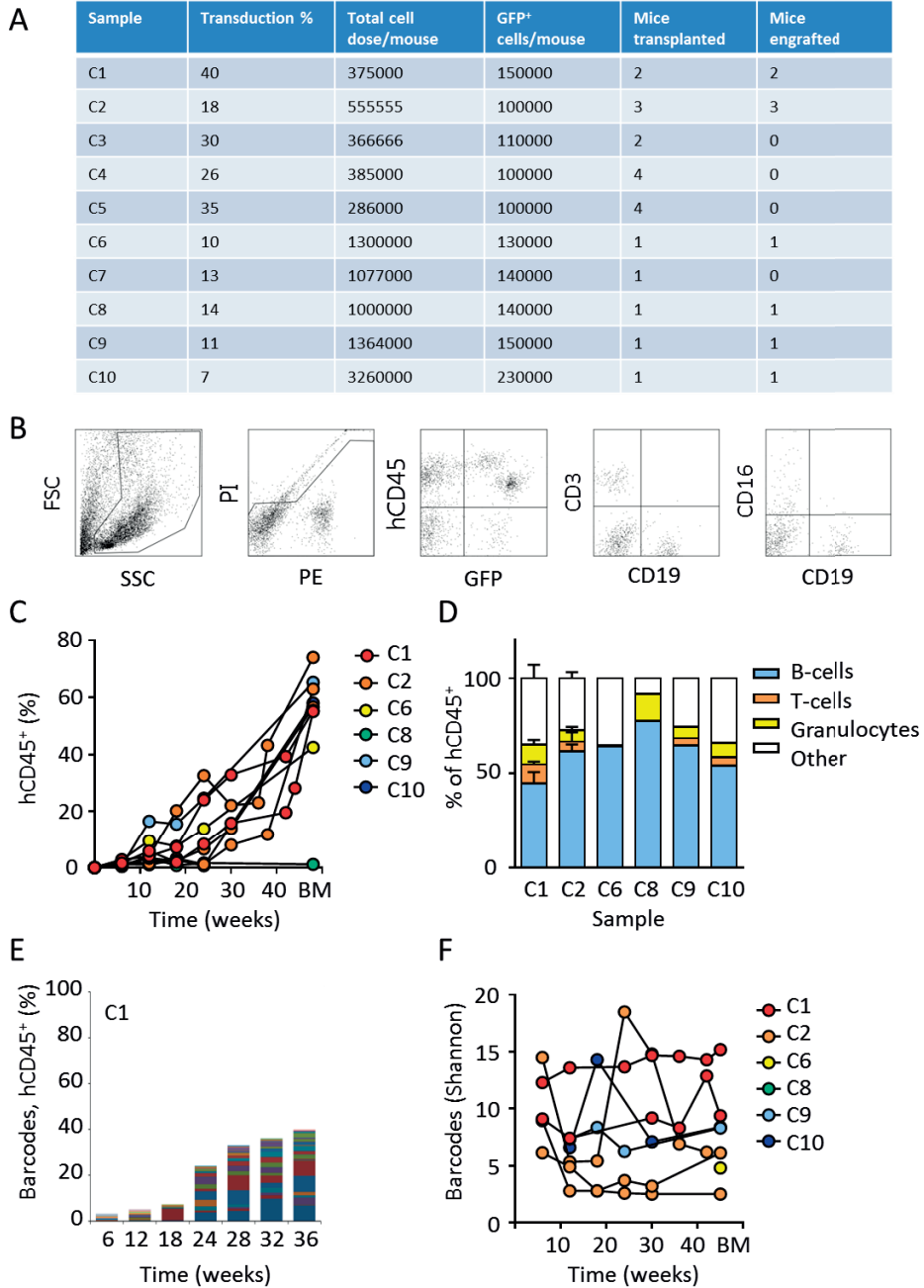

File S9: Barcode composition of patient-derived leukemia samples prior to xenotransplantation.

Barcode composition was determined by PCR and deep sequencing. Each colored bar represents one individual barcode. The numbers above the bars represent the Shannon approximation for the number of barcodes within each sample.
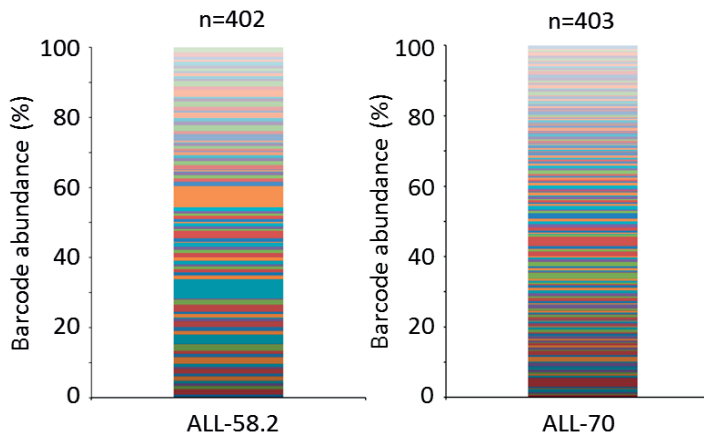
File S10: Clonal analysis of non-leukemic hematopoiesis in murine xenografts.

(A) CD34$^+$ hematopoietic progenitor cells (HPC) were isolated from umbilical cord blood of 10 individual donors by Ficoll gradient centrifugation and subsequent positive selection using CD34-beads. CD34$^+$ cells were barcoded and transplanted in bulk (GFP$^+$ and GFP$^-$) into sublethally irradiated NSG mice. (B) Human chimerism was determined by flow cytometry and defined as the %hCD45$^+$ cells of the total live population. Human B-cells were defined as hCD45$^+$/hDC19$^+$, T-cells as hCD45$^+$/hCD3$^+$, and granulocytes as hCD45$^+$/CD16$^+$. (C) Human chimerism, defined as the %hCD45$^+$ cells within the total PBMC population. Each line represents an individual mouse. (D) Bone marrow composition, determined by flow cytometry, of xenografts at sacrifice. Each bar represents the average (+SEM) of mice transplanted with the same cord blood donor. (E-F) Barcode composition of a representative mouse (E) and all mice (F), determined by PCR and deep sequencing.

File S11: Barcode complexity in serial xenografts of patient samples 58.1 and 58.2.

Diagnostic patient-derived leukemia cells were serially transplanted into immune deficient NSG mice and barcode composition in bone marrow (panels A and C) and blood (panels B and D) was determined by PCR and deep sequencing. (A and C) Barcode composition in spine bone marrow of serial xenografts. Each pie chart represents one recipient, each color represents one barcode. Arrows are used to connect each donor to its serial recipients. (B and D) Barcode complexity in blood serial xenografts. Each time point represents the average +/- SEM of three mice.
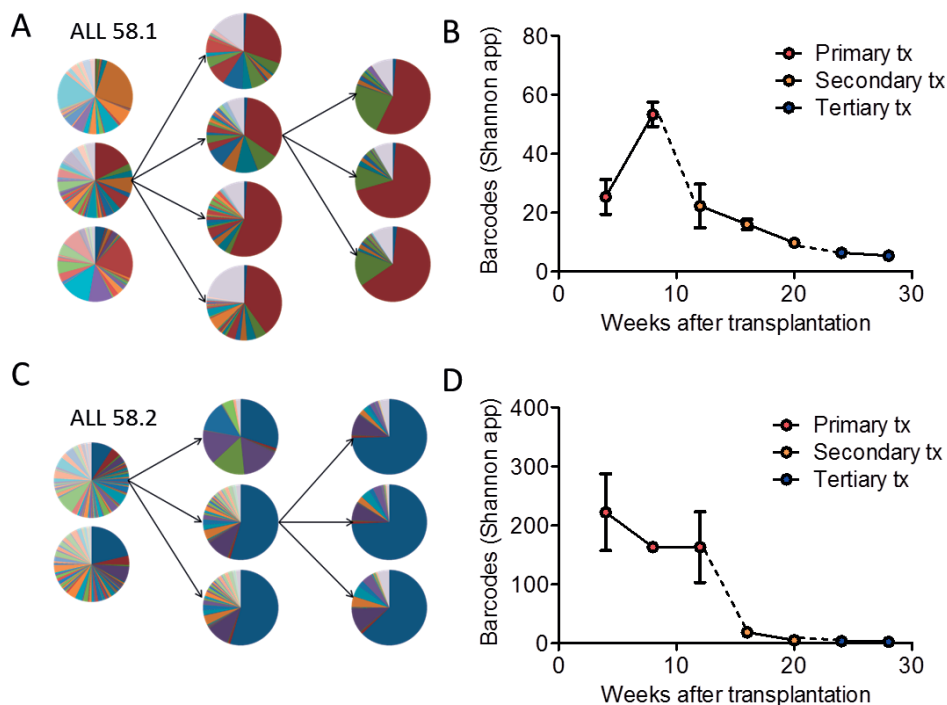
File S12: Clustering analysis of serial xenografts of patient sample ALL-70.

Hierarchical clustering based on barcode composition at sacrifice (average of bone marrow, spleen and liver) was performed using Euclidean distance as a measure of (dis)similarity. Each rectangle represents one mouse. Individual colors represent mice transplanted from the same donor. Numbers reflect the serial transplant (i.e. "1" is a primary recipient; "2" is a secondary recipient, etc.).
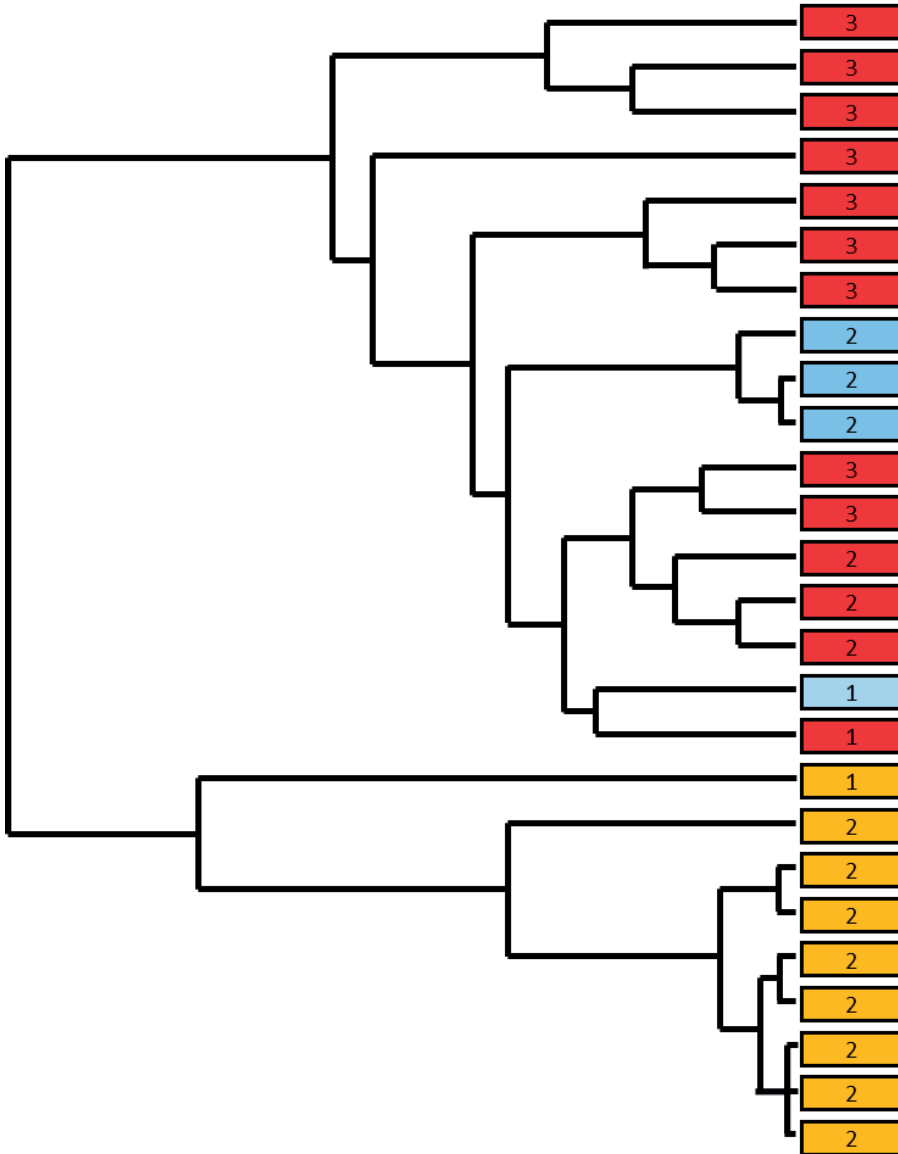
File S13: Quantitative analysis of skeletal asymmetry.

(A) Segmented pie charts for selected serial xenografts of patient sample 70. Each pie chart represents one mouse, each segment represents one anatomical location. Colors within segments represent individual barcode clones and their relative abundance. (B) Top panel: Bar graph representing barcode composition in the same mouse as in panel A. Bottom graph: Euclidean distance in barcode composition between different anatomic locations. From this, we extracted three types of distances: (1) distances between two extramedullary sites; (2) distances between an extramedullary site and a skeletal location; and (3) distances between two skeletal locations. (C) Scatter plot of euclidean distance per group, as identified in panel B.
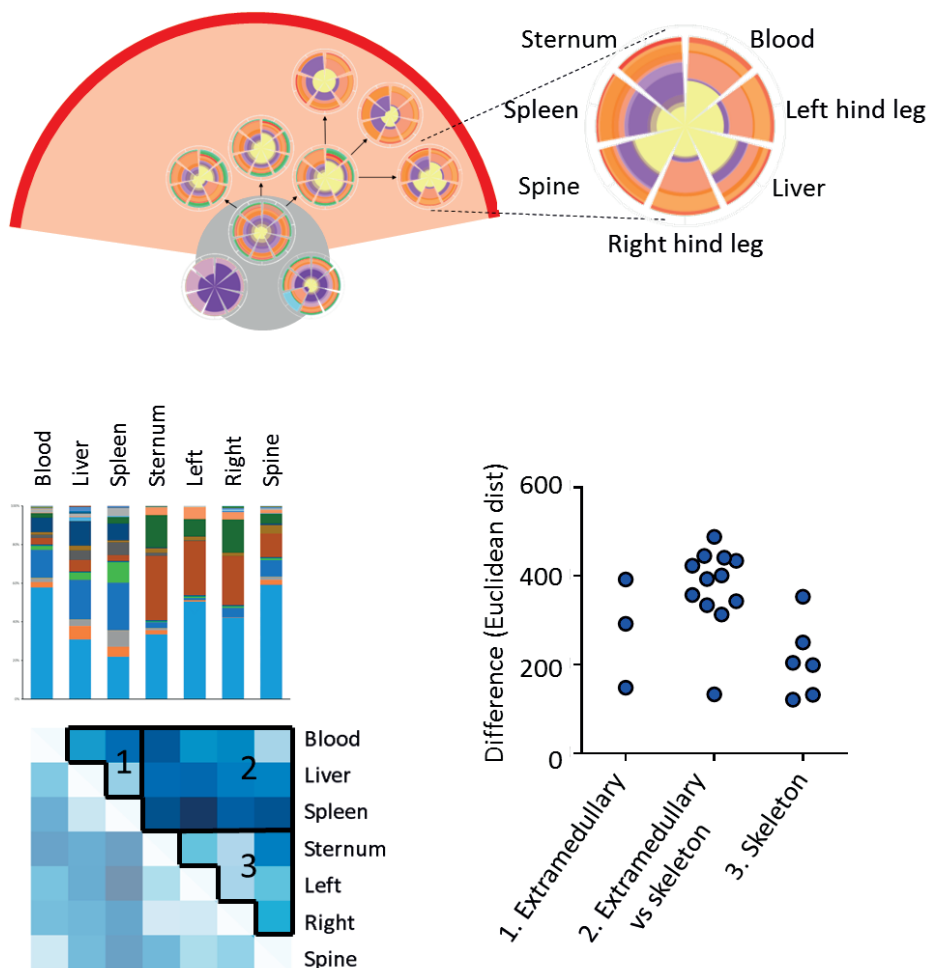
File S14: Asymmetric distribution of patient-derived leukemia clones in murine xenografts.

Barcode composition in different skeletal locations was compared using the Spearman coefficient and Euclidean distance, as explained in file S13. Each dot represents one comparison; colors are used to highlight individual mice. *; p<0.05, **; p<0.01.
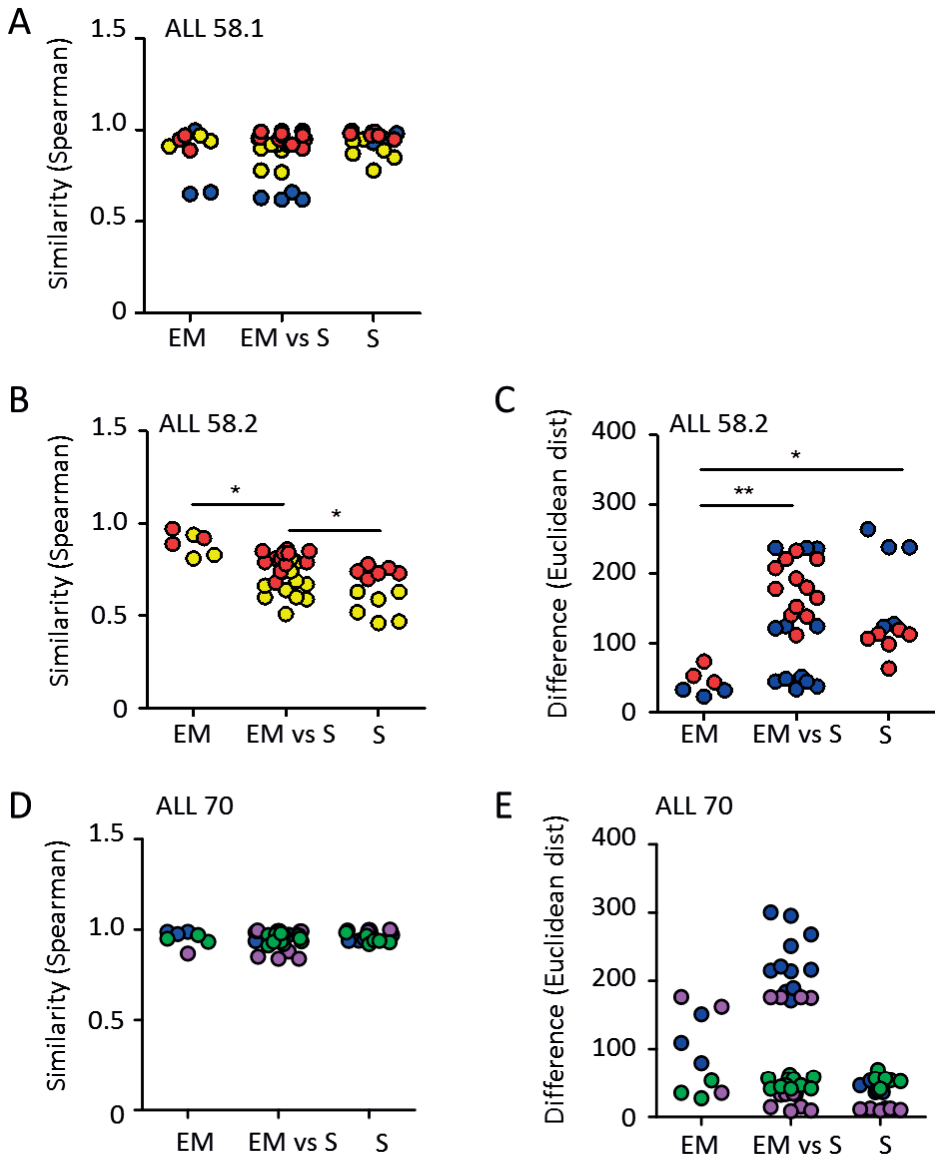
Chapter 4

Quantitative distribution of patient-derived leukemia clones in murine xenografts revealed by cellular barcodes

Sabrina Jacobs, Albertina Ausema, Erik Zwart, Ellen Weersing, Maaike J. Kingma, Yasmine A.S. El Menshawi, Gerald de Haan, Leonid V. Bystrykh and Mirjam E. Belderbos

To the editor,

Relapse affects ~10% of children diagnosed with acute lymphoblastic leukemia (ALL), and is the leading cause of cancer-related mortality in children, urging for novel diagnostic and therapeutic strategies(1–3). ALL is genetically heterogeneous, consisting of multiple clones with distinct genomic aberrations, which may alter essential cell functions (e.g. proliferation, differentiation or chemotherapeutic sensitivity)(4). Furthermore, spatial heterogeneity (i.e. diversity in the localization of ALL clones) may contribute to disease progression(5). In solid tumors, it is commonly accepted that malignant cells first proliferate at the site of origin, and only later metastasize to distant sites. Here, they may undergo further clonal selection and evolution, resulting in genomic differences between the primary tumor and its metastases(6–8). In contrast, although progenitor B-cell ALL (B-ALL) is thought to originate in the bone marrow, its exact site of origin and patterns of migration are unknown. Previously, we and others found that patient-derived B-ALL clones are asymmetrically distributed in murine xenografts(5,9). This skeletal asymmetry is relevant both from a biologic and clinical perspective, as it implies that sampling of a single site may not fully reflect the total body clonal composition, allowing for certain clones to remain undetected. However, as these previous studies only sampled a limited number of anatomic sites and did not include quantitative analysis, the quantitative distribution of leukemia clones across the total body is unknown. To assess the quantitative distribution of leukemia clones, we transplanted barcoded patient-derived B-ALL cells in Nod/SCID/IL2Rγ$^{-/-}$ (NSG) mice and determined the leukemia cell content and barcode complexity in individual anatomical locations during different stages of disease (supplementary methods).

In total, serially transplanted barcoded leukemia cells of three (out of five) patient samples engrafted successfully in 28 recipients (supplementary table 1). Using a quantitative method for leukemia-cell detection (figure 1A, supplementary figure 1A-B), we showed that at end-stage leukemia, the total murine xenograft harbored $260x10^6 \pm 115x10^6$ human leukemia cells (mean ± SD of ALL-16, ALL-17 and ALL-19; supplementary figure 2A-C). Of these, 60%±15% were located in the bone marrow and 40%±15% in extramedullary locations. The leukemia cell content (i.e. the absolute number of leukemia cells) was highly variable between anatomic locations (figure 1B, supplementary figure 2D-E), with the consistent observation that the majority of leukemia cells were located in the spine (median: 25%, IQR: 20-30%) and spleen (median: 30%, IQR: 20-40%; figure 1C, supplementary figure 2F-G). On the contrary, the blood and pelvis – locations that are routinely sampled for clinical diagnosis and follow-up – only contained a median of respectively 0.06% (IQR: 0.03-0.2%) and 9% (IQR: 8-11%) of the total body leukemia cell content.

We noted that the leukemia cell content in the same bone marrow location was markedly similar across patient samples and xenografts (figure 1B, supplementary figure 2D-E). For example, the femur consistently contained $20x10^6$ leukemia cells (median
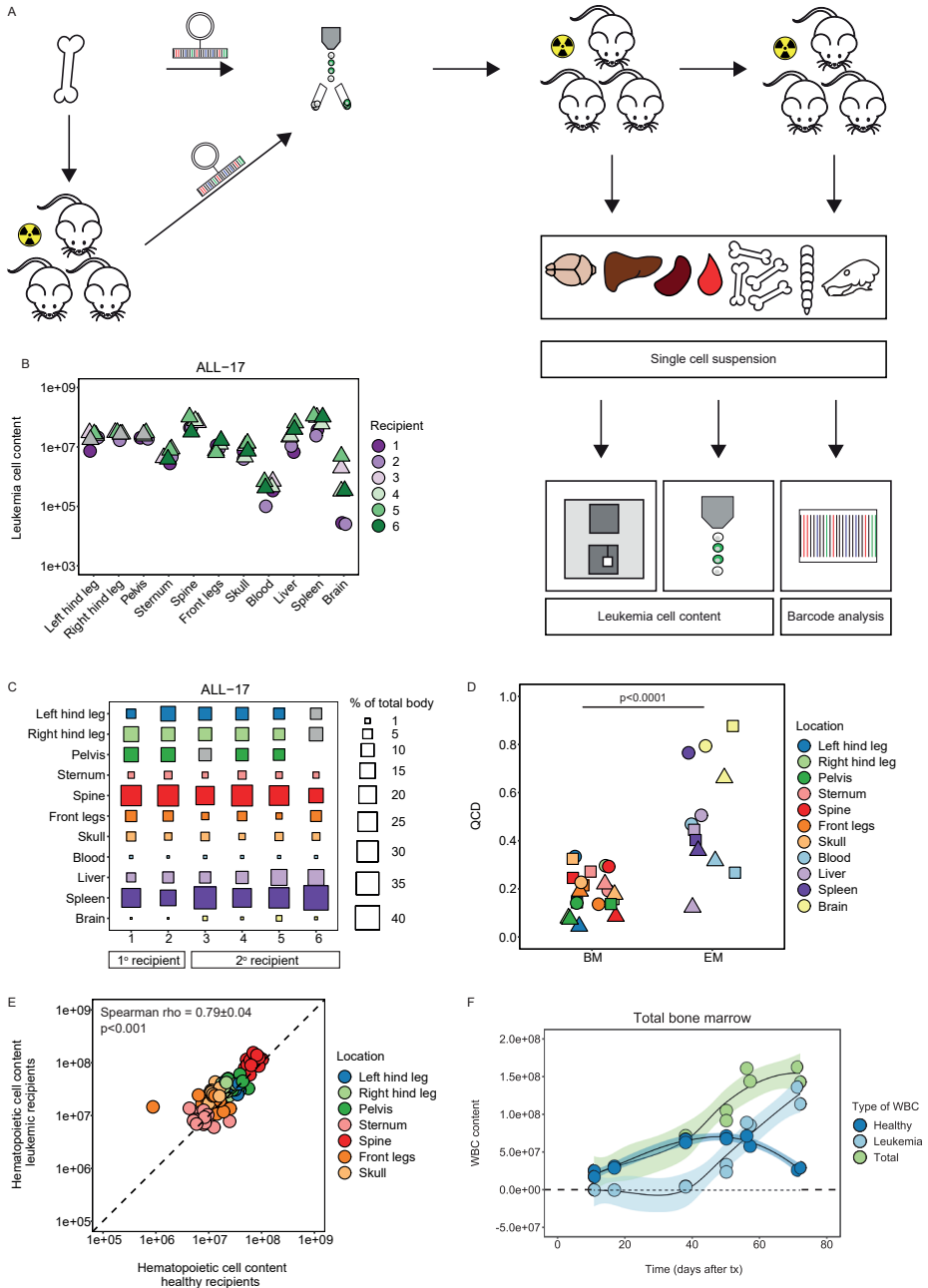
← Figure 1. The distribution of the leukemia cell content in murine xenografts was proportional to and limited by the compartment size
(A) Experimental design to quantify the leukemia cell content using the multiple platform method. Patient-derived bone marrow cells were – directly or derived from primografts – barcoded. Barcoded leukemia cells were sorted for GFP and transplanted into sublethally irradiated NSG mice. ALL-16 and ALL-17 were serially transplanted. Individual locations were analyzed for leukemia cell content and barcode composition. This multiple platform approach combines the absolute cell concentration (hematology analyzer) and cell population frequency (flow cytometry) to determine the leukemia cell content. (B) The leukemia cell content in the individual locations of murine xenografts transplanted with ALL-17. Symbols refer to primary (circle) and secondary (triangle) recipients. (C) The relative contribution of each anatomical location to the total body leukemia cell content. Grey squares; pelvis of recipient 3 was not sampled and is the average of recipient 4 and 5; hind legs of recipient 6 were analyzed together with pelvis. (D) QCD value as measurement of variability across the xenografts per individual location per patient sample (n=3). QCD values were grouped by bone marrow and extramedullary sites. Each symbol represents a patient sample: ALL-16 (circle), ALL-17 (square) and ALL-19 (triangle). Statistical analysis: two-sided Mann-Whitney U test. (E) The correlation between the number of hematopoietic cells in the bone marrow of leukemic (n=16) and healthy (n=4) NSG mice. Hereto, we used a random-comparison model which randomly assigned one out of the four healthy mice to one out of the sixteen leukemic mice to calculate the correlation (n=1000 random comparisons). Data expressed as mean ± SD. (F) The absolute number of WBCs in the total bone marrow of leukemic mice during disease progression. Distinctions were made between leukemic cells (light blue), healthy murine WBCs (dark blue) and the total number of WBCs (light green). Every dot represents a mouse. Smoothing method 'loess' with confidence interval set at 95%. Abbreviations: bone marrow (BM), extramedullary (EM).

of ALL-16, ALL-17 and ALL-19; IQR: 10-30x10^6). In contrast, the leukemia cell content in extramedullary locations was more variable. This variability was quantified by the quartile coefficient of dispersion (QCD), which was significantly lower in bone marrow locations (median: 0.20, IQR: 0.15-0.25) compared to extramedullary sites (median: 0.45; IQR: 0.35-0.70, p<0.0001, figure 1D). These data indicate that the leukemia cell content in distinct bone marrow sites at end-stage disease is highly predictable, whereas the content in extramedullary sites is more variable.

To address whether the carrying capacity of the bone dictates its leukemia cell content, we compared the number of hematopoietic cells and LSK-SLAM cells in bones of healthy NSG mice to that of mice transplanted with leukemia cells. In total, healthy mice harbored a median of 175x10^6 (IQR: 165x10^6-195x10^6) hematopoietic cells in their bone marrow (supplementary figure 3A). The distribution of these cells across the different bone marrow locations was markedly comparable to the distribution of leukemia cells (supplementary figure 3B). We found a correlation of 0.79±0.04 between the hematopoietic cell distribution in leukemic and healthy mice (Spearman rho, p<0.001, figure 1E). Similar observations were made when assessing the more stringently defined population of LSK-SLAM cells (Spearman rho: 0.62±0.03, p<0.001, supplementary figure 3C-E).

If the size of the bone indeed dictates its leukemia cell content, one might postulate that saturation occurs during disease progression. Hereto, we assessed the leukemia

cell content across the murine skeleton over time (supplementary figure 4.1A). We demonstrate that the total white blood cell (WBC) content in bone marrow of leukemic mice reached a plateau of ~150x10^6 cells (range 140-160x10^6, figure 1F) from 56 days after transplantation. This plateau was primarily due to loss of healthy WBCs throughout disease progression, whereas the leukemia cell content continued to increase over time. Similar patterns were observed when bone marrow locations were analyzed separately (supplementary figure 4.2A-G). In parallel, we observed an exponential increase in the number of splenic leukemia cells, and weight of the spleen (supplementary figure 4.1B-D). Even at late stages of disease, no plateau was reached. Together, this suggests that the size of the bone restricts its leukemia cell content, resulting in competitive loss of healthy WBCs and migration of leukemic blasts to extramedullary sites.

Next, we asked whether bones with a higher leukemia cell content also contained more clones. If so, this would imply that larger locations (by chance) would be more likely to harbor relapsing clones. Similar to our previous work, cellular barcoding revealed that patient-derived leukemia clones were asymmetrically distributed across the bone marrow locations, whereas their distribution was more homogeneous across extramedullary sites (figure 2A-B, supplementary figure 5.1A-F)(5). Notably, in contrast to the marked variation in the leukemia cell content between small and large bones (figure 1B, supplementary figure 2D-E), the number of barcodes varied only marginally across locations (supplementary figure 5.2A-C). In larger bones (e.g. spine), barcodes were generally larger, whereas smaller bones (e.g. sternum), generally contained smaller barcodes (supplementary figure 5.3A-D). Furthermore, we observed that barcodes, which were small in the overall murine xenograft, were located in a single location (supplementary figure 5.3E-H), whereas larger barcodes were often present in multiple sites. Upon serial transplantation of ALL-17, the number of leukemia clones was reduced by ~40% (supplementary figure 5.4A-B), and their distribution was more homogeneous compared to the primary recipients (confirmed by the Spearman rank analysis, supplementary figure 5.4A,C). These data once more suggest that bone size may be an important determinant of leukemic cell content and growth.

As single-site sampling is common practice in the clinic and experimental studies(10–12), we assessed to what extent blood and pelvis reflect the overall barcode complexity. At sacrifice, 40-60% of the total body leukemia clones were detected in blood, whereas the remainder stayed undetected (figure 2C, supplementary figure 5.5A-C). Detectable barcodes in the blood had an overall frequency that was significantly higher than those that remained undetected (p<0.0001, figure 2D, supplementary figure 5.6A-C). Of the undetected barcodes, 13-53% were detectable in blood samples drawn prior to sacrifice (supplementary figure 5.7A-F), and 20-45% of the barcodes were never seen in blood at any measured time point. Assessment of the pelvis showed similar results (figure 2E, supplementary figure 5.5A-C, 5.6D-F). Furthermore, combined analysis

of both locations only covered 53-66% of the total body leukemia barcodes (figure 2C, supplementary figure 5.5A-C). These data indicate that single-site sampling results in an underestimation of the clonal complexity of the disease. As each site contains unique clones (figure 2A-B, supplementary figure 5.1A-F), one would need to sample every location to fully capture the total clonal complexity.
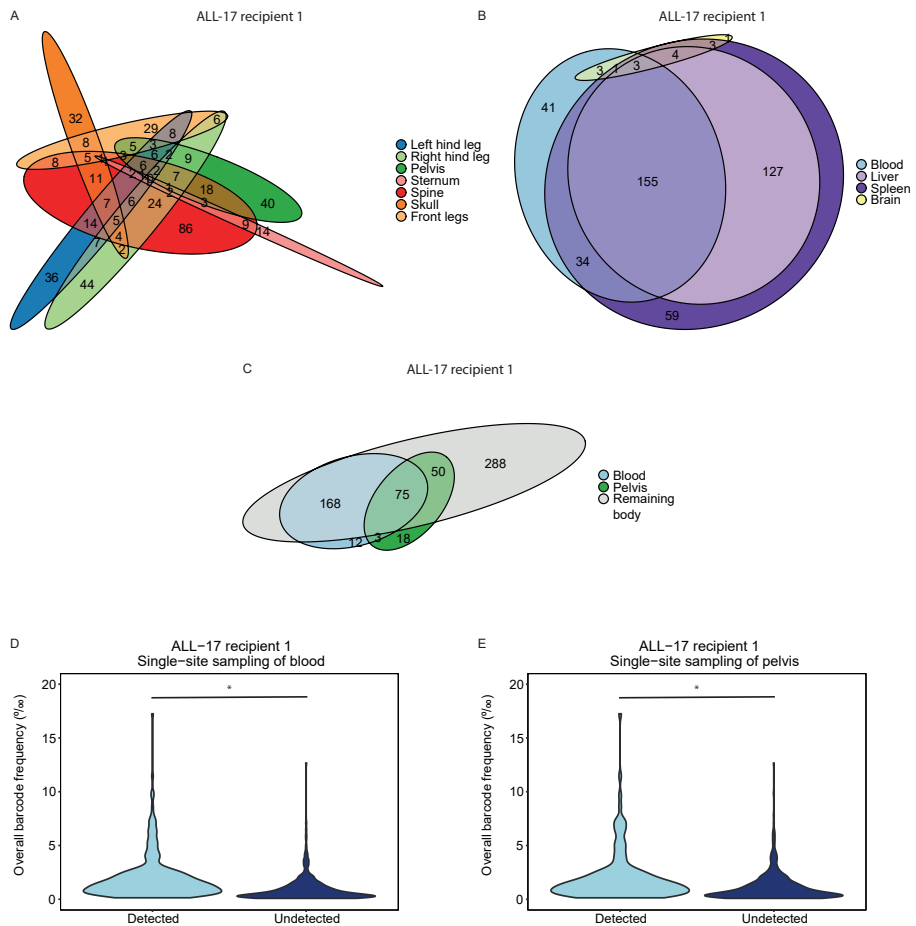
Figure 2. Single-site sampling results in underestimation of total-body leukemia clonal complexity

(A-B) Number of (non-)overlapping barcodes in the bone marrow and extramedullary locations. Barcode analysis was restricted to the top 85% most abundant barcodes to prevent false-positive barcode calling. (C) Number of (non-)overlapping barcodes from the top 85% most abundant barcodes in the blood, pelvis and remaining body. (D-E) Overall barcode frequency of the top 85% most abundant barcodes that are detected or remain undetected when blood or pelvis was sampled at end-stage leukemia (one representative recipient). Statistical analysis: two-sided Mann-Whitney U test, * p<0.0001.

To summarize, we demonstrate that, at end-stage disease, murine xenografts harbor millions of human leukemia cells, with ~10% localized in blood and pelvis. Leukemia cells are derived from hundreds of leukemia-propagating cells (LPCs), which are asymmetrically distributed across skeletal sites(5,9). Accordingly, sampling of a single-site allows for half of the LPC clones to remain undetected. Therefore, multi-site sampling of xenografts will increase the yield of cells for experimental analysis and provide a more in-depth view of the clonal heterogeneity.

These observations are in apparent contrast with clonal analysis of immunoglobulin heavy chain (IgH) rearrangements in patients, which report a symmetric distribution with >80% of IgH clones present in blood and two bone marrow sites(13). This discrepancy may be due to the choice of marker, as one IgH clone can be represented by multiple LPCs. Furthermore, the observed level of (a)symmetry may depend on the number and type of sites sampled. Although murine xenografts lack human niche factors, and may be subject to transplantation-induced clonal selection(5,14), they provide the unique advantage of allowing sampling of nearly every cell in a given location, and nearly every location in the murine body. Last, we previously showed that the degree of asymmetry depends on the number of LPCs, with more asymmetry when fewer LPCs are present(15). This may suggest that failure to detect a relapsing clone in clinical patients may not be due to its presence below detection limits of current tests, but to its presence in a non-sampled location. Future studies in chemotherapy-treated xenografts and/or clinical patients will be needed to determine whether treatment impacts on clonal asymmetry, and whether multi-site sampling improves diagnostics, monitoring and treatment-decisions of patients with ALL.

ACKNOWLEDGMENTS

FINANCIAL DISCLOSURE STATEMENT

AUTHORSHIP AND CONFLICT-OF-INTEREST STATEMENTS

MB, SJ, GdH and LB designed the research. MB, SJ, AA, EW, YEM and MK performed the research. SJ, MB, EZ and LB analyzed the data. SJ, MB, GdH and LB wrote the manuscript.

None of the authors have any conflict of interest to declare.

REFERENCES

1. van den Berg H, de Groot-Kruseman HA, Damen-Korbijn CM, de Bont ESJ., Schouten-van Meeteren AYN, Hoogerbrugge PM. Outcome after first relapse in children with acute lymphoblastic leukemia: A report based on the Dutch Childhood Oncology Group (DCOG) relapse all 98 protocol. Pediatr Blood Cancer [Internet]. 2011 Aug 1;57(2):210–6. Available from: https://doi.org/10.1002/pbc.22946

2. Pieters R, de Groot-Kruseman H, Van der Velden V, Fiocco M, van den Berg H, de Bont E, et al. Successful Therapy Reduction and Intensification for Childhood Acute Lymphoblastic Leukemia Based on Minimal Residual Disease Monitoring: Study ALL10 From the Dutch Childhood Oncology Group. J Clin Oncol [Internet]. 2016 Jun 6;34(22):2591–601. Available from: https://doi.org/10.1200/JCO.2015.64.6364

3. Bhojwani D, Pui C-H. Relapsed childhood acute lymphoblastic leukaemia. Lancet Oncol [Internet]. 2013 May;14(6):e205–17. Available from: https://doi.org/10.1016/S1470-2045(12)70580-6

4. Loh ML, Mullighan CG. Advances in the Genetics of High-Risk Childhood B-Progenitor Acute Lymphoblastic Leukemia and Juvenile Myelomonocytic Leukemia: Implications for Therapy. Clin Cancer Res [Internet]. 2012 May 15;18(10):2754–67. Available from: http://clincancerres.aacrjournals.org/cgi/doi/10.1158/1078-0432.CCR-11-1936

5. Belderbos ME, Koster T, Ausema B, Jacobs S, Sowdagar S, Zwart E, et al. Clonal selection and asymmetric distribution of human leukemia in murine xenografts revealed by cellular barcoding. Blood [Internet]. 2017 Jun 15;129(24):3210 LP – 3220. Available from: https://doi.org/10.1182/blood-2016-12-758250

6. Turajlic S, Swanton C. Metastasis as an evolutionary process. Science (80-) [Internet]. 2016 Apr 8;352(6282):169–75. Available from: http://www.sciencemag.org/cgi/doi/10.1126/science.aaf2784

7. Araf S, Wang J, Korfi K, Pangault C, Kotsiou E, Rio-Machin A, et al. Genomic profiling reveals spatial intra-tumor heterogeneity in follicular lymphoma. Leukemia [Internet]. 2018;32(5):1261–5. Available from: https://doi.org/10.1038/s41375-018-0043-y

8. Rasche L, Chavan SS, Stephens OW, Patel PH, Tytarenko R, Ashby C, et al. Spatial genomic heterogeneity in multiple myeloma revealed by multi-region sequencing. Nat Commun [Internet]. 2017;8(1):268. Available from: https://doi.org/10.1038/s41467-017-00296-y

9. Elder A, Bomken S, Wilson I, Blair HJ, Cockell S, Ponthan F, et al. Abundant and equipotent founder cells establish and maintain acute lymphoblastic leukaemia. Leukemia [Internet]. 2017 May 10;31:2577. Available from: https://doi.org/10.1038/leu.2017.140

10. van Dongen JJM, van der Velden VHJ, Bruggemann M, Orfao A. Minimal residual disease diagnostics in acute lymphoblastic leukemia: need for sensitive, fast, and standardized technologies. Blood [Internet]. 2015/05/21. 2015 Jun 25;125(26):3996–4009. Available from: http://www.bloodjournal.org/cgi/doi/10.1182/blood-2015-03-580027

11. Notta F, Mullighan CG, Wang JCY, Poeppl A, Doulatov S, Phillips LA, et al. Evolution of human BCR–ABL1 lymphoblastic leukaemia-initiating cells. Nature [Internet]. 2011 Jan 19;469:362. Available from: https://doi.org/10.1038/nature09733

12. Bardini M, Woll PS, Corral L, Luc S, Wittmann L, Ma Z, et al. Clonal variegation and dynamic competition of leukemia-initiating cells in infant acute lymphoblastic leukemia with MLL rearrangement. Leukemia [Internet]. 2014 May 6;29:38. Available from: https://doi.org/10.1038/leu.2014.154

13. Theunissen PMJ, van Zessen D, Stubbs AP, Faham M, Zwaan CM, van Dongen JJM, et al. Antigen receptor sequencing of paired bone marrow samples shows homogeneous distribution of acute lymphoblastic leukemia subclones. Haematologica [Internet]. 2017/08/31. 2017 Nov;102(11):1869–77. Available from: http://www.haematologica.org/lookup/doi/10.3324/haematol.2017.171454

14. Lane SW, Scadden DT, Gilliland DG. The leukemic stem cell niche: current concepts and therapeutic opportunities. Blood [Internet]. 2009 Aug 6;114(6):1150–7. Available from: http://www.bloodjournal.org/cgi/doi/10.1182/blood-2009-01-202606

15. Bystrykh L V, Belderbos ME. Clonal Analysis of Cells with Cellular Barcoding: When Numbers and Sizes Matter. In: Turksen K, editor. Stem Cell Heterogeneity: Methods and Protocols [Internet]. New York, NY: Springer New York; 2016. p. 57–89. Available from: https://doi.org/10.1007/7651_2016_343

SUPPLEMENTARY INFORMATION

Supplementary methods

Patient samples

Bone marrow cells from pediatric patients with B-ALL were collected as part of routine diagnostics for suspected leukemia. Residual bone marrow cells left after clinical testing were cryopreserved for research purposes (Department of Pediatric Hematology/Oncology, University Medical Center Groningen). All patients and/or their caregivers provided a written informed consent. Procedures were approved by the Medical Ethical Committee of the University Medical Center Groningen.

In total, 5 different patient samples were selected to assess the quantitative distribution of leukemia clones across the individual locations of a murine xenograft. Based on previous study, we estimated a success rate of 50% for barcoding and engraftment. Transplantation of either non-barcoded or barcoded leukemia cells in primary recipients, followed by serial transplantation into secondary recipients will generate >15 xenografts to assess the quantitative distribution of leukemia cells in >150 individual anatomical locations.

Blinding does not apply to this study as the primary outcome measures are objective measures (cell counts, frequencies and barcodes).

Mice

Male Nod/SCID/IL2Rγ$^{-/-}$ (NSG) mice, randomly assigned to an individual patient sample, were bred and housed at the Central Animal Facility of the University of Groningen. All animal experiments were approved by the Dutch Central Committee Animal Experimentation and the Animal Welfare Body of the University of Groningen.

Barcode library construction and virus production

An equimolar barcode library of approximately 800 barcodes, which were integrated into the pEGZ2 vector, was generated as previously described[1, 2]. Viral supernatant was produced by transfection of HEK293T cells. Hereto, HEK293T cells were cultured in a type-A gelatin-coated T75-cell culture flask in DMEM supplemented with 10% heat-inactivated FBS (Gibco, ThermoFisher Scientific), 1% penicillin and streptomycin (Gibco, ThermoFisher Scientific) at 0.15×10^6 cells/ml. Cells were transfected with the packaging vector pCMVΔ8.91 (3μg), the envelope vector VSV-G (0.7μg) and the barcoded pEGZ2 vector library (~800 barcodes, 3ug) in the presence of Fugene (Promega Corporation, Madison, Wisconsin, USA). Next day, culture medium was replaced by StemSpan SFEM medium (STEMCELL Technologies) supplemented with 1% penicillin and streptomycin. After approximately 24 hours, viral supernatant was collected, filtered through a 0.45μm SFCA filter and stored at -80^{0}C for later use.

Cellular barcoding and xenotransplantation of patient-derived leukemia cells

Patient-derived B-ALL cells were rapidly thawed. From each sample, 5×10^6 cells were directly transplanted into 10-20 week old, sublethally irradiated NSG mice (1.0 Gy) via tail vein injection. Direct transplantation served as backup in case the first barcoding attempt failed. The remaining cells were used for lentiviral transduction with the barcoded pEGZ2 vector library. Patient sample ALL-12 was transduced using polybrene (Sigma Aldrich, Zwijndrecht, The Netherlands) according to previous procedures described by our group[1]. Patient samples ALL-15, 16, 17 and 19 were transduced using RetroNectin® as described here. Hereto, 6-well cell culture plates were pre-coated with RetroNectin® (0.05mg/ml, Takara, Kusatsu, Shiga, Japan) followed by centrifugation at 1000g, 45 min. with varying volumes of viral supernatant containing the barcoded pEGZ2 vector library (~800 barcodes). After 4 hours of incubation at 37^0C, viral supernatant was gently removed and patient-derived leukemia cells were equally divided over the 6-well cell culture plates ($2.5 – 3.5 \times 10^6$ cells/well) followed by spinfection (900g, 45 min.). Cells were cultured in StemSpan SFEM medium (STEMCELL Technologies, Vancouver, Canada) supplemented with 10% heat-inactivated FBS (Gibco, ThermoFisher Scientific, Waltham, Massachusetts, USA), 1% penicillin and streptomycin (Gibco, ThermoFisher Scientific), human recombinant TPO (100ng/ml, PeproTech, London, UK), human recombinant IL-7 (10ng/ml, PeproTech), human recombinant FLT-3L (20ng/ml, R&D Systems, Inc., Minneapolis, Minnesota, USA) and human recombinant SCF (50ng/ml, R&D Systems). Patient samples ALL-16 and ALL-19 were successfully barcoded upon thawing (supplementary table 1). Patient sample ALL-17 required *in vivo* expansion to allow for successful barcoding. Barcoded cells were sorted for the presence of GFP using either the MoFlo XDP or Astrios flow cytometer (Beckman Coulter®, Woerden, The Netherlands) and subsequently transplanted into sublethally irradiated NSG mice with 0.5×10^6 cells/mouse via tail vein injection. For serial transplantation, pooled bone marrow of hind legs, pelvis, sternum and spine was used with 0.5×10^6 GFP+ cells/mouse. Remaining pooled bone marrow of ALL-16 was stored at -150^0C for later use.

Quantitative assessment of leukemia load

Leukemia progression was monitored based on clinical symptoms and blood analysis every other week. When mice developed leukemia, mice were sacrificed under isoflurane and perfused with saline. Bone marrow (front and hind legs, pelvis, sternum, spine and skull) and extramedullary locations (blood, liver, spleen and brain) were collected. Single cell suspensions were prepared by crushing in erythrocyte lysis buffer followed by subsequent filtering through a 100-µm filter. The absolute number of white blood cells (WBCs) was determined by differential blood count using the Medonic CA620 Hematology analyzer (Boule Medical AB, Spanga, Sweden). The number of WBCs in peripheral blood was assessed prior to erythrocyte lysis. Hereto, a fraction of the peripheral blood

was subjected to the Medonic CA620 Hematology analyzer. The output WBC count was corrected for the total circulating blood volume in an adult mouse, which is approximately 2mL. The relative frequency of leukemia cells was determined by flow cytometry using the BD FACSCanto^{TM} II flow cytometer (BD Biosciences, San Jose, California, USA; supplementary table 2). The total leukemia cell content in any given location was calculated according to one of the formulas below:

WBC $(x10^6$ cells) x PI$^-$ (% of all events) x mCD45.1$^-$hCD45$^+$(% of gated events); or

WBC $(x10^6$ cells) x PI$^-$ (% of all events) x mCD45.1$^-$hCD19$^+$(% of gated events)

All mice were included in the analysis of the leukemia cell content in individual locations. To address the total body leukemia cell content, the leukemia cell content in all individual locations was combined. In case individual locations were not samples, an estimate was calculated based on the leukemia cell content in that specific anatomical location of the other xenografts transplanted with the same patient sample.

Validation of the quantitative assessment of leukemia load

The quantitative assessment of leukemia load was validated using Count Bright absolute counting beads (ThermoFisher Scientific). Bone marrow and extramedullary locations were collected and processed to single cell suspension as described before. A total of $0.5x10^6$ cells per sample were stained according to supplementary table 2. The total sample volume and the input volume for flow cytometry (corresponding to $0.5x10^6$ cells) were determined to correct for the total sample amount. Prior to measuring the leukemia cell content using the BD FACSCanto^{TM} II flow cytometer, $0.26x10^5$ counting beads were added to each sample. A minimum of 1000 beads were recorded. The absolute leukemia cell content was calculated according to formula below:

$$\frac{\text{Total sample volume}}{\text{Input volume}} \times \frac{\text{Total \# of added counting beads}}{\text{Recorded \# of counting beads}} \times \text{Recorded \# of mCD45.1}^-\text{hCD45}^+ \text{ cells}$$

Assessment of bone marrow compartment sizes

Healthy, untreated male NSG mice (n=4) were sublethally irradiated and sacrificed under isoflurane anesthesia after 1-6 months. After perfusion, single-cell suspensions were prepared from the different bone marrow locations as described before. The overall compartment size was defined as the absolute number of murine WBCs present at steady-state conditions in a given anatomic location, as measured by Medonic CA620 Hematology analyzer. Alternatively, Lin$^-$Sca-1$^+$c-Kit$^+$CD150$^+$ (LSK-SLAM) cells (i.e. hematopoietic stem and progenitors) were used to define stem cell compartment size. The relative frequency of LSK-SLAM cells was determined by flow cytometry using the BD FACSCanto^{TM} II flow cytometer (supplementary table 2). The total number of LSK-SLAM cells in any given bone marrow sample was calculated according to the formula below:

WBC $(x10^6$ cells) x PI⁻ (% of all events) x LSK-SLAM (% of gated events)

Barcode retrieval

Genomic DNA was isolated from cell pellets using the DNeasy Blood and Tissue (Qiagen, Hilden, Germany) or QIAamp DNA micro kit (Qiagen), according to manufacturer's instructions. Barcode sequences were amplified in a 35-cycle PCR reaction using uniquely indexed eGFP forward primers (5'-TCGGCATGGACGAGCTG-3' or 5'-GGCATGGACGAGCT-GTACAAG-3') and a WPRE reverse primer (5'-GGAGAAAATGAAAGCCATACGGGAAGC-3'). Amplification of barcode sequences were confirmed on an agarose gel. Samples that did not show a clear band on the agarose gel were subjected to a nested PCR reaction, using an extra set of outer primers (forward 5'-TGCCCGACAACCACTACCTG-'3 and reverse 5'-AAACACAGTGCACACCACGC- '3). Subsequently, samples were equimolar combined in pools of max. 12 samples, which were cleaned according to the manufacturer's instructions using the QiaQuick PCR purification kit (Qiagen). All samples were pooled together in batches that contain 200-300 different samples and the quality of the sample was confirmed using the Agilent 2100 Bioanalyzer (Agilent Technologies, Inc., Santa Clara, California, USA). Next, samples were sent for paired-end next generation sequencing on an Illumina HiSeq 2500 Platform (BaseClear, Leiden, The Netherlands).

Barcode data processing

Raw sequencing reads with a minimal Phred quality score of 30 were collapsed (github: https://github.com/erikzwart/collapse-multiplex-barcodes). Collapsed reads were processed by performing an exact match of the sample tag sequence. Next, barcodes with either the GAANNNACNNNGTNNNCGNNNTANNNCANNNTAAGGAC or AG-GNNNACNNNGTNNNCGNNNTANNNCANNNTGNNNGAC backbone were retrieved using Motif Occurrence Detection Suite (MOODS, 1.0.2 https://github.com/jhkorhonen/MOODS/wiki/Installation-and-usage-(MOODS-1.0)). The generated list contained all possible barcodes per sample, which was further filtered by applying a Hamming distance of one to delete barcodes that differ one base. Samples that belonged to the same experiment were pooled into one table.

Data were further processed and analyzed using custom R scripts. First, we calculated the theoretic chance of having multiple barcode integrations into a single cell (supplementary table 2), and subsequently analyzed the actual number of cells having multiple barcode integrations. This type of analysis is based on barcode patterns: Two distinct barcodes that follow the exact same distribution pattern over time, or across the anatomical locations in all recipients, are likely the consequence of two barcode integrations into a single cell. Hereto, we performed linear regression analysis, where the frequency of each individual barcode across all anatomical locations of every recipient was compared to that of all other barcodes. In case the slope and R^2 value of two distinct barcodes were

close to one, defined as *slope – 1 < 0.05* and the $R^2 > 0.99$, these barcodes were defined as multiple integrations into a single cell and one of the barcodes was removed from further data analysis. Second, additional filtering steps were applied to remove low-noise barcodes. Hereto, the degree of noise was first visualized in a histogram plot. This plot shows a biphasic distribution, where the peak centered at the very low read frequencies likely represents sequencing noise. To select true barcode clones, we selected barcodes that were (i) present in more than three samples, and (ii) had an overall read frequency of ≥0.5‰. To confirm removal of low-noise barcodes, we re-plotted the barcode frequencies in a histogram. The resulting barcode frequency table was used as input file for further data analysis. Barcode analysis was restricted to ALL-17 and ALL-19, because the primary recipients of ALL-16 consisted of five barcodes, which was reduced to two barcodes in the secondary recipients. To prevent further false-positive barcode calling from deep sequencing data[2], we restricted our analysis to the top 85% most abundant barcodes. Raw barcode data are available upon request.

Definitions of clonality and barcode library size

Here, we defined clonality as the number of distinct barcodes in a population, and used a library consisting of ~800 individually prepared barcode preps to study the number of clones and their dynamics. Using a library of known content and complexity has the advantage of facilitating signal-noise discrimination, thus allowing for more accurate barcode calling. However, in this manuscript, the size of our library was far smaller than the number of cells subjected to the barcoding procedure. Nonetheless, we are confident that the 800-barcode library is of sufficient size for our experimental aims, because multiple observations indicate that its size exceeds the number of *clonogenic* (i.e. leukemia-propagating) cells in our *in vivo* experiments by several-fold:

First, in most *in vivo* experiments, we did not capture the full library content, which suggests that not all barcodes are integrated into a clone-producing cell. In contrast, in *in vitro* experiments with barcoded cell lines, of which every cell is in theory self-renewing, we repeatedly recovered the full library. The fact that we did not capture the full library from the leukemia xenografts, indicates an abundance of barcodes compared to the number of leukemia cells that produce a detectable clone in our model.

Second, similar to our previous publications, we observed a drastic reduction in the number of barcodes upon serial transplantation[1, 3]. We suspect that the xenotransplantation procedure itself creates a selective bottleneck. In this previous work[1] We performed random model calculations to calculate the estimate the mortality rate of the transplanted cell population, and demonstrate that >90% of administered cells fail to engraft. This was a key observation to reassess the clonal barcode representation in our survived cell population *in vivo*. With model analysis (implemented as custom python

script), we concluded that at least 80% of the surviving barcoded clones in our experiments represent a single-cell origin.

The model analysis works as follows:

1. Set a population of x cells (e.g. 1000).
2. Randomly label the cells within this population with a barcode library of size y (e.g. 10).
3. Check the barcode representation of the population and perform statistics of redundant barcoding.
4. Set the population size and a specific barcode size z. Hereto, select a random fraction of all barcoded cells until a certain number of barcodes is reached. This will address the question about the size of the subset to reduce the barcode library to the needed fraction.
5. Adjust the parameters to the actual experimental parameters: x equals number of xenotransplanted cells; y equals the barcode library size; z equals barcode numbers retrieved upon transplantation.
6. Calculate frequency of barcodes that represents a single-cell origin and residual redundancy of barcoding.

Third, the observed level of anatomic asymmetry in barcode distribution supports the conclusion that the great majority, if not each, of the barcodes represent a single LPC. Similar to our explanation above, if each barcode would represent multiple LPCs, any functional difference would be averaged out and barcode distribution would be symmetric. An extreme example of this is GFP: Because the population of GFP-positive and GFP-negative cells each consist of multiple LPCs, their distribution across anatomic locations is highly symmetric. In contrast, the asymmetric distribution of barcode clones indicates that most barcodes represent single LPCs.

Statistical analysis

Statistical analysis and data visualization was performed in R (version 3.5.3) using packages "eulerr" and "ggplot2"[4-6]. Data significance was routinely tested using standard functions in R. Differences between groups were assessed by two-sided Mann Whitney U and correlations by Spearman rank analysis. The number of barcodes within a sample was expressed using the Shannon diversity index and derivatives, as previously described[2]. The quartile coefficient of dispersion (QCD) was used to express the degree of variation for a variable between recipients. Graphpad Prism 5.0 was used to perform a nonlinear regression analysis (least squares fit, forced intercept of 0 and <5% outlier detection) between the single and multiple platform method used to quantify absolute

leukemia cell content. Data is expressed either as mean ± standard deviation or median ± interquartile range (IQR). Statistical significance was defined as p<0.05.

References

1. Belderbos ME, Koster T, Ausema B, et al (2017) Clonal selection and asymmetric distribution of human leukemia in murine xenografts revealed by cellular barcoding. Blood 129:3210 LP – 3220. https://doi.org/10.1182/blood-2016-12-758250
2. Bystrykh L V, Belderbos ME (2016) Clonal Analysis of Cells with Cellular Barcoding: When Numbers and Sizes Matter. In: Turksen K (ed) Stem Cell Heterogeneity: Methods and Protocols. Springer New York, New York, NY, pp 57–89
3. Verovskaya E, Broekhuis MJC, Zwart E, et al (2013) Heterogeneity of young and aged murine hematopoietic stem cells revealed by quantitative clonal analysis using cellular barcoding. Blood 122:523 LP – 532. https://doi.org/10.1182/blood-2013-01-481135
4. R Core Team (2019) R: A Language and Environment for Statistical Computing
5. Larsson J (2019) eulerr: Area-Proportional Euler and Venn Diagrams with Ellipses
6. Wickham H (2016) ggplot2: Elegant Graphics for Data Analysis. Springer-Verlag New York

Supplementary figures
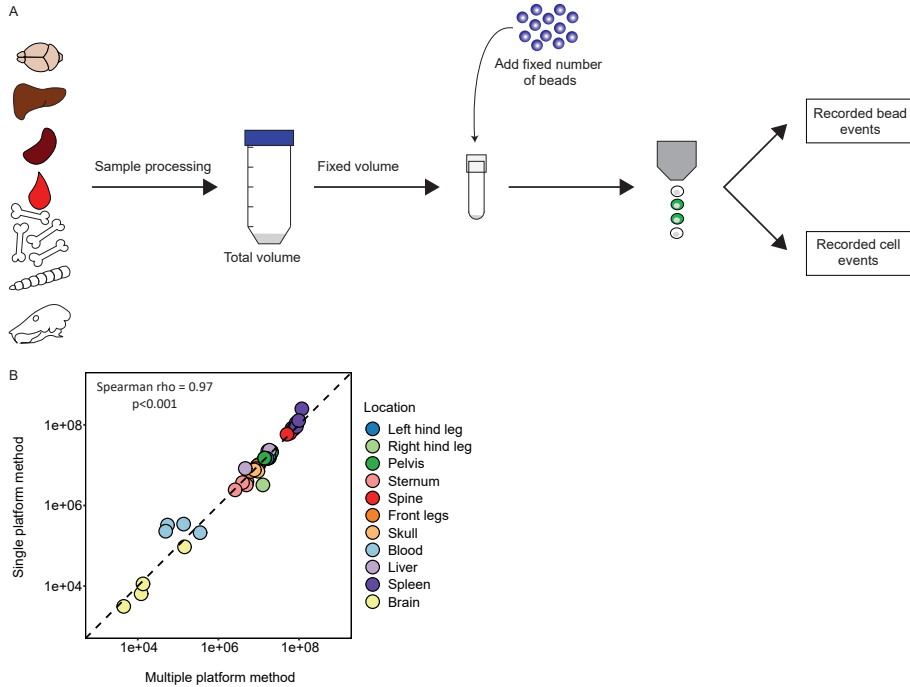
Supplementary figure 1. Validation of a multiple platform method to quantify the leukemia cell content

(A) Experimental design to quantify the leukemia cell content using a single platform method, which is based on calibrated beads by flow cytometry. (B) Spearman rank correlation of 0.97 between a single and multiple platform method to quantify leukemia cell content (n=4). Individual locations are plotted along the perfect line of y=x (dotted line). Most values are close to the expected y=x (nonlinear regression, slope=0.94±0.01, R^2=0.99). For subsequent experiments, the multiple platform method was used.
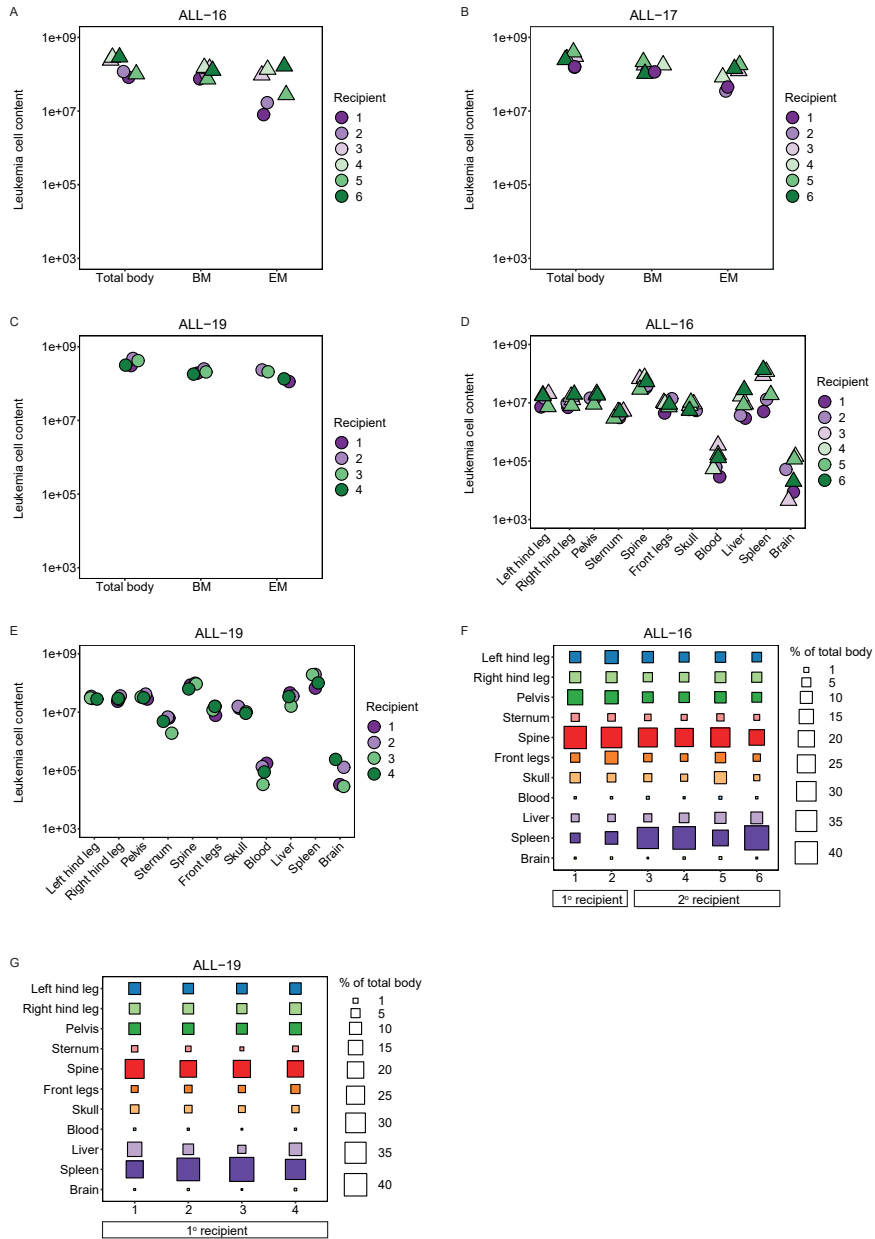
Supplementary figure 2. Quantitative distribution of leukemia cell content in murine xenografts
(A-C) The leukemia cell content in the total body, bone marrow (hind and front legs, pelvis, sternum, spine and skull) and extramedullary (blood, liver, spleen and brain) sites of murine xenografts. Symbols refer to primary (circle) and secondary (triangle) recipients. (D-E) The leukemia cell content in the individual locations of murine xenografts. Symbols refer to primary (circle) and secondary (triangle) recipients. (F-G) Relative contribution of each individual location to the total body leukemia cell content of murine xenografts.
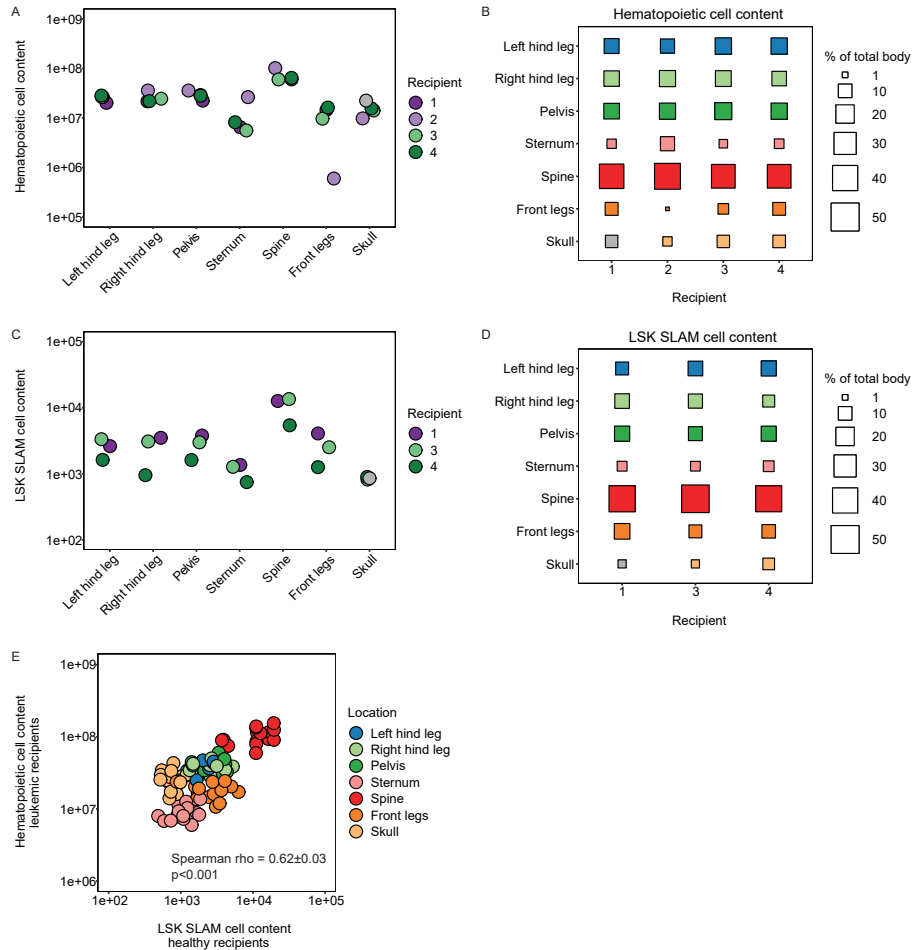
Supplementary figure 3. Leukemia load is proportional to the compartment size

(A, C) The absolute number of hematopoietic cells and LSK SLAM hematopoietic stem and progenitor cells in the individual bone marrow location of non-paired healthy NSG mice. (B, D) The contribution of each individual bone marrow location to the total hematopoietic cell content or the total LSK SLAM cell content in the bone marrow of non-paired healthy NSG mice. Grey square; skull of recipient 1 was not sampled and is the average of recipients 2-4. (E) The correlation between the number of hematopoietic cells in the bone marrow of leukemic (n=16) and the number of LSK SLAM cells in healthy (n=4) NSG mice. Hereto, we used a random-comparison model which randomly assigned one out of the four healthy mice to one out of the sixteen leukemic mice to calculate the Spearman rank correlation (n=1000 random comparisons). Data expressed as mean ± SD.
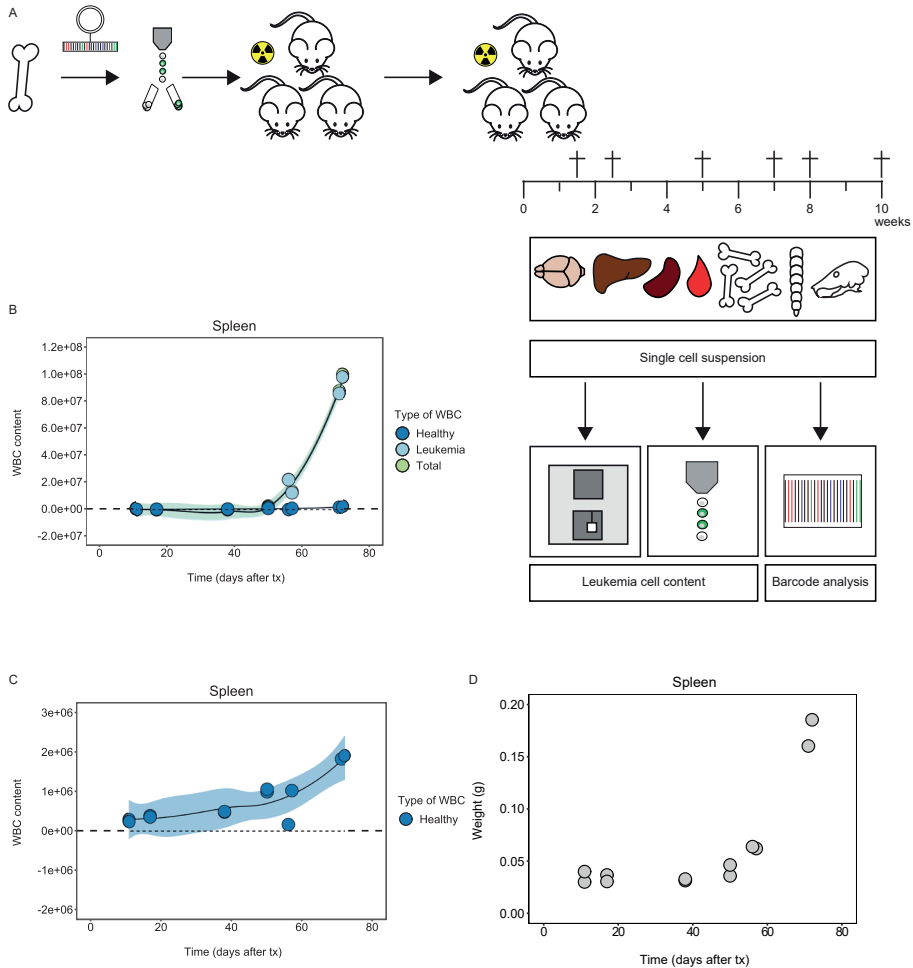
Supplementary figure 4.1. Leukemia cell content during different stages of disease progression
(A) Experimental design to quantify the leukemia cell content during different stages of disease progression. Patient-derived bone marrow cells of ALL-16 were barcoded, sorted for GFP and transplanted into sublethally irradiated NSG mice. Mice were sacrificed during different stages during disease progression (n=2 per time point). Individual locations were analyzed for their leukemia cell content and barcode composition. (B) The absolute number of WBCs in the spleen of leukemic mice during disease progression. Distinctions were made between leukemic cells (light blue), healthy murine WBCs (dark blue) and the total number of WBCs (light green). Every dot represents a mouse. Smoothing method 'loess' with confidence interval set at 95%. (C) Number of healthy murine WBCs in spleen of leukemic mice during disease progression. (D) Spleen weight of leukemic mice during disease progression.
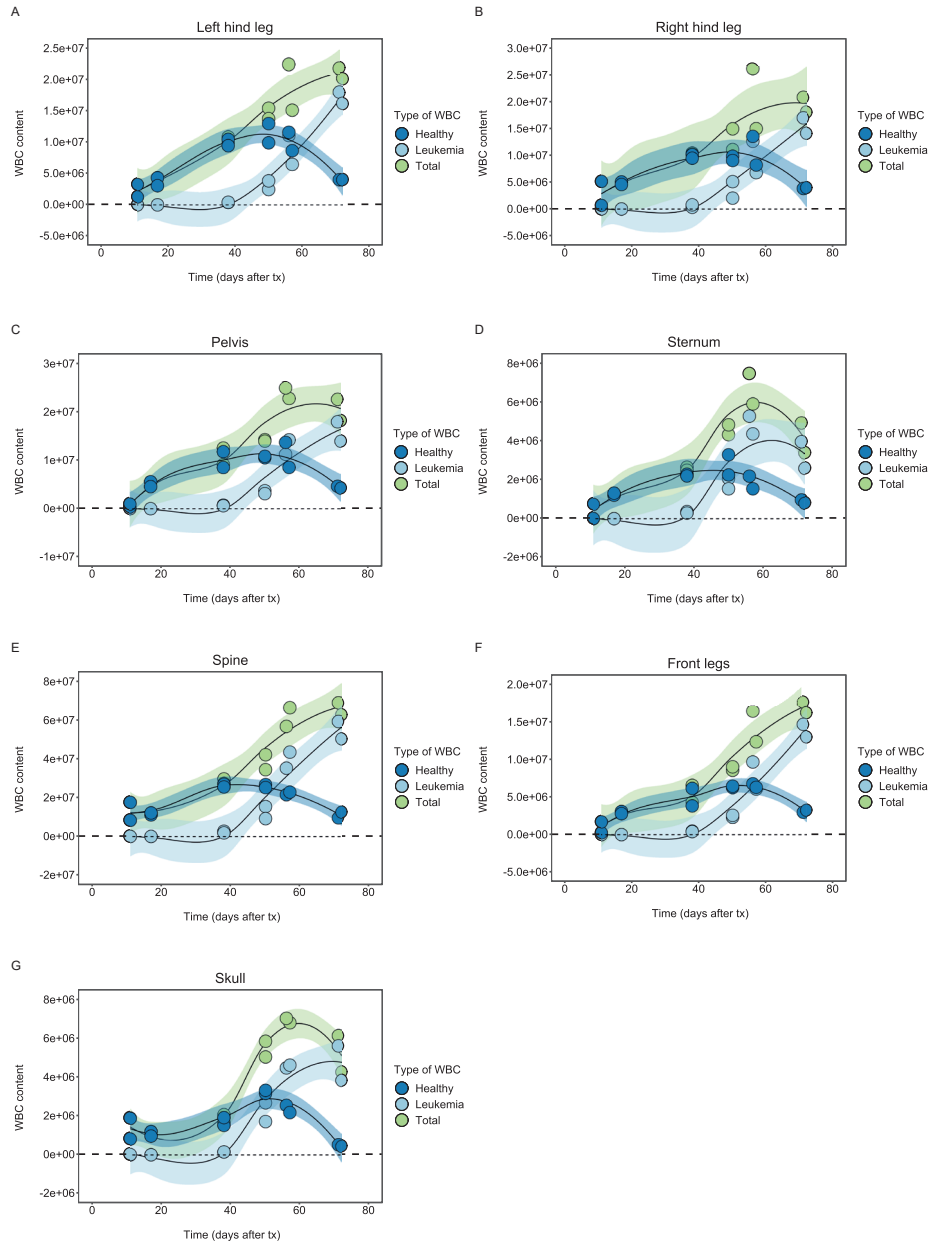
Supplementary figure 4.2. Leukemia cell content during different stages of disease progression
(A-G) The absolute number of WBCs in the individual bone marrow locations of leukemic mice during different stages of disease progression. Distinctions were made between leukemic cells (light blue), healthy murine WBCs (dark blue) and the total number of WBCs (light green). Every dot represents a mouse. Smoothing method 'loess' with confidence interval set at 95%.
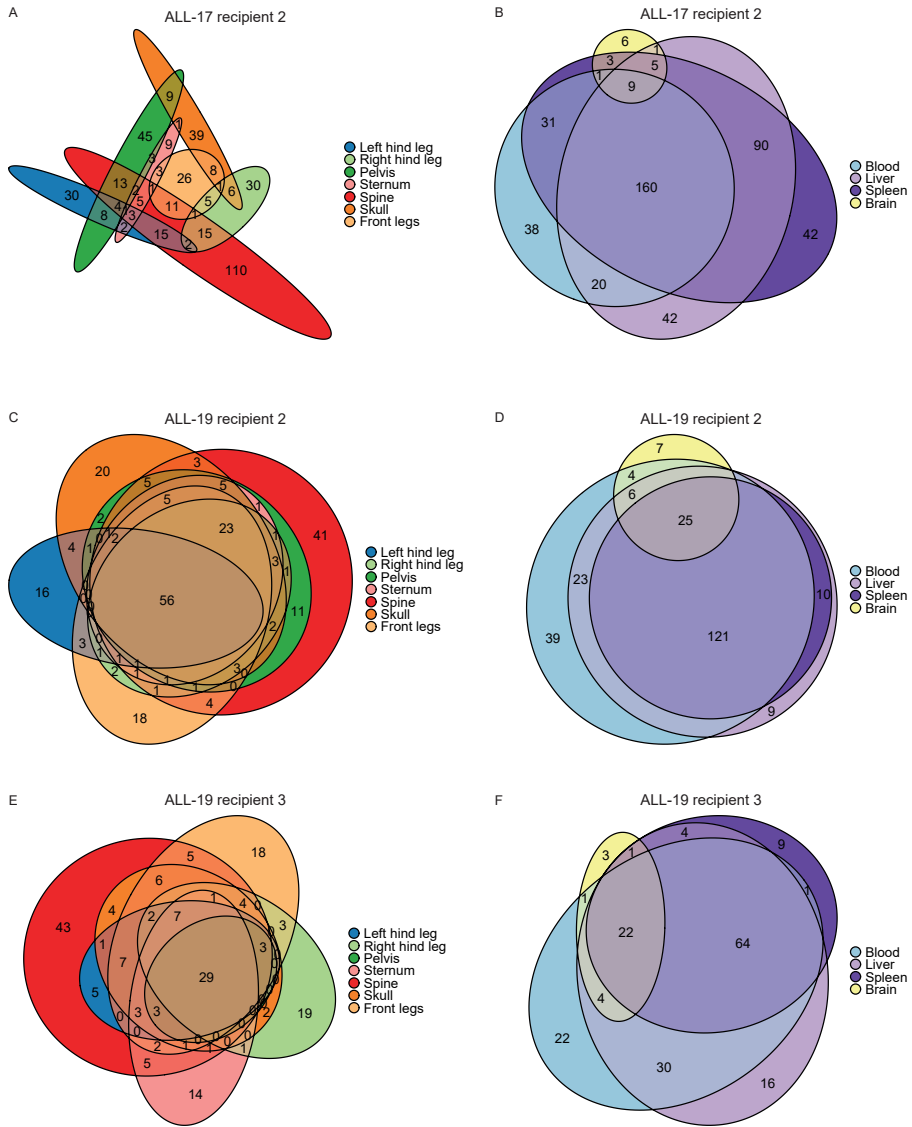
Supplementary figure 5.1. Asymmetrical distribution of human leukemia clones in the murine bone marrow

(A-F) Number of (non-)overlapping barcodes from the top 85% most abundant barcodes in the bone marrow and extramedullary locations of murine xenografts.
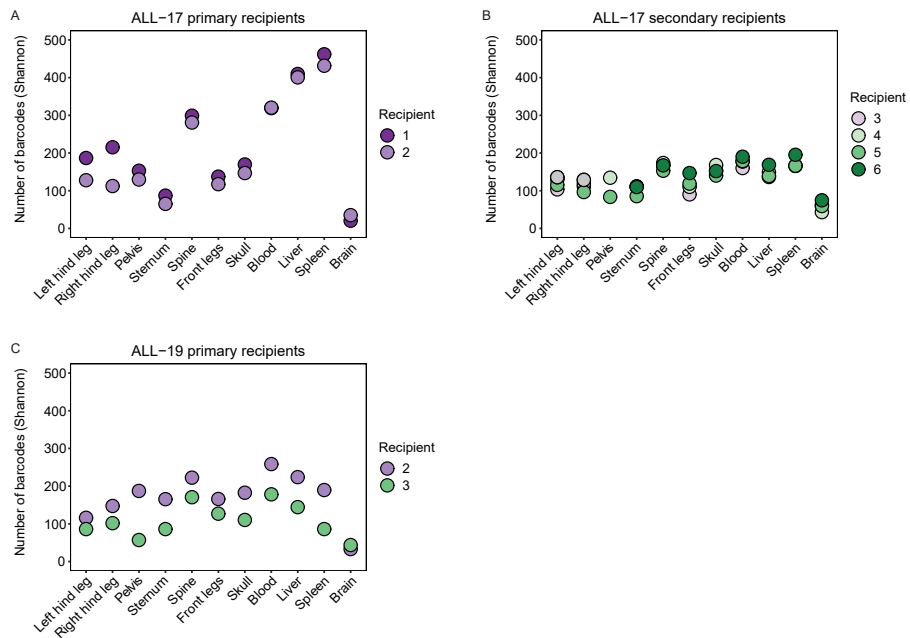
Supplementary figure 5.2. Barcode sizes in individual anatomical locations of murine xenografts
(A-C) The number of barcodes – expressed as Shannon count – in the individual anatomical locations.
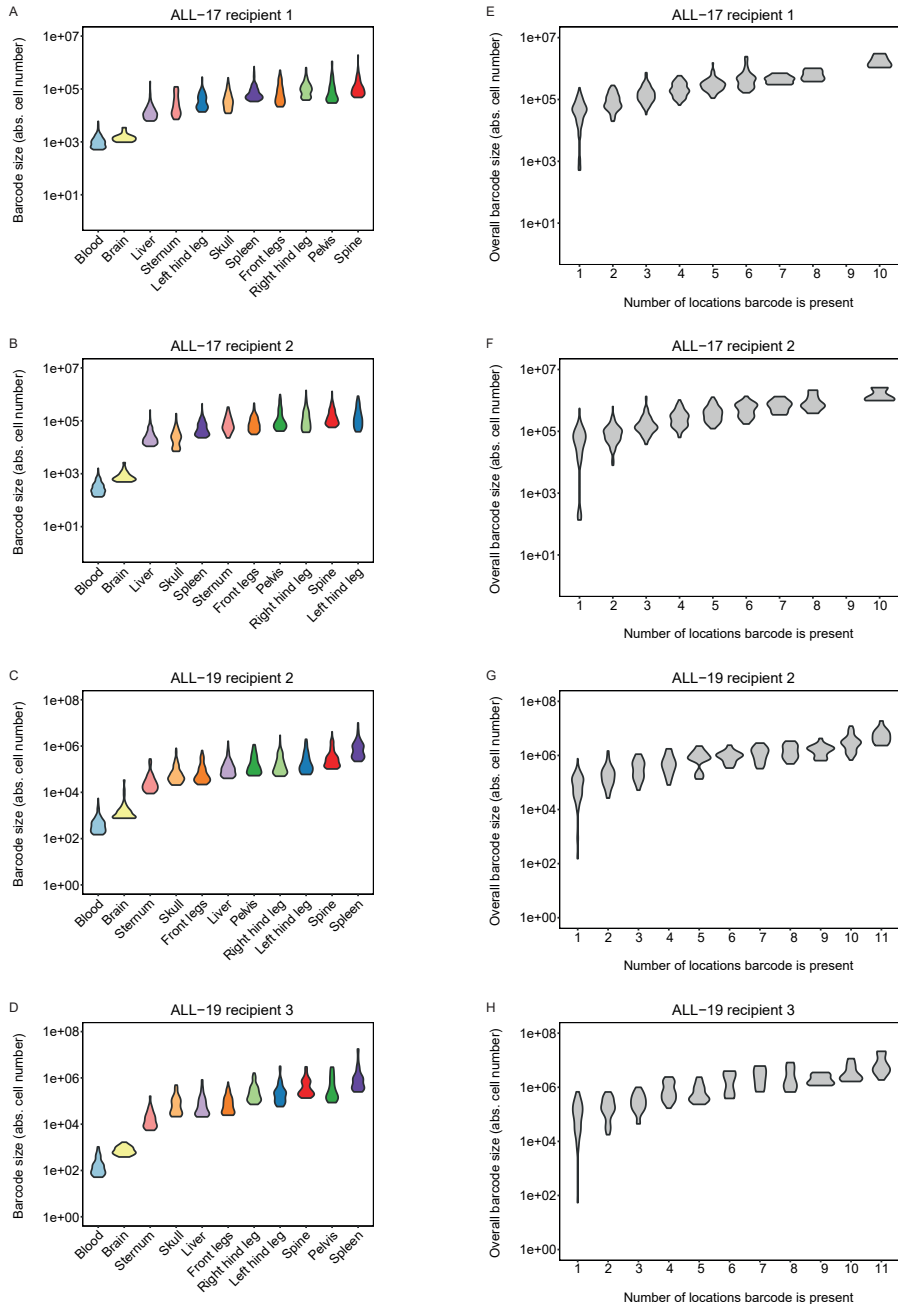
Supplementary figure 5.3. Barcode sizes in individual anatomical locations of murine xenografts
(A-D) Barcode size – expressed as absolute cell number – of the top 85% most abundant barcodes
in each individual anatomical location. (E-H) Overall barcode size of the top 85% most abundant
barcodes – expressed as absolute cell number – per number of locations in which the barcode was
present.
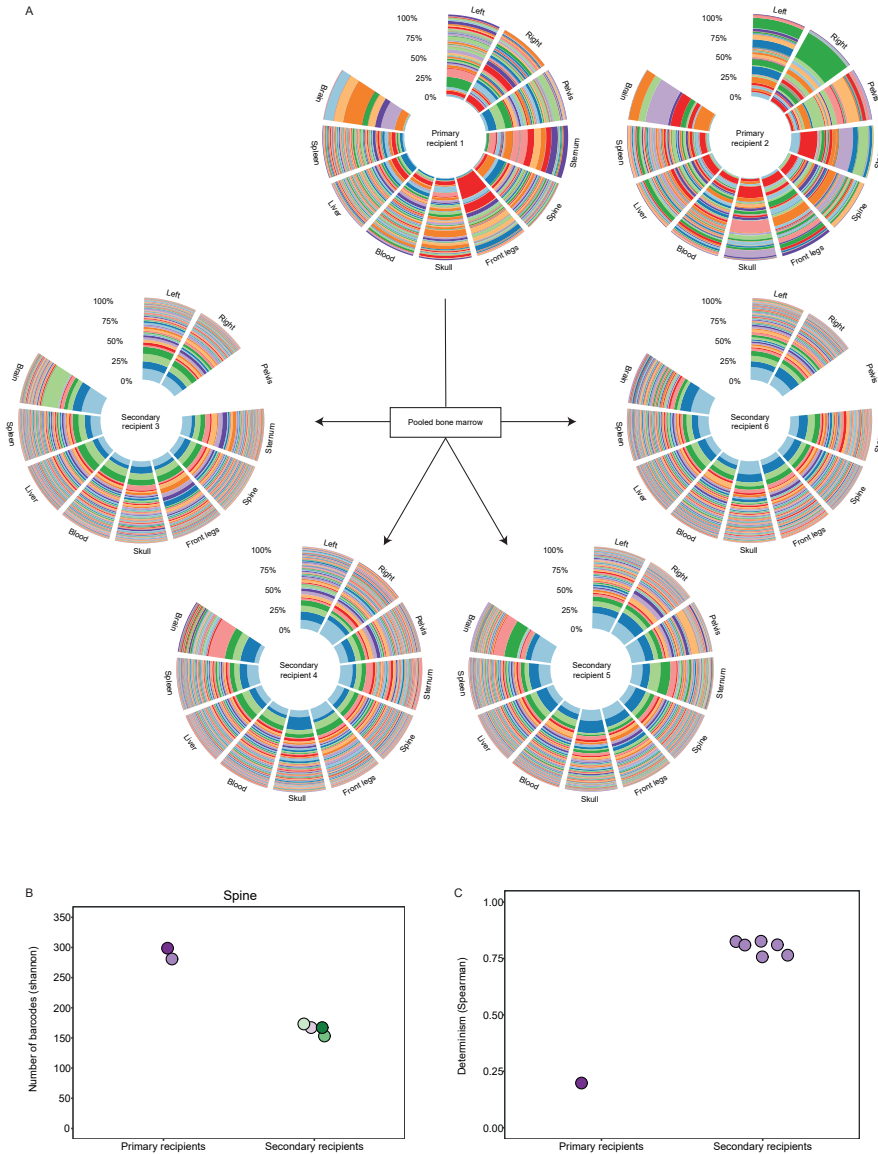
Supplementary figure 5.4. Clonal selection upon serial transplantation of ALL-17
(A) Top 100 most abundant barcodes in individual locations of serially transplanted xenografts. Each circle represents one mouse, every segment within a circle represent an anatomical location and every color represents one barcode. For serial transplantation into recipients 3-6, pooled bone marrow of the left hind leg ('Left'), right hind leg ('Right'), pelvis, sternum and spine derived from recipient 1 was used. (B) The number of barcodes – expressed as Shannon count – in the spine bone marrow of primary recipients 1 and 2, and secondary recipients 3-6. (C) Determinism (predictability) of barcode composition in primary and secondary recipients. Hereto, we compared the Spearman rank coefficient for the top 85% barcode composition in the spine bone marrow between the two primary recipients, and the four secondary recipients.
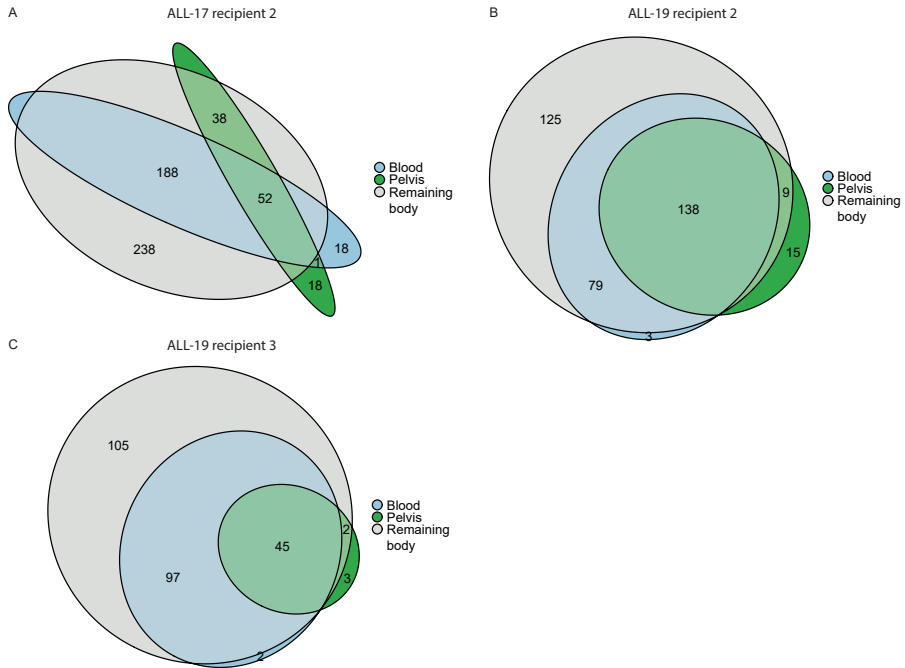
Supplementary figure 5.5. Underestimation of clonal complexity by single-site sampling
(A-C) Number of (non-)overlapping barcodes from the top 85% most abundant barcodes in the blood, pelvis and the remaining body.
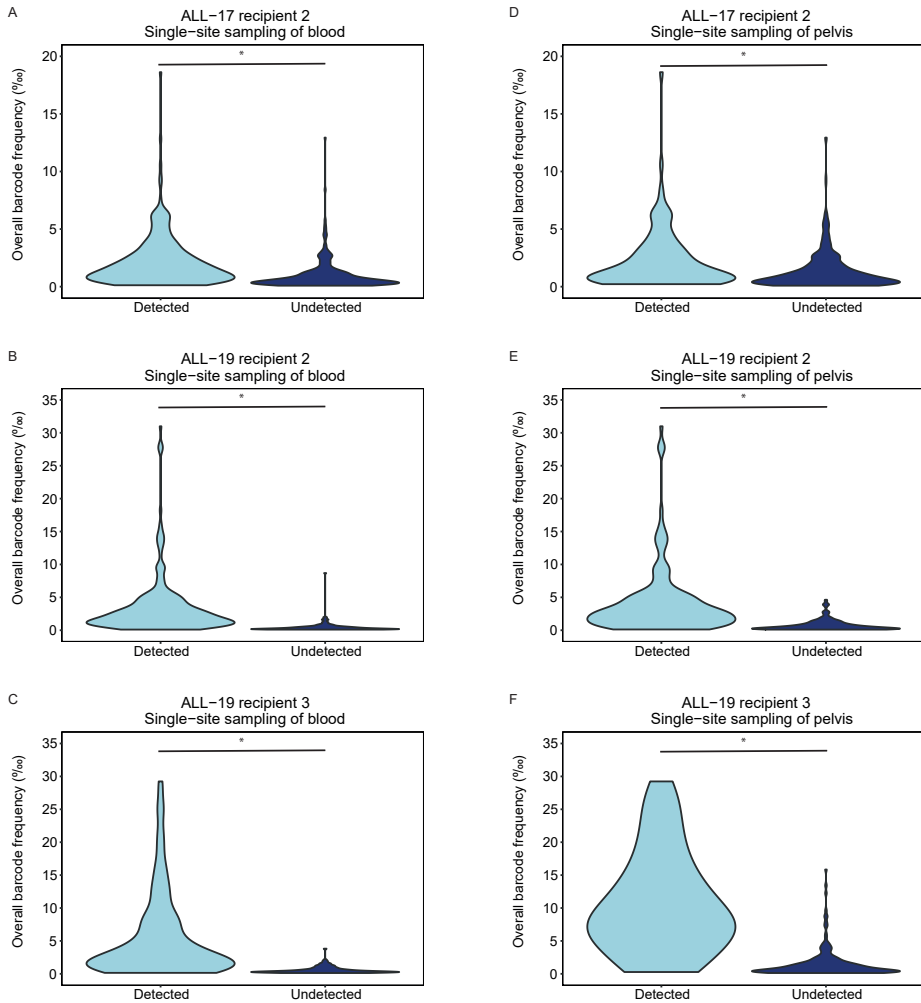
Supplementary figure 5.6. Underestimation of clonal complexity by single-site sampling
(A-F) Overall barcode frequency of the top 85% most abundant barcodes that are detected or remain undetected when blood or pelvis was sampled at end-stage leukemia. Statistical analysis: two-sided Mann-Whitney U test, * p<0.0001.
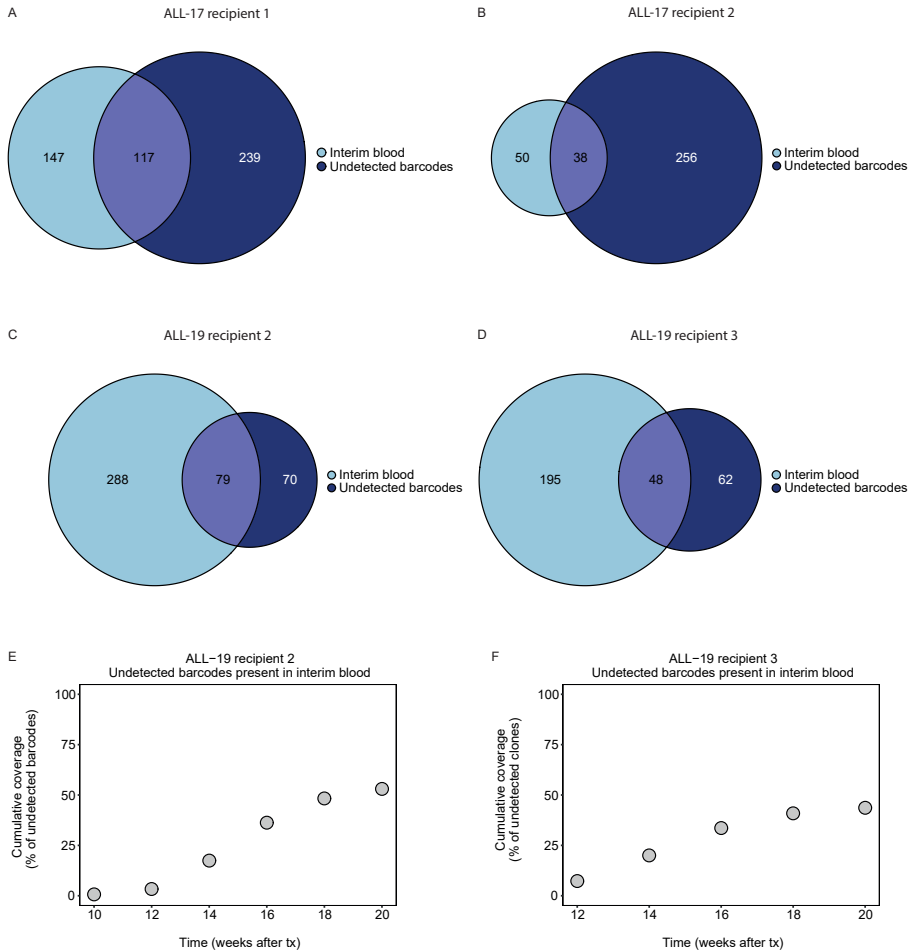
Supplementary figure 5.7. Underestimation of clonal complexity by single-site sampling
(A-D) The number of undetected clones that are detectable in interim blood samples when single-site sampling of the blood, at end-stage leukemia, is performed. (E-F) The cumulative coverage of undetected clones for single-site sampling of the blood at end-stage leukemia by multiple sampling of interim blood samples.

Supplementary tables

Supplementary table 2 "Antibodies used for flow cytometry to determine leukemia or LSK SLAM frequency" is available via the online version of this paper.

Supplementary table 1. Characteristics of patient samples used for transplantation.

Patient	Age at Dx (y)	WBC count (10⁹/L)	Blasts (%)	Karyotype	Cytogenetic aberrations	Engraftment	TE (%)	Predicted MOI (%)	Cells with multiple integrations (double hits)	Barcoding	Barcoded recipients	Un-barcoded recipients
ALL-12	10	27	76	46, XY, der(4)t(1;4)(q25;p16)[3]		No	0.19	n.a.	n.a.	n.a.	2	2
ALL-15	12	123	94	46, XX[30]	del1-5 PAX5	No	0.04	n.a.	n.a.	n.a.	1	1
ALL-16	10	57	97	47, XX, +X, -14, +mar[6]/47, idem, del(9)(p21)[9]/46, idem, der(5)t(5;9)(q3?3;q12), -9[2]/46, XX[5]	amp5 PAX5; delCDKN2A/B; gain CRLF2	Yes	2.61	n.a.	n.a.	monoclonal	17	1
ALL-17	18	295	79	46, XY	BCR-ABL	Yes	9.00	0.38	2	polyclonal	6	0
ALL-19	6	7.6	45	54,XY,+X,+Y,+8,+9,+14,+18,+21,+21[11]/46,XY[4]	DelIKZF1	Yes	7.50	0.27	1	polyclonal	2	2

Abbreviations: multiplicity of infection (MOI), transduction efficiency (TE).

Chapter 5

Detection of chemotherapy-resistant patient-derived acute lymphoblastic leukemia clones in murine xenografts using cellular barcodes

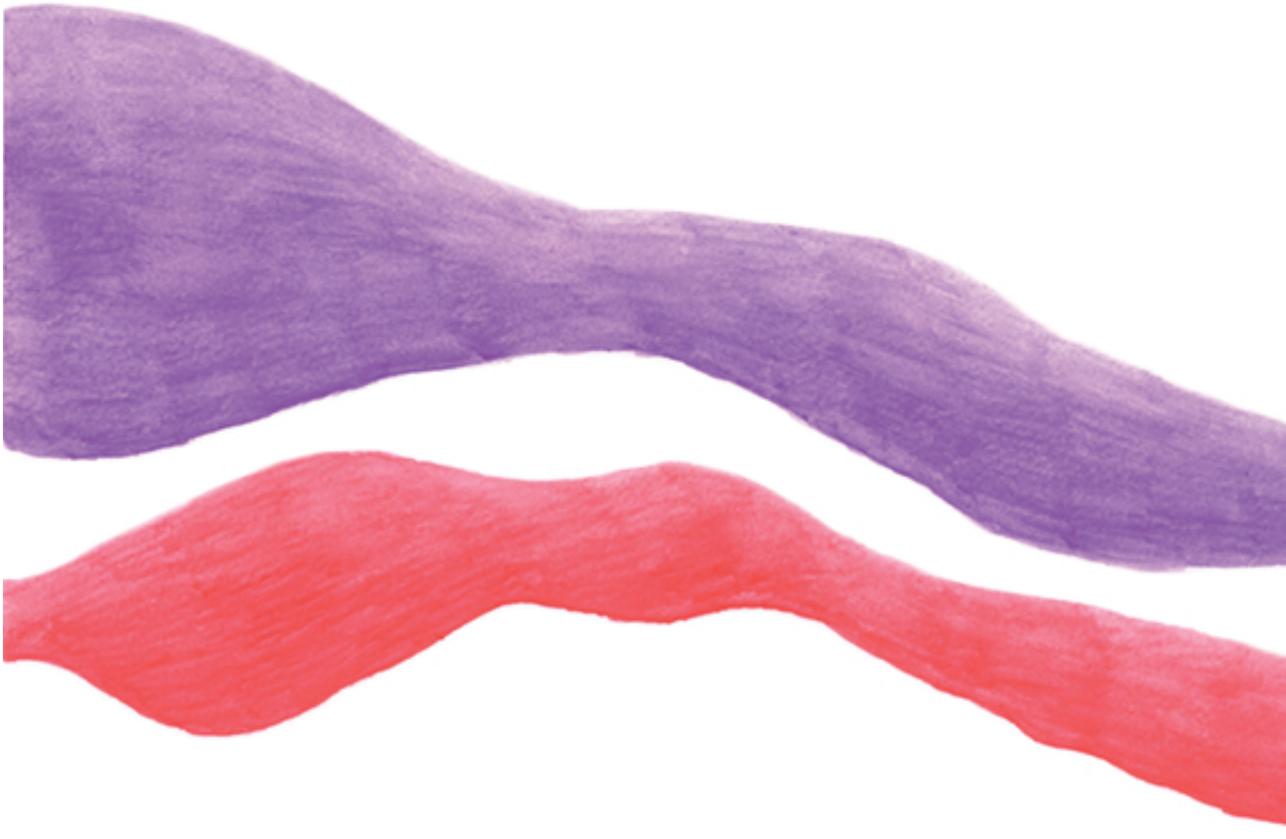Sabrina Jacobs, Albertina Ausema, Erik Zwart, Ellen Weersing, Gerald de Haan, Leonid V. Bystrykh and Mirjam E. Belderbos

ABSTRACT

Clonal heterogeneity fuels leukemia evolution, therapeutic resistance and relapse. Up-front detection of therapy-resistant leukemia clones at diagnosis may allow adaptation of treatment and prevention of relapse, but this is hampered by a paucity of methods to identify and trace single leukemia-propagating cells and their clonal offspring.

Here, we tested methods of cellular barcoding analysis, to trace the *in vivo* competitive dynamics of hundreds of patient-derived leukemia clones upon chemotherapy-mediated selective pressure. We transplanted Nod/Scid/Il2Rγ$^{-/-}$ (NSG) mice with barcoded patient-derived or SupB15 acute lymphoblastic leukemia (ALL) cells, and assessed clonal responses to dexamethasone, methotrexate and vincristine, longitudinally and across nine anatomical locations. We demonstrate that chemotherapy reduced clonal diversity in a drug-dependent manner. At end-stage disease, methotrexate-treated patient-derived xenografts had significantly fewer clones compared to placebo-treated mice (100±10 versus 160±15 clones, p=0.0005), while clonal complexity in vincristine- and dexamethasone-treated xenografts was unaffected (115±33 and 150±7 clones; p=NS). Using tools developed to assess differential gene expression, we determined whether these clonal patterns resulted from random clonal drift or selection. We identified five clones that were reproducibly enriched in methotrexate-treated patient-derived xenografts, suggestive of pre-existent resistance. Finally, we found that chemotherapy-mediated selection resulted in a more asymmetric distribution of leukemia clones across anatomic sites.

Altogether, we demonstrate that cellular barcoding is a powerful method to trace the clonal dynamics of human patient-derived leukemia cells in response to chemotherapy. In future, integration of cellular barcoding with single-cell sequencing technology may allow in-depth characterization of therapy-resistant leukemia clones and identify novel targets to prevent relapse.

INTRODUCTION

Although improved treatment protocols have substantially increased the survival of pediatric patients with acute lymphoblastic leukemia (ALL), ~10-15% of these children still suffer from relapse and have a poor prognosis[1–3]. ALL is a clonally heterogeneous disease, consisting of cells with variable (epi-)genetic characteristics which may diversify their responses to selective pressures, such as chemotherapy[4–7]. Sequencing of bulk diagnostic and relapsed ALL has shown that the majority of relapses originate from minor clones that were already present at diagnosis, with additional mutations suggestive of clonal evolution[5,6,8]. Early detection of therapy-resistant clones may allow adaptation of treatment and prevention of relapse[9]. However, upfront detection of these minor clones in diagnostic samples, and characterization of the clonal properties that enable drug resistance, remains challenging. On a cell-population level, several studies have demonstrated enrichment of drug-resistance mechanisms in relapsed samples compared to diagnostic material[5,6]. However, relapse samples have typically undergone several rounds of chemotherapy, and it is unknown whether the mechanisms causing drug-resistance were already present prior to therapy or evolved de novo during treatment[10,11]. A recent study, using limiting dilution to isolate single leukemia subclones, has demonstrated that relapse-fated subclones are metabolically and transcriptionally distinct from their non-relapsing counterparts[12]. However, single-clone transplant studies do not take into account the extensive interactions and competition between subclones that typically occur in patients. Therefore, there is a clear need for complimentary methods, enabling identification and characterization of chemotherapy-resistant subclones within a polyclonal population of cells.

We and others have previously shown that cellular barcoding is a powerful method to study the competitive dynamics of leukemic[13–16] and normal hematopoietic stem cell clones[17–19] in murine xenografts. Here, we aimed to determine whether cellular barcodes can be used to prospectively trace the clonal dynamics of diagnostic, patient-derived ALL cells in response to chemotherapy.

METHODS

Cells

Diagnostic bone marrow cells from an 18-year old patient with BCR-ABL[+] precursor B-cell ALL (B-ALL) were collected as part of routine diagnostics for suspected leukemia. At diagnosis, the patient had a white blood cell count of 295×10^9/L, of which 79% were blasts. Except for the (9;11) translocation, no additional cytogenetic abnormalities were found. The patient was treated with multi-agent chemotherapy, but had a poor response and

eventually died of treatment-related complications after allogeneic transplantation. For the current project, residual bone marrow cells, leftover after diagnostic testing, were used (Department of Pediatric Hematology/Oncology, University Medical Center Groningen). Procedures were approved by the Medical Ethical Committee of the University Medical Center Groningen, and informed consent was provided. Patient-derived B-ALL cells were cultured in StemSpan SFEM medium (STEMCELL Technologies, Vancouver, Canada) supplemented with 10% heat-inactivated FBS, 1% penicillin and streptomycin, human recombinant TPO (100ng/ml, PeproTech, London, UK), human recombinant IL-7 (10ng/ml, PeproTech), human recombinant FLT-3L (20ng/ml, R&D Systems, Inc., Minneapolis, Minnesota, USA) and human recombinant SCF (50ng/ml, R&D Systems). The pediatric BCR-ABL[+] SupB15 cell line was obtained from the American Type Culture Collection (ATCC), and maintained in RPMI 1640 medium supplemented with 10% heat-inactivated fetal bovine serum (Gibco, ThermoFisher Scientific, Waltham, Massachusetts, USA) and 1% penicillin and streptomycin (Gibco, ThermoFisher Scientific).

Cellular barcoding and xenotransplantation

Patient-derived B-ALL cells and SupB15 cells were barcoded as previously described[13]. In short, patient-derived B-ALL cells were thawed rapidly and transplanted directly into sublethally irradiated (1.0 Gy) Nod/SCID/IL2Ry^{-/-} (NSG) primografts (figure 1A). This direct transplant served to increase the total number of leukemia cells available for transduction, and to increase the transduction efficiency[13]. Pooled bone marrow cells of primografts and SupB15 cells were transduced with a lentiviral library of ~800 barcodes for 24 hours, after which barcoded cells were sorted for the presence of GFP on a MoFlo XDP flow cytometer (Beckman Coulter®, Woerden, The Netherlands). Sorted GFP[+] barcoded leukemia cells were transplanted via tail vein injection into sublethally irradiated (1.0 Gy) NSG mice, at a dose of $5x10^6$ cells/mouse. For serial transplantation, pooled bone marrow cells of hind legs, spine and sternum were used ($2.5x10^6$ cells/mouse). All animal experiments were approved by the Dutch Central Committee for Animal Experiments and the Animal Welfare Body of the University of Groningen.

In vivo chemotherapy

Xenografts of barcoded SupB15 cells or patient-derived B-ALL cells were randomly assigned to one of the following treatment groups: (1) Control: saline 10 ml/kg/day intraperitoneally (i.p.), 5 days per week; (2) Dexamethasone (DEX): 15 mg/kg/day i.p., 5 days per week; (3) Methotrexate (MTX): 5.0 mg/kg/day, 5 days per week every other week; (4) Vincristine (VCR): 0.5 mg/kg/day i.p., one day per week. Treatment of SupB15 and patient-derived xenografts was started 17 days and 18 days after transplantation, respectively, and continued for a total duration of four weeks. Treatment was stopped early in case of severe treatment-related toxicity or leukemia progression. Leukemia

development was monitored based on clinical symptoms and on the amount of leukemia cells in blood, assessed by bimonthly analysis of ~100µl peripheral blood, collected via orbital puncture. Differential blood counts were performed on a Medonic CA620 Hematology analyzer (Boule Medical AB, Spanga, Sweden) and the frequency of leukemia cells was determined by flow cytometry using a BD FACSCanto™ II flow cytometer (BD Biosciences, San Jose, California, USA; table S1). At end-stage leukemia, mice were sacrificed under isoflurane and perfused with saline. Bone marrow (hind legs, pelvis, sternum and spine) and extramedullary locations (blood, liver, spleen and brain) were collected. Single cell suspensions of bone marrow samples were prepared by crushing in erythrocyte lysis buffer, followed by filtering through a 100µm filter. The brain was mechanically dissociated and filtered through a 100µm filter, after which erythrocytes were lysed and myelin was removed using a percoll gradient buffer. Liver and spleen samples were directly filtered through a 100µm filter in erythrocyte lysis buffer. The absolute number of white blood cells in these samples was measured using a Medonic CA620 Hematology analyzer; the percentage of leukemia cells was determined by flow cytometry on a BD FACSCanto™ II (table S1). Cell pellets of 1-5 x 10^6 cells were stored at -20°C for barcode analysis.

Barcode retrieval and analysis

Genomic DNA was isolated using the DNAeasy Blood and Tissue (Qiagen, Hilden, Germany) or QIAamp DNA micro kit (Qiagen), according to the manufacturer's instructions. Barcode sequences were amplified in duplicate by PCR using uniquely indexed primers, and the multiplexed PCR product was sent for paired-end next-generation sequencing on an Illumina HiSeq 2500 Platform (BaseClear, Leiden, The Netherlands). Details on the methods for barcode data analysis are provided in supplemental file S1.

RESULTS

Chemotherapy delays human leukemia development in murine xenografts

To trace the dynamics of patient-derived leukemia clones in response to chemotherapy, we serially transplanted barcoded patient-derived or SupB15 leukemia cells into sublethally irradiated NSG mice, and treated the secondary recipients with clinically relevant chemotherapeutics: methotrexate, vincristine, dexamethasone or placebo (figure 1A). We chose to perform serial transplantation, to ensure that all xenografts had similar clonal composition at baseline[13], allowing comparison between treatment groups. The SupB15 xenografts were included to control for random fluctuations in clone numbers and/or dynamics.

In total, 209 chemotherapeutic doses were administered to 24 xenografts (76.8% of the planned regimen, table S2). All chemotherapeutic agents were well-tolerated (figure S1). The main reason for dose omission was progressive disease (patient-derived xenografts, dexamethasone, n=48 omitted doses). Two SupB15 xenografts did not have any detectable levels of leukemia up to ~6 weeks after completion of treatment; the remaining xenografts all developed leukemia. As expected, chemotherapeutic treatment significantly delayed leukemia development in a drug- and sample-dependent manner (figure 1). In patient-derived xenografts, both vincristine and methotrexate effectively extended survival, from a median of 30 days in control mice ((IQR: 29.5-30.3), to 51 days upon methotrexate treatment (IQR: 48.0-54.3, p=0.007) and 65.5 days upon vincristine treatment (IQR: 61-68, p=0.007, figure 1B-D). Dexamethasone did not affect disease free remission (figure 1B) nor overall survival of patient-derived xenografts (figure 1D), suggestive of population-level steroid-resistance. Notably, these responses resemble the course of disease in the patient, who responded poorly to induction therapy, necessitating high-risk chemotherapy and allogeneic stem cell transplantation, which ultimately led to his death. In SupB15 xenografts, all drugs prolonged disease-free remission (figure 1C) and overall survival (figure 1E), although the effect of dexamethasone did not reach significance (P=0.09).

Chemotherapy reduces clonal complexity

Our major aim was to assess potential heterogeneity in chemotherapeutic responses at a clonal level. Hereto, we analyzed the number and type of barcodes in each xenograft at end-stage disease (figure 2). We anticipated several scenarios; (1) homogeneous drug-resistance, resulting in similar number and types of clones between drug-treated and placebo-treated xenografts; (2) homogeneous drug-sensitivity; resulting in a (random) reduction of the number of barcode clones; (3) heterogeneous drug-sensitivity, in which the number of clones is reduced, and in which certain clones reproducibly gain dominance.

In line with our previous studies[13,14], all xenografts were highly polyclonal. In patient-derived xenografts, the number of clones was significantly reduced upon treatment with methotrexate (median ± standard deviation 100±10 clones versus 160±15 clones in control mice, p=0.0005), but not upon treatment with vincristine (115±33 clones) or dexamethasone (150±7 clones; figure 2A-B). In contrast, in SupB15 xenografts, all chemotherapeutic agents reduced the number of leukemia clones compared to placebo-treatment, consistent with homogeneous sensitivity (figure 2C-D). Using a linear regression model, including survival time and treatment group as potential predictors of barcode complexity, we identified treatment group as the most important determinant of the number of clones at sacrifice in patient-derived xenografts (figure S2).
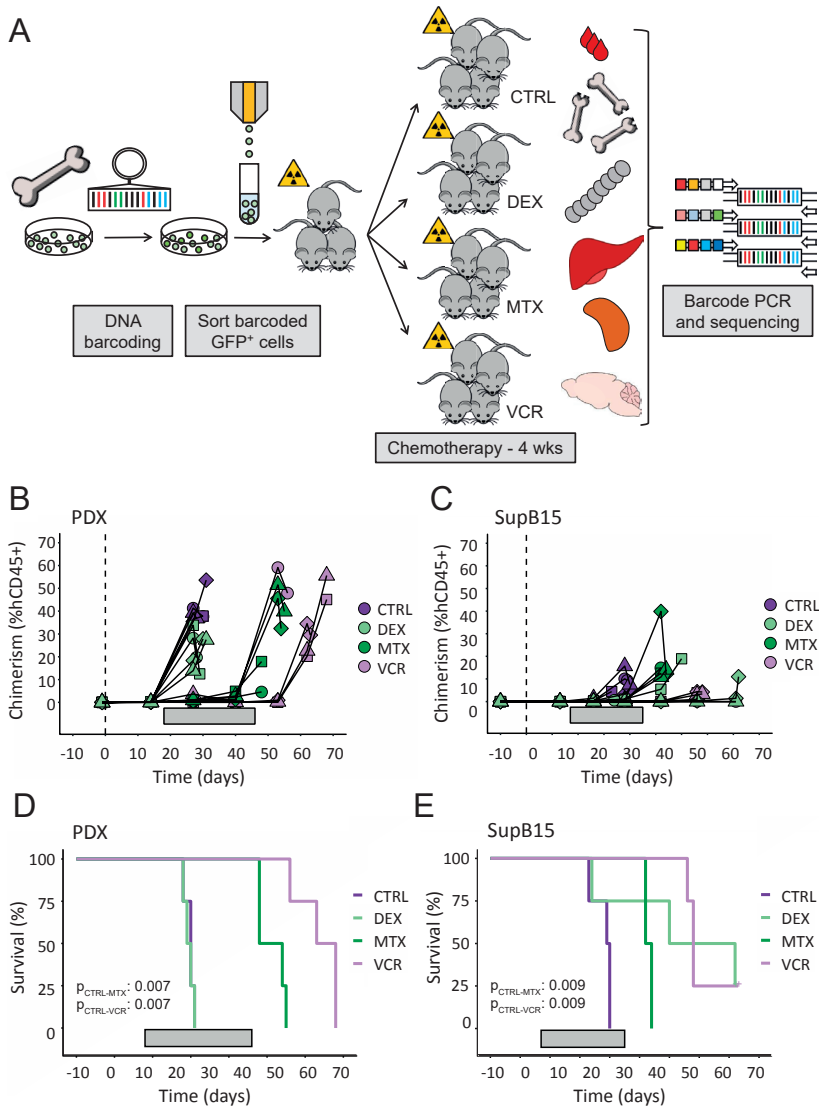
Figure 1. Identification of chemotherapy-resistant leukemia clones using cellular barcodes
(A) Experimental design. Sublethally irradiated Nod/SCID/IL2Rγ$^{-/-}$ mice were transplanted with bar-coded SupB15 cells (n=16 mice) or patient-derived B-ALL cells (n=16 mice), and randomly assigned to one of four treatment groups: control (saline), dexamethasone, methotrexate, or vincristine. Treatment was continued for 4 weeks, or until clinically evident leukemia. At end-stage disease, xenografts were sacrificed, after which blood, bone marrow and extramedullary sites were ana-lyzed for leukemia cell content and barcode composition. (B-C) Leukemia development in blood of chemotherapy-treated patient-derived (B) and SupB15 xenografts (C). Shapes indicate individual xe-nografts within a treatment group. The grey beam depicts the treatment period. (D-E) Kaplan-meier survival curves of chemotherapy-treated patient-derived (D) and SupB15 (E) xenografts. Abbrevia-tions: CTRL; Control; DEX: dexamethasone; MTX: methotrexate; VCR: vincristine; PDX: patient-derived xenografts.

Notably, while comparing the type of clones between patient-derived xenografts, we observed a striking similarity in barcode patterns in recipients that had received the same treatment. This was confirmed by unsupervised clustering of the clonal composition in the total body (figure 2E) and by principal component analysis (PCA) of the clonal composition in individual anatomical locations (figure 3A). In contrast, treatment-dependent clustering was less evident in SupB15 xenografts (figure 2F, figure 3B). To account for potential artefacts due to arbitrary decisions on the number of clones included in the analysis, we repeated these analyses using different cutoffs, which consistently showed the same results (figure S3-S4). Moreover, in SupB15 xenografts, chemotherapeutic treatment primarily eliminated small clones (figure S5). This is consistent with random, size-based selection, which is expected for a homogeneous population of cells. In contrast, in recipients transplanted with patient-derived leukemic cells, treatment with methotrexate eliminated small as well large clones (figure S6). Altogether, these findings indicate that cellular barcoding provides a relevant method to assess clonal selection upon chemotherapy. Furthermore, they suggest that the observed clonal patterns are not solely due to random selection or clonal drift, but driven (in part) by heterogeneity in clonal responses to chemotherapy[10].

Identification of chemotherapy-resistant leukemia clones

We subsequently aimed to determine which clones were consistently more abundant in chemotherapy-treated patient-derived xenografts compared to controls (figure 3). Hereto, we applied differential gene expression (DGE)-type analyses, which are normally used for transcriptomic data, to our barcode DNA sequencing data (figure 3, table S3-4). We identified 28 patient-derived leukemia clones, together accounting for 41.5±4.3% of the total body leukemia load, that were significantly more abundant in methotrexate-treated xenografts than in controls (in which these clones occupied 11.3±1.3% of the total body leukemia load; figure 3D). Of these clones, clone #12, #17 and #99 (ranked by abundance) contributed significantly to the dimensions that separated methotrexate-treated xenografts from the other treatment groups (figure 3A). In contrast, in SupB15 xenografts, no treatment-related enrichment of specific clones was observed (figure 3B, 3D). Collectively, these data indicate that DGE-analysis of barcode data is an effective approach to identify chemotherapy-enriched, and thus potentially resistant, patient-derived leukemia clones in murine xenografts.

Chemotherapy increases the spatial asymmetry of patient-derived leukemia clones

In previous work, we demonstrated that patient-derived leukemia clones are asymmetrically distributed across anatomic sites in murine xenografts, especially when the number of contributing leukemia-propagating cells is low[13,14]. Here, to address the im-
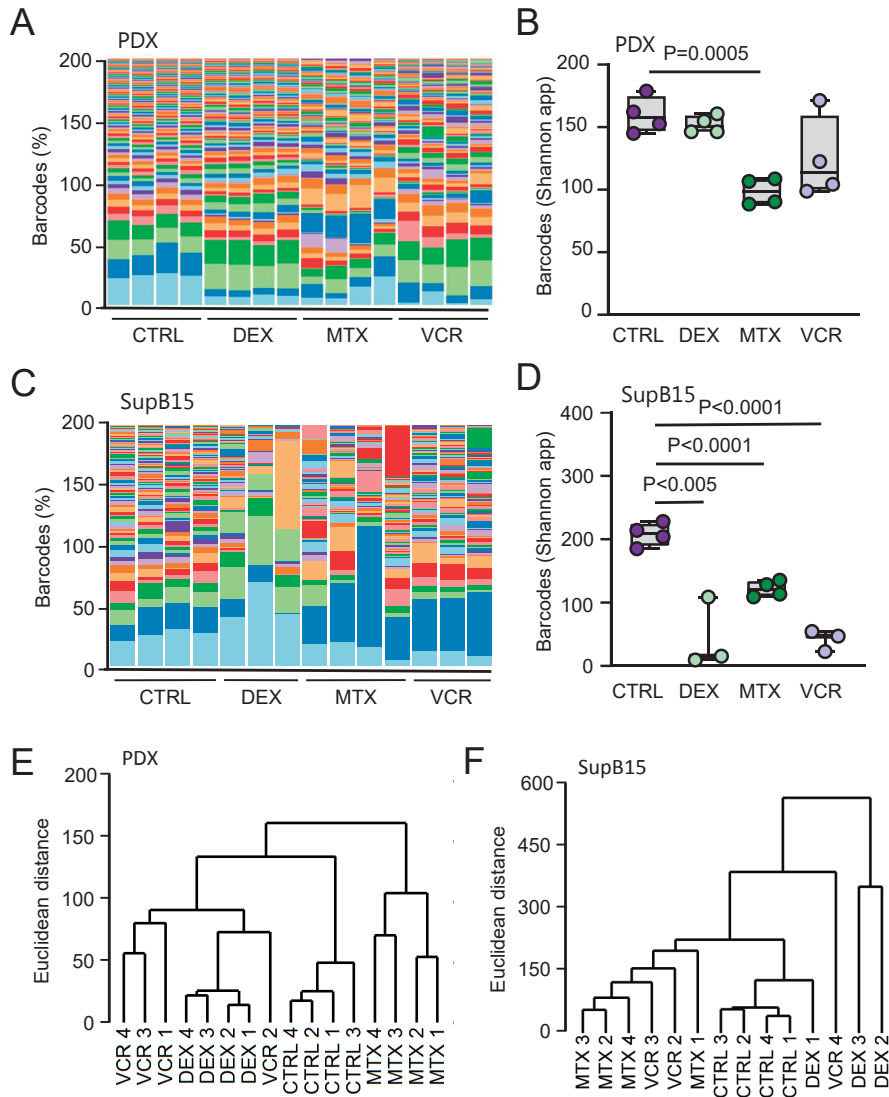
Figure 2. Chemotherapy reduces ALL clonal complexity in a drug- and sample-dependent manner

(A-D) Barcode composition in patient-derived (A, B) and SupB15 (C, D) xenografts. (A and C): The top 100 most abundant barcode clones in the total body of individual xenografts. Each bar represents an individual mouse, colors depict individual barcodes. Barcodes were sorted from large to small, based on their size in control-treated mice. (B and D): Quantification of barcode complexity in the total body of patient-derived and SupB15 xenografts, using the Shannon approximation. Each dot represents an individual mouse, colors are used to depict the different treatment groups. P-values represent the result of one-way ANOVA with post-hoc Dunnett's multiple comparisons test. (E-F): Clustering analysis of patient-derived (E) and SupB15 leukemia (F) xenografts, based on the Euclidean distance between barcode profiles. Abbreviations: CTRL; Control; DEX: dexamethasone; MTX: methotrexate; VCR: vincristine; PDX: patient-derived xenografts.
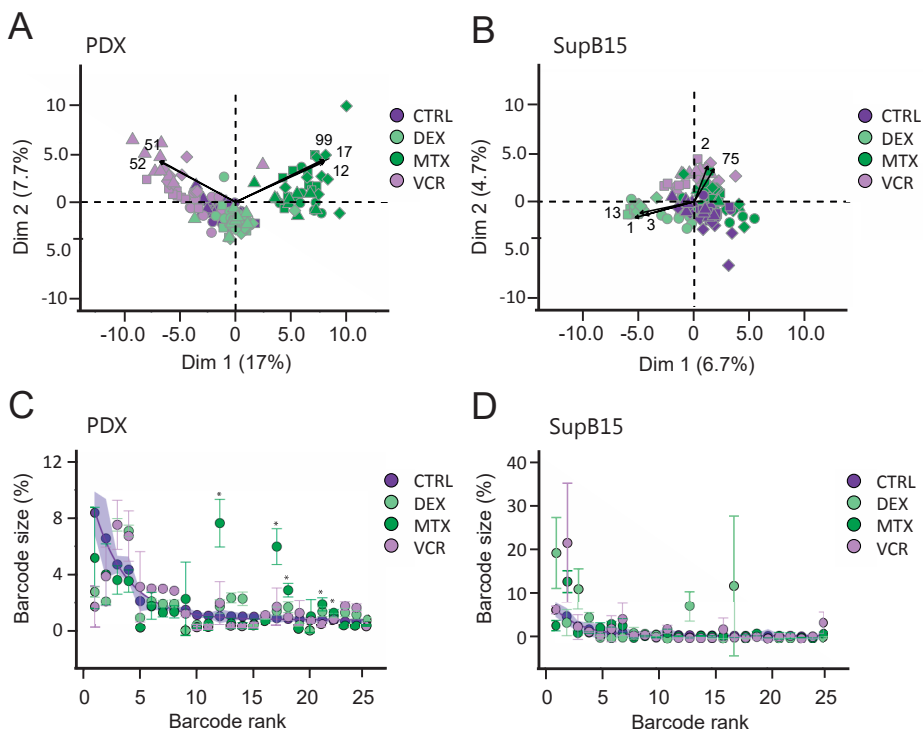
Figure 3. Identification of chemotherapy-resistant leukemia clones using cellular barcodes
(A-B) Principal component analysis of the top 100 most abundant barcode clones across anatomic locations of chemotherapy-treated patient-derived (A) and SupB15 (B) xenografts. Every dot represents an anatomic location; the different shapes depict individual xenografts within a treatment group. The arrows indicate the top 5 clones – indicated by their rank number – that contribute to the dimensions. (C-D) Relative abundance of the 25 largest clones in patient-derived (C) and SupB15 (D) xenografts, ranked by their average size in the total body of control-treated xenografts. Clones that were significantly more abundant in methotrexate-treated xenografts compared to control-treated xenografts are indicated with an asterisk. Significance was assessed by differential gene expression analysis, using the barcode data of SupB15 xenografts to determine the cut-off p-value for significance. Abbreviations: CTRL; Control; DEX: dexamethasone; MTX: methotrexate; VCR: vincristine; PDX: patient-derived xenografts.

pact of chemotherapy-based selection on clonal asymmetry, we analyzed the anatomic distribution of the 100 most abundant barcode clones across different locations (figure 4, S7-S17). We assessed asymmetry in two dimensions: (I) relative asymmetry, defined as the difference in clone sizes between locations; and (II) absolute asymmetry, defined as the difference in clone presence/absence between locations. To quantify the degree of relative asymmetry, we used the cumulative coefficient of variation (CV), which reflects the dispersion of clone sizes in individual locations around their average size in the total body[14]. In general, the

anatomic distribution of SupB15-clones was more asymmetric than the distribution of patient-derived leukemia clones, and unaffected by chemotherapy (fig S17). In contrast,

in patient-derived xenografts, treatment with methotrexate resulted in a significant increase in both relative and absolute clonal asymmetry (median CV CTRL: 53.9, IQR: 53.4-55.8; MTX: 76.1, IQR: 74.3-78.3; p=0.028; figure 4A-C). For example, in control-treated patient-derived xenografts, 32±6 clones were present in all eight locations, whereas only 9±3 clones were present in all anatomic locations in methotrexate-treated mice (figure 4D). Of the clones present in control-treated xenografts, 15±2 and 10±7 clones were not detected in any location upon, respectively, methotrexate and vincristine treatment.
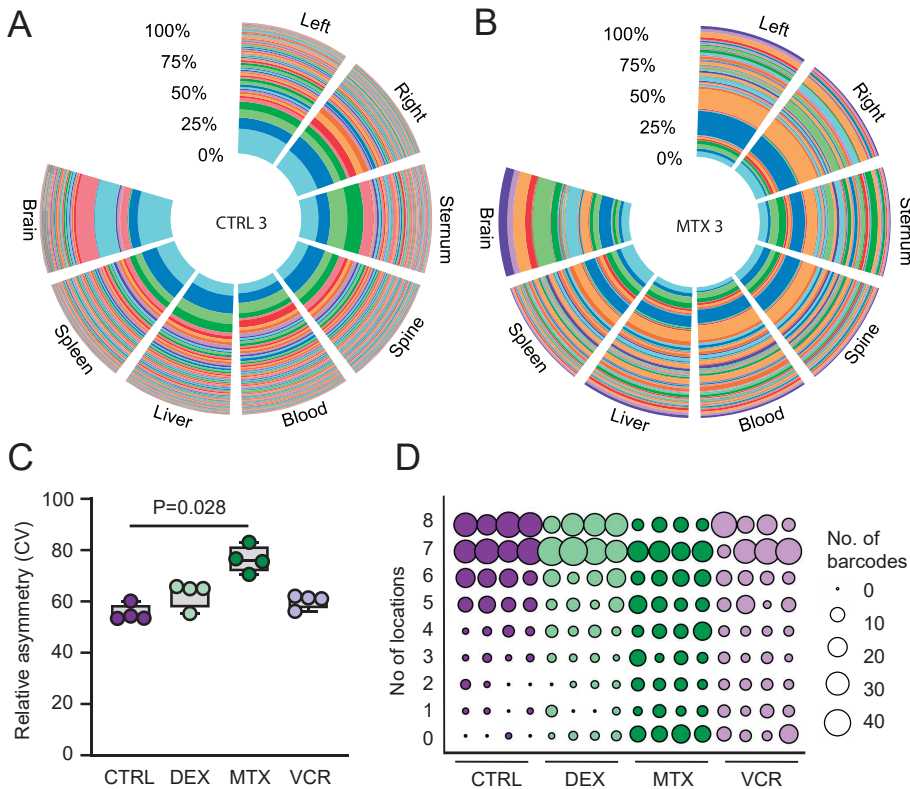
Figure 4. Chemotherapy increases the anatomic asymmetry of patient-derived leukemia clones
(A-B) Barcode composition in individual anatomic locations of representative control-treated (A) and methotrexate-treated (B) patient-derived xenografts. The top 100 most abundant barcodes are shown, ordered from large to small based on their abundance in the total body of control-treated mice. (C) Summary of the relative clonal asymmetry in all patient-derived xenografts, quantified by the cumulative coefficient of variation for the top 100 most abundant clones (CV). Every dot represents an individual xenograft; the p-value depicts the result of one-way ANOVA with post-hoc Dunnett's test. (D) Absolute clonal asymmetry in patient-derived xenografts, shown as the presence/absence of a barcode in n of the eight sampled anatomic locations (i.e. left/right hind legs, sternum, spine, blood, liver, spleen, brain). The size of the circles reflects the number of clones that were observed in n locations. Abbreviations: CTRL; Control; DEX: dexamethasone; MTX: methotrexate; VCR: vincristine; PDX: patient-derived xenografts.

Remarkably, the brain consistently contained far fewer clones than any other location (figure S3-S4, S18). This may be due to detection limits, or to blood-brain barrier-mediated clonal selection. Altogether, these data demonstrate that chemotherapy can increase clonal asymmetry, allowing for certain clones to escape detection when a single site is sampled.

DISCUSSION

In summary, this study demonstrates that cellular barcoding is a powerful method to study the dynamics of patient-derived leukemia clones in response to chemotherapy-mediated selection. Barcoding enables parallel tracing of hundreds of clones from the same patient in a quantitative, unbiased approach, which cannot be easily achieved with somatic mutation-based clone-tracing methods. Its application in murine xenografts allows assessment of responses to single chemotherapeutic agents, over time and across anatomic locations.

Barcodes enable parallel tracing of hundreds of leukemia clones

One particular advantage of the cellular barcoding method is the possibility to trace the behavior of individual clones within a polyclonal population of cells. This is especially relevant in light of recent studies, which demonstrate that interactions between heterogeneous subpopulations of tumor cells are of crucial importance for cancer initiation and progression. For instance, cancer subclones have been shown to negatively affect each other's survival, by competition for essential resources such as oxygen and nutrients[7,20]. In fact, clonal competition is considered a key force driving cancer evolution and progression[21,22]. Conversely, cancer subclones may cooperate and improve each other's fitness, including increased growth rate and mobilizing potential[23,24]. Importantly, a recent study, using short-tandem repeats to trace glioblastoma subclones *in vitro*, revealed that two drug sensitive clones can develop resistance *de novo* by cooperating together[24]. Altogether, these studies identify that clonal interactions are important regulators of clonal behavior, which may provide therapeutic targets. Cellular barcoding provides insight into the dynamics of hundreds of individual clones in the context of these interactions, thus providing a biologically relevant method to study the fundamental mechanisms that underlie drug resistance.

Identification of chemotherapy-resistant subclones

Key challenges for lineage tracing studies in highly polyclonal samples, such as ALL, are to reliably discriminate "true" subclones from sequencing noise, and to distinguish between clonal selection and random fluctuations in clonal abundance. In previous

work, we have shown that estimation of the number of clones in polyclonal samples is highly dependent on the definitions of clonal complexity and methods for their assessment, with the Shannon approximation being the most reliable[13,14]. Nonetheless, although the Shannon index accurately counts the *number* of subclones in set of samples, it does not tell *which* subclones are enriched/lost in one sample versus the other. In the current manuscript. we present a complementary data analysis method, which enables identification of single subclones that are significantly enriched/lost from a population. We adapted an edgeR protocol originally used to recover differentially expressed genes in RNA sequencing data[25–27], and used this method to assess enrichment/loss of barcode subclones after *in vivo* chemotherapy. We demonstrate that, with minimal adjustments, DGE analyses can be successfully applied to DNA barcode data. The potential applications of this type of analysis range much further. In future, DGE-like analysis can be employed to identify escape clones for various selective pressures, using several types of lineage tracing markers.

Chemotherapy induces clonal asymmetry

The observation that chemotherapy increases the asymmetric distribution of ALL clones across skeletal locations is in line with our previous work, demonstrating skewed localization of normal hematopoietic stem cells, as well as leukemia clones in untreated recipients[13,14,28]. Collectively, these studies support a model in which any reduction in the number of leukemia clones (e.g. by serial transplantation, by chemotherapy) increases the level of asymmetry in murine xenografts. If a similar model applies to human patients, this urges for extreme caution in the monitoring of treatment responses and assessment of minimal residual disease status, which are often based on analysis of a single bone marrow site.

Clonal origins of chemotherapeutic resistance

Having established efficient methods to label, trace and identify chemotherapy-resistant subclones, the next challenge will be to characterize the underlying mechanisms that allow these subclones to escape therapy. Currently, one of the major disadvantages of cellular barcoding is that the barcode composition of a sample can only be determined retrospectively, by sequencing bulk populations of cells. Accordingly, formal evidence of durable subclonal chemotherapeutic resistance and investigation of the underlying mechanisms, requires large-scale limiting dilution assays in high numbers of laboratory mice. Recent advances in single-cell technology and next-generation sequencing may address this issue, enabling prospective identification and sorting of barcode subclones[29,30]. The majority of barcode vectors include a potent promotor, which drives expression of a fluorescent protein (used to identify barcoded cells), including the downstream barcode sequence. These expressed barcode transcripts are unlikely to affect cell function, but

they can be detected by RNA sequencing. In the future, integration of cellular barcoding with single-cell RNA and DNA sequencing may enable genomic and transcriptomic characterization of therapy-resistant clones, potentially identifying clonal patterns or molecular pathways that can be used to predict and prevent leukemia relapse.

In conclusion, this study demonstrates that cellular barcoding and xenotransplantation is a relevant strategy to identify and trace the clonal dynamics of patient-derived leukemia clones in response to chemotherapy. In the future, combining cellular barcoding of larger cohorts of patients, and integration of cellular barcoding with single cell sequencing technology will provide a powerful tool to study the clonal evolution of chemotherapeutic resistance and to optimize patient treatment.

ACKNOWLEDGMENTS

FINANCIAL DISCLOSURE STATEMENT

AUTHORSHIP AND CONFLICT-OF-INTEREST STATEMENTS

MB, SJ, GdH and LB designed the research. MB, SJ, AA and EW performed the research. SJ, MB, EZ and LB analyzed the data. SJ, MB, GdH and LB wrote the manuscript.

None of the authors have any conflict of interest to declare.

REFERENCES

1. Hunger, S. P. & Mullighan, C. G. Acute Lymphoblastic Leukemia in Children. *N. Engl. J. Med.* **373**, 1541–1552 (2015).

2. Bhojwani, D. & Pui, C.-H. Relapsed childhood acute lymphoblastic leukaemia. *Lancet Oncol.* **14**, e205–e217 (2013).

3. Wiemels, J. L. *et al.* Prenatal origin of acute lymphoblastic leukaemia in children. *Lancet (London, England)* **354**, 1499–503 (1999).

4. Anderson, K. *et al.* Genetic variegation of clonal architecture and propagating cells in leukaemia. *Nature* **469**, 356–361 (2011).

5. Mullighan, C. G. *et al.* Genomic analysis of the clonal origins of relapsed acute lymphoblastic leukemia. *Science* **322**, 1377–1380 (2008).

6. Ma, X. *et al.* Rise and fall of subclones from diagnosis to relapse in pediatric B-acute lymphoblastic leukaemia. *Nat. Commun.* **6**, 6604 (2015).

7. Greaves, M. & Maley, C. C. Clonal evolution in cancer. *Nature* **481**, 306–13 (2012).

8. Notta, F. *et al.* Evolution of human BCR-ABL1 lymphoblastic leukaemia-initiating cells. *Nature* **469**, 362–367 (2011).

9. Aparicio, S. & Caldas, C. The implications of clonal genome evolution for cancer medicine. *N. Engl. J. Med.* **368**, 842–51 (2013).

10. Li, B. *et al.* Therapy-induced mutations drive the genomic landscape of relapsed acute lymphoblastic leukemia. *Blood* **135**, 41–55 (2020).

11. Alexandrov, L. B. *et al.* Signatures of mutational processes in human cancer. *Nature* **500**, 415–421 (2013).

12. Dobson, S. M. *et al.* Relapse-fated latent diagnosis subclones in acute B lienage leukemia are drug tolerant and possess distinct metabolic programs. *Cancer Discov.* **10**, 1–20 (2020).

13. Belderbos, M. E. *et al.* Clonal selection and asymmetric distribution of human leukemia in murine xenografts revealed by cellular barcoding. *Blood* **129**, 3210–3220 (2017).

14. Jacobs, S. *et al.* Quantitative distribution of patient-derived leukemia clones in murine xenografts revealed by cellular barcodes. *Leukemia* **34**, 1669–1674 (2019).

15. Elder, A. *et al.* Abundant and equipotent founder cells establish and maintain acute lymphoblastic leukemia. *Leukemia* (2017). doi:10.1038/leu.2017.140

16. Williams, M. T. S. *et al.* The ability to cross the blood-cerebrospinal fluid barrier is a generic property of acute lymphoblastic leukemia blasts. *Blood* **127**, 1998–2006 (2016).

17. Belderbos, M. E. *et al.* Donor-to-Donor Heterogeneity in the Clonal Dynamics of Transplanted Human Cord Blood Stem Cells in Murine Xenografts. *Biol. Blood Marrow Transplant.* (2019). doi:10.1016/j.bbmt.2019.08.026

18. Cheung, A. M. S. *et al.* Analysis of the clonal growth and differentiation dynamics of primitive barcoded human cord blood cells in NSG mice. *Blood* **122**, 3129–37 (2013).

19. Gerrits, A. *et al.* Cellular barcoding tool for clonal analysis in the hematopoietic system. *Blood* **115**, 2610–2618 (2010).

20. Bardini, M. *et al.* Clonal variegation and dynamic competition of leukemia-initiating cells in infant acute lymphoblastic leukemia with MLL rearrangement. *Leukemia* **29**, 38–50 (2015).

21. Ferrando, A. A. & López-Otín, C. Clonal evolution in leukemia. *Nat. Med.* **23**, 1135–1145 (2017).

22. Yates, L. R. & Campbell, P. J. Evolution of the cancer genome. *Nat. Rev.* **13**, 795–806 (2012).

23. Williams, J. B. *et al.* Tumor heterogeneity and clonal cooperation influence the immune selection of IFN-γ-signaling mutant cancer cells. *Nat. Commun.* **11**, 602 (2020).

24. Davis, J. B. *et al.* A new model isolates glioblastoma clonal interactions and reveals unexpected modes for regulating motility, proliferation, and drig resistance. *Sci. Rep.* **22**, 17380 (2019).

25. McCarthy, D. J., Chen, Y. & Smyth, G. K. Differential expression analysis of multifactor RNA-Seq experiments with respect to biological variation. *Nucleic Acids Res.* **40**, 4288–4297 (2012).

26. Robinson, M. D., McCarthy, D. J. & Smyth, G. K. edgeR: a Bioconductor package for differential expression analysis of digital gene expression data. *Bioinformatics* **26**, 139–140 (2010).

27. Ritchie, M. E. *et al.* limma powers differential expression analyses for RNA-sequencing and microarray studies. *Nucleic Acids Res.* **43**, e47–e47 (2015).

28. Verovskaya, E. *et al.* Asymmetry in skeletal distribution of mouse hematopoietic stem cell clones and their equilibration by mobilizing cytokines. *J. Exp. Med.* **211**, 487–97 (2014).

29. Alemany, A., Florescu, M., Baron, C. S., Peterson-Maduro, J. & van Oudenaarden, A. Whole-organism clone tracing using single-cell sequencing. *Nature* **556**, 108–112 (2018).

30. Kester, L. & van Oudenaarden, A. Single-Cell Transcriptomics Meets Lineage Tracing. *Cell Stem Cell* **23**, 166–179 (2018).

SUPPLEMENTARY INFORMATION

Supplementary methods

Barcode retrieval

Genomic DNA was isolated from cell pellets using the DNeasy Blood and Tissue (Qiagen, Hilden, Germany) or QIAamp DNA micro kit (Qiagen), according to manufacturer's instructions. Barcode sequences were amplified *in duplicate* in a 35-cycle PCR reaction using uniquely indexed eGFP forward primers (5'-TCGGCATGGACGAGCTG-3' or 5'-GGCATGGACGAGCTGTACAAG-3') and a WPRE reverse primer (5'-GGAGAAAAT-GAAAGCCATACGGGAAGC-3'). Duplicates of amplified barcode sequences were pooled together and amplification was confirmed on an agarose gel. Samples that did not show a clear band on the agarose gel were redone or subjected to a nested PCR reaction using an extra set of outer primers (forward 5'-TGCCCGACAACCACTACCTG-'3 and reverse 5'-AAA-CACAGTGCACACCACGC- '3). Subsequently, samples derived from SupB15 xenografts and patient-derived xenografts were respectively pooled together in batches of 24 samples or equimolar combined in pools of max. 12 samples. Pooled samples were cleaned according to the manufacturer's instructions using the QiaQuick PCR purification kit (Qiagen). All cleaned-up samples were pooled together in batches that contain 200-300 different samples and the quality of the sample was confirmed using the Agilent 2100 Bioanalyzer (Agilent Technologies, Inc., Santa Clara, California, USA). Next, samples were sent for paired-end next generation sequencing on an Illumina HiSeq 2500 Platform (BaseClear, Leiden, The Netherlands).

Barcode data processing

Barcode data processing was performed as previously described[3]. In short, raw sequencing reads with a minimal Phred quality score of 30 were collapsed (github: https://github.com/erikzwart/collapse-multiplex-barcodes). Collapsed reads were processed by performing an exact match of the sample tag sequence. Next, barcodes with either the GAANNNACNNNGTNNNCGNNNTANNNCANNNTAAGGAC or AG-GNNNACNNNGTNNNCGNNNTANNNCANNNTGNNNGAC backbone were retrieved using Motif Occurrence Detection Suite (MOODS, 1.0.2 https://github.com/jhkorhonen/MOODS/wiki/Installation-and-usage-(MOODS-1.0)). The generated list contained all possible barcodes per sample, which was further filtered by applying a Hamming distance of one to merge frequencies of barcodes that had the exact same sequence or barcodes that differ by one nucleotide. Samples that belonged to the same experiment were pooled into one table.

Data were further processed and analyzed using custom R scripts. First, we assessed the theoretical and actual chance of multiple barcode integrations into a single cell. Us-

ing linear regression analysis, we identified possible multiple integrations into a single cell (criteria: *slope – 1 < 0.05* and the $R^2 > 0.99$). If we identified samples with similar behavior across samples, we removed one of the barcodes from further data analysis. Second, low-noise barcodes were reduced by removing barcodes that were (i) present in only one sample, and (ii) had an overall read frequency of <0.5‰. Reduction of low-noise barcodes was confirmed by plotting the barcode frequencies in a histogram. The resulting barcode frequency table was used as input file for further data analysis. Samples with <500 reads were excluded from further analysis.

Statistical analysis
Statistical analysis and data visualization were performed in R (version 3.5.3)[4]. Data was visualized using package "ggplot2"[5]. Data significance was routinely tested by Mann-Whitney U and Student's t-test using standard packages in R. Principal component analysis was performed and visualized in R using packages "ade4" and "factoextra"[6,7]. Relevant plotting data for unsupervised clustering was extracted using package "ggdendro"[8]. The number of barcodes within a sample was expressed using the Shannon diversity index and derivatives, as previously described[1]. Statistical significance was defined as p<0.05.

Quantification of the absolute leukemia cell content
The absolute leukemia cell content was assessed at end-stage leukemia for all individual locations as described before[3].

Determining total body barcode composition
To calculate the total body barcode composition, barcode compositions in individual anatomical locations were summed, corrected for the contribution of that specific anatomical location to the total body leukemia load[3]. To assess the number of barcodes in the total body, the Shannon diversity index and derivatives were calculated using the total body barcode frequencies as input data.

Assessing differentially expressed barcodes in patient-derived xenografts
To identify barcodes that were differentially expressed in chemotherapy-treated patient-derived xenografts, we applied differentially gene expression analysis using packages "limma" and "edgeR" in R (version 3.5.3)[9–11]. First, to determine the cut-off p-value for significantly, differentially expressed barcodes, we applied this analysis to the total body barcode composition data of SupB15 xenograft. Hereto, we compared the total body barcode composition of control-treated SupB15 xenografts to the total body barcode composition of dexamethasone-, methotrexate- or vincristine-treated SupB15 xenografts. Next, we applied the differentially gene expression analysis to the total body barcode composition data of patient-derived xenografts. The total body barcode composition

data of control-treated patient-derived xenografts was compared to dexamethasone-, methotrexate-, or vincristine-treated xenografts. Differentially expressed barcodes were defined by: (1) a p-value that was equal to or lower compared to the cut-off p-value retrieved from the SupB15 barcode data; (2) a false discovery rate lower than 0.00125, since the occurrence of a type I error equals 1/800 when using a library of 800 unique barcodes.

Assessment of clonal asymmetry

To assess the degree of clonal asymmetry, analysis was restricted to hind legs, sternum, spine, blood, liver, spleen and brain for patient-derived xenografts, and to hind legs, pelvis, sternum, spine, blood, liver and spleen for SupB15 xenografts.

To determine the degree of relative clonal asymmetry between individual anatomical locations, we assessed the cumulative coefficient of variation (CV) of barcode frequencies for the top 100 barcodes (i) between sampled locations (see formula below). Hereto, we first calculated the CV value of barcode frequencies for each individual barcode between all locations. Next, we added up de individual CV values for the top 100 barcodes.

$$cumulative\ CV = \sum_{i=1}^{100} CV = \left(\frac{\delta}{\mu}\right)_i + \left(\frac{\delta}{\mu}\right)_{i+1} + \cdots + \left(\frac{\delta}{\mu}\right)_{100}$$

To determine the degree of absolute asymmetry between individual locations, we assessed the selective presence or absence of barcodes in sampled location. Hereto, for each sample barcodes were first ordered from large to small based on their frequency. Next, barcodes up to 85% of the total barcode frequency were defined as 'present' and values were set at 1. The remaining barcodes, ~15% of the total barcode frequency, were defined as 'absent' and values were set at zero.

Data sharing

For original data, please contact the corresponding author Dr. M.E. Belderbos: m.e.belderbos@prinsesmaximacentrum.nl.

References

1. Bystrykh L V, Belderbos ME. Clonal Analysis of Cells with Cellular Barcoding: When Numbers and Sizes Matter. In: Turksen K, ed. *Stem Cell Heterogeneity: Methods and Protocols*. New York, NY: Springer New York; 2016:57-89. doi:10.1007/7651_2016_343

2. Belderbos ME, Koster T, Ausema B, et al. Clonal selection and asymmetric distribution of human leukemia in murine xenografts revealed by cellular barcoding. *Blood*. 2017;129(24):3210-3220. doi:10.1182/blood-2016-12-758250

3. Jacobs S, Ausema A, Zwart E, et al. Quantitative distribution of patient-derived leukemia clones in murine xenografts revealed by cellular barcodes. *Leukemia*. December 2019. doi:10.1038/s41375-019-0695-2

4. R Core Team. R: A Language and Environment for Statistical Computing. 2019. https://www.r-project.org/.

5. Wickham H. *Ggplot2: Elegant Graphics for Data Analysis*. Springer-Verlag New York; 2016. https://ggplot2.tidyverse.org.

6. Dray S, Dufour A-B. The ade4 Package: Implementing the Duality Diagram for Ecologists. *J Stat Softw*. 2007;22(4):1-20. doi:10.18637/jss.v022.i04

7. Kassambara A, Mundt F. factoextra: Extract and Visualize the Results of Multivariate Data Analyses. 2019. https://cran.r-project.org/package=factoextra.

8. de Vries A, Ripley BD. ggdendro: Create Dendrograms and Tree Diagrams Using "ggplot2." 2016. https://cran.r-project.org/package=ggdendro.

9. Ritchie ME, Phipson B, Wu D, et al. limma powers differential expression analyses for RNA-sequencing and microarray studies. *Nucleic Acids Res*. 2015;43(7):e47-e47. doi:10.1093/nar/gkv007

10. Robinson MD, McCarthy DJ, Smyth GK. edgeR: a Bioconductor package for differential expression analysis of digital gene expression data. *Bioinformatics*. 2010;26(1):139-140. doi:10.1093/bioinformatics/btp616

11. McCarthy DJ, Chen Y, Smyth GK. Differential expression analysis of multifactor RNA-Seq experiments with respect to biological variation. *Nucleic Acids Res*. 2012;40(10):4288-4297. doi:10.1093/nar/gks042

Supplementary figures
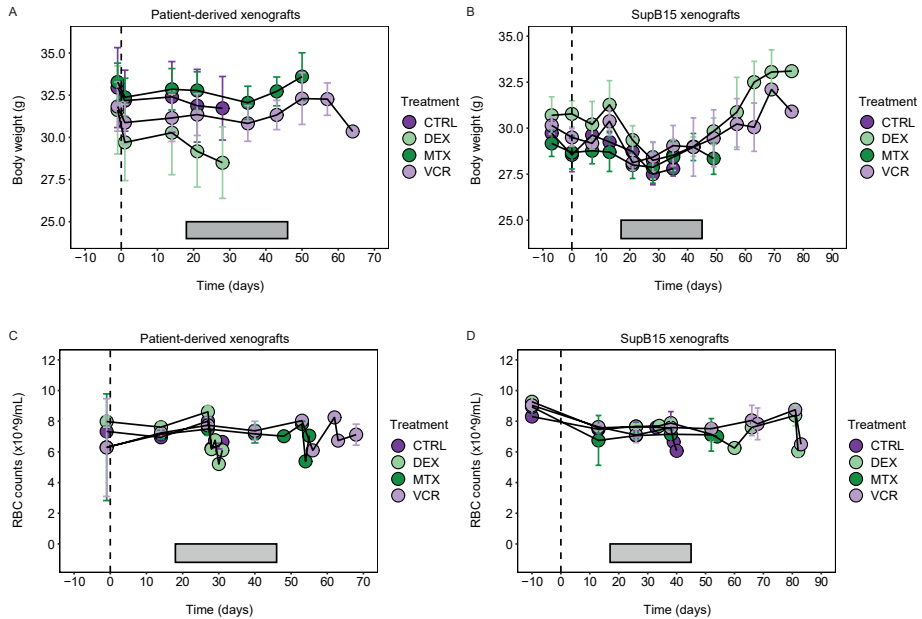
Figure S1. Treatment-related toxicity in SupB15 and patient-derived xenografts.
(A-B) Body weight of xenografts treated with dexamethasone, methotrexate, vincristine and saline as vehicle control (n=4 per treatment group). Grey beams indicate the treatment periods. Data are expressed as mean ± standard deviation. (C-D) The red blood cell counts measured in the peripheral blood of patient-derived and SupB15 xenografts treated with dexamethasone, methotrexate, vincristine or saline (n=4 per treatment group). Grey beams indicate the treatment periods. Data are expressed as mean ± standard deviation. Abbreviations; CTRL: control; DEX: dexamethasone; MTX: methotrexate; RBC: red blood cell; VCR: vincristine.
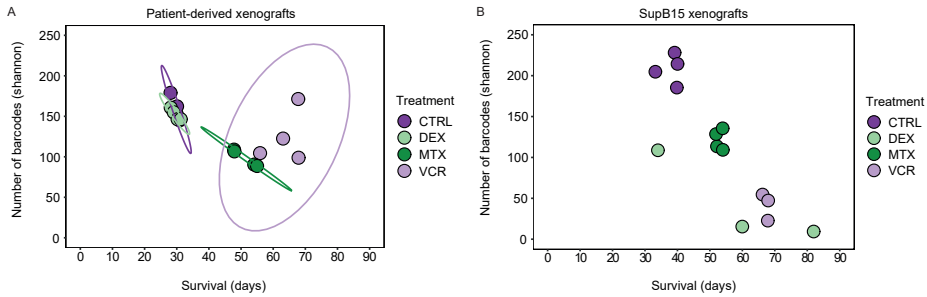
Figure S2. Barcode patterns in chemotherapy-treated xenografts

(A) The number of clones in the total body of patient-derived leukemia xenografts, as a function of the survival time. Ellipses reflect the 95% confidence interval, assuming a multivariate t-distribution. Linear regression modelling revealed that the number of clones was best predicted by the treatment (R^2=0.68 , $F(3, 12)$=8.54, p=0.0026), and not by survival time. Moreover, we observed multicollinearity between both variables (R^2=0.96, $F(3, 12)$=91.7, p=1.5×10^{-8}), excluding contributions and/or interactions between the survival time and treatment as predictors of the number of clones. (B) Number of clones in SupB15 xenografts, which was best predicted by the combination of survival and treatment (R^2=0.96 , $F(4, 9)$=51.3, p=3.4×10^{-6}), compared to either survival time (R^2= 0.74, $F(1, 12)$=34.2, p=7.9×10^{-5}) and treatment (R^2=0.89, $F(3, 10)$=26.83, p=4.3×10^{-5}) alone.
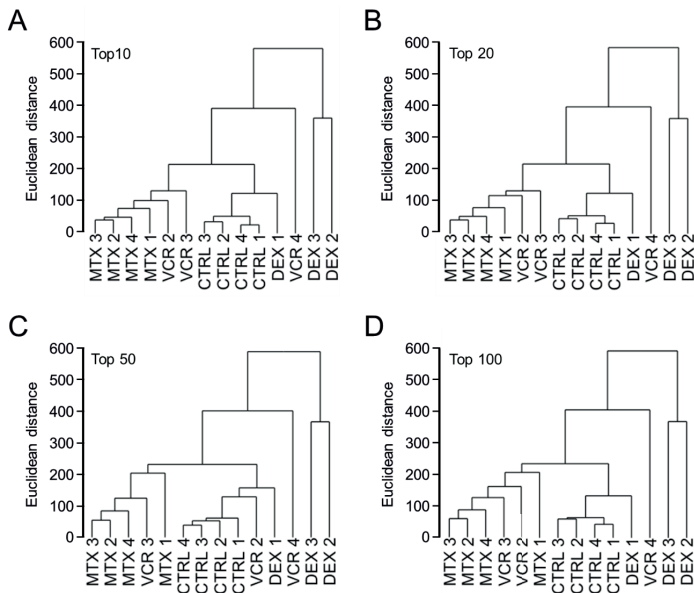
Figure S3. Clustering analysis of SupB15 leukemia xenografts, using different cutoffs for the number of barcodes included in the analysis.

Mice were clustered based on the Euclidean distance between barcode profiles. To account for semi-arbitrary decisions on the number of barcodes included in the analyses, we used different cutoffs, including the top 10 (A), top 20 (B), top 50 (C) or top 100 (D) clones in the total body of control mice in the analysis. Abbreviations: CTRL; Control; DEX: dexamethasone; MTX: methotrexate; VCR: vincristine; PDX: patient-derived xenografts
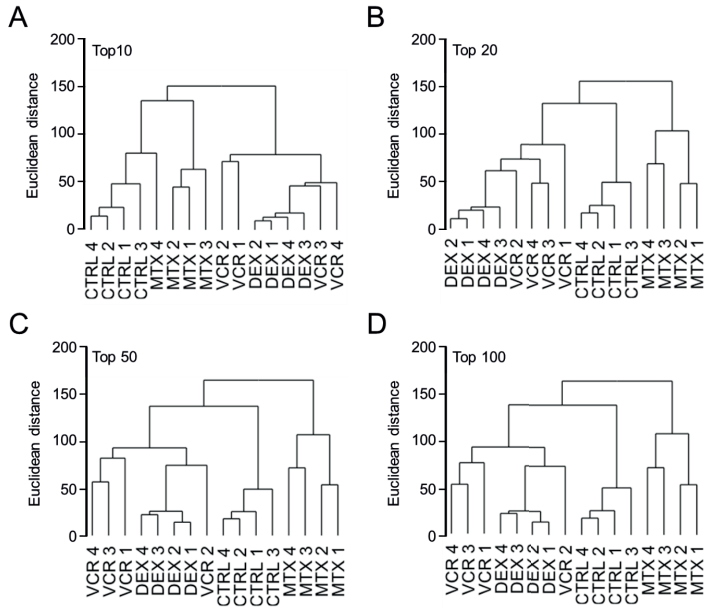
Figure S4. Clustering analysis of patient-derived xenografts, using different cutoffs for the number of barcodes included in the analysis.

Mice were clustered based on the Euclidean distance between barcode profiles. To account for semi-arbitrary decisions on the number of barcodes included in the analyses, we used different cutoffs, including the top 10 (A), top 20 (B), top 50 (C) or top 100 (D) clones in the total body of control mice in the analysis. Abbreviations: CTRL; Control; DEX: dexamethasone; MTX: methotrexate; VCR: vincristine; PDX: patient-derived xenografts.
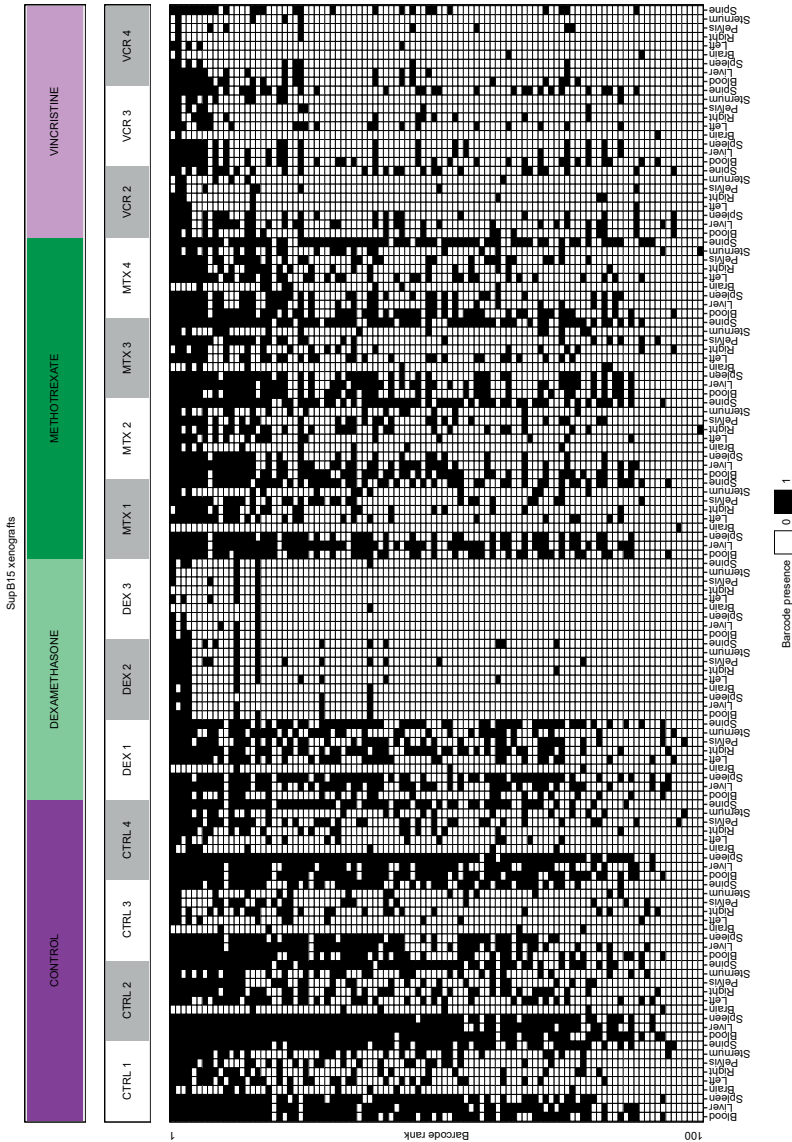
Figure S5. The absolute presence or absence of the top 100 clones in individual locations of SupB15 xenografts.
Overview of the top 100 overall largest barcode clones that were present (black) or absent (white) in individual locations of control-, dexamethasone-, methotrexate- and vincristine-treated SupB15 xenografts. Clones were ranked from large to small based on their average size in the total body of control-treated xenografts. Abbreviations; CTRL: control; DEX: dexamethasone; MTX: methotrexate; VCR: vincristine.
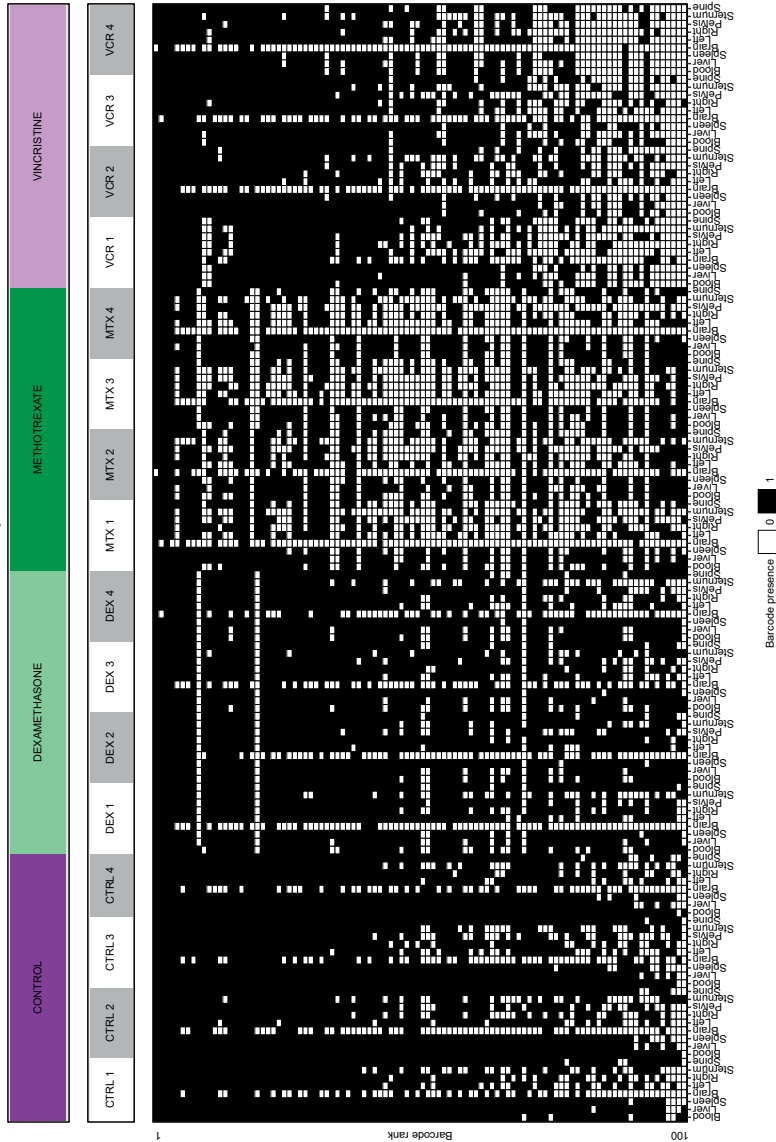
Figure S6. The absolute presence or absence of the top 100 clones in individual locations of patient-derived xenografts.
An overview of the top 100 overall largest barcode clones that were present (black) or absent (white) in individual locations of control-, dexamethasone-, methotrexate- and vincristine-treated patient-derived xenografts. Clones are ranked by their average size in the total body of control-treated xenografts. Abbreviations; CTRL: control; DEX: dexamethasone; MTX: methotrexate; VCR: vincristine.
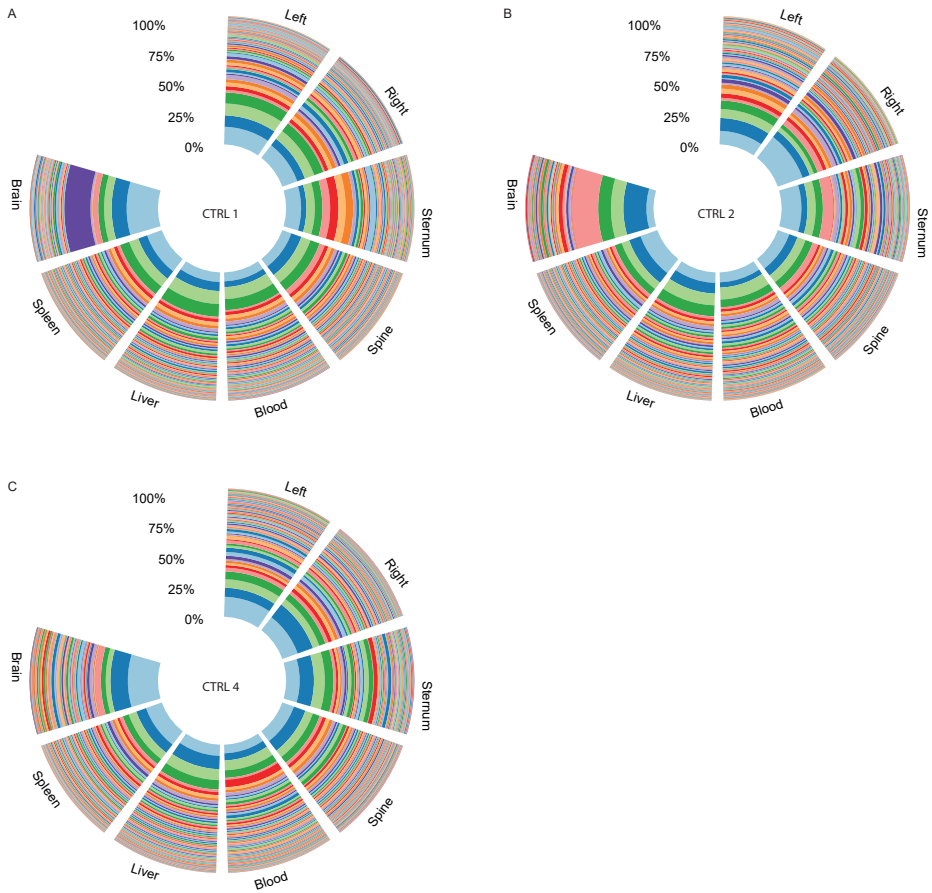
**Figure S7. Clonal composition in individual anatomic locations of control-treated patient-de-
rived xenografts.**

(A-C) Clonal composition of the top 100 overall largest barcode clones in the individual locations of
control-treated patient-derived xenografts. Clones are ordered from large to small based on their
average size in the total body. Abbreviation: CTRL: control.
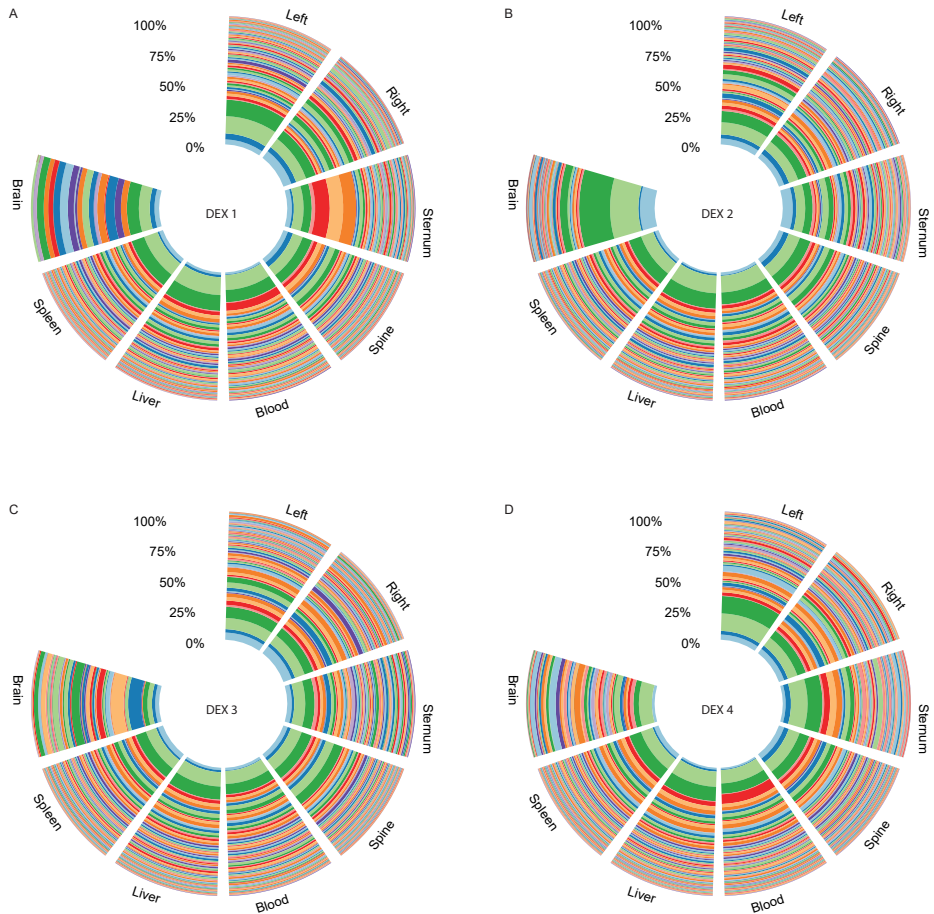
Figure S8. Clonal composition in individual anatomic locations of dexamethasone-treated patient-derived xenografts.

(A-D) Clonal composition of the top 100 overall largest barcode clones in the individual locations of dexamethasone-treated patient-derived xenografts. Clones are ordered from large to small based on their average size in the total body of control-treated patient-derived xenografts. Abbreviation; DEX: dexamethasone.

Figure S9. Clonal composition in individual anatomic locations of methotrexate-treated patient-derived xenografts.

(A-D) Clonal composition of the top 100 overall largest barcode clones in the individual locations of methotrexate-treated patient-derived xenografts. Clones are ordered from large to small based on their average size in the total body of control-treated patient-derived xenografts. Abbreviation; MTX: methotrexate.

Figure S10. Clonal composition in individual anatomic locations of vincristine-treated patient-derived xenografts.
(A-D) Clonal composition of the top 100 overall largest barcode clones in the individual locations of vincristine-treated patient-derived xenografts. Clones are ordered from large to small based on their average size in the total body of control-treated patient-derived xenografts. Abbreviation: VCR: vincristine.
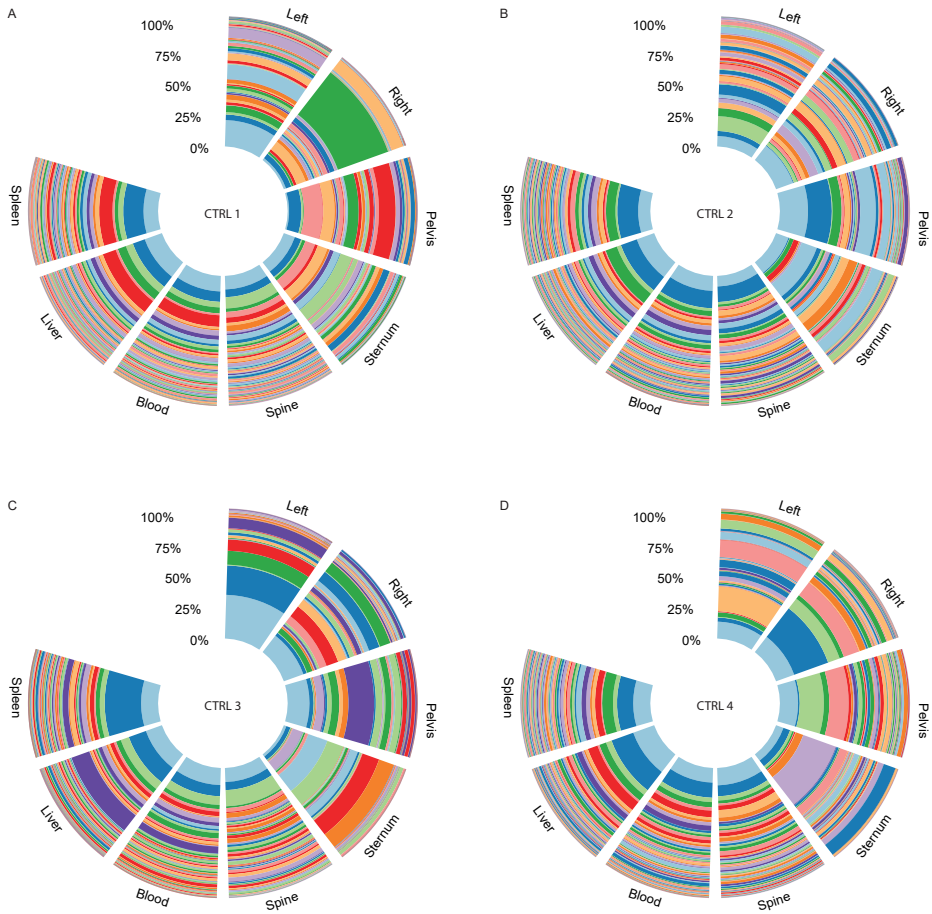
Figure S11. Clonal composition in individual anatomic locations of control-treated SupB15 xenografts.

(A-D) Clonal composition of the top 100 overall largest barcode clones in the individual locations of control-treated SupB15 xenografts. Clones are ordered from large to small based on their average size in the total body. Abbreviation; CTRL: control.
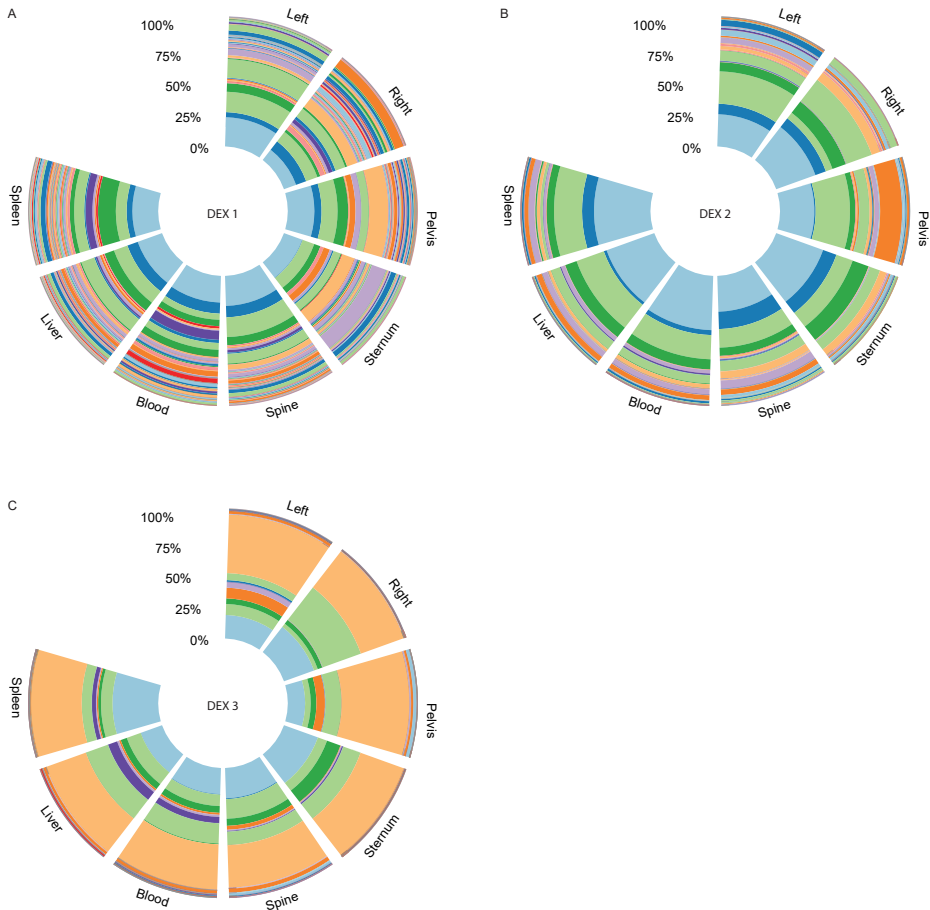
Figure S12. Clonal composition in individual anatomic locations of dexamethasone-treated SupB15 xenografts.
(A-C) Clonal composition of the top 100 overall largest barcode clones in the individual locations of dexamethasone-treated SupB15 xenografts. Clones are ordered from large to small based on their average size in the total body of control-treated SupB15 xenografts. Abbreviation; DEX: dexamethasone.
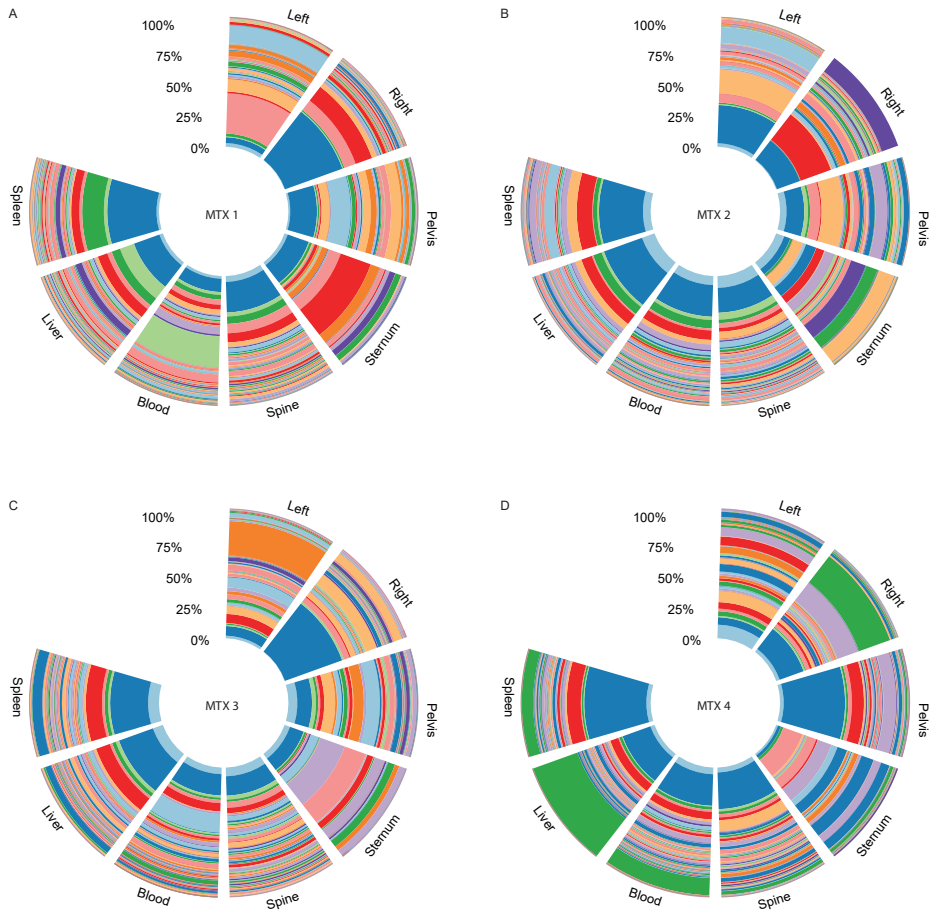
Figure S13. Clonal composition in individual anatomic locations of methotrexate-treated SupB15 xenografts.

(A-D) Clonal composition of the top 100 overall largest barcode clones in the individual locations of methotrexate-treated SupB15 xenografts. Clones are ordered from large to small based on their average size in the total body of control-treated SupB15 xenografts. Abbreviation; MTX: methotrexate.
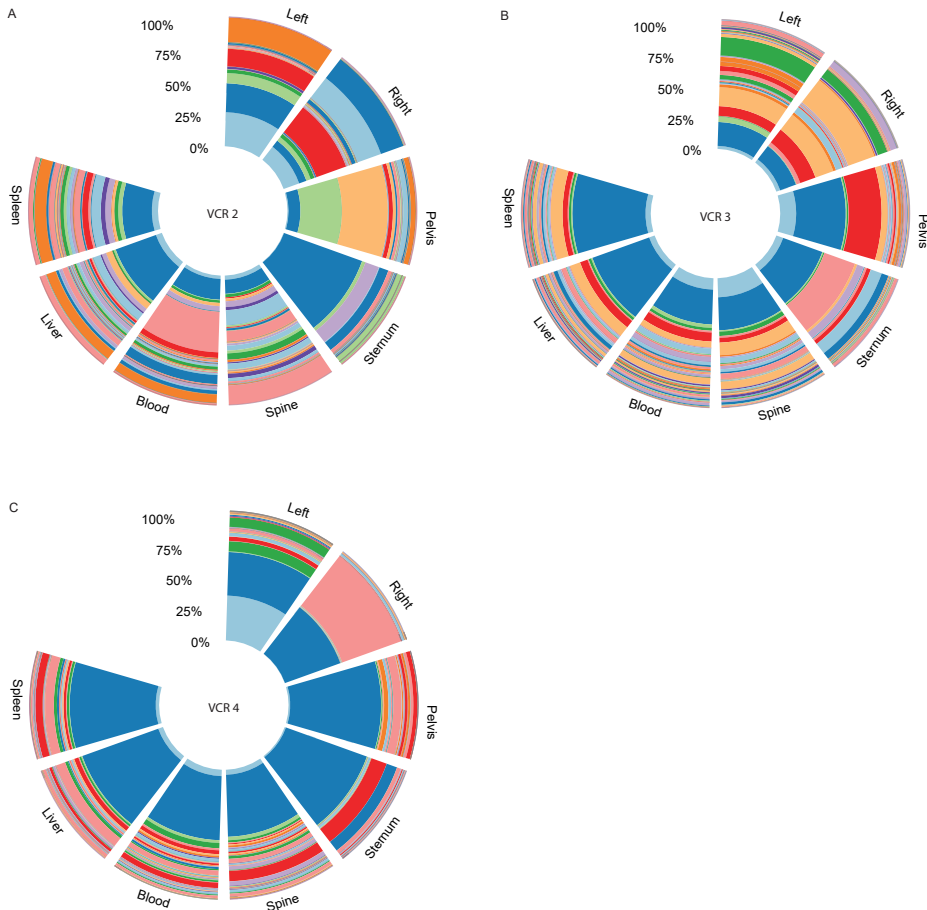
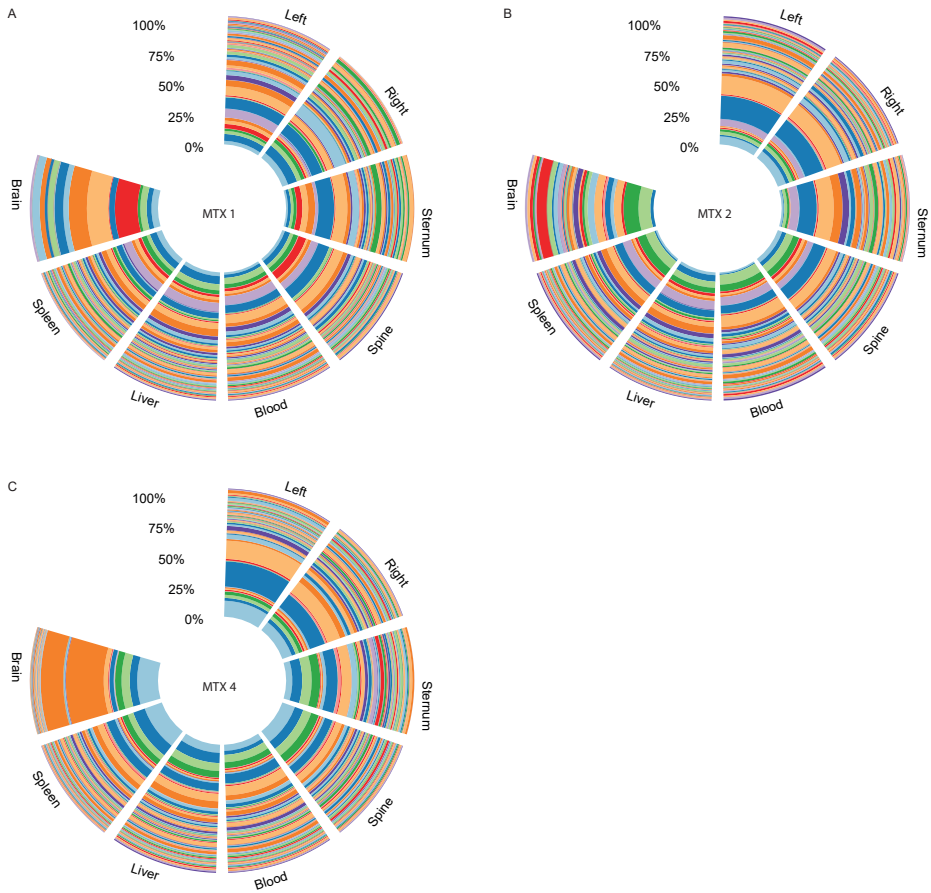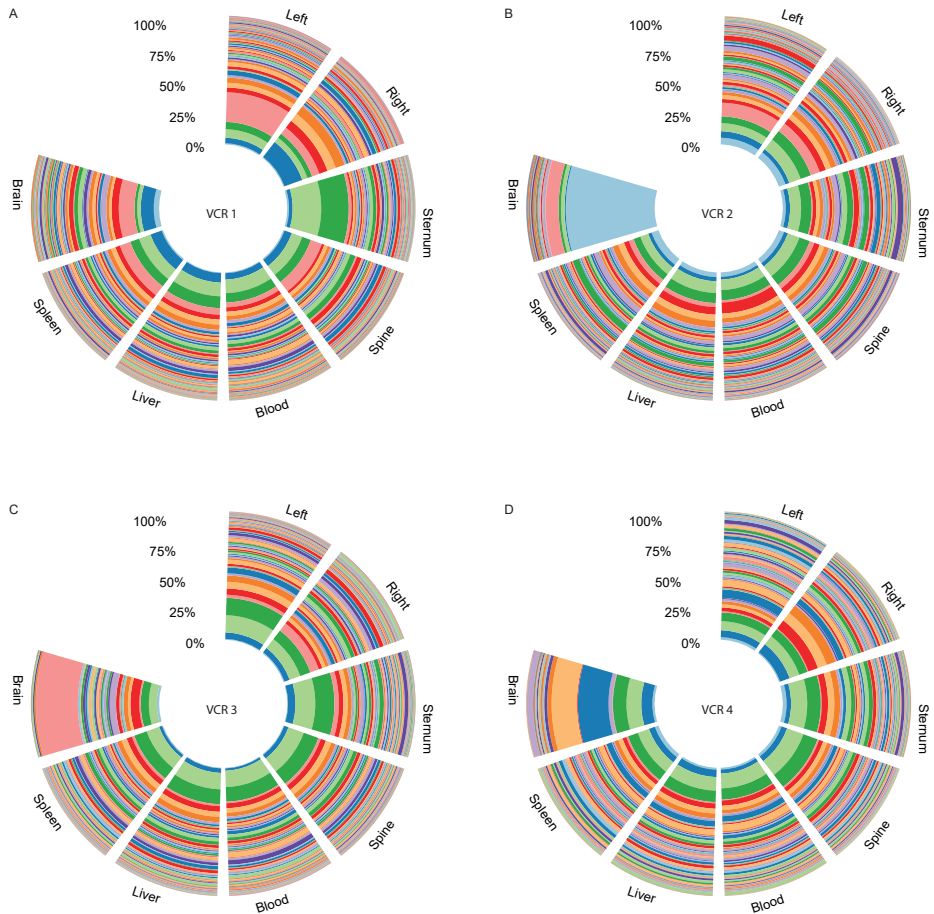**Figure S14. Clonal composition in individual anatomic locations of vincristine-treated SupB15 xenografts.**
(A-C) Clonal composition of the top 100 overall largest barcode clones in the individual locations of vincristine-treated SupB15 xenografts. Clones are ordered from large to small based on their average size in the total body of control-treated SupB15 xenografts. Abbreviation; VCR: vincristine.
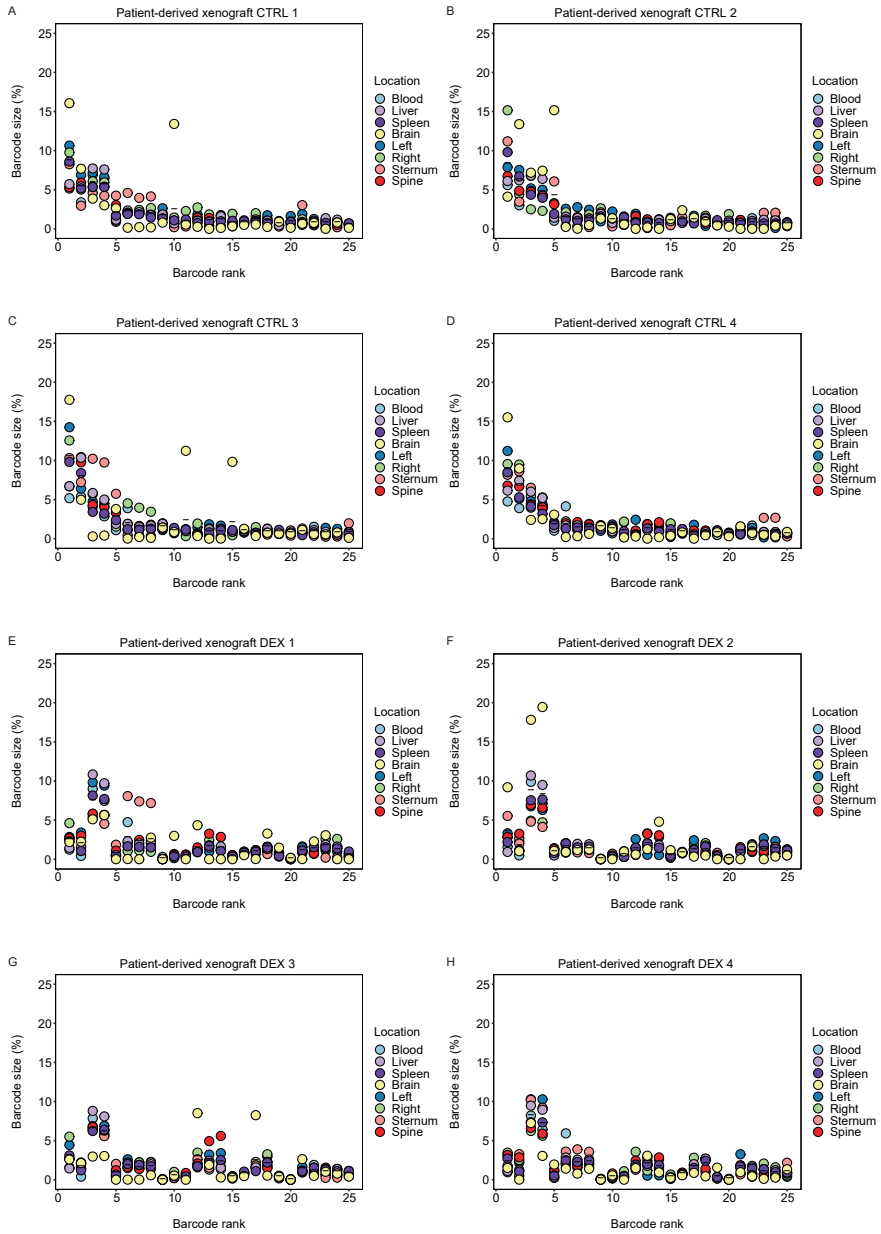
**Figure S15. Relative clonal asymmetry in patient-derived xenografts.**
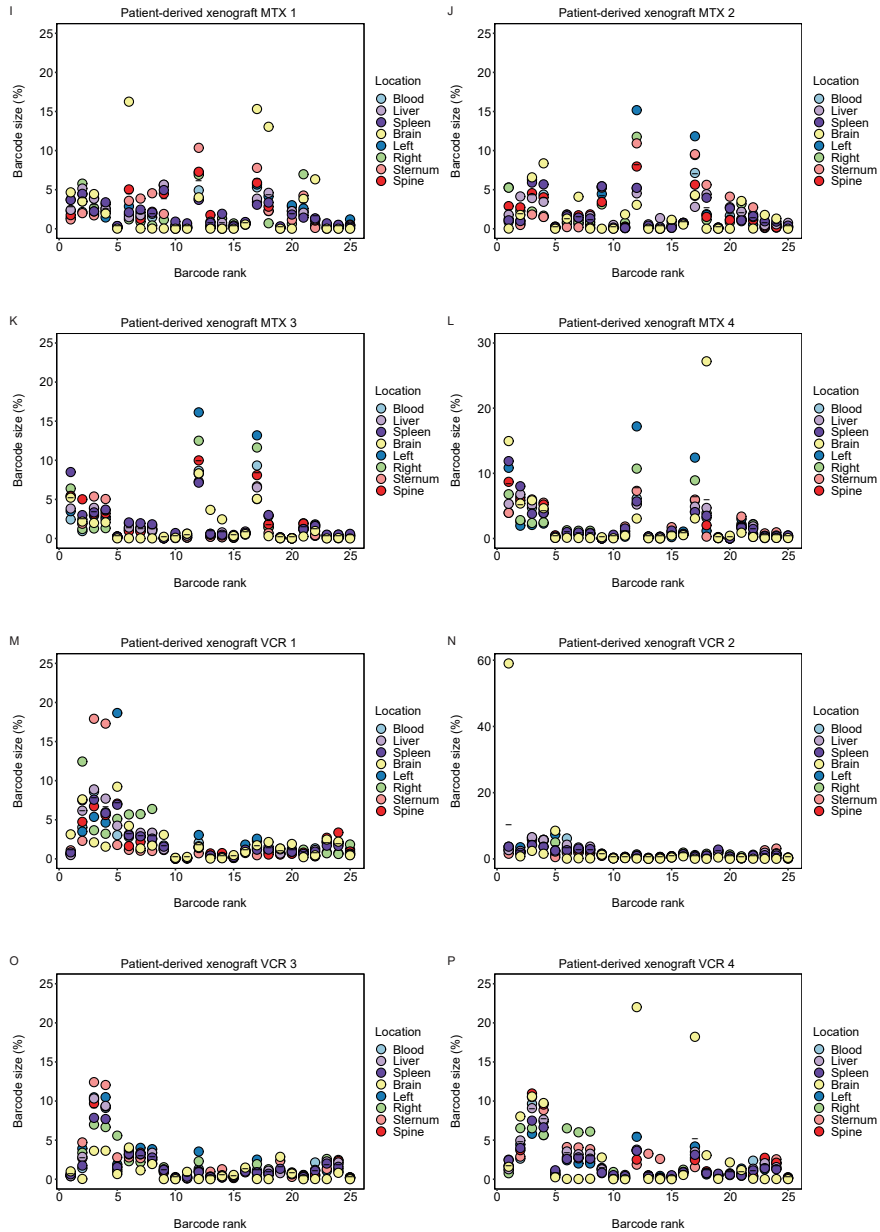
Figure S15. Relative clonal asymmetry in patient-derived xenografts.
(A-P) Clone sizes in individual locations in control- (A-D), dexamethasone- (E-H), methotrexate- (I-L) and vincristine-treated (M-P) patient-derived xenografts. Clones were ranked from large to small based on their size in control-treated patient-derived xenografts. Each dot represents the size of that specific clone in a certain location; lines represent the median clone size. Clones with a high degree of asymmetry have a greater degree of variation compared to clones that are symmetrically distributed. For clarity, only the top 25 clones are shown. Abbreviations; CTRL: control; DEX: dexamethasone; MTX: methotrexate; VCR: vincristine.
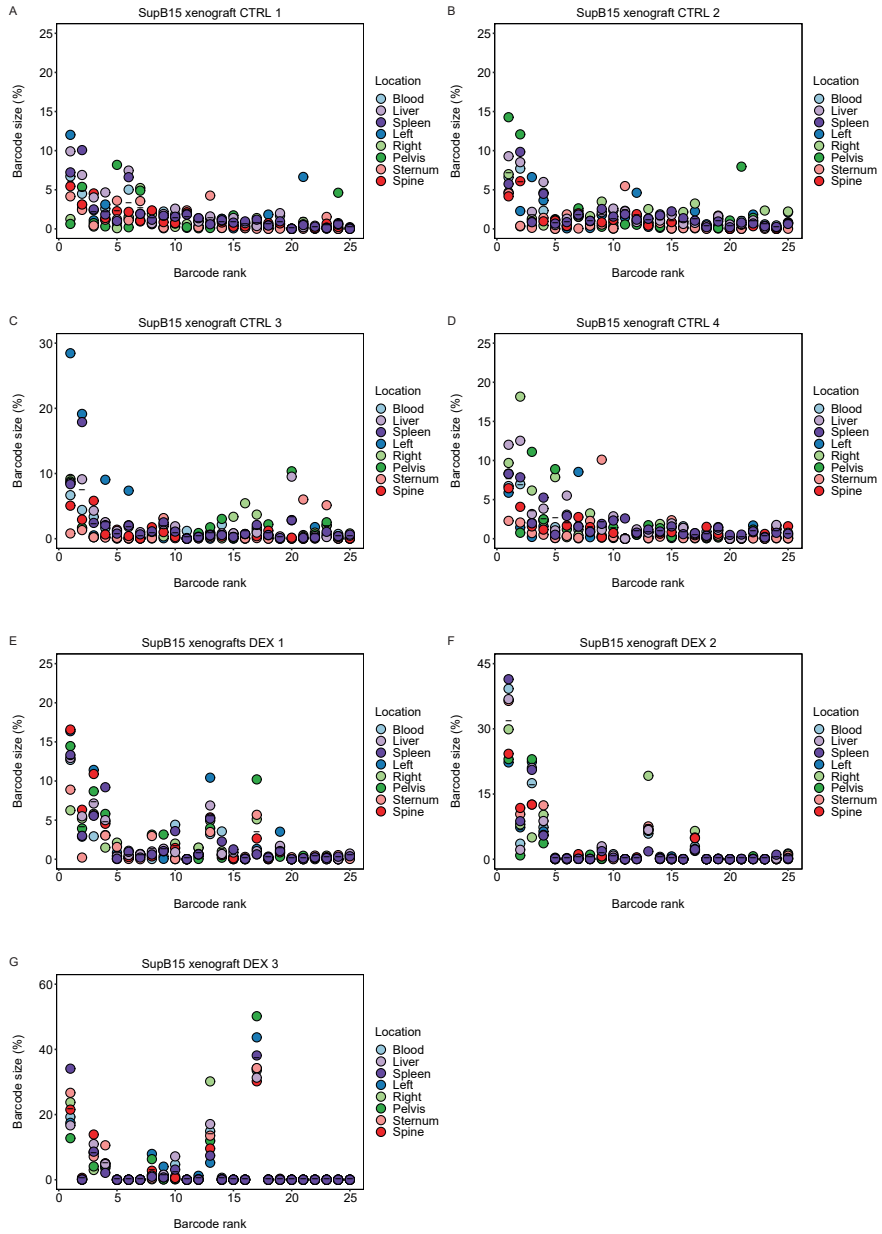
Figure S16. Relative clonal asymmetry in SupB15 xenografts.
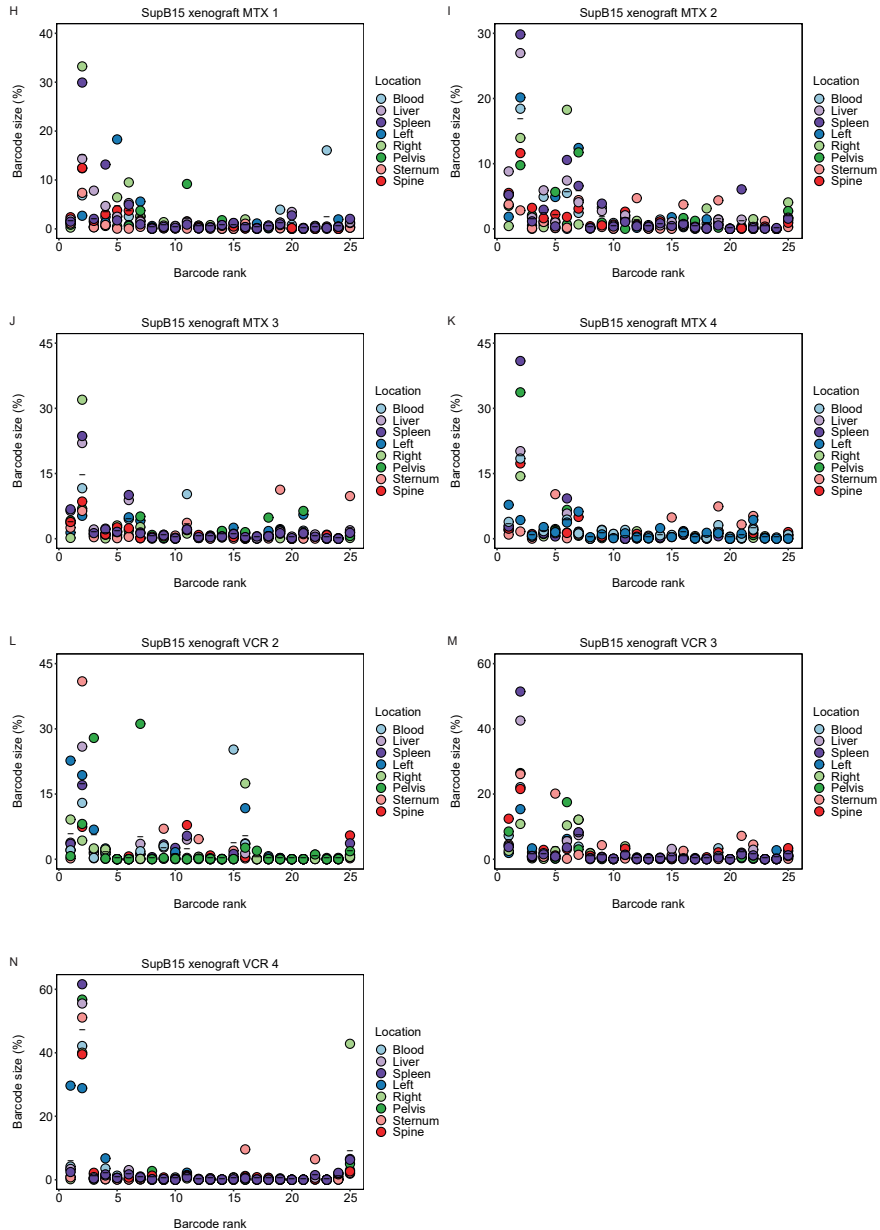
Figure S16. Relative clonal asymmetry in SupB15 xenografts.
(A-P) Clone sizes in individual locations in control- (A-D), dexamethasone- (E-H), methotrexate- (I-L) and vincristine-treated (M-P) SupB15 xenografts. Clones were ranked from large to small based on their size in control-treated xenografts. Each dot represents the size of that specific clone in a certain location; lines represent the median clone size. Clones with a high degree of asymmetry have a greater degree of variation compared to clones that are symmetrically distributed. For clarity, only the top 25 clones are shown. Abbreviations; CTRL: control; DEX: dexamethasone; MTX: methotrexate; VCR: vincristine.
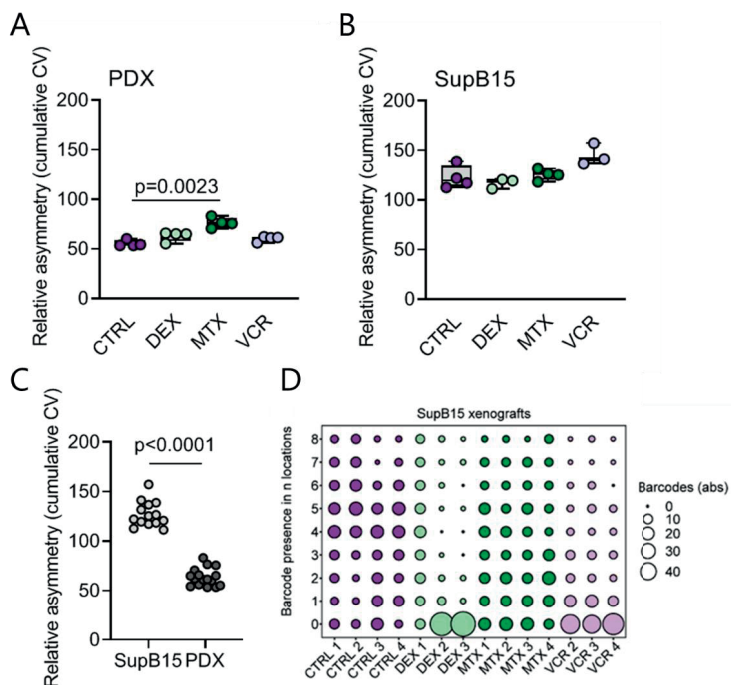
Figure S17. Clonal asymmetry in SupB15 xenografts.
(A-C) Relative clonal asymmetry in patient-derived xenografts (A) and in SupB15 (B) xenografts, quantified by the cumulative coefficient (CV) of variation for the top 100 most abundant barcode clones. Every dot represents the cumulative CV of an individual xenograft. (C) CV of all xenografts, irrespective of treatment group. Each dot represents an individual mouse. (D) Absolute asymmetry, depicted as the presence/absence of the top 100 barcode clones in n of the eight sampled anatomical locations (hind legs, pelvis, sternum, spine, blood, liver and spleen) of SupB15 xenografts. The size of the dot reflects the absolute number of clones that are present in n locations. Abbreviations; CTRL: control; DEX: dexamethasone; MTX: methotrexate; VCR: vincristine; PDX: Patient-derived xenografts.
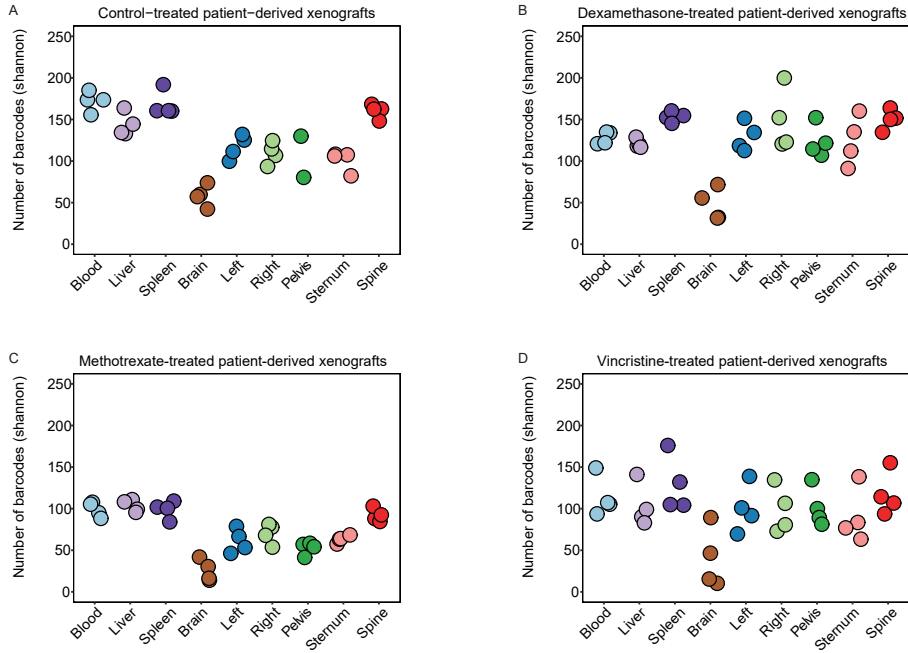
Figure S18. Chemotherapy-mediated clonal selection in individual anatomic locations.
(A-D) The number of clones – expressed as Shannon approximation – in individual locations of control- (A), dexamethasone- (B), methotrexate- (C) and vincristine-treated (D) patient-derived xenografts. Every dot represents an individual xenograft.

Supplementary tables

Supplementary tables are available via the online version of this paper.

Supplementary table S1 "Antibodies used for flow cytometry".

Supplementary table S2 "Administered doses of chemotherapy".

Supplementary table S3 "Output of differentially gene expression analysis of chemotherapy-treated SupB15 xenografts".

Supplementary table S4 "Output of differentially gene expression analysis of chemotherapy-treated patient-derived xenografts".

Chapter 6

Summary and general discussion

SUMMARY

Tissue-specific stem cells have the potential to self-renew and to give rise to a multi-lineage progeny of more differentiated cells. From a biological perspective, all descendants that are derived from the same ancestor are considered to constitute a clone and to share certain heritable features. However, it is becoming increasingly clear that these descendants are not completely identical. Rather, due to ongoing accumulation of (epi-)genetic alterations, they form a heterogeneous population of cells that differ in essential cell functions, such as proliferation, differentiation and survival. Moreover, especially in humans, these descendants are continuously exposed to a wide range of selective pressures, which fuel clonal selection and evolution. Together, the processes of clonal diversification, selection and evolution result in a continuously changing, heterogeneous population of cells. In the introduction of this thesis, we first summarized various clone-tracing methods which aim to track individual cells and their (clonal) progeny. We conclude that the degree of clonal complexity of a population of cells varies between these methods, due to differences in the definition, identification and approach to trace clones. In the past, our group has developed a cellular barcoding method, which allowed accurate and quantitative clonal tracking of murine hematopoietic stem cells (HSCs) and leukemia stem cells[1–4].

The overall aim of this thesis was to apply cellular barcoding to normal and malignant human hematopoietic stem and progenitor cell populations. We determined its applicability to quantify umbilical cord blood-derived HSCs and to assess their lineage output in murine xenografts (**chapter 2**), to quantify the number leukemia propagating cells and to assess their clonal distribution (**chapter 3 and 4**) and dynamics upon chemotherapeutic pressure (**chapter 5**).

In **chapter 2,** we assessed the impact of different data analysis strategies on conclusions regarding clonal dynamics and stem cell frequencies. Hereto, human umbilical cord blood-derived CD34+ hematopoietic stem progenitor cells (HSPCs) were barcoded and transplanted into sublethally irradiated Nod/Scid IL2Rγ$^{-/-}$ mice. Bone marrow, blood and spleen were collected to assess the human HSPC frequency and clonal dynamics using different data filtering and analysis strategies. We show that differences in data filtering and measures of population diversity can affect the frequency of CD34+ HSPCs by several orders of magnitude. These differences were predominantly caused by discrepancies in signal-noise discrimination and calling of small barcode clones. The Shannon diversity index takes both the number and relative abundance of barcodes into account. Therefore, the Shannon diversity index is less sensitive to PCR and sequencing noise. In line with this, the frequency of barcode HSPCs derived from the Shannon diversity index remained most consistent between different data filtering strategies. In contrast, nominal counts and selected nonparametric asymptotic estimators of population diversity

were more sensitive to the different data filtering strategies. Using the Shannon diversity index, we showed that the frequency of HSPCs, that generate multi-lineage offspring in murine xenografts, can vary several-fold between different umbilical cord blood donors.

In **chapter 3,** we introduced barcode sequences into patient-derived B-cell acute lymphoblastic leukemia cells to assess their clonal dynamics and anatomic distribution in murine xenografts. We first validated the barcode library in the SupB15 pediatric leukemia cell line. We showed that the majority of barcodes are present at equimolar ratios within the library and that barcode sequences can be relatively simple and accurately retrieved from deep sequencing data. We subsequently performed serial transplantations of barcoded patient-derived leukemia cells in sublethally irradiated Nod/Scid IL2Rγ$^{-/-}$ mice. A selected number of skeletal and extramedullary locations were assessed for their clonal composition. Variable numbers of barcode clones were retrieved from xenografts, but all were highly polyclonal and harbored tens to hundreds of barcode clones. Individual primary xenografts transplanted with the same patient-derived leukemia cells were different in their clonal composition, while secondary and tertiary recipients were increasingly similar. Moreover, leukemia barcode clones were asymmetrically distributed across the murine body. The clonal composition varies both between individual skeletal sites and between skeletal and extramedullary sites. This has important implications for experimental studies and for clinical diagnosis and follow-up, where single-site sampling is common practice.

In **chapter 4,** we elaborate on the anatomical asymmetry of individual leukemia clones in murine xenografts. Here, we provide a quantitative assessment of leukemia clonal composition in the total body, by combining differential blood counts (i.e. absolute white blood cell counts) and flow cytometry (i.e. the relative frequency of leukemia cells). At end-stage leukemia, murine xenografts harbored millions of leukemia cells. The absolute number of leukemia cells varied between the anatomic locations, with the majority of the cells localized in the spine and the spleen. Only a minor fraction of leukemia cells was located in the blood. Moreover, the leukemia cell content in bone marrow locations was consistent between xenografts and patient's samples. On the contrary, the extramedullary sites were more variable in their leukemia cell content. This contrast can potentially be explained by the inability of bones to expand, whereas extramedullary locations can expand. Together, these findings suggest that the leukemia cell content in a given anatomic location is dictated (and restricted) by its 'carrying' capacity. This was confirmed by proportional hematopoietic cell content in the bone marrow locations of leukemic and healthy recipients. In line with **chapter 3**, leukemia barcode clones were asymmetrically distributed across skeletal sites. As a consequence, only half of the clones are detected when only the blood and pelvic bones are assessed for their leukemia content. This has important implications for experimental studies and clinical diagnosis

and follow-up, as single site sampling might result in an underestimation of the clonal complexity of the disease.

In **chapter 5,** we assessed the applicability of cellular barcoding to study the clonal dynamics of patient-derived leukemia clones in response to chemotherapy-induced selective pressure. Hereto, sublethally irradiated Nod/Scid IL2Rγ$^{-/-}$ mice were transplanted with barcoded patient-derived leukemia cells and secondary recipients were treated with either dexamethasone, methotrexate or vincristine. To control for random fluctuations in clonal dynamics, we transplanted sublethally irradiated Nod/Scid IL2Rγ$^{-/-}$ mice with the SupB15 pediatric leukemia cell line. We showed that all chemotherapeutic agents were well tolerated. Methotrexate and vincristine treatment both delayed leukemia development and prolonged survival of patient-derived xenografts. On the contrary, dexamethasone treatment did not affect leukemia development nor survival in patient-derived xenografts, suggestive of steroid-resistance at population level. When we assessed the clonal composition of these mice, we observed that the barcode composition was highly similar between patient-derived xenografts that received the same treatment. Moreover, methotrexate treatment significantly reduced the number of leukemia barcode clones and eliminated both smaller and larger clones, suggestive for heterogeneous drug sensitivity. Next, we applied differential gene expression analyses to our DNA barcode sequencing data, using the SupB15 xenografts as a control. We identified several barcode clones in methotrexate-treated patient-derived xenografts that were significantly enriched compared to control-treated mice. In contrast, in SupB15 xenografts, no enrichment was observed, suggesting that these patient-derived clones may be resistant. Notably, methotrexate treatment increased both the absolute and relative anatomic asymmetry of patient-derived xenografts. Altogether, cellular barcoding and xenotransplantation are a useful method to identify and trace leukemia clones in response to single chemotherapeutic agents.

GENERAL DISCUSSION

Relevance of clone-tracing

The development of more advanced sequencing technology has provided crucial insight into clonal heterogeneity of leukemia. Similar to a range of solid tumors[5-9], acute lymphoblastic leukemia consist of multiple (epi-)genetically diverse populations of cells which are subjected to a Darwinian-like process of clonal evolution[10-13]. The acquisition of (epi-)genetic aberrations was initially thought to be a linear process, where sequential acquisition of mutations resulted in the generation of new clones[14]. However, genomic analysis of paired diagnostic and relapsed leukemia blasts suggests that clonal evolution is a more complex branching process that results in a continuously changing

heterogeneous population of leukemia cells[10–12]. Relapsing clones are frequently present as minor subpopulation at diagnosis and acquire additional genomic aberrations at relapse, suggestive of clonal evolution. Comparison of diagnostic and relapsed leukemia blasts also resulted in the identification of mutations in relapse-associated genes[10–12,15–21]. Moreover, sequencing of serial bone marrow-derived leukemia blasts suggests selection of chemotherapy-induced mutations as an alternative mechanism of therapy resistance and driver of relapse[22]. However, validation and a better understanding of the potential therapy-resistant mechanisms (e.g. self-renewal capacity, clonal evolution, therapy-resistant mutations and microenvironment) of subclones as driver of relapse largely rely on experimental studies, including *in vitro* assays, murine models and patient-derived xenografts[15–17,19–21,23–28]. Altogether, current clone tracing methods underline the biological relevance of clonal heterogeneity as driver of leukemia progression, therapy resistance and relapse. However, it remains to be determined how the proposed mechanisms drive relapsing clones in human patients.

Despite our increased understanding of clonal heterogeneity in acute lymphoblastic leukemia, it is not completely understood how relapsing clones arise and how their expansion is maintained and/or regulated during disease progression. This is primarily due to the lack of a noninvasive method to identify and prospectively trace individual leukemia propagating cells and their progeny in human patients. Retrospective sequencing of naturally occurring somatic mutations in the nuclear genome is currently the primary method to reconstruct evolutionary trajectories[29–31]. However, bulk or single-cell sequencing of mutations in human patients usually provides a snapshot of the mutational state of leukemia cells in time (i.e. diagnosis and relapse) and space (i.e. blood and one bone marrow site). Based on these snapshots the mutational dynamic is computationally reconstructed and the intermediate mutational states are derivatives of these snapshots[32,33]. Moreover, sequencing of mutations does not always provide insights into the mechanisms that drive relapsing clones. In addition, due to technical difficulties, sequencing of the genome is rarely combined with other single-cell sequencing approaches. However, the applicability of the many experimental clonal markers that are compatible with other single-cell sequencing technology is problematic and unethical in human patients. Moreover, with the exception of easily accessible tissues such as the blood, a biopsy in human patients is invasive. Therefore, prospective assessment of the temporal and spatial clonal heterogeneity of leukemia in human patients is challenging and largely relies on preclinical studies.

Clone-tracing using DNA barcodes: advantages and pitfalls

In this thesis, we have shown that DNA barcoding is a relatively simple and affordable method to study the dynamics of individual patient-derived HSC and leukemia clones in murine xenografts[34–37]. With proper library design, hundreds of clones can be accurately

traced in parallel[38,39]. Moreover, DNA barcodes are quantitative and do not require the use of complex computational analysis[38–40]. In addition, the application of DNA barcodes in murine xenografts allows us to study the dynamics of patient-derived leukemia clones over time, across different anatomical locations and in response to selective pressures such as serial transplantations and chemotherapy[27,35–37]. However, our approach also faces limitations. First, DNA barcoding might result in the loss of leukemia propagating cells due to selective pressures, including *in vitro* cell culture and *in vivo* transplantation. Second, the clonal composition and dynamic of a population of leukemia cells are determined retrospectively through bulk sequencing. Accordingly, individual leukemia cells cannot be sorted based on their barcode sequence for subsequent molecular analysis. Finally, the potential risks of viral transduction and integration of DNA barcode sequences into the target cells (i.e. insertional mutagenesis) hamper the application of DNA barcoding in human patients. To confirm current preclinical views on clonal heterogeneity and evolution of leukemia, non-invasive prospective clone-tracing strategies that are applicable in human patients are required. Moreover, to understand how the different mechanisms of therapy resistance contribute to relapse, the clone-tracing strategy should allow linkage of extensive molecular information to the fate of an individual cell at multiple stages during leukemia development. In the next paragraph, we will discuss features of the ideal clone-tracing method and provide examples of studies that address different aspects of the ideal clone-tracing method.

The ideal clone-tracing method/strategy

In the absence of ethical, technical and financial boundaries, we can define the characteristics of the ideal method to study the dynamics of individual leukemia clones in human patients. The ideal clone-tracing strategy should fulfill several criteria. First, to accurately trace the progeny of individual leukemia clones in their polyclonal environment, the marker should be heritable, stable and allow discrimination of a sufficient number of individual cells. Second, the marker should acquire additional, predetermined genomic alterations related to every cell division to circumvent the use of complex mathematical modeling and accurately reconstruct the evolutionary trajectory. Third, to accurately identify individual clones, the generation and retrieval of the marker library should be unbiased. Moreover, upfront knowledge of the complexity of the library will facilitate more precise quantification of clone sizes. Fourth, to link clonal dynamics to molecular information, this marker should not affect the behavior of individual cells and be compatible with other (single-cell) technologies, such as transcriptomics, proteomics or metabolomics. Fifth, ideally, this approach is affordable, reproducible and universal, to facilitate repetitive use in diverse laboratories and in a wide variety of cancer types. Finally, to consider the actual fate of an individual patient-derived leukemia cell and not its potential in experimental studies, this approach should be applicable in human

patients. Altogether, such a method could predict the developmental fate of individual cancer cells in response to treatment and potentially provide the knowledge to create an evolutionary trap[41] to eradicate all cancer propagating cells in human patients.

The first steps towards this ideal clone-tracing method have been made in developmental studies, which aim to understand how a single cell becomes a full-grown multicellular organism[42,43]. For instance, parallel sequencing of clonal markers and the transcriptome of individual cells allowed reconstruction of the developmental lineages of multiple organs of zebrafish[44–47] and mice[48]. In these studies, CRISPR-Cas9-based genetic 'scars' were introduced during early and late developmental stages to determine clonal relationships between individual cells. Sequencing of the transcriptome was used to provide information on cell types. Parallel sequencing of the transcriptome and 'scars' at a later stage during development is of added value as it provides insights into the clonal origin of adult cell types. As another example, recent studies used DNA barcoding and transcriptomics to study the differentiation process of murine hematopoietic progenitor cells[49,50]. By comparing the transcriptome of clonally related cells at multiple time points during development, the authors identified transcriptomic changes related to the fate of cells[49]. Remarkably, this study also revealed that transcriptionally similar daughter cells can have a different development fate[49]. Other factors, such as the chromatin accessibility, proteome, metabolome or environment, could potentially affect the developmental fate of a cell. Moreover, assessment of transcriptomic differences between functionally diverse clones can identify genes related to this phenotypic heterogeneity[50]. Currently, the first publications appear where simultaneous clone-tracing and single-cell transcriptome analysis identified genetic alterations related to cancer progression[51,52]. In a third example, clone-tracing has been combined with *in situ* readout, which could potentially address transcriptomic changes of clonally related cells in their spatial context[53,54]. As a last example, several studies have assessed the possibility of clonal markers to be inducible by environmental signals[46,47,55] or to be continuously introduced[48,56]. Although potential off-target effects should be considered, these studies pave the way to mitotic-dependent clonal marking. Altogether, pre-clinical studies showed that clone-tracing is compatible with single-cell technologies and potential conservation of the spatial context. The next challenge relies on combining clone-tracing with methods to detect (epi-)genetic, transcriptomic, proteomic and metabolomics changes in their spatial context and at multiple time points during development.

The compatibility of clone-tracing methods with other single-cell technologies is not only restricted to cell culture or transplantation assays. In human patients, sequencing of mutations in the mitochondrial DNA (mtDNA) has been proposed as an alternative clone-tracing method to sequencing mutations in the nuclear genome. Using mtDNA as a clonal marker is particularly interesting because it can be detected in parallel to single-cell transcriptome sequencing or assay for transposase accessible chromatin (ATAC)

sequencing[57–59]. Moreover, sequencing of mtDNA has the advantage that the mtDNA is small in size and therefore relatively affordable compared to sequencing of the whole nuclear genome[60]. In addition, as individual cells contain multiple mitochondria, mtDNA is relatively abundant in individual cells and thereby less sensitive to amplification bias. However, mutations in mtDNA as clonal markers also face limitations. First, notwith-standing the multiplicity of mitochondria, the frequency of *de novo* mutations may be too low to be detected. Second, clonal relationships may be inaccurate as mitochondria are randomly distributed across daughter cells upon cell division, some mutations may negatively affect mitochondrial fitness and individual cells may exchange their mito-chondria in pathological conditions such as leukemia[61,62]. Although these limitations should be considered and mutations in mtDNA might not be applicable as clonal markers in all conditions, it is a new step in combining clone-tracing with transcriptomic and epigenomic changes in human patients.

Patient-derived xenografts provide a pre-clinical model that allows to study leukemia pathogenesis at different stages of leukemia development in the context of the patient´s clonal complexity. However, xenografts lack human niche factors and patient-derived leukemia cells may be subjected to selection upon transplantation. Where xenograft models allow cell collection from virtually all anatomical locations, in human patients collecting cells from most tissues is an invasive procedure. Blood is the least invasive location from which repetitively cells can be collected. In solid tumors, circulating tumor DNA represents tumor heterogeneity and is used complementary to tissue biopsies[63]. Although spatial heterogeneity needs to be confirmed in human leukemia patients, patient-derived xenograft models suggest that collecting cells from solely the blood will not fully capture the clonal complexity[27,35,36]. To do so, this would require a symmetric distribution of leukemia propagating cells, which could potentially be achieved by mobilization of leukemia propagating cells to the circulating blood system. In murine skeletal sites, hematopoietic stem cell clones were equally redistributed upon a single challenge with a mobilizing agent[3]. Moreover, treatment of patient-derived xenografts with the mobilizing agents inhibited engraftment, mobilized leukemia cells to the pe-ripheral blood and increased chemotherapeutic efficacy resulting in fewer circulating leukemic cells and prolonged survival[64–66]. Mobilizing agents are routinely used in the clinic to mobilize HSCs to the blood circulation for allogeneic and autologous stem cell transplantations[67]. Moreover, clinical trials aimed to determine its safety and efficacy as complementary treatment to chemotherapy in leukemia patients[68–71]. Although the potential beneficial effect on clinical outcome remains unclear, mobilizing agents can be relatively safely administered to leukemia patients in combination with chemotherapy, to mobilize leukemia cells to the peripheral blood. As complementary treatment with mobilizing agents is safe, it is tempting to speculate that repetitive sampling of peripheral blood in the context of such therapies might improve our view on the degree of clonal

complexity in human patients. Relapsing clones, potentially hiding in locations that are not routinely assessed in the clinic, might become detectable upon their mobilization to the peripheral blood. Follow-up studies in human patients could determine whether complementary treatment with mobilizing agents could provide a more in-depth view of the clonal complexity. Understanding the overall clonal complexity of leukemia and their dynamics in response to therapy could result in new therapeutic interventions and improve diagnostics and monitoring of patients with acute lymphoblastic leukemia.

REFERENCES

1. Gerrits A, Dykstra B, Kalmykowa OJ, et al. Cellular barcoding tool for clonal analysis in the hematopoietic system. *Blood*. 2010;115(13):2610-2618. doi:10.1182/blood-2009-06-229757

2. Verovskaya E, Broekhuis MJC, Zwart E, et al. Heterogeneity of young and aged murine hematopoietic stem cells revealed by quantitative clonal analysis using cellular barcoding. *Blood*. 2013;122(4):523-532. doi:10.1182/blood-2013-01-481135

3. Verovskaya E, Broekhuis MJC, Zwart E, et al. Asymmetry in skeletal distribution of mouse hematopoietic stem cell clones and their equilibration by mobilizing cytokines. *J Exp Med*. 2014;211(3):487-497. doi:10.1084/jem.20131804

4. Klauke K, Broekhuis MJC, Weersing E, et al. Tracing Dynamics and Clonal Heterogeneity of Cbx7-Induced Leukemic Stem Cells by Cellular Barcoding. *Stem Cell Reports*. 2015;4(1):74-89. doi:10.1016/j.stemcr.2014.10.012

5. Thirlwell C, Will OCC, Domingo E, et al. Clonality Assessment and Clonal Ordering of Individual Neoplastic Crypts Shows Polyclonality of Colorectal Adenomas. *Gastroenterology*. 2010;138(4):1441-1454.e7. doi:10.1053/j.gastro.2010.01.033

6. Shah SP, Roth A, Goya R, et al. The clonal and mutational evolution spectrum of primary triple-negative breast cancers. *Nature*. 2012;486(7403):395-399. doi:10.1038/nature10933

7. Gerlinger M, Rowan AJ, Horswell S, et al. Intratumor Heterogeneity and Branched Evolution Revealed by Multiregion Sequencing. *N Engl J Med*. 2012;366(10):883-892. doi:10.1056/NEJMoa1113205

8. Bashashati A, Ha G, Tone A, et al. Distinct evolutionary trajectories of primary high-grade serous ovarian cancers revealed through spatial mutational profiling. *J Pathol*. 2013;231(1):21-34. doi:10.1002/path.4230

9. Zhang J, Fujimoto J, Zhang J, et al. Intratumor heterogeneity in localized lung adenocarcinomas delineated by multiregion sequencing. *Science (80-)*. 2014;346(6206):256-259. doi:10.1126/science.1256930

10. Mullighan CG, Phillips LA, Su X, et al. Genomic Analysis of the Clonal Origins of Relapsed Acute Lymphoblastic Leukemia. *Science (80-)*. 2008;322(5906):1377-1380. doi:10.1126/science.1164266

11. Anderson K, Lutz C, van Delft FW, et al. Genetic variegation of clonal architecture and propagating cells in leukaemia. *Nature*. 2011;469(7330):356-361. doi:10.1038/nature09650

12. Ma X, Edmonson M, Yergeau D, et al. Rise and fall of subclones from diagnosis to relapse in pediatric B-acute lymphoblastic leukaemia. *Nat Commun*. 2015;6(1):6604. doi:10.1038/ncomms7604

13. Ferrando AA, López-Otín C. Clonal evolution in leukemia. *Nat Med*. 2017;23(10):1135-1145. doi:10.1038/nm.4410

14. Nowell P. The clonal evolution of tumor cell populations. *Science (80-)*. 1976;194(4260):23-28. doi:10.1126/science.959840

15. Mullighan CG, Zhang J, Kasper LH, et al. CREBBP mutations in relapsed acute lymphoblastic leukaemia. *Nature*. 2011;471(7337):235-239. doi:10.1038/nature09727

16. Meyer JA, Wang J, Hogan LE, et al. Relapse-specific mutations in NT5C2 in childhood acute lymphoblastic leukemia. *Nat Genet*. 2013;45(3):290-294. doi:10.1038/ng.2558

17. Tzoneva G, Perez-Garcia A, Carpenter Z, et al. Activating mutations in the NT5C2 nucleotidase gene drive chemotherapy resistance in relapsed ALL. *Nat Med*. 2013;19(3):368-371. doi:10.1038/nm.3078

18. Mar BG, Bullinger LB, McLean KM, et al. Mutations in epigenetic regulators including SETD2 are gained during relapse in paediatric acute lymphoblastic leukaemia. *Nat Commun.* 2014;5(1):3469. doi:10.1038/ncomms4469

19. Li B, Li H, Bai Y, et al. Negative feedback–defective PRPS1 mutants drive thiopurine resistance in relapsed childhood ALL. *Nat Med.* 2015;21(6):563-571. doi:10.1038/nm.3840

20. Tzoneva G, Dieck CL, Oshima K, et al. Clonal evolution mechanisms in NT5C2 mutant-relapsed acute lymphoblastic leukaemia. *Nature.* 2018;553(7689):511-514. doi:10.1038/nature25186

21. Yu S-L, Zhang H, Ho B-C, et al. FPGS relapse-specific mutations in relapsed childhood acute lymphoblastic leukemia. *Sci Rep.* 2020;10(1):12074. doi:10.1038/s41598-020-69059-y

22. Li B, Brady SW, Ma X, et al. Therapy-induced mutations drive the genomic landscape of relapsed acute lymphoblastic leukemia. *Blood.* 2020;135(1):41-55. doi:10.1182/blood.2019002220

23. Cheung LC, Tickner J, Hughes AM, et al. New therapeutic opportunities from dissecting the pre-B leukemia bone marrow microenvironment. *Leukemia.* 2018;32(11):2326-2338. doi:10.1038/s41375-018-0144-7

24. Cox C V., Diamanti P, Evely RS, Kearns PR, Blair A. Expression of CD133 on leukemia-initiating cells in childhood ALL. *Blood.* 2009;113(14):3287-3296. doi:10.1182/blood-2008-04-154187

25. Notta F, Mullighan CG, Wang JCY, et al. Evolution of human BCR–ABL1 lymphoblastic leukaemia-initiating cells. *Nature.* 2011;469(7330):362-367. doi:10.1038/nature09733

26. Bardini M, Woll PS, Corral L, et al. Clonal variegation and dynamic competition of leukemia-initiating cells in infant acute lymphoblastic leukemia with MLL rearrangement. *Leukemia.* 2015;29(1):38-50. doi:10.1038/leu.2014.154

27. Elder A, Bomken S, Wilson I, et al. Abundant and equipotent founder cells establish and maintain acute lymphoblastic leukaemia. *Leukemia.* 2017;31(12):2577-2586. doi:10.1038/leu.2017.140

28. Oshima K, Khiabanian H, da Silva-Almeida AC, et al. Mutational landscape, clonal evolution patterns, and role of RAS mutations in relapsed acute lymphoblastic leukemia. *Proc Natl Acad Sci.* 2016;113(40):11306-11311. doi:10.1073/pnas.1608420113

29. Woodworth MB, Girskis KM, Walsh CA. Building a lineage from single cells: genetic techniques for cell lineage tracking. *Nat Rev Genet.* 2017;18(4):230-244. doi:10.1038/nrg.2016.159

30. Wu S-H (Sam), Lee J-H, Koo B-K. Lineage Tracing: Computational Reconstruction Goes Beyond the Limit of Imaging. *Mol Cells.* 2019;42(2):104-112. doi:10.14348/molcells.2019.0006

31. Baron CS, van Oudenaarden A. Unravelling cellular relationships during development and regeneration using genetic lineage tracing. *Nat Rev Mol Cell Biol.* 2019;20(12):753-765. doi:10.1038/s41580-019-0186-3

32. El-Kebir M, Oesper L, Acheson-Field H, Raphael BJ. Reconstruction of clonal trees and tumor composition from multi-sample sequencing data. *Bioinformatics.* 2015;31(12):i62-i70. doi:10.1093/bioinformatics/btv261

33. Tarabichi M, Salcedo A, Deshwar AG, et al. A practical guide to cancer subclonal reconstruction from DNA sequencing. *Nat Methods.* 2021;18(2):144-155. doi:10.1038/s41592-020-01013-2

34. Belderbos ME, Jacobs S, Koster TK, et al. Donor-to-Donor Heterogeneity in the Clonal Dynamics of Transplanted Human Cord Blood Stem Cells in Murine Xenografts. *Biol Blood Marrow Transplant.* 2020;26(1):16-25. doi:10.1016/j.bbmt.2019.08.026

35. Belderbos ME, Koster T, Ausema B, et al. Clonal selection and asymmetric distribution of human leukemia in murine xenografts revealed by cellular barcoding. *Blood.* 2017;129(24):3210-3220. doi:10.1182/blood-2016-12-758250

36. Jacobs S, Ausema A, Zwart E, et al. Quantitative distribution of patient-derived leukemia clones in murine xenografts revealed by cellular barcodes. *Leukemia*. 2020;34(6):1669-1674. doi:10.1038/s41375-019-0695-2

37. Jacobs S, Ausema A, Zwart E, et al. Detection of chemotherapy-resistant patient-derived acute lymphoblastic leukemia clones in murine xenografts using cellular barcodes. *Exp Hematol*. 2020;91:46-54. doi:10.1016/j.exphem.2020.09.188

38. Bystrykh L V, de Haan G, Verovskaya E. Barcoded Vector Libraries and Retroviral or Lentiviral Barcoding of Hematopoietic Stem Cells. In: Bunting KD, Qu C-K, eds. New York, NY: Springer New York; 2014:345-360. doi:10.1007/978-1-4939-1133-2_23

39. Bystrykh L V, Belderbos ME. Clonal Analysis of Cells with Cellular Barcoding: When Numbers and Sizes Matter. In: Turksen K, ed. *Stem Cell Heterogeneity: Methods and Protocols*. New York, NY: Springer New York; 2016:57-89. doi:10.1007/7651_2016_343

40. Bystrykh L V, Verovskaya E, Zwart E, Broekhuis M, de Haan G. Counting stem cells: methodological constraints. *Nat Methods*. 2012;9(6):567-574. doi:10.1038/nmeth.2043

41. Lin KH, Rutter JC, Xie A, et al. Using antagonistic pleiotropy to design a chemotherapy-induced evolutionary trap to target drug resistance in cancer. *Nat Genet*. 2020;52(4):408-417. doi:10.1038/s41588-020-0590-9

42. Kester L, van Oudenaarden A. Single-Cell Transcriptomics Meets Lineage Tracing. *Cell Stem Cell*. 2018;23(2):166-179. doi:10.1016/j.stem.2018.04.014

43. Wagner DE, Klein AM. Lineage tracing meets single-cell omics: opportunities and challenges. *Nat Rev Genet*. 2020;21(7):410-427. doi:10.1038/s41576-020-0223-2

44. Spanjaard B, Hu B, Mitic N, et al. Simultaneous lineage tracing and cell-type identification using CRISPR–Cas9-induced genetic scars. *Nat Biotechnol*. 2018;36(5):469-473. doi:10.1038/nbt.4124

45. Alemany A, Florescu M, Baron CS, Peterson-Maduro J, van Oudenaarden A. Whole-organism clone tracing using single-cell sequencing. *Nature*. 2018;556(7699):108-112. doi:10.1038/nature25969

46. Raj B, Wagner DE, McKenna A, et al. Simultaneous single-cell profiling of lineages and cell types in the vertebrate brain. *Nat Biotechnol*. 2018;36(5):442-450. doi:10.1038/nbt.4103

47. Raj B, Gagnon JA, Schier AF. Large-scale reconstruction of cell lineages using single-cell readout of transcriptomes and CRISPR–Cas9 barcodes by scGESTALT. *Nat Protoc*. 2018;13(11):2685-2713. doi:10.1038/s41596-018-0058-x

48. Chan MM, Smith ZD, Grosswendt S, et al. Molecular recording of mammalian embryogenesis. *Nature*. 2019;570(7759):77-82. doi:10.1038/s41586-019-1184-5

49. Weinreb C, Rodriguez-Fraticelli A, Camargo FD, Klein AM. Lineage tracing on transcriptional landscapes links state to fate during differentiation. *Science (80-)*. 2020;367(6479):eaaw3381. doi:10.1126/science.aaw3381

50. Rodriguez-Fraticelli AE, Weinreb C, Wang S-W, et al. Single-cell lineage tracing unveils a role for TCF15 in haematopoiesis. *Nature*. 2020;583(7817):585-589. doi:10.1038/s41586-020-2503-6

51. Eyler CE, Matsunaga H, Hovestadt V, Vantine SJ, van Galen P, Bernstein BE. Single-cell lineage analysis reveals genetic and epigenetic interplay in glioblastoma drug resistance. *Genome Biol*. 2020;21(1):174. doi:10.1186/s13059-020-02085-1

52. Quinn JJ, Jones MG, Okimoto RA, et al. Single-cell lineages reveal the rates, routes, and drivers of metastasis in cancer xenografts. *Science (80-)*. 2021;371(6532):eabc1944. doi:10.1126/science.abc1944

53. Frieda KL, Linton JM, Hormoz S, et al. Synthetic recording and in situ readout of lineage information in single cells. *Nature*. 2017;541(7635):107-111. doi:10.1038/nature20777

54. Askary A, Sanchez-Guardado L, Linton JM, et al. In situ readout of DNA barcodes and single base edits facilitated by in vitro transcription. *Nat Biotechnol*. 2020;38(1):66-75. doi:10.1038/s41587-019-0299-4

55. Pei W, Feyerabend TB, Rössler J, et al. Polylox barcoding reveals haematopoietic stem cell fates realized in vivo. *Nature*. 2017;548(7668):456-460. doi:10.1038/nature23653

56. Kalhor R, Kalhor K, Mejia L, et al. Developmental barcoding of whole mouse via homing CRISPR. *Science (80-)*. 2018;361(6405):eaat9804. doi:10.1126/science.aat9804

57. Ludwig LS, Lareau CA, Ulirsch JC, et al. Lineage Tracing in Humans Enabled by Mitochondrial Mutations and Single-Cell Genomics. *Cell*. 2019;176(6):1325-1339.e22. doi:10.1016/j.cell.2019.01.022

58. Xu J, Nuno K, Litzenburger UM, et al. Single-cell lineage tracing by endogenous mutations enriched in transposase accessible mitochondrial DNA. *Elife*. 2019;8. doi:10.7554/eLife.45105

59. Lareau CA, Ludwig LS, Muus C, et al. Massively parallel single-cell mitochondrial DNA genotyping and chromatin profiling. *Nat Biotechnol*. August 2020:1-11. doi:10.1038/s41587-020-0645-6

60. Abyzov A, Vaccarino FM. Cell Lineage Tracing and Cellular Diversity in Humans. *Annu Rev Genomics Hum Genet*. 2020;21:101-116. doi:10.1146/annurev-genom-083118-015241

61. Mishra P, Chan DC. Mitochondrial dynamics and inheritance during cell division, development and disease. *Nat Rev Mol Cell Biol*. 2014;15(10):634-646. doi:10.1038/nrm3877

62. Griessinger E, Moschoi R, Biondani G, Peyron JF. Mitochondrial Transfer in the Leukemia Microenvironment. *Trends in Cancer*. 2017;3(12):828-839. doi:10.1016/j.trecan.2017.10.003

63. Martins I, Ribeiro IP, Jorge J, et al. Liquid Biopsies: Applications for Cancer Diagnosis and Monitoring. *Genes (Basel)*. 2021;12(3):349. doi:10.3390/genes12030349

64. Juarez J, Dela Pena A, Baraz R, et al. CXCR4 antagonists mobilize childhood acute lymphoblastic leukemia cells into the peripheral blood and inhibit engraftment. *Leukemia*. 2007;21(6):1249-1257. doi:10.1038/sj.leu.2404684

65. Parameswaran R, Yu M, Lim M, Groffen J, Heisterkamp N. Combination of drug therapy in acute lymphoblastic leukemia with a CXCR4 antagonist. *Leukemia*. 2011;25(8):1314-1323. doi:10.1038/leu.2011.76

66. Welschinger R, Liedtke F, Basnett J, et al. Plerixafor (AMD3100) induces prolonged mobilization of acute lymphoblastic leukemia cells and increases the proportion of cycling cells in the blood in mice. *Exp Hematol*. 2013;41(3):293-302.e1. doi:10.1016/j.exphem.2012.11.004

67. To LB, Haylock DN, Simmons PJ, Juttner CA. The biology and clinical uses of blood stem cells. *Blood*. 1997;89(7):2233-2258. doi:10.1182/blood.v89.7.2233

68. Srinivasan A, Panetta JC, Cross SJ, et al. Phase I Study of the Safety and Pharmacokinetics of Plerixafor in Children Undergoing a Second Allogeneic Hematopoietic Stem Cell Transplantation for Relapsed or Refractory Leukemia. *Biol Blood Marrow Transplant*. 2014;20(8):1224-1228. doi:10.1016/j.bbmt.2014.04.020

69. Cooper TM, Sison EAR, Baker SD, et al. A phase 1 study of the CXCR4 antagonist plerixafor in combination with high-dose cytarabine and etoposide in children with relapsed or refractory acute leukemias or myelodysplastic syndrome: A Pediatric Oncology Experimental Therapeutics Investigators' Co. *Pediatr Blood Cancer*. 2017;64(8):e26414. doi:10.1002/pbc.26414

70.   Roboz GJ, Ritchie EK, Dault Y, et al. Phase I trial of plerixafor combined with decitabine in newly diagnosed older patients with acute myeloid leukemia. *Haematologica*. 2018;103(8):1308-1316. doi:10.3324/haematol.2017.183418

71.   Heiblig M, Elhamri M, Thomas X, Plesa A, Raffoux E, Hayette S. A phase 1 study of chemo-sensitization with plerixafor plus G-CSF in adults with relapsed acute myeloid leukemia. *Leuk Res*. 2018;72:7-11. doi:10.1016/j.leukres.2018.07.017

Appendices

NEDERLANDSE SAMENVATTING VOOR NIET-INGEWIJDEN

De klonale diversiteit van kanker is belangrijk voor het ontstaan van kanker, voor de het stellen van de diagnose en voor de behandeling. In dit proefschrift hebben we barcodes gebruikt om de klonale diversiteit van acute leukemie te bestuderen. Leukemie is klonaal heterogeen, wat betekent dat de leukemie van één patiënt bestaat uit meerdere groepen cellen. Deze klonen verschillen van elkaar waardoor bijvoorbeeld niet alle klonen even goed reageren op therapie en sommige klonen sneller groeien dan anderen. Om de behandeling van patiënten met leukemie te verbeteren, moeten we begrijpen hoe deze verschillende klonen zich gedragen. Hoeveel klonen zitten er bijvoorbeeld in een patiënt, hoe verdelen deze klonen zich over het lichaam van een patiënt en hoe gevoelig zijn de voor de verschillende chemotherapie waaraan ze in een patiënt worden blootgesteld? Om dit soort vragen te kunnen beantwoorden, hebben wij gebruik gemaakt van proefdieren. We hebben leukemiecellen van patiënten voorzien van een barcode en deze getransplanteerd in muizen. Hieronder de belangrijkste bevindingen van dit proefschrift, die vervolgens nader zullen worden toegelicht:

- Een accurate telling van het aantal klonen vereist transparantie in de barcode data-analyse.
- In het lichaam van een muis bevinden zich tientallen tot honderden leukemie klonen die zich asymmetrisch verdelen over de verschillende botten en organen.
- Doordat leukemie klonen zich asymmetrisch verdelen over de verschillende botten en organen van de muis, missen we ruim de helft van de klonen wanneer we slechts één locatie analyseren.
- Met behulp van barcodes kunnen we in muizen leukemie klonen identificeren die ongevoelig zijn voor chemotherapie.

Wat zijn stamcellen?

Ons lichaam bestaat uit miljarden cellen, oorspronkelijk ontstaan uit de samensmelting van een zaadcel en eicel, die samen één cel vormden. Deze miljarden cellen vormen de verschillende organen en weefsels in ons lichaam, en bestaan uit meerdere celtypes met elk hun eigen functie. De meeste organen en weefsel beschikken over weefselspecifieke stamcellen. Zo'n stamcel is een uniek celtype dat zich karakteriseert door twee eigenschappen. Ten eerste kan deze cel zich ontwikkelen tot alle celtypen binnen een bepaald orgaan of weefsel (i.e. differentiatie). Ten tweede kan deze cel zichzelf vernieuwen (i.e. proliferatie) en gaat een leven lang mee, waardoor ze onmisbaar zijn voor het menselijk lichaam. Een voorbeeld zijn de bloedvormende stamcellen. De bloedvormende stamcellen kunnen zich ontwikkelen tot de verschillende type bloedcellen - rode bloedcellen, witte bloedcellen en bloedplaatjes – die ervoor zorgen dat zuurstof wordt getransporteerd door het lichaam, het lichaam wordt beschermd tegen infecties en wondjes worden

hersteld door middel van stolling van het bloed. Deze verschillende type bloedcellen kunnen zichzelf echter niet vernieuwen, hebben een beperkte levensduur en moeten worden vervangen. Om ervoor te zorgen dat er gedurende het hele leven nieuw bloed kan worden aangemaakt, kunnen deze bloedvormende stamcellen zichzelf vernieuwen. De eigenschappen van de verschillende cellen liggen vastgelegd in het genetische materiaal. Dit genetische materiaal wordt DNA genoemd en is opgebouwd uit de vier bouwstenen Adenosine (A), Thymine (T), Cytosine (C) en Guanine (G). Deze bouwstenen komen in een bepaalde volgorde voor en vormen een codeboek voor alle eigenschappen van een cel. Zo'n eigenschap ligt opgeslagen in een gen, een klein stuk van het DNA dat codeert voor een eiwit dat een bepaalde functie uitvoert in de cel. Er zijn meerdere genen, denk bijvoorbeeld aan de genen die de kleur van je ogen bepalen. Ook zijn er genen die betrokken zijn bij complexere en essentiële functies van de cel, zoals bijvoorbeeld celdeling en overleving van de cel waardoor deze zijn functie kan blijven uitvoeren. Ons lichaam bestaat dus uit vele verschillende type cellen, waarvan de eigenschappen liggen vastgelegd in het DNA.

Wat is een kloon?

In theorie is het DNA in alle cellen van een individu uniek. Alle cellen zijn namelijk afkomstig van dezelfde bevruchte eicel. Alle cellen die afkomstig zijn van dezelfde voorloper cel en daarmee dus bepaalde genetische eigenschappen delen, worden een kloon genoemd. Hiermee vormen alle cellen waaruit ons lichaam is opgebouwd dus een kloon. In de volksmond is het een term die wordt geassocieerd met 'identiek', maar het wordt steeds duidelijker dat de nakomelingen van cellen niet volledig identiek zijn. Gedurende ons leven ontstaan er namelijk veranderingen in de bouwstenen van het DNA van cellen. Zo'n verandering wordt een mutatie genoemd en kan bijvoorbeeld spontaan ontstaan tijdens een celdeling of door invloeden van buitenaf zoals ultraviolette straling. Vaak zijn deze mutaties onschuldig en in de meeste gevallen worden ze gerepareerd door de cel. Echter, blijvende mutaties van het DNA kunnen ervoor zorgen cellen niet meer identiek zijn en variëren in essentiële functies. Deze veranderingen in de bouwstenen van het DNA zorgen er dus voor dat er diverse populaties van cellen ontstaan, in andere woorden meerdere klonen. Ondanks dat de biologische definitie van een "kloon" helder is, is de term "kloon" een begrip dat vanuit experimenteel perspectief op verschillende manieren wordt gedefinieerd. Verschillende definities voor de term kloon kan een negatieve invloed hebben op de interpretatie van experimentele studies en onderstreept het belang van een heldere definitie. Een eenvoudigere definitie van de term kloon, met name vanuit experimenteel oogpunt, vereist dat de populatie van cellen afkomstig is van dezelfde voorloper cel, maar daarmee niet per se volledig identiek zijn aan elkaar.

Klonale diversiteit in leukemie

Aangezien klonen kunnen verschillen in essentiële functies, krijgt het bestuderen van klonen steeds meer aandacht in verschillende onderzoeksvelden, waaronder kanker. De diversiteit van klonen (i.e. klonale heterogeniteit) wordt gezien als belangrijke drijfveer voor de start, de ontwikkeling en terugkeren van kanker. Kanker is een ziekte waarbij lichaamscellen ongecontroleerd delen, bijvoorbeeld ten gevolge van verandering in het DNA van genen die betrokken zijn bij celdeling. Een voorbeeld is leukemie (i.e. bloedkanker) waarbij witte bloedcellen ongecontroleerd delen en niet hun normale functie kunnen uitoefenen. Deze leukemiecellen verspreiden zich via het bloed naar verschillende locaties in het lichaam en verdringen de gezonde bloedcellen. Leukemie is klonaal heterogeen, wat betekent dat leukemie bestaat uit verschillende klonen. Klonen kunnen bijvoorbeeld verschillen in de snelheid waarmee ze delen en de mogelijkheid om zich staande kunnen houden tegen chemotherapeutische behandelingen (i.e. klonale evolutie), met als gevolg dat de leukemie niet volledig verdwijnt en op een later moment eventueel weer terugkeert. Om ervoor te zorgen dat patiënten genezen van leukemie moeten we alle klonen van de leukemie uitroeien. Om dit mogelijk te maken is het belangrijk om een beter begrip te krijgen van hoeveel leukemie klonen er in een patiënt zijn, hoe deze klonen zijn verdeeld over het lichaam en hoe deze klonen reageren op chemotherapie. Alleen als we begrijpen hoe de verschillende leukemie klonen zich gedragen, kunnen we daarop anticiperen en ze uitroeien.

Het gebruik van barcodes om klonale diversiteit te bestuderen

In wetenschappelijk onderzoek worden verschillende methodes gebruikt om klonen te bestuderen. In de introductie van dit proefschrift gaan we uitvoerig in op de meest gebruikte methodes om klonen te volgen en bespreken we de voor- en nadelen van iedere methode. In de rest van dit proefschrift hebben we gebruik gemaakt van zogenaamde barcodes om klonen te identificeren, te tellen en de dynamiek van verschillende klonen over de tijd en in reactie op chemotherapie te volgen. Een barcode is een combinatie van de verschillende bouwstenen van het DNA die kan worden gebruikt om individuele klonen van een genetisch label te voorzien. Zo kun je bijvoorbeeld de code "ACTG" en "CTGA" creëren, die je kunt inbouwen in het DNA van de cel die je wilt volgen. Deze code wordt bij iedere celdeling doorgegeven aan de dochtercellen, waardoor je in dit specifieke voorbeeld twee verschillende klonen kunt volgen. Uiteraard kun je veel meer en complexere varianten van dit soort barcodes creëren, waardoor je vele verschillende individuele klonen kunt volgen. Je kunt deze barcodes het beste vergelijken met de streepjescodes in de supermarkt, die het mogelijk maken om alle verschillende producten van elkaar te onderscheiden. Net zoals dat je in de supermarkt individuele producten kunt scannen, kunnen wij in het laboratorium ook de barcode van individuele cellen uitlezen (i.e. 'sequencen'). In dit proefschrift hebben we de toepasbaarheid van

barcodes in het bestuderen van klonale heterogeniteit onderzocht. Hiervoor hebben we gebruik gemaakt van normale bloedvormende stamcellen en leukemiecellen, waarvan we de klonale dynamiek in muizen hebben bestudeerd.

Het aantal klonen dat je telt, verschilt tussen data analysemethodes

Het uitlezen van de barcodes van individuele cellen is een techniek waarbij foutjes worden gemaakt, er worden barcodes uitgelezen die eigenlijk niet bestaan. Als we dit vergelijken met de supermarkt-analogie betekent dit dat er in het kassa-systeem barcodes zijn ingevoerd, terwijl er geen producten met die barcode worden verkocht. Wanneer je deze foutjes niet uit je kassa-systeem zou halen, lijkt het erop dat je meer producten te koop aanbiedt dan dat daadwerkelijk het geval is. Ditzelfde geldt voor de barcodes, we moeten ervoor zorgen dat we de foutjes er zo goed mogelijk uithalen zodat we nauwkeurig het aantal barcode klonen kunnen tellen. Er zijn echter verschillende strategieën om deze foutjes eruit te halen. Door de verschillende strategieën toe te passen op dezelfde barcode dataset laten we zien dat het aantal barcode klonen dat je telt varieert tussen deze strategieën. Dit betekent dat experimentele conclusies met betrekking tot het tellen van het aantal klonen en biologische interpretaties afhankelijk zijn van de gekozen data-analyse strategie. Transparantie in gekozen data-analyse strategieën zorgt ervoor dat verschillende studies met elkaar vergeleken kunnen worden en de juiste conclusies getrokken kunnen worden. Daarnaast laten we zien dat de Shannon-diversiteitsindex, één van de strategieën om foutjes eruit te halen, de meest robuuste methode is om het aantal barcode klonen te tellen en deze strategie hebben wij dan ook in de rest van dit proefschrift toegepast.

Leukemie klonen zijn asymmetrisch verdeeld in de muis

In dit proefschrift hebben we barcodes gebruikt om het aantal leukemie klonen te tellen die de mogelijkheid hebben om de ziekte voort te zetten in de muis. Immers, hoe meer klonen er aanwezig zijn in leukemie, des te groter de kans dat er een kloon tussen zit die ongevoelig is voor chemotherapie en ervoor zorgt dat de leukemie uiteindelijk terugkeert. Om te bepalen hoeveel leukemie klonen de mogelijkheid hebben de ziekte voort te zetten in de muis, hebben we leukemiecellen van patiënten voorzien van een barcode. Deze gebarcodeerde leukemiecellen hebben we getransplanteerd in muizen. Op het moment dat deze muizen leukemie hadden ontwikkeld, hebben we gekeken welke barcode klonen er aanwezig waren in de verschillende botten en organen van de muis. We vonden honderden leukemie barcode klonen; wat betekent dat leukemie bestaat uit honderden cellen, die ieder opnieuw de ziekte kunnen voortzetten. Deze barcode klonen waren asymmetrisch verdeeld over de botten en organen van de muis: de barcode klonen in de linker poot van de muis verschilden bijvoorbeeld van de barcode klonen in de rechter poot van de muis. Door de klonen in alle lichaamsdelen te vergelijken, berekenden we

dat we ruim de helft van de leukemie klonen missen, wanneer we alleen één lichaamslokalisatie analyseren. Met andere woorden, wanneer men slechts een beperkt aantal locaties analyseert, krijgt men geen compleet beeld van de leukemie. Dit is belangrijk, omdat de meeste wetenschappelijke studies gebruikelijk slechts naar één locatie kijkt. Dit betekent dat experimentele conclusies en biologische interpretaties mogelijk onvolledig kunnen zijn. Daarnaast is het in patiënten gebruikelijk om bij de diagnose en controles alleen in het bloed en bekken te kijken. Dit zou mogelijk kunnen betekenen dat we ook bij patiënten leukemie klonen missen. Dit betekent dat de behandeling die patiënten krijgen mogelijk suboptimaal is en dat we bij controles kunnen denken dat de behandeling goed heeft gewerkt terwijl er nog wel leukemie klonen aanwezig zijn in de patiënt. Echter, de conclusies zijn gebaseerd op onderzoeken in muizen en uiteraard zal de asymmetrische verdeling eerst in mensen moeten worden bevestigd voordat we conclusies kunnen trekken over het ziektebeeld in de mens.

Met barcodes kunnen we leukemie klonen detecteren die ongevoelig zijn voor chemotherapie

Daarnaast hebben we onderzocht of barcodes kunnen worden gebruikt om de gevoeligheid van individuele leukemieklonen voor chemotherapie te testen. We hebben eerder al laten zien dat de leukemie in een patiënt bestaat uit tientallen tot honderden verschillende klonen. Als één van deze klonen ongevoelig is voor chemotherapie, zal de behandeling uiteindelijk onvoldoende effectief zijn en komt te ziekte terug. Het zou dus handig zijn als we de gevoeligheid van deze leukemie klonen vóóraf kunnen vaststellen en daarmee de meest effectieve behandeling te kunnen selecteren. Om te onderzoeken of barcodes gebruikt kunnen worden om chemotherapie-ongevoelige cellen op te sporen, hebben we eveneens gebruik gemaakt van gebarcodeerde leukemiecellen verkregen uit patiënten, die we hebben getransplanteerd in muizen. Deze muizen hebben we vervolgens behandeld met verschillende chemotherapie. Met behulp van barcodes en het gebruik van de juiste controles in de experimentele opzet waren we in staat om verschillen in gevoeligheid van barcode leukemieklonen te detecteren. Zo vonden we bijvoorbeeld meerdere barcode klonen die ongevoelig zijn voor de chemotherapie methotrexaat. Dit is belangrijk omdat deze klonen ervoor kunnen zorgen dat de leukemie niet verdwijnt of uiteindelijk weer terugkeert. Het gebruik van barcodes in ons muismodel is een waardevolle methode om de dynamiek van leukemieklonen na blootstelling aan chemotherapie te bestuderen. Hoe de gevoeligheid van leukemie klonen in muizen zich verhoudt tot de gevoeligheid in mensen zal nog nader moeten worden onderzocht.

Conclusie

Al met al laten we in dit proefschrift zien dat DNA-barcodes een relevante, relatief eenvoudige methode is om het gedrag van individuele leukemie klonen in muizen te be-

studeren. Naast DNA barcodes zijn er nog veel meer manieren om de eigenschappen van leukemie klonen te onderzoeken. Zo zijn er methodes die kijken naar het RNA of naar de stofwisseling van deze klonen. Door deze verschillende methodes te combineren met DNA barcodes zullen we nog beter gaan begrijpen hoe leukemie klonen zich gedragen. Verdere combinaties van methodes en de ontwikkeling van nieuwe technieken zullen in de toekomst onze kennis over het gedrag van leukemie klonen vergroten en mogelijk resulteren in nieuwe en verbeterde behandelstrategieën.

CURRICULUM VITAE

Sabrina Jacobs is op 11 november 1990 geboren in Zeist en opgegroeid in Den Dolder. In 2009 haalde zij haar VWO-diploma aan Het Nieuwe Lyceum te Bilthoven. Aansluitend daarop is zij gestart met de bachelor Life, Science and Technology, major Biomedische Wetenschappen, aan de Rijksuniversiteit Groningen. Na het behalen van haar bachelor diploma in 2012 vervolgde zij haar studie aan de Rijksuniversiteit Groningen met de master Biomedische Wetenschappen. Tijdens haar master heeft zij twee onderzoeksprojecten afgerond. Het eerste onderzoeksproject was bij de afdeling voor neurowetenschappen van het Universitair Medisch Centrum Groningen, waar ze onder begeleiding van prof. dr. Erik Boddeke, prof. dr. Bart Eggen, dr. Peter Meerlo en dr. Wandert Schaafsma onderzoek heeft gedaan haar de inflammatoire response van microglia. Voor haar tweede onderzoeksproject ging zij naar het Verenigd Koninkrijk, waar ze regulatie van oligodendrocyten door Sox2 heeft bestudeerd bij de afdeling voor klinische neurowetenschappen van de Universiteit van Cambridge onder begeleiding van prof. dr. Robin Franklin, dr. Chao Zhao, en dr. Wia Baron. In September 2014 rondde ze de masteropleiding *cum laude* af, waarna zij in 2015 begon aan haar promotieonderzoek op de afdeling voor neurowetenschappen van het Universitair Medisch Centrum Groningen. Na het afbreken van dit promotieonderzoek is zij in 2016 begonnen als analist op de afdeling verouderingsbiologie en stamcellen van het Universitair Medisch Centrum Groningen. In 2018 heeft zij haar werkzaamheden voortgezet als promovendus onder begeleiding van prof. dr. Gerald de Haan, dr. Mirjam Belderbos en dr. Leonid Bystrykh. In dit promotieonderzoek heeft zij met behulp van DNA barcodes de klonale heterogeniteit van leukemie bestudeerd. De resultaten van haar promotieonderzoek staan beschreven in dit proefschrift, die zij zal verdedigen op 27 september 2021. Sinds mei 2021 werkt Sabrina als data steward bij de 'Cohort and Biobank Coordination Hub' in het Universitair Medisch Centrum Groningen te Groningen.

DANKWOORD

Mijn proefschrift is een feit en wat een werk is er verricht! Van het sorteren van cellen en het prakken van muizenbotjes tot aan het analyseren van de data en het schrijven van verschillende publicaties. Met de bouw van ons nieuwe huis en de komst van Luuk, was het laatste jaar van mijn promotietraject toch wat stressvol. Waar menig mens óf een nieuw huis koopt óf zwanger is óf zijn promotietraject afrond, stond er bij mij in een keer overal én tussen. Ik ben dan ook trots op dat we dit proefschrift hebben afgerond en bovenal enorm dankbaar voor alle hulp en steun die ik heb gekregen van mijn collega's, vrienden en familie om dit mogelijk te maken.

Allereerst wil ik mijn promotor prof. dr. **Gerald de Haan** en mijn co-promotoren dr. **Mirjam Belderbos** en dr. **Leonid Bystrykh** bedanken voor het gestelde vertrouwen in mij en jullie supervisie tijdens de verschillende projecten. Bedankt voor de kans die jullie mij hebben gegeven om na twee jaar als analist de werkzaamheden als promovendus voort te mogen zetten met dit proefschrift als mooie resultaat.

Lieve **Mirjam**, toch best knap dat we dit zo voor elkaar hebben weten te krijgen! Jij in Utrecht en ik 200km verderop in Groningen. Zeker in de eerste jaren ging je telefoon dan ook met regelmaat over. Ondanks de drukte in de kliniek wist je altijd tijd vrij te maken om mijn vragen te beantwoorden. Als er te veel muizen op het punt stonden om te vallen, gooide je weekendplannen overhoop en kwam je naar Groningen toe om te helpen. Dankjewel, want daardoor kon ook ik van mijn kerstdagen genieten! Een terugkerend verhaal, waar we deze dagen nog steeds om kunnen lachen, is toch wel het pelvis botje dat in de septobox belandde. Ook in mijn persoonlijke ontwikkeling heb je me altijd gesteund en het beste in mij naar boven weten te halen. Zo heb ik met jouw hulp op meerdere congressen en voor het Prinses Máxima Centrum met zeker 100 aanwezige artsen een praatje gegeven. Voor mij is dat een enorme overwinning. Ik wens je veel succes met het opzetten van je eigen onderzoeksgroep. Jij als kinderoncoloog bij de transplantatieafdeling (ja, ook een fulltimebaan, hoe doe je het allemaal toch) kan dit! En denk maar zo, er is nog altijd dat koffietentje. Mirjam, ik hoop dat je door de regels heen kunt lezen dat ik je ontzettend dankbaar ben voor alles wat je voor mij op professioneel en persoonlijk vlak betekent! Ik ben blij dat onze paden hebben gekruist en ik ga onze samenwerking en gezellige heidagen zeker missen! Wat betreft dit proefschrift, we hebben mooi werk geleverd en er rest mij nog één ding te zeggen: "Strikje erom".

Beste **Gerald**, in de eerste periode van mijn aanstelling hadden we wat minder contact omdat de dagelijkse begeleiding via Mirjam liep. Hier kwam echter verandering in toen mijn aanstelling werd voortgezet als promovendus en tevens de eerste publicaties geschreven moesten worden. Zo kwamen er de maandelijkse voortgangsgesprekken waarin we uitvoerig ingingen op de behaalde resultaten. Ik wil je dan ook bedanken voor alle input die je daarin hebt geleverd. Daarnaast wil ik je in het bijzonder bedanken voor de mogelijkheid die je me hebt gegeven om mijzelf op persoonlijk professioneel vlak te

ontwikkelen. Je deur stond altijd open om het te hebben over vervolgstappen in mijn carrière. Een mooie brug om jou succes te wensen in de volgende stap van jouw carrière!

Dear **Leonid**, although I was sometimes a bit hesitant to go into your office, I always came back more knowledgeable and I can genuinely say it was nice to work together with you. Your creative thoughts on how to present the data and your help with the statistical analysis, I could always stop by your office. I would especially like to thank you for helping me with my presentations. There have been some changes in the stem cell biology department and I want to wish you the best of luck with the next and last stages in your career!

I would like to thank the members of the reading committee, prof. dr. ir. **F. Foijer**, prof. dr. **B. Fehse** and prof. dr. **H.J. Vormoor**, for their effort on reading and judging my thesis.

Daarnaast wil ik alle co-auteurs bedanken voor de suggesties en hulp bij het uitvoeren van het onderzoek en het schrijven van de publicaties.

Mijn paranimfen Daniëlle en Lisette.
Lieve **Daniëlle**, we zijn op hetzelfde moment gestart en nu mogen we ook op vrijwel hetzelfde moment allebei ons proefschrift verdedigen. Waar we begonnen als collega's is onze relatie uitgegroeid tot een mooie vriendschap. Ik heb altijd veel bewondering gehad voor je tomeloze inzet en je positieve karakter. Daarnaast sta je altijd klaar om andere mensen te helpen! Niet alleen voor werk, maar ook daarbuiten. Zo stonden jij en Erik voor ons klaar, toen ik hoogzwanger ging verhuizen van De Brink naar Tuikwerd en er nog behoorlijk wat moest worden ingepakt (en de lift die het niet deed!). Ik zal mijn presentatie op het CRCG-congres ook nooit vergeten. Vol spanning stond ik klaar om mijn presentatie te beginnen, waarna ik vervolgens jou achterin de zaal als een idioot (geluidloos) zag juichen. Ik proestte het bijna uit en mijn spanning verdween als sneeuw voor de zon. Twee weken na mijn verdediging is het jouw beurt om te promoveren en dan zal ik jou stilletjes (maar wel idioot) in de zaal aanmoedigen!

Lieve **Lisette**, wat ben ik blij dat wij huisgenoten werden op Damsterdiep! Eigenlijk kan ik bij jou alles in één woord samenvatten: "Topper!", maar zo makkelijk kom je er niet vanaf. Je staat voor me klaar op het moment dat ik steun nodig heb, maar gelukkig ben je er ook altijd bij als er iets gevierd moet worden. Zo ook bij mijn promotie (waarbij steun en feest toch wel erg dicht bij elkaar liggen) en ik zou niemand liever naast me te hebben dan jij. Al wil ik je vragen om de sing star-sessies, die tot laat in de avond doorgingen, tijdens de verdediging zelf maar achterwege te laten. Dit bewaren we wel voor tijdens het feestje. Samen met **Lizette** hebben we het altijd erg gezellig; bordspelletjes spelen, gamen, formule-1 kijken, racefietsen, wandelen en passen jullie met liefde op

Luuk. Tegen beide wil ik zeggen, dankjewel daarvoor. Samen gaan we hier nog veel meer mooie herinneringen aan toevoegen! Bedankt voor alles toppers!

Dan wil ik graag mijn collega's van de stamcelbiologie bedanken voor de ontzettend gezellige tijd die ik samen met jullie heb gehad. Al met al zijn het succesvolle experimenten geweest en dit was zonder jullie hulp niet mogelijk geweest. **Bertien**, ik had me geen betere leermeester kunnen wensen voor de muisexperimenten. Bedankt voor alles wat je mij hebt geleerd. De handigheid waarmee jij bloedafnames doet en de snelheid waarmee jij botjes schoonmaakt en prakt, is ongekend. Ook wil ik je bedanken voor je hulp bij de uitvoer van de experimenten. Dit viel soms niet mee, met muizen die op ieder moment konden omvallen van de leukemie en chemotherapie waarvan we niet wisten hoe ze erop gingen reageren. **Ellen**, bij jou kon ik altijd terecht voor vragen over en hulp met celweekexperimenten. O en laten we de onmogelijk vele PCRs, dit zijn er zeker een paar duizend(!), en gelletjes die gerund moesten worden niet vergeten! Dankzij jou hebben we onze transductie efficiëntie flink omhoog weten te schroeven en ook samples met een laag aantal gebarcodeerde cellen succesvol kunnen sequencen. Bedankt voor al je hulp! **Erik**, help! En gelukkig was je er ook altijd om me te helpen. Dankzij jouw hulp heb ik leren programmeren. Ik moet zeggen dat ik na mijn studie een hekel had aan R, maar doordat je mij zelf liet puzzelen en hielp wanneer het nodig was, ben ik het programmeren oprecht leuk gaan vinden. Bedankt voor hulp hierbij, de gezellige wandelingen tijdens de pauzes, je hulp bij het verhuizen en bij het in elkaar zetten van de box voor Luuk. We blijven elkaar zien! **Sonja**, een MD PhD met fundamenteel onderzoek en ik ben erg onder de indruk van hoe jij dit allemaal hebt gedaan. Het was altijd gezellig om samen te werken, te oefenen voor onze presentaties ('less is more') en koffie te halen aan de andere kant van het UMCG. Ook zal ik ons congres in Papendal niet snel vergeten. Wat hebben we gelachen om het penthouse van Jason. **Jason**, speaking about Papendal! We had such a laughter when we realized you booked a penthouse for the conference. I am still laughing when I think about it. In your defense, it was the last available room. Thank you for the great time in the lab. You are a kind person and I enjoyed working with you. **Arthur**, your commitment to research is impressive! I want to thank you for your help and sharing your knowledge with me. You are a kind person and I was always very happy that I could steal your FACS appointments. Thank you for the nice time we had in the lab, the barbeques and the New Year's Eve parties with the rest of the lab.

Ook heb ik met veel plezier samen mogen werken met een aantal studenten. **Maaike**, jij was de eerste studenten die ik onder mijn hoede kreeg. Je hebt me geholpen bij het opzetten van de chemotherapie experimenten en daar ben ik je dankbaar voor. Ik heb je leren kennen als een harde werker en iemand die ook precies te werk gaat. Je bent na het afronden van je HBO-opleiding verdergegaan met de master. Ik wist dat het in je zat! **Yasmine**, de muisexperimenten die we voor ogen hadden bleken toch wat complexer te

zijn dan we hadden verwacht. Na wat aanpassingen in jouw project heb je je goed kunnen ontwikkelen. Ik wil je bedanken voor je hulp in het lab en voor het mooie figuur dat je hebt gemaakt voor de leukemieontwikkeling in de muis over de tijd. **Samuel**, during the project you developed as a skilled and independent student. I am sure that you will have further developed your scientific skill and I wish you all the best in your career.

I would also like to thank my former colleagues **Johannes**, **Seka** and **Alexander** for their support and great time in the lab. To the new PhD-students **Nathalia** and **Anne**, I wish you all the best of luck.

To **Tosca**, **Eduardo, Irena, Marlinde** and **Ina**, when you joined the Eriba (and we had to share our lab-space ;)) it took some adjustment from our group. I think it worked out very well! Although it was for a short period of time, it was nice working together.

To the **Foijer group**, the **CRISPR-Cas facility** and the **research sequencing facility** of the Eriba, thank you for the great time. I enjoyed our lunches, tea-/coffee-breaks and the delicious cake everybody brought to celebrate their birthdays. **Bjorn**, ik wil jou bedanken voor je hulp bij het complexe script voor loopdy loop loop. **Laura**, fijn om me te kunnen identificeren met een mede-zwangere tijdens een PhD. **Diana**, bedankt voor je input tijdens de lunchmeetings. **Nancy**, **Karina** en **Jennefer**, bedankt voor jullie hulp bij het testen van de kwaliteit van mijn samples voordat ze werden opgestuurd voor sequencen. **Yin Fai**, het valt niet te onderschatten hoe fijn het is dat alles schoon en klaar staat als je het nodig hebt. Bedankt voor de gezellige tijd!

Annet en **Sylvia** van het secretariaat en **Henk**, **Arnoud** en **Kevin** van het management-team, bedankt voor jullie hulp in de afgelopen jaren.

Voor alle medewerkers van de **CDP**, bedankt voor al jullie goede zorgen voor mijn mui-zen. Dankzij jullie kon ik ook van mijn weekenden genieten. In het bijzonder wil ik graag **Catriene**, **Michel**, **Annemieke**, **Magda**, **Juliëtte** en **Liana** bedanken voor jullie hulp!

Geert, **Johan**, **Theo** en **Henk** van de FACS-faciliteit, het was altijd gezellig om bij jullie te komen kletsen en tegelijkertijd ook nog cellen sorteren. Bedankt voor de fijne tijd.

Mijn oud-collega's van de neurowetenschappen, dank voor de hulp die ik heb gekregen en in het bijzonder, **Evelyn** en **Ietje**, bedankt voor jullie hulp bij het kleuren van de coupes.

Voorlopig blijf ik nog in het Hoge Noorden! Met veel enthousiasme ben ik de nieuwe uitdaging als data steward bij het **CBCH** aangegaan. **Wim**, **Rogier**, **Janny**, **Joëlle**, **Kim**,

Adriaan, **Nancy**, **Julissa**, **Efi**, **Anco**, **Jitka** en **Jone**, ik wil jullie bedanken voor het vertrouwen dat jullie mij geven door mij aan te nemen voor deze baan. Aan alle andere afdelingen waarmee ik nauw samenwerk, ik heb het erg naar mijn zin en kijk uit naar onze toekomstige samenwerkingen.

Aan al mijn lieve vrienden, van wie ik ongetwijfeld wat mensen ga vergeten (sorry, dit is niets persoonlijks ;)) maar ik ga toch proberen wat mensen in willekeurige volgorde benoemen, **Melissa** en **Jasper**, **Lauren** en **Robin**, **Aranka** en **Hugo**, **Martijn** en **Linda**, **Emma**, **Wandert** en **Laura**, **Hiske** en **Leon**, **Astrid** en **Wout**, **Pieter** en **Sus**, **Duco** en **Annelies**, **Corien** en **Jakob**, **Ramon** en **Nina**, alle medewerkers van **Van Drie**; een promotieonderzoek doe je niet alleen, maar doe je ook met hulp van vrienden. Vrienden die een luisterend oor bieden, die interesse tonen, die er zijn om met je te lachen, waar je even kan klagen als het niet lukt, maar bovenal waarmee je kan vieren als het goed gaat. Dank jullie voor alle plezier en steun die ik tijdens mijn PhD heb gehad!

Lieve **Gert** en **Marion**, ik wil jullie graag bedanken voor jullie steun van de afgelopen jaren en jullie interesse in mijn promotieonderzoek. Jullie waren altijd een en al oor als ik wat vertelde over onze nieuwe bevindingen. En voor al die presentaties, trek wat moois aan en vergeet geen lippenstift op te doen! Als je er mooi uitziet, straal je zelfvertrouwen uit. Niets is minder waar. Bedankt voor alles en ik kan me geen lievere schoonouders wensen!

Lieve **oma**, gezellig bij u op de koffie en er is altijd wat lekkers in huis! We kletsen over van alles en u bent altijd geïnteresseerd als ik vertel wat ik op mijn werk doe. Ik vind het heel bijzonder dat u dit mee kan maken en ik hoop dat we er nog veel bijzondere herinneringen aan toe mogen voegen.

Lieve **paps** en **mams**, jullie hebben mij altijd aangemoedigd het beste in mijzelf naar boven te halen. Jullie hebben me altijd gesteund in de keuzes die ik maakte; toen ik Den Dolder achter me liet om te gaan studeren in Groningen, mijn uitstapje naar Cambridge om uiteindelijk weer terug te gaan naar Groningen om daar te promoveren. Zonder jullie steun was dit nooit gelukt! De geboorte van Luuk, mijn promotie en we gaan er samen nog vele mooie herinneringen aan toevoegen.

Lieve **Natas**, jij geloofde altijd in mij dat ik het kon. Bedankt voor al je steun van de afgelopen jaren. De heerlijke high-teas en lekker kletsen. Gezellig samen gamen – old time favorite Mario – of bordspelletjes spelen om even te ontspannen net als toen we jong waren.

Lieve **Koen**, al grappend vroeg je mij of je een ode kreeg. Eerlijk gezegd heb je die wel verdiend! Iedereen weet inmiddels wel dat mijn eerste poging van een promotietraject geen succes was en jij was daar om mij te steunen met mijn zoektocht naar een baan die op dat moment beter bij me paste. Maar ook je aanmoediging en steun om toch weer een promotieonderzoek te gaan doen toen die mogelijkheid zich voordeed: "Ik ga de keuze niet voor je maken", en "Als je het niet doet, krijg je er misschien wel spijt van". We zullen het nooit weten, want ik heb het gedaan! Je hulp bij mijn experimenten, ja ja ook jij hebt muizenbotjes schoongemaakt. Je eindeloze steun bij het voorbereiden van mijn presentaties en het lezen van mijn artikelen. Je steun bij het afronden van mijn proefschrift, de laatste loodjes wegen het zwaarst. Met de geboorte van Luuk is er voor ons beide een nieuw hoofdstuk aangebroken in ons leven. Hij is onze nummer één! Ik kijk uit naar alles wat wij samen als gezinnetje gaan beleven!

Lieve **Luuk**, mijn blije ei van 1 jaar oud! Er zijn veel dingen die papa en ik jou gaan leren, maar in deze tijd dat jij bij ons bent heb ik ook al zoveel van jou geleerd. Het is cliché, maar door jou besef ik me weer dat je van vallen en opstaan leert en dat goed, goed genoeg is. Jij hebt me gemotiveerd om dit proefschrift af te ronden. Hoe bijzonder het afronden van dit proefschrift ook is, het valt in het niet bij jou en alles wat je doet. Ik hou ontzettend veel van je! Liefs mama.